UiT
THE ARCTIC UNIVERSITY OF NORWAY

Faculty or Science and Technology

A Holocene palaeoceanographic multi-proxy study on the variability of Atlantic water inflow and sea ice distribution along the pathway of Atlantic water

—

Sarah MP Berben

A dissertation for the degree of Philosophiae Doctor – August 2014

DISSERTATION FOR THE DEGREE OF PHILOSOPHIAE DOCTOR

A Holocene palaeoceanographic multi-proxy study on the variability of Atlantic water inflow and sea ice distribution along the pathway of Atlantic water

Sarah MP Berben

UNIVERSITY OF TROMSØ

Faculty of Science and Technology

August 2014

By endurance we conquer!

Acknowledgements

I would like to take the opportunity to thank all the people who supported and guided me throughout this entire PhD journey.

First of all, I would like to thank my supervisor Dr. Katrine Husum for giving me this wonderful opportunity in the first place. Further, I'm very grateful for all of her scientific advice, moral support, patience, freedom and trust to develop my own ideas, not to mention the many loud laughs we had. Secondly, I would like to thank Dr. Steffen Aagaard-Sørensen for the many scientific discussions, constructive feedback and assistance regarding my PhD-work.

The entire CASE group is thanked for the always pleasant and inspiring meetings, training sessions and social gatherings scattered over Europe. Special thanks go to Prof. Simon Belt and the chemical sisters for a warm welcome in Plymouth and a highly enthusiastic guidance in my biomarker adventure. It has been very contagious (*or should I scream contamination!)*. My gratitude is also expressed to my fellow 'ESRs' for the many scientific discussions, supporting friendships and enjoyable stays abroad. In particular, to Diane for being, this entire time, my Tromsø partner in crime!

Thank you to Frank Peeters for an enthusiastic introduction to the fascinating world of paleoceanography and the encouragement to continue. You were so right when you told me *"Saar, ik weet wat je het liefste zou doen, en volgens mij weet je dat zelf ook"*…and that is exactly what I did.

Thanks are also extended to the entire staff at the department of geology, UiT, for their technical and organizational assistance. Special thanks go to Jan P. Holm, Trine Dahl, Julia Sen and Karina Monsen for their always professional and kind help when and wherever I needed it.

To all my colleagues and friends in Tromsø, I would like to say thank you for all the support (in many ways), the different kind of social get-togethers and successful distractions, especially to Noortje for being such a great and always helpful friend from the early beginning. It all contributed to this great experience of living in the Arctic.

Thank you to all my friends and family in Belgium for not forgetting me, taking an interest in what it is again that I actually do, but most of all, for always making it such a pleasure to

come back home. Some of you were even crazy enough to come and visit me so far up north which I appreciate a lot.

Finally, the biggest thank you is for my mother and her never-ending support and believe in my (sometimes crazy) dreams and ambitions which is an inspiration on itself.

Tusen takk!

Sarah

Table of contents

Preface

This PhD thesis was carried out from 2011 to 2014 at the University of Tromsø within the Initial Training Network programme "Changing Arctic and Subarctic Environments" (CASE-ITN) funded by the European Commission within the 7th Framework Programme FP7 2007/2013, Marie Curie Actions. The overall aim of the project was to reconstruct and elucidate the Holocene natural variability of physical parameters such as Atlantic water inflow and sea ice distribution in the Arctic and Subarctic environment (Nordic Seas). Further, it provided intensive training sessions (including a marine geology and geophysics cruise in the Fram Strait with the R/V Helmer Hanssen, University of Tromsø) and progress meetings which all resulted in a close collaboration with five institutes across Europe (i.e. University of Bordeaux, Amsterdam, Plymouth, Geomar (Kiel) and the Geological Survey of Norway (Trondheim)). This collaboration also included a personal research stay during spring 2013 at the Biogeochemistry Research Centre, University of Plymouth, focusing on the analyses of sea ice and phytoplankton biomarkers.

Additionally, a Marie Curie "toppfinansiering" was received from the Research Council of Norway, whereas the Norwegian Research School in Climate Dynamics provided funding for their annual all staff meetings, several specialized courses and participation of the 2nd Young Scientist Meeting/4th Open Science Meeting organized by PAGES in Goa, India.

The results of this thesis were presented in 5 posters and 8 talks during national and international workshops, project meetings and conferences. The thesis consists of an introduction and three scientific papers regarding the investigation and reconstruction of the natural variability of Atlantic water inflow and sea ice distribution in the high latitude North Atlantic and adjacent Barents Sea. The scientific papers presented are:

Paper I

Berben SMP, Husum K, Cabedo-Sanz P and Belt ST (2014) **Holocene sub-centennial evolution of Atlantic water inflow and sea ice distribution in the western Barents Sea.** *Clim. Past* 10: 181-198, doi:10.5194/cp-10-181-2014.

Paper II

Berben SMP, Husum K, Navarro-Rodriguez A, Belt ST and Aagaard-Sørensen S **Atlantic water inflow and sea ice distribution in the northern Barents Sea: A Holocene palaeoceanographic evolution.**
Submitted to Paleoceanography

Paper III

Berben SMP, Husum K and Aagaard-Sørensen S **A late Holocene multi-proxy record from the northern Norwegian margin: temperature and salinity variability.**
In prep. Intended for The Holocene

1 Introduction and objectives

Atlantic water is transported through the North Atlantic via the Fram Strait and Barents Sea into the Arctic Ocean where it interacts with sea ice, affects salinity regulation and hence, the Atlantic Meridional Overturning Circulation (AMOC) (e.g. Rudels et al., 1996; Dieckmann and Hellmer, 2008). The latter is of great importance for the global climate and plays an influential role for the relatively warm north-western European climate. Further, the inflow of Atlantic water results in an oceanic heat advection towards the Arctic and mainly defines the Arctic sea ice extent, especially within the high latitude North Atlantic and adjacent Barents Sea (Hopkins, 1991). Nonetheless, the extent of Arctic sea ice is also influenced by different processes such as atmospheric circulation variability, local wind patterns and ice import (Hopkins, 1991). The Barents Sea is considered to be the main gateway of Atlantic water inflow towards the Arctic Ocean and thus, a region characterized by a significant heat exchange between the ocean and atmosphere (Broecker, 1991; Serreze et al., 2007). Furthermore, the dramatic decline in Arctic sea ice cover throughout recent decades is most pronounced within the northern Barents Sea (e.g. Comiso et al., 2008; Screen and Simmonds, 2010) and it has been argued that a recent enhanced advection of Atlantic water inflow has contributed to a further decline in sea ice cover (e.g. Kinnard et al., 2011; Spielhagen et al., 2011; Årthun et al., 2012). Additionally, an increased loss of Arctic sea ice, related to an enhanced Arctic warming, is presumed to had a severe impact on climatic conditions far beyond the Arctic region (e.g. extreme winters in Europe) (Francis et al., 2009; Yang and Christensen, 2012). As such, both Atlantic water and sea ice cover are pivotal elements of the climate system (e.g. Hopkins, 1991; Kvingedal, 2005; Stroeve et al., 2012) with the high latitude North Atlantic, including the Barents Sea, representing a key area for which to focus investigations into ocean-sea ice-atmosphere interactions (Vinje, 2001). In order to obtain a better comprehension of the interaction between Atlantic water inflow and sea ice distribution it is crucial to determine the degree of natural variability and thus, acquire more high resolution palaeo-records of sub-surface water masses and sea ice cover (e.g. Voronina et al., 2001; Polyak et al., 2010).

Previously, climate fluctuations throughout the Holocene (ca. 11 700 – 0 cal yr BP) have been associated with North Atlantic Ocean circulation changes (e.g. Bianchi and McCave, 1999; Bond et al., 2001). In particular, proxy records have indicated several changes of sea ice distribution and surface water masses (i.e. Atlantic, Arctic and Polar water) within the high latitude North Atlantic (e.g. Bauch and Weinelt, 1997; Bond et al., 1997; Jennings et al., 2002; Sarnthein et al., 2003; Hald et al., 2007), the Svalbard margin (e.g. Slubowska et al., 2005; Rasmussen et al., 2007; Spielhagen et al., 2011; Müller et al., 2012; Werner et al., 2013) and the Barents Sea (e.g. Duplessy et al., 2001; Lubinski et al., 2001; Duplessy et al., 2005; Risebrobakken et al., 2010; Risebrobakken et al., 2011; Klitgaard Kristensen et al., 2013). A strong influence of Atlantic water related to the Holocene Thermal Maximum (HTM) has been observed throughout the early Holocene (e.g. Duplessy et al., 2001; Sarnthein et al., 2003; Husum and Hald, 2004; Slubowska et al., 2005; Hald et al., 2007; Slubowska-Woldengen et al., 2007; Risebrobakken et al., 2010). The HTM is primarily attributed to a solar insolation maximum at these latitudes, although various other factors such as land-cover feedbacks and coupled atmospheric-oceanic dynamics and in particular, the northward penetration of relatively warm Atlantic water might have contributed (e.g. Berger, 1978; Koç et al., 1993; Kaufman et al., 2004). Nevertheless, palaeo-temperature reconstructions based on alkenones (Calvo et al., 2002), diatoms (Koç and Jansen, 1994; Birks and Koç, 2002; Andersen et al., 2004) and planktic foraminifera (Andersson et al., 2003; Risebrobakken et al., 2003; Sarnthein et al., 2003) have different temporal signatures of the HTM which are attributed to the influence of regional variations, different depth habitat and/or response time of the various proxies to atmospheric changes (Moros et al., 2004). This emphasizes the important role of atmosphere-ocean interactions (Kaufman et al., 2004; Moros et al., 2004; Hald et al., 2007). After the HTM, a dominance of Arctic water and increased sea ice cover has been observed by marine records in the high latitude North Atlantic (e.g. Sarnthein et al., 2003; Hald et al., 2007), the Svalbard margin (e.g. Rasmussen et al., 2007; Müller et al., 2012; Rasmussen et al., 2012; Werner et al., 2013) and the Barents Sea (e.g. Duplessy et al., 2001; Risebrobakken et al., 2010; Klitgaard Kristensen et al., 2013). This period characterized by cooler conditions is referred to Neoglacial cooling and is consistent with decreasing summer insolation at high latitudes (Wanner et al., 2008). Finally, during the late Holocene, marine records have indicated a reduced influence of Atlantic water inflow, the dominant presence of cold Arctic water and cooler conditions (e.g. Slubowska et al., 2005; Hald et al., 2007; Skirbekk et al., 2010). This general cooling trend has been ascribed to reduced insolation at high latitudes (e.g. Kaufman et al., 2009) and has also been recorded by

several terrestrial records such as ice core records from Greenland and Svalbard (e.g. Dahl-Jensen et al., 1998; Divine et al., 2011) and lake and tree records from north-western Europe (e.g. Bjune et al., 2009; Kaufman et al., 2009). Contradictory, marine records also showed evidence of a strengthened inflow of Atlantic water at the Vøring plateau (Andersson et al., 2003; Risebrobakken et al., 2003; Andersson et al., 2010), at the Svalbard margin (Slubowska-Woldengen et al., 2007; Jernas et al., 2013; Werner et al., 2013; Zamelczyk et al., 2013) and in the Barents Sea (Duplessy et al., 2001; Lubinski et al., 2001). Additionally throughout the late Holocene, observations of fluctuating climatic conditions attributed to different causes such as solar forcing, volcanic eruptions (e.g. Bryson and Goodman, 1980; Lean, 2002; Jiang et al., 2005; Wanner et al., 2008) or the North Atlantic Oscillation (NAO) have been found in the Nordic Seas (e.g. Giraudeau et al., 2004; Goosse and Holland, 2005; Nyland et al., 2006; Rousse et al., 2006; Solignac et al., 2006; Slubowska-Woldengen et al., 2007; Semenov et al., 2009) and in north-western Europe (e.g. Lauritzen and Lundberg, 1999; Bjune and Birks, 2008).

These Holocene observations highlight the importance of atmospheric changes as they influence the strength of the surface water masses, the AMOC and hence, Earth's global heat distribution. Nonetheless, the natural variations of Atlantic water inflow and sea ice distribution, including the precise nature and driving forces behind them, are not well constrained. Therefore, the overarching main objective of this thesis is to investigate the natural variability of Atlantic water inflow and sea ice distribution throughout the Holocene by reconstructing a series of new high resolution multi-proxy records of sub-surface water mass properties (i.e. temperature and salinity) and sea ice distribution. In order to obtain a better understanding of potential driving mechanisms, additional focus is placed on: a) the Holocene palaeoceanographic evolution in the western and northern Barents Sea; b) the interaction between surface water masses and sea ice extent; and c) the interplay between Atlantic and Coastal water during the fluctuating climatic conditions of the late Holocene and the possible relationship to the North Atlantic Oscillation.

2 Present day oceanography of the study area

The North Atlantic Current (NAC) transports warm and saline Atlantic water (>2 °C, >35 ‰; Hopkins, 1991) from the south and enters the high latitude North Atlantic as two major topographically steered branches of the Norwegian Atlantic Current (NwAC) (Orvik and

Niiler, 2002) (Figure 1). The western branch enters the Norwegian Sea through the Iceland-Faroe Ridge as the Iceland-Faroe frontal jet (Perkins et al., 1998). The eastern branch passes through the Faroe-Shetland channel continuing its north-eastwards pathway along the Norwegian shelf edge (Orvik and Niiler, 2002). Subsequently, Atlantic water is brought into the Arctic Ocean by different branches of the NwAC. The NwAC continues northwards as the West Spitsbergen Current (WSC) along the western Barents Sea slope into the Fram Strait where it splits into three branches, the Return Atlantic Current (RAC), the Yermak Branch (YB) and the Svalbard Branch (SB) (Manley, 1995) (Figure 1). North of Svalbard, the SB flows as an eastwards sub-surface current beyond the Franz Victoria and St. Anna Trough and thereby influences the Barents Sea by south-westwards advected Atlantic water (Abrahamsen et al., 2006) (Figure 1). The eastern branch of the NwAC turns as the North Cape Current (NCaC) into the Barents Sea where it flows partly northwards as a submerged flow and partly eastwards parallel to the Coastal current system (Loeng, 1991) (Figure 1).

The Norwegian Coastal Current (NCC) transports fresh Coastal water (2 - 13 °C, 32 - 35 ‰; Hopkins, 1991) from the North Sea, the Baltic and the Norwegian coast northwards and parallel between the Norwegian margin and the NwAC (Figure 1). It flows into the south-western Barents Sea continuing along the Norwegian and Russian coastline (Aure and Strand, 2001). Due to the influence of freshwater runoff from the Norwegian mainland it is characterized by low salinities (Blindheim, 1987). The NCC is a density driven current mainly influenced by its salinity distribution and, due to mixing with Atlantic water, its salinity increases, whereas stratification reduces on its pathway northwards. The boundary between Coastal and Atlantic water is formed as a well-defined Coastal front with Coastal water above Atlantic water in the upper 50 to 100 m of the water column as a westwards thinning wedge (Ikeda et al., 1989).

The inflow of Atlantic water into the Arctic Ocean is balanced by the outflow of cold, less saline and ice-loaded Polar water (0 - 2 °C, 33 - 34.4 ‰; Hopkins, 1991). From the Arctic Ocean, Polar water is brought into the Atlantic Ocean by the East Greenland Current (EGC) (Rudels et al., 2005) and into the Barents Sea by the East Spitsbergen Current (ESC) and Bear Island Current (BIC) (Hopkins, 1991) (Figure 1).

Arctic water (~0.5 °C, ~34.8 ‰; Hopkins, 1991) is characterized by a reduced temperature and salinity as well as by a seasonal sea ice cover and is formed when Polar water and Atlantic water meet and mix (Hopkins, 1991). In the northern Barents Sea, Arctic water

dominates the area with progressively decreasing temperature and salinity towards the north-east.

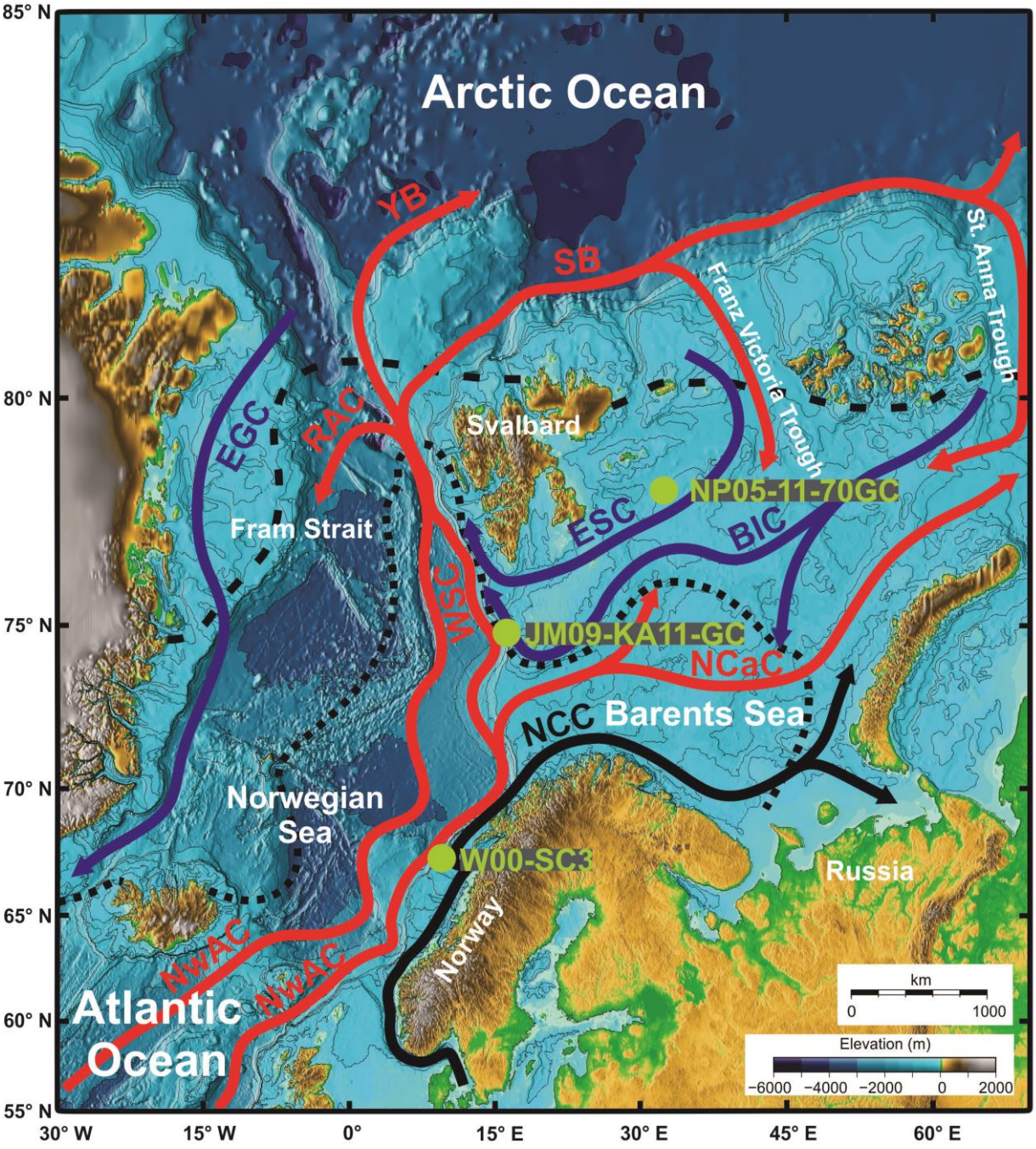

Figure 1: The present day oceanography of the study area is presented on a bathymetric map. The main surface currents and sea ice extent of the high latitude North Atlantic and Barents Sea are indicated. Summer sea ice margin (black dashed). Winter sea ice margin (black dotted). Atlantic water (red): Norwegian Atlantic Current (NwAC), West Spitsbergen Current (WSC), Return Atlantic Current (RAC), Yermak Branch (YB), Svalbard Branch (SB) and North Cape Current (NCaC). Polar water (blue): East Greenland Current (EGC), East Spitsbergen Current (ESC) and Bear Island Current (BIC). Coastal water (black): Norwegian Coastal Current (NCC). The locations of the three marine sediment cores used in this study are indicated with green circles.

One of the main oceanographic features of the Barents Sea are the Oceanic fronts which divide the different water masses by forming boundaries that are defined as a sharp climatic gradient in terms of temperature, salinity and sea ice coverage (Hopkins, 1991; Pfirman et al., 1994). The boundaries between Polar/Arctic and Arctic/Atlantic waters correspond to the Polar and Arctic front, respectively.

In the northern North Atlantic and the Barents Sea, the positions of the Polar and Arctic front are closely related to the overall extent of sea ice distribution and align with the average summer and winter sea ice margins, respectively (Vinje, 1977) (Figure 1). The north-eastern Barents Sea is dominated by Arctic water and characterized by large changes in seasonal sea ice distribution with sea ice mainly formed during fall and winter (Loeng, 1991; Vinje, 2001; Sorteberg and Kvingedal, 2006). Due to cooling and brine rejection during sea ice growth, dense and cold deep waters are formed. In addition, the extensive sea ice formation, subsequent brine rejection in winter and the seasonal melting of sea ice in the summer results in a stable and strong stratification (Wassmann et al., 2006). Contrary, in the south-western Barents Sea the inflow of relative warm Atlantic water affects the sea ice extent which results in a mainly ice-free Atlantic domain (Årthun et al., 2012). The position of the marginal ice zone (MIZ), an area characterized by high surface productivity during the summer season (Smith and Sakshaug, 1990), is strongly influenced by the interplay among the different water masses. A peak algal bloom during spring, as sea ice retreats along the ice edge, is responsible for nearly all the biological primary production in the Barents Sea (Sakshaug et al., 1992).

3 Material and methods

In this thesis, the results of multi-proxy analyses preformed on marine sediment samples are presented and discussed. Along the pathway of Atlantic water, three marine sediment cores were collected (Figure 1). At the northern Norwegian margin (Vøring plateau in front of Trænadjupet, south of the Lofoten) sediment core W00-SC3 (67.24° N, 08.31° E; 1184 m water depth) was retrieved by the SV *Geobay* in 2000 (Laberg et al., 2002) (Paper III). In 2009, sediment core JM09-KA11-GC (74.87° N, 16.48° E; 345 m water depth) was retrieved by the RV *Jan Mayen* in the western Barents Sea (Rüther et al., 2012) (Paper I). Sediment core NP05-11-70GC (78.40° N, 32.42° E; 293 m water depth) was retrieved within the northern Barents Sea, south of Kong Karls Land (Olga Basin) by the RV Lance in 2005 (Paper II).

A description of the methods applied in this PhD thesis is given below. All three papers consist of planktic foraminiferal fauna and their preservation indicators analyses, as well as stable isotope ($\delta^{18}O$, $\delta^{13}C$) measurements of *Neogloboquadrina pachyderma*. Additionally, in paper I and III, summer sub-surface temperatures (SST) were reconstructed via the application of a transfer function. In paper I and II, sea ice and phytoplankton biomarkers were analyzed, whereas in paper III geochemical and trace element analyses were performed.

3.1 Chronology

The chronologies are based on accelerator mass spectrometry (AMS) ^{14}C dates. Eight AMS ^{14}C dates performed on molluscs (Rüther et al., 2012) complemented with five AMS ^{14}C dates on benthic foraminifera were used to develop the depth-age model of JM09-KA11-GC (Paper I). To construct the depth-age model of NP05-11-70GC (Paper II) three AMS ^{14}C dates obtained from benthic foraminifera were used, whereas for W00-SC3 (Paper III) three published AMS ^{14}C dates (Laberg et al., 2002) and one additional AMS ^{14}C date on *N. pachyderma* were used. All AMS ^{14}C dates were calibrated to calendar years Before Present (cal yr BP) using the Calib 6.1.1 software (Stuiver and Reimer, 1993) and the Marine09 calibration curve (Reimer et al., 2009) for NP05-11-70GC (Paper II), and the Calib 7.0.0 software (Stuiver and Reimer, 1993) and the Marine13 calibration curve (Reimer et al., 2013) for JM09-KA11-GC (Paper I) and W00-SC3 (Paper III). For each sediment core a region-specific local reservoir age correction was applied. The calibration was constrained by a 2-σ range and the final depth-age models were developed using linear interpolation. In addition, an extrapolation was applied towards the core top for W00-SC3 (Paper III).

3.2 Planktic foraminifera

The distribution of planktic foraminifera is mainly controlled by water mass properties such as temperature, salinity, nutrition and sea ice cover (e.g. Johannessen et al., 1994; Carstens et al., 1997). The planktic foraminiferal fauna thus reflects the sea surface conditions and is therefore often used to reconstruct sea surface and sub-surface temperatures (e.g. Eynaud, 2011). Quantitative palaeo-temperature estimates can be obtained through the application of a transfer function including a modern training set (e.g. Imbrie and Kipp, 1971; Pflaumann et al., 2003; Kucera et al., 2005). Nonetheless, the composition of foraminiferal assemblages

might be modified by carbonate dissolution associated with ocean circulation and climate which can affect planktic foraminifera, in particular smaller species such as *Turborotalita quinqueloba*, *Globigerina bulloides*, *Globigerinita glutinata* and *Globigerinita uvula* (e.g. Berger, 1970; Archer and Maier-Reimer, 1994; Archer, 1996; Zamelczyk et al., 2013).

All samples were freeze-dried, wet-sieved into different size fractions (1000, 100 and 63 µm) and dried in an oven at 40 °C. Due to a low abundance of planktic foraminifera in the bottom samples (90 - 130 cm) of JM09-KA11-GC (Paper I), the planktic foraminifera and sediment in these samples were divided by heavy liquid separation using sodium polytungstate diluted with distilled water to a specific gravity of 1.8 g mL^{-1} following Knudsen (1998). From the 100 - 1000 µm size fraction, planktic foraminiferal assemblages (>300 specimens) were determined following Knudsen (1998). Although a minimum of 300 specimens was aimed for, species-specific relative abundances were calculated for samples containing more than 50 specimens in samples from JM09-KA11-GC (Paper I) and at least 25 specimens in samples from NP05-11-70GC (Paper II) following the recommendations of Forcino (2012). The identification of left and right coiling *N. pachyderma* was achieved following Darling et al. (2006) and thus, the right coiling form is identified as *Neogloboquadrina incompta* (Cifelli, 1961). In addition to the species-specific relative abundances (%), the total planktic foraminiferal concentration (#/g sediment), the total and the species-specific planktic foraminiferal flux (#/cm^2/yr) were calculated, with the latter calculated according to Ehrmann and Thiede (1985).

3.2.1 Preservation indicators

In order to quantify the state of foraminiferal preservation, the potential dissolution of foraminiferal tests was analyzed by measuring the mean shell weight (µg) of *N. pachyderma* (Broecker and Clark, 2001; Barker and Elderfield, 2002; Beer et al., 2010) and calculating the fragmentation (%) of planktic foraminiferal tests (Conan et al., 2002). The mean shell weight was obtained using a Mettler Toledo microbalance (0.1 µg sensitivity). Well-preserved (visually) and square-shaped tests of *N. pachyderma* were chosen from narrow size ranges in order to reduce problems of ontogeny and size difference induced variability (Barker et al., 2004). The fragmentation of planktic foraminiferal tests was analyzed within the 100 - 1000 µm size fraction and calculated following the method of Pufhl and Shackleton (2004).

3.2.2 Transfer function derived summer sub-surface temperature

A transfer function and the Arctic training set of Husum and Hald (2012), based on the >100 µm size fraction, were used in order to reconstruct summer (July-August-September) sub-surface temperature (SST) estimates for a water depth of 100 m. The reconstruction was carried out using the C2 version 1.7.2. software (Juggins, 2010) applying the Weighted Average-Partial Least Square (WA-PLS) and Maximum Likelihood (ML) statistical model with a leave-one-out cross validation (Ter Braak and Juggins, 1993; Telford and Birks, 2005).

3.4 Stable isotope analysis ($\delta^{18}O$, $\delta^{13}C$)

The stable oxygen and carbon isotopic compositions ($\delta^{18}O$, $\delta^{13}C$) of foraminiferal calcite tests reflect several properties of the ambient sea water masses in which they have been calcified. More specifically, $\delta^{18}O$ is controlled by temperature and salinity changes, whereas $\delta^{13}C$ is influenced by the primary production and stratification characteristics of the water mass (e.g. Spielhagen and Erlenkeuser, 1994; Katz et al., 2010).

A stable isotope analysis was carried out on the polar planktic foraminiferal tests of *N. pachyderma*. The tests were selected from narrow size fractions in order to minimize size dependent effects on isotopic composition (Aksu and Vilks, 1988; Keigwin and Boyle, 1989; Oppo and Fairbanks, 1989; Donner and Wefer, 1994; Bauch et al., 2000). All measurements were analyzed using a Finnigan MAT 253 mass spectrometer coupled to an automated Kiel device at the Geological Mass Spectrometer (GMS) Laboratory of the University of Bergen. The ice volume effect was corrected for the obtained $\delta^{18}O$ records of JM09-KA11-GC (Paper I) and NP05-11-70GC (Paper II) according to Fairbanks (1989). These records were not corrected for their species-specific vital effect as published offsets of *N. pachyderma* are often inconsistent (e.g. Kohfeld et al., 1996; Bauch et al., 1997; Stangeew, 2001; Simstich et al., 2003). However, to the $\delta^{18}O$ results from W00-SC3 (Paper III) a vital effect of 0.6 ‰ was applied based on previous suggestions for the Nordic Seas (Simstich et al., 2003) and Norwegian Sea (Nyland et al., 2006).

3.5 Biomarker analysis

The sea ice biomarker IP_{25} is produced specifically by Arctic sea ice diatoms and remains relatively stable in marine sediments (Brown et al., 2011; Belt and Müller, 2013; Stein and Fahl, 2013; Brown et al., 2014). Previous studies indicated that sedimentary IP_{25} concentrations have been consistent with known sea ice trends and thus, provide a tool to reconstruct palaeo sea ice conditions (Belt and Müller, 2013 and references therein). In addition, an integrated analysis of IP_{25} with other phytoplankton lipids such as brassicasterol has been used to distinguish between either open water conditions or perennial ice cover (Müller et al., 2009; Müller et al., 2011; Belt and Müller, 2013).

Samples were freeze-dried and stored at -20 °C prior to the biomarker analysis being performed. The previously described general methodology for biomarker analysis (IP_{25} and sterols) was applied with some modifications (Belt et al., 2012; Brown and Belt, 2012). In order to permit quantification of the biomarkers using gas chromatography-mass spectrometry (GC-MS), three internal standards were added (Belt et al., 2012). A total organic extract (TOE) was obtained following previous descriptions (Belt et al., 2012; Brown and Belt, 2012). The presence of elemental sulfur that interfered with the subsequent chromatographic analyses was removed from the TOE prior fractionation into individual lipids. Subsequently, all individual fractions were analyzed using GC-MS with operating conditions according to Belt et al. (2012). The identification of individual lipids was done on the basis of their characteristic GC retention indices and mass spectra obtained from standards in total ion current chromatogram (TIC). The lipids were quantified by comparison of peak area integrations of selected ions with those of the internal standard in selected ion monitoring (SIM) mode, and subsequently normalized according to instrumental response factors and sediment masses (and total organic carbon content) (Brown et al., 2011; Belt et al., 2012). These ratios were also converted to biomarker fluxes ($\mu g/cm^2/yr$) (Belt et al., 2012). Concentrations of IP_{25} and brassicasterol from NP05-11-70GC (Paper II) were further combined to derive the so-called P_BIP_{25} index that has the potential to provide semi-quantitative estimates of sea ice cover (Müller et al., 2011).

3.6 Geochemical analysis

The weight percentages (wt. %) of total carbon (TC) and total organic carbon (TOC) were analyzed using a LECO SC-444 (ES-2) at the Laboratory of the Geological Survey of Norway (NGU). The calcium carbonate content ($CaCO_3$) was calculated using the equation of Espitalié et al. (1977) (Equation 1).

$$CaCO_3 = (TC - TOC) * 8.33 \quad \text{[Equation 1]}$$

3.7 Trace element analysis

The incorporation of Mg into planktic foraminiferal calcite is mainly controlled by the ambient sea water temperature (e.g. Nürnberg, 1995). The positive correlation between foraminiferal Mg/Ca ratios and sea water temperature allows for the reconstruction of sub-surface temperature (SST) estimates (e.g. Mashiotta et al., 1999; Elderfield and Ganssen, 2000; Kozdon et al., 2009). Additionally, a combined analysis of Mg/Ca and $\delta^{18}O$ measurements of planktic foraminiferal tests enables the reconstruction of sub-surface salinity (SSS) estimates by using a modern $\delta^{18}O_{seawater}$:salinity relationship (e.g. Thornalley et al., 2009; Elderfield et al., 2010).

Trace element analysis was performed on well-preserved (visually) specimens of *N. pachyderma*. The tests were selected from a narrow size fraction (150 - 250 µm) in order to reduce the possible size-dependent bias on the Mg/Ca measurements (Elderfield et al., 2002). A chemical cleaning procedure, including a reduction step to remove metal oxides and an oxidation step to remove any organic matter, was carried out (e.g. Boyle and Keigwin, 1985). The samples were then analyzed by ICP-MS method for foraminiferal analysis, including simultaneous measurements of Mg, Mn, Al, and Fe, on a Finnigan Element2 at the Marine Science Institute, UC Santa Barbara. In order to identify post cleaning sample contamination which potentially biased the measured Mg/Ca ratios in foraminiferal calcite, tracers of contaminating phases (Fe, Al and Mn) were investigated (Barker et al., 2003).

3.7.1 Sub-surface temperature and salinity

The species-specific temperature:Mg/Ca equation of Kozdon et al. (2009) was used to reconstruct Mg/Ca derived SST estimates. This equation assumes a linear temperature function for the narrow temperature range occupied by *N. pachyderma* which is appropriate for reconstructed temperatures above ca. 2.5 °C. For water masses below 2.5 °C associated with salinities less than 34.5 ‰ the method loses its precision (Kozdon et al., 2009).

SSS estimates were reconstructed based on the $\delta^{18}O$ measurements of *N. pachyderma* ($\delta^{18}O_c$) and the calculated Mg/Ca derived SST ($T_{Mg/Ca}$) estimates. The temperature:$\delta^{18}O$ equation of Shackleton (1974) modified after O'Neil et al. (1969) and an equation to convert $\delta^{18}O_w$ from VPDB to VSMOW values (Hut, 1987) were rearranged in order to calculate the oxygen isotope ratios of the ambient seawater ($\delta^{18}O_w$) VSMOW. This result in the following equation previously presented by Nyland et al. (2006) (Equation 2).

$$\delta^{18}O_w = \delta^{18}O_c + 0.27 - \left[\frac{4.38 - \sqrt{4.38^2 - 0.4 * (16.9 - T_{Mg/Ca})}}{0.2}\right] \quad \text{[Equation 2]}$$

Subsequently, the salinity (S) to $\delta^{18}O_w$ relation for the central and eastern Nordic Seas by Simstich et al. (2003) (Equation 3) was applied to reconstruct palaeo SSS estimates.

$$\delta^{18}O_w = -12.17 + 0.36 * S \quad \text{[Equation 3]}$$

4 Summary of papers

Paper I

Berben SMP, Husum K, Cabedo-Sanz P and Belt ST (2014) **Holocene sub-centennial evolution of Atlantic water inflow and sea ice distribution in the western Barents Sea.** *Clim. Past* 10: 181-198, doi:10.5194/cp-10-181-2014.

The NAC brings warm and saline Atlantic water into the Arctic Ocean. This inflow is balanced by the outflow of cold Polar water and by the formation of deep water to the south, which is part of the AMOC. Changes of the AMOC can greatly affect the global ocean circulation and climate, especially in the high-latitude North Atlantic and adjacent Barents Sea where the inflow of warm water, heat exchange and its effect on sea ice formation is

essential for the environment and society. It is suggested that the recent decline in Arctic sea ice might have been partly caused by an enhanced advection of Atlantic water into the Arctic Ocean (Kinnard et al., 2011; Spielhagen et al., 2011). To fully understand the nature and driving forces of Atlantic water inflow and its interaction with sea ice, it is crucial to establish the natural range of oceanographic fluctuations within this area.

In this study, a continuous high resolution record from the Kveithola Through, western Barents Sea, is investigated in order to elucidate the Holocene variability of Atlantic water inflow and sea ice distribution. Palaeo SST estimates and temporal changes in sea ice cover are reconstructed by analyzing planktic foraminiferal fauna and their preservation indicators, planktic foraminiferal stable isotopes ($\delta^{18}O$, $\delta^{13}C$) and biomarkers (including IP_{25}).

The resulting multi-proxy data indicates the following palaeoceanographic changes. A dominance of the polar species *N. pachyderma* and low SST values (ca. 4 °C) indicate the existence of cold water and a reduced Atlantic water inflow during the early Holocene (ca. 11 900 – 10 400 cal yr BP). Additionally, the biomarker data argues for a transition from severe sea ice conditions to a marginal ice zone scenario. From ca. 10 900 to 10 700 cal yr BP, the planktic fauna and stable isotope data record a clear cooling event correlating to the Preborial Oscillation. The early-mid Holocene (ca. 10 400 – 7300 cal yr BP) is characterized by an increased influence of Atlantic water. This is indicated by the dominance of *T. quinqueloba*, increased $\delta^{18}O$ values indicative of increased salinity and SST values up to 6 °C. Further, the biomarker data argues for a decline in seasonal sea ice cover. Throughout the mid-late Holocene (ca. 7300 – 1100 cal yr BP) stable conditions with a pronounced influence of Atlantic water are reflected by high abundances of *T. quinqueloba* and relatively warm SST values (ca. 5.9 °C), whereas biomarker data indicates predominantly ice-free conditions at the study site. After ca. 1100 cal yr BP, a higher abundance of *G. uvula* argues for a reduced salinity, whereas biomarker concentrations reflect the reappearance of low-frequency seasonal sea ice. The late Holocene (ca. 1100 – 0 cal yr BP) is further characterized by more unstable conditions as indicated by the rapidly fluctuating proxy records.

Paper II

Berben SMP, Husum K, Navarro-Rodriguez A, Belt ST and Aagaard-Sørensen S **Atlantic water inflow and sea ice distribution in the northern Barents Sea: A Holocene palaeoceanographic evolution.**
Submitted to Paleoceanography

Previous research suggested that the observed Arctic sea ice decline during recent decades might be partly attributed to an enhanced advection of Atlantic water into the Arctic Ocean (Årthun et al., 2012). An increasing loss of sea ice will result in an enhanced Arctic warming and eventually, lead to severe consequences for the climate system. It is thus important to understand the interaction between sea ice and Atlantic water. In the northern Barents Sea, the oceanic fronts dividing different water masses are closely related to the overall extent of sea ice distribution, in particular the average winter and summer sea ice margins.

Therefore, the purpose of this study is to investigate the Holocene natural variability and interaction between Atlantic water inflow and sea ice distribution. This is achieved by multi-proxy analyses performed on a marine sediment core from the Olga Basin, northern Barents Sea. The analyses include planktic foraminiferal fauna and their preservation indicators, planktic foraminiferal stable isotopes ($\delta^{18}O$, $\delta^{13}C$), in addition to sea ice biomarkers (including the P_BIP_{25} index; Müller et al., 2011). The reconstructed sub-centennial record illustrates that the area experienced gradual but distinct changes in seasonal sea ice cover and Atlantic water inflow. Based on these results, different oceanographic scenarios emphasizing the interaction between surface water masses and sea ice distribution are proposed.

The results suggest overall warm subpolar conditions characterized by short spring and long productive summers throughout the early Holocene (ca. 9500 – 5800 cal yr BP). Additionally, the proxy records argue for a strong influence of Atlantic water which contributed to a reduced sea ice extent via an active ocean feedback mechanism. A proxy-specific response is indicated by the different recording times of the Holocene Thermal Optimum between ca. 9300 and 5800 cal yr BP. Throughout the mid Holocene (ca. 5800 – 2200 cal yr BP) an overall cooling trend characterized by cold Arctic water, well-ventilated water masses and an advanced seasonal sea ice cover is indicated. These observations are consistent with the lowered summer insolation likely affecting the sea ice production which resulted in a more southwards position of the sea ice edge. During the late Holocene (ca. 2200 – 0 cal yr BP), the proxy data indicates more unstable palaeoceanographic conditions most likely associated with

a more pronounced positive NAO-mode. In addition, both a sub-surface warming linked to the increased inflow of Atlantic water and an extended sea ice cover attributed to decreasing insolation are recorded. This argues for a decoupling between ocean and atmosphere which result in a long spring and short summer season causing the most extended sea ice cover recorded in this study.

Paper III

Berben SMP, Husum K and Aagaard-Sørensen S **A late Holocene multi-proxy record from the northern Norwegian margin: temperature and salinity variability.**
In prep. Intended for The Holocene

The late Holocene is characterized by fluctuating climatic conditions in the Nordic Seas (e.g. Nyland et al., 2006) and north-western Europe (e.g. Lauritzen and Lundberg, 1999; Bjune and Birks, 2008) including the 'Roman Warm Period' (RWP, ca. BCE 50 – CE 400), the 'Dark Ages' (DA, ca. CE 400 – 800), the 'Medieval Warm Period' (MWP, CE 900 – 1500) and the 'Little Ice Age' (LIA, ca. CE 1500 – 1900) (e.g. Lamb, 1977). Previously, shifting NAO conditions have been referred to as a possible forcing mechanism for the observed fluctuating climatic conditions (e.g. Trouet et al., 2009; Olsen et al., 2012). Positive and negative NAO modes affect the westerlies and thereby, the strength of Atlantic water inflow and Coastal water influence along the Norwegian margin (e.g. Sætre, 2007; Hurrell et al., 2013). As it strongly influences north-western Europe climatic conditions, it is of importance to understand the natural variability of Atlantic water inflow in the Nordic Seas.

Therefore, in order to investigate the fluctuating interplay of Atlantic and Coastal water possibly linked to a variable NAO, palaeo SST and SSS estimates are reconstructed throughout the late Holocene. This is achieved by analyses of planktic foraminiferal fauna, preservation indicators, stable isotopes ($\delta^{18}O$, $\delta^{13}C$) and paired Mg/Ca and $\delta^{18}O$ measurements of *N. pachyderma* performed on a marine sediment core from the northern Norwegian margin.

The two independently reconstructed SST-records (i.e. $SST_{Mg/Ca}$ and $SST_{Transfer}$) reveal a discrepancy between their values which is attributed to a combination of several factors. In particular, the low Mg/Ca ratios are primarily caused by the overall poor preservation conditions linked to the continental margin. This resulted in most likely underestimated

$SST_{Mg/Ca}$ and SSS values. Nonetheless, the $SST_{Transfer}$ record corresponds well to modern sea temperatures within the upper 300 m of the water column.

The presented high-resolution multi-proxy data indicates some fluctuating influences of Atlantic and Coastal water at the core site. Period I (ca. 3500 – 2900 cal yr BP) is influenced by relatively cool (ca. 6.9 °C, $SST_{Transfer}$) Coastal water and an enhanced stratification attributed to a dominating negative NAO-like mode. Warmer (ca. 7.3 °C, $SST_{Transfer}$) Atlantic water associated with more favorable preservation and positive NAO conditions dominates throughout Period II (ca. 2900 – 1600 cal yr BP). The RWP might be reflected by the last part of Period II. During period III (ca. 1600 – 950 cal yr BP), the core site experiences stable and relatively cool (ca. 6.6 °C, $SST_{Transfer}$) conditions attributed to an increased influence of Coastal water. This correlates with the colder and dryer DA. A stronger influence of Atlantic water is observed during Period IV (ca. 950 – 550 cal yr BP) and attributed to prevailing positive NAO conditions correlating with the MWP. However, due to the overall late Holocene cooling, Atlantic water was less warm (ca. 6.3 °C, $SST_{Transfer}$) compared to Period II.

5 Synthesis

This study represents multi-proxy high resolution reconstructions of water mass properties of the high latitude North Atlantic and adjacent Barents Sea. They reflect the natural variability of Atlantic water inflow and sea ice distribution over the Holocene. To elucidate the Holocene palaeoceanographic evolution and obtain an improved understanding of driving factors, the interaction between sub-surface water masses, mutually, and sea ice distribution was investigated.

The results illustrate the natural oceanic variability in the Norwegian and Barents Seas, in particular along the pathway of Atlantic water. Additionally, potential forcing mechanisms and aspects of ocean-sea ice-atmosphere dynamics, as part of the climate system, are suggested. Furthermore, using multi-proxy data from the same horizons highlighted the importance of a full comprehension of proxy behaviour as they each have their proxy-specific response to environmental and/or climatic changes. With respect to the analyses of planktic foraminifera, the assessment of preservation conditions has proven to be important for the interpretation of planktic foraminiferal proxy data. In particular, as calcite dissolution affects

both faunal assemblages and Mg/Ca ratios of *N. pachyderma*, the palaeo SST estimates might show over or under-estimated values. Finally, the main conclusions of this study are presented below.

The earliest timing of the Holocene (ca. 11 900 – 10 400 cal yr BP) is in the western Barents Sea characterized by a transition from severe sea ice to marginal ice zone conditions and a dominance of cold Arctic water. Both the western and northern Barents Sea experienced overall warm sub-polar conditions including a pronounced influence of Atlantic water and a decline in seasonal sea ice cover during the early Holocene (ca. 10 400 – 7300 and ca. 9500 – 5800 cal yr BP respectively). These palaeoceanographic conditions are attributed primarily to the high summer insolation at these latitudes. Throughout the mid Holocene, contradictory environmental conditions reconstructed for the western and northern Barents Sea indicate the regional different responses to climatic forcing mechanisms. Whereas the northern Barents Sea was characterized by cold Arctic water and an advanced seasonal sea ice extent between ca. 5800 and 2200 cal yr BP, the western Barents Sea was influenced by relatively warm, high saline Atlantic water and predominantly ice-free conditions between ca. 7300 and 1100 cal yr BP. The overall cooling trend associated with the Neoglacial cooling and attributed to the lowered insolation observed in the northern Barents Sea does not seem to affect the western Barents Sea similarly. Eventually, all studies show that the late Holocene experiences an overall period of unstable oceanographic conditions along the pathway of Atlantic water.

Throughout the late Holocene (ca. 2200 – 0 cal yr BP), the northern Barents Sea experienced an enhanced influence of Atlantic water and a seasonal sea ice cover that experienced its greatest extent at any point within the record. Superimposed on this trend, elevated levels of Atlantic water inflow and seasonal sea ice cover were recorded. In the western Barents Sea, a minor cooling trend and the reappearance of low-frequency seasonal sea ice was indicated in addition to rapidly fluctuating oceanographic conditions between ca. 1100 and 0 cal yr BP. The observed fluctuating conditions throughout the late Holocene were investigated in more detail at the northern Norwegian margin. These results show an overall cooling trend throughout the late Holocene (ca. 3500 – 550 cal yr BP) which consist of alternating oceanographic conditions between a dominant influence of Atlantic versus Coastal water. Further, these periods correspond to a dominating positive versus negative NAO mode respectively, with the exception of period III. Seemingly contradictory is the overall cooling trend observed at the northern Norwegian margin and in the western Barents sea versus the well-pronounced increased influence of Atlantic water observed in the northern Barents Sea.

This might be explained by overall more positive NAO conditions resulting in a stronger inflow of Atlantic water northwards but not necessarily in warmer Atlantic water temperatures. The recorded cooler temperatures of Atlantic water are most likely due to a lowered summer insolation.

The investigation of integrated sub-surface water mass and sea ice records suggest that the interaction between Atlantic water and sea ice depends on additionally interfering factors such as insolation and the NAO. In particular for the northern Barents Sea, high insolation throughout the early Holocene resulted in a reduced sea ice cover allowing for a strong heat flux between ocean and atmosphere. This led to an active ocean feedback mechanism that additionally contributed to the decline in sea ice extent. Contrary, throughout the late Holocene, a reduced insolation caused the overall increased sea ice cover that co-existed with an increased influence of Atlantic water. A decoupling between ocean and atmosphere, with the sea ice acting as a barrier between the two, might have prohibited a strong heat flux which resulted in the observed simultaneous sub-surface warming and sea surface cooling. Hereby, the palaeo-records illustrate the complexity of the interacting elements of the climate system leading to different possible natural scenarios of the environmental conditions.

6 Future research

The reconstructed Holocene palaeoceanographic evolution has shown natural fluctuations of Atlantic water inflow and sea ice distribution. Although these results provided new insights, it also highlighted certain issues that deserve more attention in the future.

In this PhD-study, the planktic foraminiferal fauna was analyzed in order to investigate palaeo water mass properties. In particular, the faunal assemblages were used to quantify sub-surface water temperatures via the application of a transfer function. However, the planktic foraminiferal fauna is known to be also influenced by other properties besides temperature (e.g. Johannessen et al., 1994; Carstens et al., 1997). For instance, *T. quinqueloba* has been associated with warm Atlantic water, but is also found nearby the sea ice margin and thus associated with oceanic front conditions (e.g. Volkmann, 2000). With regard to this species, it has been pointed out in this PhD-study that the available nutrients might have played an important role, especially in the Arctic region with the proximity of the sea ice edge and its associated high primary production. Therefore, the resulting transfer function derived SST

record (Paper I) possibly contains overestimated SST values. And thus, a more detailed investigation on the preference of high food supply, and consequent incorporation of this knowledge into a modern database, would be appropriated and strengthen transfer function derived SST estimates. This could also lead to a better interpretation of the past influence of Atlantic water whereby a change in strength and temperature are not necessarily occuring at the same time.

Additionally, transfer function derived SST estimates can be biased due to selective dissolution which might alter the species composition of foraminiferal assemblages (e.g. Zamelczyk et al., 2013). In particular, planktic foraminiferal species such as *T. quinqueloba*, *G. bulloides*, *G. glutinata* and *G. uvula* are more sensitive to carbonate dissolution than others such as *N. pachyderma* and *N. incompta* (e.g. Berger, 1970; Archer and Maier-Reimer, 1994; Archer, 1996). Furthermore, calcite dissolution might also be responsible for the removal of Mg-rich parts in foraminiferal tests and thus bias the Mg/Ca ratios (Brown and Elderfield, 1996; Rosenthal et al., 2000; Johnstone et al., 2011). It has been indicated that, beside the calcification temperature, the Mg-uptake is also controlled by environmental factors such as the carbonate ion concentration (Hendry et al., 2009). In this PhD study, preservation indicators such as mean shell weight, planktic foraminiferal fragmentation and sedimentary $CaCO_3$ were analyzed in order to obtain an overview of the preservation conditions. However, these parameters do not identify the responsible factors of dissolution and their connection to environmental conditions. Therefore, a more detailed study of calcite dissolution, its causes and effects is necessary to limit biased palaeo-temperature estimates. For example, an investigation of the B/Ca ratio of foraminiferal calcite, a proxy for past seawater carbonate ion concentration, could contribute to a better understanding of the calcium carbonate preservation state (e.g. Yu and Elderfield, 2007).

To fully examine the dynamics of the density driven AMOC and its involvement in climate changes, it is important to obtain both palaeo SST and SSS estimates (e.g. Thornalley et al., 2009) and thus, a further investigation in order to improve the potential of the Mg/Ca proxy should be carried out. In addition, assuming a future establishment of the species-specific calcification depth, paired Mg/Ca and $\delta^{18}O$ measurements of different species might further deliver SST and SSS data for different water depths. Thereby, it would provide a better understanding of the vertical stratification of the water column.

The biomarker analysis has shown the potential to reconstruct high resolution palaeo seasonal sea ice distribution in the Arctic. Recently, Brown et al. (2014) identified the source of the sea ice biomarker IP_{25}. Nevertheless, to clarify the interpretation of IP_{25} and brassicasterol, the production regulating factors of these biomarkers, in addition to a better knowledge on the source and specificity of brassicasterol, should be better identified (Belt and Müller, 2013). This should be investigated by collecting sea ice and phytoplankton samples from different areas which then contribute to an improved P_BIP_{25} index (potentially region-specific) and thus, a more quantitative assessment of seasonal sea ice cover. In addition, several related biomarkers such as Diene II and Triene could provide additional oceanographic information. Therefore, these biomarkers should be assessed in order to determine their source origin and palaeoenvironmental significance as well as degradation in marine sediments throughout time.

In this PhD study, it was indicated that proxies have their specific responses to oceanographic changes and reflect different elements of the climate system. This led to a better understanding of responsible mechanisms behind the natural variability of Atlantic water inflow and sea ice extent. In order to obtain a better overview of palaeo-environmental conditions, it is important to further identify proxy-specific responses.

Finally, new multi-proxy records along the pathway of Atlantic water (similar to the ones presented here) would strongly contribute to a better spatial interpretation of the sea ice extent and Atlantic water inflow interaction. In addition, similar multi-proxy studies from a broader area in the Arctic Ocean, including the Polar water outflow pathways, might lead to an advanced understanding of sea ice-ocean changes in general and a better constrain of the spatial and temporal variability.

7 References

Abrahamsen E, Østerhus S and Gammelsrød T (2006) Ice draft and current measurements from the north-western Barents Sea, 1993-96. *Polar Res.* 25: 25-37.

Aksu AE and Vilks G (1988) Stable isotopes in planktonic and benthic foraminifera from Arctic Ocean surface sediments. *Can. J. Earth Sci.* 25: 701-709.

Andersen C, Koç N, Jennings AE and Andrews JT(2004) Nonuniform response of the major surface currents in the Nordic Seas to insolation forcing: implications for the Holocene climate variability. *Paleoceanography* 19: PA200310.1029/2002PA000873.

Andersson C, Risebrobakken B, Jansen E and Dahl SO (2003) Late Holocene surface ocean conditions of the Norwegian Sea (Voring Plateau). *Paleoceanography* 18: PA1044, doi: 10.1029/2001PA000654.

Andersson C, Pausata FSR, Jansen E, Risebrobakken B and Telford RJ (2010) Holocene trends in the foraminifer record from the Norwegian Sea and the North Atlantic Ocean. *Clim. Past* 6: 179-193.

Archer D (1996) A data-driven model of the global calcite lysocline. *Global Biogeochem. Cy.* 10: 511-526.

Archer D and Maier-Reimer E (1994) Effect of deep-sea sedimentary calcite preservation on atmospheric CO_2 concentration. *Nature* 367: 260-263.

Årthun MT, Eldevik LH, Smedsrud Ø, Skagseth R and Ingvaldsen R (2012) Quantifying the influence of Atlantic heat on Barents Sea ice variability and retreat. *J. Clim.* 25: 4736-4743.

Aure J and Strand Ø (2001) Hydrographic normals and long-term variations at fixed surface layer stations along the Norwegian coast from 1936 to 2000. *Fisken og Havet* 13: 1-24.

Barker S and Elderfield H (2002) Foraminiferal calcification response to glacial interglacial changes in atmospheric CO_2. *Science* 297: 883-836.

Barker S, Greaves M and Elderfield H (2003) A study of cleaning procedures used for foraminiferal Mg/Ca paleothermometry. *Geochem. Geophys. Geosyst.* 4(9): 8407, doi:10.1029/2003GC000559.

Barker S, Kiefer T and Elderfield H (2004) Temporal changes in North Atlantic circulation constrained by planktonic foraminiferal shell weights. *Paleoceanography* 19: PA3008.

Bauch HA and Weinelt MS (1997) Surface water changes in the Norwegian Sea during last deglacial and Holocene times. *Quaternary Sci. Rev.* 16: 1115-1124.

Bauch D, Carstens J, Wefer G and Thiede J (2000) The imprint of anthropogenic CO_2 in the Arctic Ocean: evidence from planktic $d^{13}C$ data from water column and sediment surfaces. *Deep-Sea Res. Pt. II* 9(11): 1791–1808.

Beer C J, Schiebel R and Wilson PA (2010) Testing planktic foraminiferal shell weight as a surface water [CO_3^{2-}] proxy using plankton net samples. *Geology* 38: 103-106.

Belt ST and Müller J (2013) The Arctic sea ice biomarker IP_{25}: a review of current understanding, recommendations for future research and applications in palaeo sea ice reconstructions. *Quaternary Sci. Rev. Doi: 10.1016/j.quascirev.2012.12.001.*

Belt ST, Brown TA, Navarro Rodriguez A, Cabedo Sanz P, Tonkin A and Ingle R (2012) A reproducible method for the extraction, identification and quantification of the Arctic sea ice proxy IP_{25} from marine sediments. *Anal. Method.* 4: 705-713.

Berger A (1978) Long-term variations of daily insolation and quaternary climatic changes. *J. Atmos. Sci.* 35: 2363-2367.

Berger WH (1970) Planktonic foraminifera: Selective solution and the lysocline. *Mar. Geol.* 8: 111-138.

Bianchi GG and McCave IN (1999) Holocene periodicity in North Atlantic climate and deep-ocean flow south of Iceland. *Nature* 297: 515-517.

Birks CJA and Koç N (2002) A high-resolution diatom record of late-quaternary sea-surface temperatures and oceanographic conditions from the eastern Norwegian Sea. *Boreas* 31: 323-344.

Bjune AE and Birks HJB (2008) Holocene vegetation dynamics and inferred climate changes at Svanåvatnet, Mo i Rana, northern Norway. *Boreas* 37: 146-156.

Bjune AE, Seppä H and Birks HJB (2009) Quantitative summer temperature reconstructions for the last 2000 years based on pollen-stratigraphical data from northern Fennoscandia. *J. Paleolimnol.* 41: 43-56.

Blindheim J (1987) The seas of Norden. In: Varjo U and Tietze W (eds) *Norden: Man and environment*. Gebrüder Borntraeger, Berlin, 20-32.

Bond G, Showers W, Cheseby M, Lotti R, Almasi P, deMenocal P, Priore P, Cullen H, Hajdas I and Bonani G (1997) A pervasive millennial-scale cycle in North Atlantic Holocene and glacial climates. *Science* 278: 1257-1266.

Bond G, Kromer B, Beer J, Muscheler R, Evans MN, Showers W, Hoffmann S, Lotti-Bond R, Hajdas I and Bonani G (2001) Persistent solar influence on north Atlantic climate during the Holocene. *Science* 294: 2130-2136.

Boyle EA and Keigwin LD (1985) Comparison of Atlantic and Pacific paleochemical records for the last 215,000 years: Changes in deep ocean circulation and chemical inventories. *Earth Planet. Sci. Lett.* 76: 135-150.

Broecker WS (1991) The great ocean conveyor. *Oceanography* 4: 79-89.

Broecker WS and Clark E (2001) An evaluation of Lohmann's foraminifera weight dissolution index. *Paleoceanography* 16: 531-534.

Brown SJ and Elderfield H (1996) Variations in Mg/Ca and Sr/Ca ratios of planktonic foraminifera caused by post depositional dissolution: Evidence of shallow Mg-dependent dissolution. *Paleoceanography* 11(5): 543-551.

Brown TA and Belt ST (2012) Identification of the sea ice diatom biomarker IP_{25} in Arctic benthic macrofauna: Direct evidence for a sea ice diatom diet in Arctic heterotrophs. *Polar Biol.* 35: 131-137.

Brown TA, Belt ST, Philippe B, Mundy CJ, Massé G, Poulin M and Gosselin M (2011) Temporal and vertical variations of lipid biomarkers during a bottom ice diatom bloom in the Canadian Beaufort Sea: Further evidence for the use of the IP_{25} biomarker as a proxy for spring Arctic sea ice. *Polar Biol.* 34: 1857-1868.

Brown TA, Belt ST, Tatarek A and Mundy CJ (2014) Source identification of the Arctic sea ice proxy IP_{25}. *Nat. Commun.* 5:4197 doi: 10.1038/ncomms5197.

Bryson RA and Goodman BM (1980) Volcanic activity and climate change. *Science* 207: 1041-1044.

Calvo E, Grimalt J and Jansen E (2002) High resolution U_K^{37} sea surface temperature reconstruction in the Norwegian Sea during the Holocene. *Quaternary Sci. Rev.* 21: 1385-1394.

Carstens J, Hebbeln D and Wefer G (1997) Distribution of planktic foraminifera at the ice margin in the Arctic (Fram Strait). *Mar. Micropaleontol.* 29: 257-269.

Cifelli R (1961) Globigerina incompta, a new species of pelagic foraminifera from the North Atlantic. *Contributions Cushman Foundation Foraminiferal Research* 12: 83-86

Comiso JC, Parkinson CL, Gersten R and Stock L (2008) Accelerated decline in the Arctic sea ice cover. *Geophys. Res. Lett.* 35: L01703, doi:10.1029/2007GL031972.

Conan SMH, Ivanova EM and Brummer GJA (2002) Quantifying carbonate dissolution and calibration of foraminiferal dissolution indices in the Somali Basin. *Mar. Geol.* 182: 325-349.

Dahl-Jensen DK Moesgaard, Gundestrup N, Clow GD, Johnsen SJ, Hansen AW and Balling N (1998) Past temperatures directly from the Greenland Ice Sheet. *Science* 282: 268-271.

Darling KF, Kucera M, Kroon D and Wade CM (2006) A resolution for the coiling direction paradox in Neogloboquadrina pachyderma. *Paleoceanography* 21: PA2011, doi:10-1029/2005PA001189.

Dieckmann GS and Hellmer HH (2008) The importance of sea ice: An overview. In: Thomas DN and Dieckmann GS (eds) *Sea ice: An introduction to its physics, chemistry, biology and geology* Blackwell Science Ltd, Oxford, UK, doi: 10.1002/9780470757161.ch1.

Divine D, Isaksson E, Martma, T., Meijer HAJ, Moore J, Pohjola V, van de Wal RSW and Godtliebsen F (2011) Thousand years of winter surface air temperature variations in Svalbard and northern Norway reconstructed from ice-core data. *Polar Research* 30: 7379, doi: 10.3402/polar.v30i0.7379.

Donner B and Wefer G (1994) Flux and stable isotope composition of Neogloboquadrina pachyderma and other planktonic foraminifers in the Southern Ocean (Atlantic sector). *Deep-Sea Res. Pt. I* 41: 1733-1743.

Duplessy JC, Ivanova E, Murdmaa I, Paterne M and Labeyrie L (2001) Holocene paleoceanography of the northern Barents Sea and variations of the northward heat transport by the Atlantic Ocean. *Boreas* 30: 2-16.

Duplessy JC, Cortijo E, Ivanova E, Khusid T, Labeyrie L, Levitan M, Murdmaa I and Paterne M (2005) Paleoceanography of the Barents Sea during the Holocene. *Paleoceanography* 20: A4004.

Ehrmann WU and Thiede J (1985) History of Mesozoic and Cenozoic sediment fluxes to the North Atlantic Ocean. *Contributions to Sedimentology E. Schweizerbart'sche Verlagsbuchhandlung*, Stuttgart 15: 1-109, ISBN 3-510-57015-4.

Elderfield H and Ganssen G (2000) Past temperature and d18O of surface ocean waters inferred from foraminiferal Mg/Ca ratios. *Nature* 405: 442-445, doi:10.1038/35013033.

Elderfield H, Vautravers M and Cooper M (2002) The relationship between shell size and Mg/Ca, Sr/Ca, δ18O, and δ13C of species of planktonic foraminifera. *Geochem. Geophys. Geosyst.* 3(8): 1-13.

Elderfield H, Greaves M, Barker, S, Hall IR, Tripati A, Ferretti P, Crowhurst S, Booth L and Daunt C (2010) A record of bottom water temperature and seawater [delta]18O for the Southern Ocean over the past 440 kyr based on Mg/Ca of benthic foraminiferal Uvigerina spp. *Quaternary Sci. Rev.* 29: 160-169.

Espitalié J, Laporte JL, Madec M, Marquis F, Leplat P, Paulet J and Boutefeu A (1977) Méthode rapide de characterisation des roches-mere, de leur potential petrolier et de leur degre d'évolution. *Revue de l'Institute Francais du Petrole* 32: 23-42.

Eynaud F (2011) Planktonic foraminifera in the Arctic: Potentials and issues regarding modern and quaternary populations. IOP Conf. Series: Earth and Environmental Science, 14.

Fairbanks RG (1989) A 17 000-year glacia-eustatic sea level record: Influence of glacial melting rates on the Younger Dryas event and deep-ocean circulation. *Nature* 342: 637-642.

Forcino FL (2012) Multivariate assessment of the required sample size for community paleoecological research. *Palaeogeogr. Palaeocl.* 315-316: 134-141.

Francis JA, Chan W, Leathers DJ, Miller JR and Veron DE (2009) Winter Northern Hemisphere weather patterns remember summer Arctic sea-ice extent. *Geophys. Res. Lett.* 36: L07503, doi:10.1029/2009GL037274.

Giraudeau J, Jennings AE and Andrews JT (2004) Timing and mechanisms of surface and intermediate water circulation changes in the Nordic seas over the last 10,000 cal years: A view from the north Iceland shelf. *Quaternary Sci. Rev.* 23: 2127-2139.

Goosse H and Holland M (2005) Mechanisms of decadal and interdecadal Arctic variability in the Community Climate System Model CCSM2. *J. Climate* 18: 3552-3570.

Hald M, Andersson C, Ebbesen H, Jansen E, Klitegaard-Kristensen D, Risebrobakken B, Salomonsen GR, Sejrup HP, Sarnthein M and Telford R (2007) Variations in temperature and extent of Atlantic water in the northern North Atlantic during the Holocene. *Quaternary Sci. Rev.* 26: 3423-3440.

Hendry KR, Rickaby REM, Meredith MP, Elderfield H (2009) Controls on stable isotope and trace metal uptake in Neogloboquadrina pachyderma (sinistral) from an Antarctic sea-ice environment. *Earth Planet. Sci. Lett.* 278: 67-77.

Hopkins TS (1991) The GIN Sea: A synthesis of its physical oceanography and literature review, 1972–1985. *Earth Sci. Rev.* 30: 175-318.

Hurrell JW, Kushnir Y, Ottersen G and Visbeck M (2013) An overview of the North Atlantic Oscillation. The North Atlantic Oscillation: Climatic significance and environmental impact. American Geophysical Union, 1-35.

Husum K and Hald M (2004) A continuous marine record 8000-1600 cal. yr BP from the Malangenfjord, north Norway: Foraminiferal and isotopic evidence. *Holocene* 14: 877-887.

Husum K and Hald M (2012) Arctic planktic foraminiferal assemblages: Implications for subsurface temperature reconstructions. *Mar. Micropaleontol.* 96-97: 38-47.

Hut G (1987) Stable isotope reference samples for geochemical and hydrological investigations. paper presented at Consultants Group Meeting, Int. At. Energy Agency, Vienna.

Ikeda M, Johannessen JA, Lygre K and Sandven S (1989) A process study of mesoscale meanders and eddies in the Norwegian Coastal Current. *J. Phys. Oceanogr.* 19: 20-35.

Imbrie J and Kipp NG (1971) A new micropaleontological method for quantitative paleoclimatology: Applications to a late Pleistocene Caribbean core. In: Turkian KK (ed) *Late Cenozoic Glacial Ages*. Yale University Press, New Haven, 71-191.

Jennings A, Knudsen KL, Hald M, Hansen CV and Andrews JT (2002) A mid-Holocene shift in Arctic sea-ice variability on the East Greenland shelf. *Holocene* 12: 49-58.

Jernas P, Klitgaard Kristensen D, Husum K, Wilson L and Koç N (2013) Palaeoenvironmental changes of the last two millennia on the western and northern Svalbard shelf. *Boreas* 42: 236-255.

Jiang H, Eiriksson J, Schulz M, Knudsen KL, Seidenkrantz MS (2005) Evidence for solar forcing of sea-surface temperature on the North Icelandic Shelf during the Late Holocene. *Geology* 33(1): 73-76.

Johannessen T, Jansen E, Flatøy A and Ravelo AC (1994) The relationship between surface water masses, oceanographic fronts and plaeoclimatic proxies in surface sediments of the Greenland, Iceland, Norwegian Seas. NATO, ASI Series, 61-86.

Johnstone HJH, Yu J, Elderfield H and Schulz M (2011) Improving temperature estimates derived from Mg/Ca of planktonic foraminifera using X-ray computed tomography-based dissolution index, XDX. *Paleoceanography* 26(1): PA1215, DOI: 10.1029/2009pa001902.

Juggins S (2010) C2 1.7.2 available at http://www.staff.ncl.ac.uk/staff/stephen.juggins/.

Katz ME, Cramer BS, Franzese A, Hönisch B, Miller KG, Rosenthal Y and Wright J (2010) Traditional and emerging geochemical proxies in foraminifera. *J. Foramin. Res.* 40(2): 165-192.

Kaufman D, Ager TA, Anderson NJ, Anderson PM, Andrews JT, Bartlein PJ, Brubakker LB, Coats LL, Cwynar LC, Duvall ML, Dyke AS, Edwards ME, Eisner WR, Gajewski K, Geirsdottir A, Hu FS, Jennings AE, Kaplan MR, Kerwin MW, Loshkin AV, MacDonald GM, Miller GH, Mock CJ, Oswald WW, Otto-Bliesner BL, Porinchu DF, Rühland K, Smol JP, Steig EJ and Wolfe BB (2004) Holocene thermal maximum in the western Arctic (0 - 180 °N). *Quaternary Sci. Rev.* 23: 529-560.

Kaufman DS, Schneider DP, McKay NP, Ammann CM, Bradley RS, Briffa KR, Miller GH, Otto-Bliesner BL, Overpeck JT, Vinther BM and Arctic Lakes 2k Project Members (2009) Recent warming reverses long-term Arctic cooling. *Science* 325: 1236-1239.

Keigwin LD and Boyle EA (1989) Late Quaternary paleochemistry of high-latitude surface waters. *Palaeogeogr. Palaeocl.* 73: 85-106.

Kinnard C, Zdanowicz CM, Fisher AF, Isaksson E, de Vernal A and Thompson LG (2011) Reconstructed changes in Arctic sea ice over the past 1,450 years. *Nature* 479: 509-512, doi:10.1038/nature10581.

Klitgaard Kristensen D, Rasmussen TL and Koç N (2013) Paleoceanographic changes in the northern Barents Sea during the last 16 000 years – new constraints on the last deglaciation of the Svalbard-Barents Ice Sheet. *Boreas* 42: 798-813.

Knudsen KL (1998) Foraminiferer i Kvartær stratigrafi: Laboratorie og fremstillingsteknik samt udvalgte eksempler. *Geologisk Tidsskrift* 3: 1-25.

Koç N and Jansen E (1994) Response of the high-latitude Northern hemisphere to orbital climate forcing: evidence from the Nordic Seas. *Geology* 22: 523-526.

Koç N, Jansen E and Haflidason H (1993) Paleoceanographic reconstructions of surface ocean conditions in the Greenland, Iceland and Norwegian seas through the last 14 ka based on diatoms. *Quaternary Sci. Rev.* 12: 115-140.

Kohfeld KE, Fairbanks RG and Smith SL (1996) *Neogloboquadrina pachyderma* (sinistral coiling) as paleoceanographic tracers in polar oceans: Evidence from northeast water polynya plankton tows, sediments traps, and surface sediments. *Paleoceanography* 11: 679-699.

Kozdon R, Eisenhauer A, Weinelt M, Meland MY and Nuernberg D (2009) Reassessing Mg/Ca temperature calibrations of Neogloboquadrina pachyderma (sinistral) using paired d44/40Ca and Mg/Ca measurements. *Geochem. Geophys. Geosyst.* 10: Q03005, doi:10.1029/2008GC002169.

Kucera M, Weinelt M, Kiefer T, Pflaumann U, Hayes A, Weinelt M, Chen MT, Mix AC, Barrows TT and Cortijo E (2005) Reconstruction of sea-surface temperatures from assemblages of planktonic foraminifera: Multi-technique approach based on geographically constrained calibration data sets and its application to glacial Atlantic and Pacific Oceans. *Quaternary Sci. Rev.* 24: 951-998.

Kvingedal B (2005) Sea-ice extent and variability in the Nordic Seas, 1967-2002. In: Drange H, Dokken T, Furevik T, Gerdes R and Berger W (eds): T*he Nordic seas: An integrated perspective*. American Geophysical Union, Geophysical Monograph, 158: 39-49.

Laberg JS, Vorren TO, Mienert J, Bryn P and Lien R (2002) The Trænadjupet slide: a large slope failure affecting the continental margin of Norway 4,000 years ago. *Geo. Mar. Lett.* 22: 19-24.

Lamb HH (1977) Climate, Present, Past and Future. Volume 2. Climatic History and the Future. Methuen & Co Ltd, London, 835.

Lauritzen SE and Lundberg J (1999) Calibration of the speleothem delta function: an absolute temperature record for the Holocene in northern Norway. *The Holocene* 9(6): 650-669.

Lean J (2002) Solar forcing of climate change in recent millennia. In: Wefer G, Berger WH, Behre KE and Jansen E (eds) *Climate development and history of the North Atlantic realm*. Berlin, Springer-Verlag, 75-88.

Loeng H (1991) Features of the physical oceanographic conditions of the Barents Sea. *Polar Res.* 10: 5-18.

Lubinski DJ, Polyak L and Forman SL (2001) Freshwater and Atlantic water inflows to the deep northern Barents and Kara seas since ca 13 ^{14}Cka: foraminifera and stable isotopes. *Quaternary Sci. Rev.* 20: 1851-1879.

Manley TO (1995) Branching of Atlantic water within the Greenland—Spitsbergen passage: an estimate of recirculation. *J. Geophys. Res.* 100: 20627-20634.

Mashiotta TA, Lea DW and Spero HJ (1999) Glacial interglacial changes in Subantarctic sea surface temperature and d18O-water using foraminiferal Mg. *Earth Planet. Sci. Lett.* 170: 417-432, doi:10.1016/S0012-821X(99)00116-8.

Moros M, Emeis K, Risebrobakken B, Snowball I, Kuijpers A, McManus J and Jansen E (2004) Sea surface temperatures and ice rafting in the Holocene North Atlantic: Climate influences on northern Europe and Greenland. *Quaternary Sci. Rev.* 23: 2113-2126.

Müller J, Massé G, Stein R and Belt ST (2009) Variability of sea-ice conditions in the Fram Strait over the past 30000 years. *Nat. Geosci.* 2(11): 772-776.

Müller J, Wagner A, Fahl K, Stein R, Prange M, and Lohman G (2011) Towards quantitative sea ice reconstructions in the northern North Atlantic: A combined biomarker and numerical modelling approach. *Earth Planet. Sci. Lett.* 306: 137-148.

Müller J, Werner K, Stein R, Fahl K, Moros M and Jansen E (2012) Holocene cooling culminates in sea ice oscillations in Fram Strait. *Quaternary Sci. Rev.* 47: 1-14.

Nürnberg D (1995) Magnesium in tests of Neogloboquadrina pachyderma sinistral from high northern and southern latitudes. *J. Foraminiferal Res.* 25(4): 350-368.

Nyland B, Jansen E, Elderfield H and Andersson C (2006) Neogloboquadrina pachyderma (dex. and sin.) Mg/Ca and d18O records from the Norwegian Sea. *Geochem. Geophys. Geosyst.* 7: Q10P17, doi:10.1029/2005GC001055.

Olsen J, Anderson NJ and Knudsen MF (2012) Variability of the North Atlantic Oscillation over the past 5200 years. *Nature Geoscience* 5: 808-812.

O'Neil JR, Clayton RN and Mayeda TK (1969) Oxygen isotope fractionation in divalent metal carbonates. *J. Chem. Phys.* 51(12): 5547-5558, doi:10.1063/1.1671982.

Oppo DW and Fairbanks RG (1989) Carbon isotope composition of tropical surface water during the past 22,000 years. *Paleoceanography* 4: 333-351.

Orvik KA and Niiler P (2002) Major pathways of Atlantic water in the northern North Atlantic and Nordic Seas toward Arctic. *Geophys. Res. Lett.* 29(19): 1896, doi:10.1029/2002GL015002.

Perkins H, Hopkins TS, Malmberg SA, Poulain PM and Warn-Varnas A (1998) Oceanographic conditions east of Iceland. *J. Geophys. Res.* 103: 21531-21542.

Pfirman SL, Bauch D and Gammelsrød T (1994) The Northern Barents Sea: water mass distribution and modification. In: Johannessen OM, Muench RD and Overland JE (eds) *The Polar Oceans and Their Role in Shaping the Global Environment.* AGU Geoph. Monog. Series., 85: 77-94.

Pflaumann U, Sarnthein M, Chapman M, d'Abreu L, Funnell B, Huels M, Kiefer T, Maslin M, Schulz H, Swallow J, van Kreveld S, Vautravers M, Vogelsang E and Weinelt M (2003) Glacial North Atlantic sea-surface conditions reconstructed by GLAMAP 2000. *Paleoceanography* 18: 22.

Polyak L, Alley RB, Andrews JT, Brigham-Grette J, Cronin TM, Darby DA, Dyke AS, Fitzpatrick JJ, Funder S, Holland M, Jennings AE, Miller GH, O´Regan M, Savelle J, Serreze M, John KS, White JWC and Wolff E (2010) History of sea ice in the Arctic. *Quaternary Sci. Rev.* 29: 1757-1778.

Pufhl HA and Shackleton NJ (2004) Two proximal, high-resolution records of foraminiferal fragmentation and their implications for changes in dissolution. *Deep-Sea Res. Pt. I* 51: 809-832.

Rasmussen TL, Thomsen E, Slubowska MA, Jessen S, Solheim A and Koç N (2007) Paleoceanographic evolution of the SW Svalbard margin (76 °N) since 20 000 ^{14}C yr BP. *Quaternary Res.* 67: 100-114.

Rasmussen TL, Forwick M and Mackensen A (2012) Reconstruction of inflow of Atlantic Water to Isfjorden, Svalbard during the Holocene: Correlation to climate and seasonality. *Mar. Micropaleontol.* 94-95: 80-90.

Reimer PJ, Baillie MGL, Bard E, Bayliss A, Beck JW, Blackwell PG, Ramsey CB, Buck CE, Burr GS, Edwards RL, Friedrich HM, Grootes PM, Guilderson TP, Hajdas I, Heaton TJ, Hogg AG, Hughen KA, Kaiser KF, Kromer B, Mccormac FG, Manning SW, Reimer RW, Richards DA, Southon JR, Talamo S, Turney CSM, Van Der Plicht J and Weyhenmeyer CE (2009) IntCal09 and Marine09 radiocarbon age calibration curves, 0-50 000 years cal BP. *Radiocarbon* 51: 1111-1150.

Reimer PJ, Bard E, Bayliss A, Beck JW, Blackwell PG, Ramsey CB, Buck CE, Cheng H, Edwards RL, Friedrich M, Grootes PM, Guilderson TP, Haflidason H, Hajdas I, Hatté C, Heaton TJ, Hoffmann DL, Hogg AG, Hughen KA, Kaiser KF, Kromer B, Manning SW, Niu M, Reimer RW, Richards DA, Scott EM, Southon JR, Staff RA, Turney CSM and van der Plicht J (2013) Intcal13 and Marine13 radiocarbon age calibration curves. *Radiocarbon* 55(4): 1869-1887.

Risebrobakken B, Jansen E, Andersson C, Mjelde E and Hevrøy K (2003) A high-resolution study of Holocene paleoclimatic and paleoceanographic changes in the Nordic Seas. *Paleoceanography* 18: doi:10.1029/2002PA000764.

Risebrobakken B, Morros M, Ivanova EV, Chistyakova N and Rosenberg R (2010) Climate and oceanographic variability in the SW Barents Sea during the Holocene. *Holocene* 20: 609-621.

Risebrobakken B, Dokken T, Smedsrud LH, Andersson C, Jansen E, Moros M and Ivanova EV (2011) Early Holocene temperature variability in the Nordic Seas: The role of oceanic heat advection versus changes in orbital forcing. *Paleoceanography* 26: PA4206.

Rosenthal Y, Lohmann GP, Lohmann KC and Sherrell RM (2000) Incorporation and preservation of Mg in *Globigerinoides sacculifer*: Implications for reconstructingthe temperature and 18O/16O of seawater. *Paleoceanography* 15(1): 135-145.

Rousse S, Kissel C, Laj C, Eiriksson J and Knudsen KL (2006) Holocene centennial to millenial-scale climatic variability: Evidence from high resolution magnetic analyses of the last 10 cal. kyr of North Iceland (core MD99-2275). *Earth Planet. Sci. Lett.* 242: 390-405.

Rudels B, Anderson LG and Jones EP (1996) Formation and evolution of the surface mixed layer and the halocline of the Arctic Ocean. *J. Geophys. Res.* 101: 8870-8821.

Rudels B, Björk G, Nilsson J, Winsor P, Lake I and Nohr C (2005) The interaction between waters from the Arctic Ocean and the Nordic Seas north of Fram Strait and along the East Greenland Current: Results from the Arctic Ocean-O2 Oden expedition. *J. Marine Syst.* 55: 1-30.

Rüther DC, Bjarnadóttir LJ, Junttila J, Husum K, Rasmussen TL, Lucchi RG and Andreassen K (2012) Pattern and timing of the northwestern Barents Sea Ice Sheet deglaciation and indications of episodic Holocene deposition. *Boreas* 10.1111/j.1502-3885.2011.00244.x. ISSN 0300-9483.

Sætre R (2007) The Norwegian coastal current. Tapir academic press, Trondheim, 89-99.

Sakshaug E, Bjørge A, Gulliksen B, Loeng H and Mehlum F (1992) Økosystem Barentshavet, Norges Allmenvitenskapelige Forskningsråd, Norges Fiskeriforskningsråd, Miljøverndepartementet, 304.

Sarnthein M, Van Kreveld S, Erlenkeuser H, Grootes PM, Kucera M, Pflaumann U and Schulz M (2003) Centennial- to millennial-scale periodicities of Holocene climate and sediment injections off the western Barents shelf, 75 N. *Boreas*, 32: 447-461.

Screen JA and Simmonds I (2010) The central role of diminishing sea ice in recent Arctic temperature amplification. *Nature*, 464: 1334-1337.

Semenov VA, Park W and Latif M (2009) Barents Sea inflow shutdown: A new mechanism for rapid climate changes. *Geophys. Res. Lett.* 36: L14709, doi:10.1029/2009GL038911.

Serreze M, Barrett A, Slater A, Steele M, Zhang J and Trenberth K (2007) The large-scale energy budget of the Arctic. *J. Geophys. Res.* 112, D11122, doi.:10.1029/2006JD008230.

Shackleton NJ (1974) Attainment of isotopic equilibrium between ocean water and the benthonic foraminifera genus uvigerina: Isotopic changes in the ocean during the last glacial. *Colloq. Int. CNRS* 219: 203-209.

Simstich J, Sarnthein M and Erlenkeuser H (2003) Paired δ18O signals of N. pachyderma (s) and T. quinqueloba show thermal stratification structure in the Nordic seas. *Mar. Micropaleontol.* 48: 107–125.

Skirbekk K, Klitgaard Kristensen D, Rasmussen TL, Koç N and Forwick M (2010) Holocene climate variations at the entrance to a warm Arctic fjord: evidence from Kongsfjorden trough, Svalbard. *Geological society, London, Special Publications*, 344: 289-304, doi:10.1144/SP344.20.

Slubowska MA, Koç N, Rasmussen TL and Klitgaard-Kristensen D (2005) Changes in the flow of Atlantic water into the Arctic Ocean since the last deglaciation: Evidence from the northern Svalbard continental margin, 80N. *Paleoceonography* 20: PA4014, doi:10.1029/2005PA001141.

Slubowska-Woldengen M, Rasmussen TL, Koç N, Klitgaard-Kristensen D, Nilsen F and Solheim A (2007) Advection of Atlantic Water to the western and northern Svalbard shelf since 17 500 cal yr BP. *Quaternary Sci. Rev.* 26: 463-478.

Smith WO and Sakshaug E (1990) Polar phytoplankton. In Smith WO (ed) *Polar oceanography, Part B: Chemistry, Biology and Geology.* Academic Press, New York, 447-525.

Solignac S, Giraudeau J and De Vernal A (2006) Holocene sea surface conditions in the western North Atlantic: Spatial and temporal heterogeneities. *Paleoceanography* 21: PA2004, doi:10.1029/2005PA001175.

Sorteberg A and Kvingedal B (2006) Atmospheric forcing on the Barents Sea winter ice extent. *J. Clim.* 19: 4772-4784.

Spielhagen RF and Erlenkeuser H (1994) Stable oxygen and carbon isotopes in planktic foraminifera from the Arctic Ocean surface sediments: Reflection of the low salinity surface water layer. *Mar. Geol.* 119: 227-250.

Spielhagen RF, Werner K, Aagaard-Sørensen S, Zamelczyk K, Kandiano E, Budeus G, Husum K, Marchitto T and Hald M (2011) Enhanced modern heat transfer to the Arctic by warm Atlantic water. *Science* 331: 450-453.

Stangeew, E. (2001), Distribution and isotopic composition of living planktonic foraminifera N. pachyderma (sinistral) and T. quinqueloba in the high latitude North Atlantic, Ph.D. thesis, Math.-Naturwiss. Fak., Christian-Albrechts-Univ., Kiel, Germany. (Available at http://e-diss.uni-kiel.de/diss_464/pp).

Stein R and Fahl K (2013) Biomarker proxy shows potential for studying the entire Quaternary Arctic sea ice history. *Org. Geochem.* 55: 98-102.

Stroeve JC, Kattsov V, Barrett A, Serreze M, Pavlova T, Holland M and Meier WN (2012) Trends in Arctic sea ice extent from CMIP5, CMIP3 and observations. *Geophys. Res. Lett.* 39: L16502, doi:10.1029/2012GL052676.

Stuiver M and Reimer PJ (1993) Extended 14C data base and revised CALIB 3.0 14C age calibration program. *Radiocarbon* 35: 215-230.

Telford RJ and Birks HJB (2005) The secret assumption of transfer functions: Problems with spatial autocorrelation in evaluating model performance. *Quaternary Sci. Rev.* 24: 2173-2179.

Ter Braak CJF and Juggins S (1993) Weighted averaging partial least squares regression (WA-PLS): An improved method for reconstructing environmental variables from species assemblages. *Hydrobiologia* 269(270): 485-502.

Thornalley DJR, Elderfield H and McCave IN (2009) Holocene oscillations in temperature and salinity of the surface subpolar North Atlantic. *Nature* 457: 711-714.

Trouet V, Esper J, Graham NE, Baker A, Scourse JD and Frank DC (2009) Persistent positive North Atlantic Oscillation mode dominated the Medieval Climate Anomaly. *Science* 324: 78-80.

Vinje TE (1977) Sea ice conditions in the European sector of the marginal seas of the Arctic, 1966-75. *Aarb. Nor. Polarinst.* 1975: 163-174.

Vinje T (2001) Anomalies and trends of sea-ice extent and atmospheric circulation in the Nordic Seas during the period 1864-1998. *J. Clim.* 14(3): 255-267.

Volkmann R (2000) Planktic foraminifers in the outer Laptev Sea and the Fram Strait: Modern distribution and ecology. *J. Foramin. Res.* 30: 157-176.

Voronina E, Polyak L, de Vernal A and Peyron O (2001) Holocene variations of sea-surface conditions in the southeastern Barents Sea, reconstructed from dinoflagellate cyst assemblages. *J. Quaternary Sci.* 16: 717-726.

Wanner H, Beer J, Bütikofer J, Crowley TJ, Cubasch U, Flückiger J, Goosse H, Grosjean M, Joos F, Kaplan JO, Küttel M, Müller SA, Prentice C, Solomina O, Stocker TF, Tarasov P, Wagner M and Widmann M (2008) Mid- to Late Holocene climate change: An overview. *Quat. Sci. Rev.* 27(19–20): 791-1828.

Wassmann P, Reigstad M, Haug T, Rudels B, Carroll ML, Hop H, Gabrielsen GW, Falk-Petersen S, Denisenko SG, Arashkevich E, Slagstad D and Pavlova O (2006) Food webs and carbon flux in the Barents Sea. *Prog. Oceanogr.* 71: 232-287.

Werner K, Spielhagen RF, Bauch D, Hass HC and Kandiano E (2013) Atlantic Water advection versus sea-ice advances in the eastern Fram Strait during the last 9 ka: Multiproxy evidence for a two-phase Holocene. *Paleoceaonography* 28: 283-295.

Yang S and Christensen JH (2012) Arctic sea ice reduction and European cold winters in CMIP5 climate change experiments. *Geophys. Res. Lett.* 39: L20707, doi:10.1029/2012GL053338.

Yu J and Elderfield H (2007) Benthic foraminiferal B/Ca ratios reflect deep water carbonate saturation state. *Earth Planet. Sci. Lett.* 258: 73-86.

Zamelczyk K, Rasmussen TL, Husum K and Hald M (2013) Marine calcium carbonate preservation vs. climate change over the last two millennia in the Fram Strait: Implications for planktic foraminiferal paleostudies. *Mar. Micropaleontol.* 98: 14-27.

Paper I

Berben SMP, Husum K, Cabedo-Sanz P and Belt ST (2014) **Holocene sub-centennial evolution of Atlantic water inflow and sea ice distribution in the western Barents Sea.** *Clim. Past* 10: 181-198, doi:10.5194/cp-10-181-2014.

Clim. Past, 10, 181–198, 2014
www.clim-past.net/10/181/2014/
doi:10.5194/cp-10-181-2014

Climate of the Past
Open Access

Holocene sub-centennial evolution of Atlantic water inflow and sea ice distribution in the western Barents Sea

S. M. P. Berben[1], **K. Husum**[1], **P. Cabedo-Sanz**[2], **and S. T. Belt**[2]

[1]Department of Geology, University of Tromsø, 9037 Tromsø, Norway
[2]Biogeochemistry Research Centre, School of Geography, Earth and Environmental Sciences, University of Plymouth, Drake Circus, Plymouth PL4 8AA, UK

Correspondence to: S. M. P. Berben (sarah.m.berben@uit.no)

Received: 8 July 2013 – Published in Clim. Past Discuss.: 22 August 2013
Revised: 27 November 2013 – Accepted: 2 December 2013 – Published: 23 January 2014

Abstract. A marine sediment core (JM09-KA11-GC) from the Kveithola Trough at the western Barents Sea margin has been investigated in order to reconstruct sub-surface temperatures and sea ice distribution at a sub-centennial resolution throughout the Holocene. The relationship between past variability of Atlantic water inflow and sea ice distribution has been established by measurement of planktic foraminifera, stable isotopes and biomarkers from sea ice diatoms and phytoplankton.

Throughout the early Holocene (11 900–7300 cal yr BP), the foraminiferal fauna is dominated by the polar species *Neogloboquadrina pachyderma* (sinistral) and the biomarkers show an influence of seasonal sea ice. Between 10 900 and 10 700 cal yr BP, a clear cooling is shown both by fauna and stable isotope data corresponding to the so-called Preboreal Oscillation. After 7300 cal yr BP, the sub-polar *Turborotalita quinqueloba* becomes the most frequent species, reflecting a stable Atlantic water inflow. Sub-surface temperatures reach 6 °C and biomarker data indicate mainly ice-free conditions. During the last 1100 cal yr BP, biomarker abundances and distributions show the reappearance of low-frequency seasonal sea ice and the planktic fauna show a reduced salinity in the sub-surface water. No apparent temperature decrease is observed during this interval, but the rapidly fluctuating fauna and biomarker distributions indicate more unstable conditions.

1 Introduction

Sea ice is a pivotal element of the climate system (e.g. Kvingedal, 2005; Stroeve et al., 2012) and plays a major role in determining ocean circulation in the North Atlantic. There has been a dramatic reduction in Arctic sea ice cover in recent decades (e.g. Comiso et al., 2008) and, in summer 2012, this loss reached its maximum extent within the ca. 30 yr record of satellite sea ice observations (Schiermeier, 2012). Increased sea ice loss in the Arctic Ocean will result in an enhanced Arctic warming, and this will also have a severe impact on climatic conditions in the Northern Hemisphere in general (e.g. extreme winters in Europe) (Francis et al., 2009).

The underlying water masses are of great importance in determining sea ice extent, especially in the high-latitude North Atlantic and adjacent Barents Sea, where sea ice interacts with the inflow of warm saline Atlantic water (Hopkins, 1991). Indeed, some recent studies have suggested that enhanced advection of Atlantic water into the Arctic might be one of the main causes of the recent sea ice decline (Kinnard et al., 2011; Spielhagen et al., 2011), so ice conditions in the Barents Sea are especially influenced by changing oceanic fronts. The interaction between sea ice and Atlantic water also affects salinity regulation and hence the Atlantic Meridional Overturning Circulation (AMOC) (e.g. Rudels et al., 1996; Dieckmann and Hellmer, 2008). As such, the high-latitude North Atlantic, including the western Barents Sea, represents a key study area as it is the main gateway for Atlantic water into the Arctic Ocean (Broecker, 1991).

Previous studies indicate that Atlantic water inflow in the high-latitude North Atlantic and adjacent Barents Sea has changed throughout the Holocene (Bauch and Weinelt, 1997; Bond et al., 1997; Jennings et al., 2002; Jiang et al., 2002; Sarnthein et al., 2003; Duplessy et al., 2005; Hald et al., 2007; Risebrobakken et al., 2010), and an overall decrease in atmospheric and oceanic temperatures is generally linked to decreasing solar insolation (Berger, 1978; Koç et al., 1993; Kaufman et al., 2004). During the early Holocene, when solar insolation reached a maximum at these latitudes (Laskar et al., 2004), a strong advection of Atlantic water has been observed (e.g. Husum and Hald, 2004; Slubowska et al., 2005; Slubowska-Woldengen et al., 2007); however, several reconstructions of palaeo-temperatures based on alkenones (e.g. Calvo et al., 2002), diatoms (e.g. Andersen et al., 2004; Birks and Koç, 2002; Koç and Jansen, 1994) and planktic foraminifera (e.g. Andersson et al., 2003; Risebrobakken et al., 2003; Sarnthein et al., 2003) show a different timing of this Holocene maximum. Such differences might be explained in terms of regional variations or influences attributed to the different depth habitats or seasonal responses of the various proxies (Moros et al., 2004). For example, Andersson et al. (2010) suggested that discrepancies in SST records could be explained by differences in hydrographic settings (i.e. sea surface versus sub-surface), while Risebrobakken et al. (2011) showed that a strong insolation at high northern latitudes affects temperatures within the summer mixed layer, but not within the waters underneath, thereby amplifying the different roles of oceanic heat advection and orbital forcing.

Superimposed on this overall trend, observations of several millennial-scale changes in surface ocean circulation also exist (e.g. Bauch and Weinelt, 1997; Bond et al., 1997; Duplessy et al., 2001; Jennings et al., 2002; Jiang et al., 2002; Hald et al., 2007). These changes have been attributed to several influences, including the North Atlantic Oscillation (NAO), the Arctic Oscillation and sea ice (Giraudeau et al., 2004; Solignac et al., 2006; Rousse et al., 2006; Slubowska-Woldengen et al., 2007; Goosse and Holland, 2005; Semenov et al., 2009). Further, Orvik and Skagseth (2003) suggested that wind stress curls affect the variability of Atlantic water inflow. Thus, atmospheric changes are important as they influence the strength of the surface water masses, the AMOC and hence Earth's global heat distribution. The precise nature and driving forces behind the variability of Atlantic water inflow and sea ice extent are, however, not well constrained and large uncertainties prevent an accurate prediction of the future state of these polar regions. In order to determine the degree of natural variability, more well-dated and high-resolution records are required (e.g. Voronina et al., 2001), especially those that include records of sea ice distribution (Polyak et al., 2010).

In this paper, we describe a new high-resolution record of surface water properties and sea ice distribution in the western Barents Sea in order to provide a better understanding of their variability throughout the Holocene. The core site (Fig. 1) is situated close to the modern day position of the Arctic front (Hopkins, 1991) and is situated in a glacial trough, which acts as a natural sediment trap containing relatively thick Holocene sediments (Rüther et al., 2012). It therefore represents an excellent location for carrying out such a study using planktic foraminiferal fauna, stable isotopes (δ^{18}O, δ^{13}C) and sea ice and phytoplankton biomarkers.

2 Regional oceanography

An overview of the main surface currents in the high-latitude North Atlantic and adjacent Barents Sea is shown in Fig. 1a. The North Atlantic Current (NAC) is drawn from the south, pushing relatively warm salty Atlantic water ($T > 2\,^{\circ}$C, $S > 35\,‰$; Hopkins, 1991) into the northern North Atlantic (Swift, 1986) (Fig. 1a). Subsequently, this Atlantic water spreads into adjoining regions by different branches of the NAC, i.e. the West Spitsbergen Current (WSC) into the Arctic Ocean and the North Cape Current (NCaC) into the Barents Sea (Fig. 1a). The latter current flows partly northwards into the Barents Sea, whereas another branch turns eastwards, parallel with the coastal current system (Loeng, 1991).

Cold, less saline and ice-loaded polar water (T 0–2 °C, S 33–34.4 ‰; Hopkins, 1991) coming from the Arctic Ocean is brought into the Atlantic Ocean by the East Greenland Current (EGC) (Rudels et al., 2005) and into the Barents Sea by the East Spitsbergen Current (ESC) and Bear Island Current (BIC). The ESC continues northwards along the inner shelf of western Svalbard (Fig. 1a). When polar and Atlantic water meet in the Barents Sea, they mix and form Arctic water ($T \sim 0.5\,^{\circ}$C, $S \sim 34.8\,‰$; Hopkins, 1991), which is characterized by a reduced temperature and salinity, as well as by a seasonal sea ice distribution (Hopkins, 1991). The boundaries between polar/Arctic and Arctic/Atlantic waters correspond to the polar front and Arctic front, respectively. Both fronts represent a sharp climatic gradient in terms of temperature, salinity and sea ice coverage and are amongst the main oceanographic features of the Barents Sea (Hopkins, 1991). Further north, dense deep water is generated due to brine rejection during winter freezing (Midttun, 1985).

Warm and fresh coastal water (T 2–13 °C, S 32–35 ‰; Hopkins, 1991) is found on the shelves and off the coast of Norway, with its reduced salinity resulting from freshwater runoff from the Norwegian mainland and Baltic Sea (Blindheim, 1987). This water mass is transported northwards by the Norwegian Coastal Current (NCC) into the south-western Barents Sea, where it continues along the Norwegian and Russian coastline (Aure and Strand, 2001). The coastal front represents the boundary between coastal and Atlantic water. It typically overlies Atlantic water as a westward thinning wedge although, more northwards, the two water masses mix (Sætre, 2007).

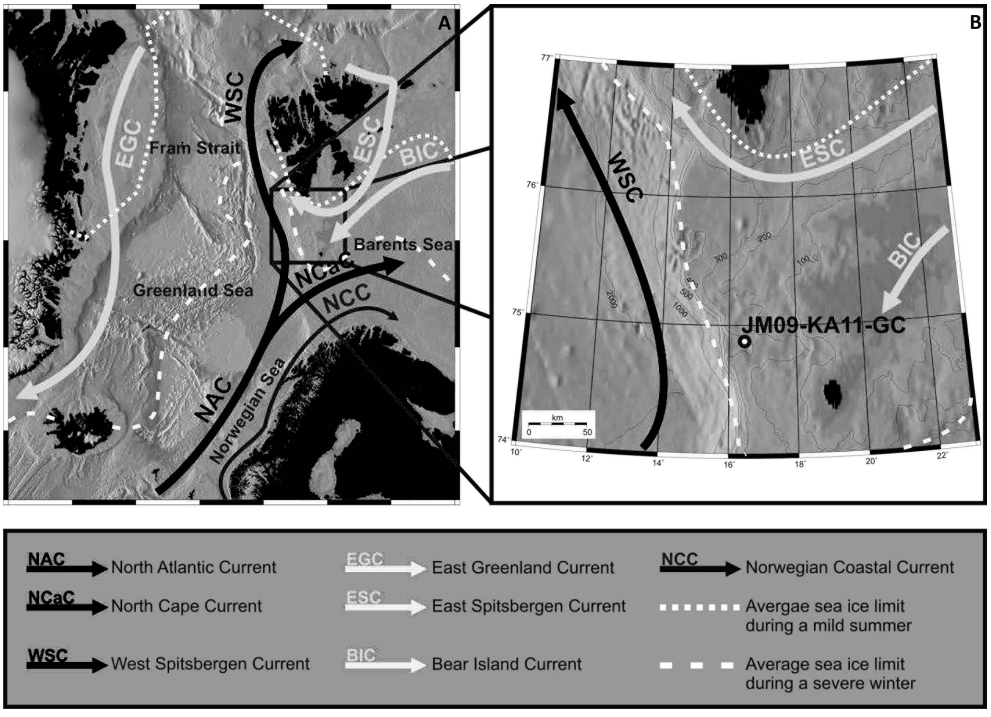

Fig. 1. (A) Surface currents in the high-latitude North Atlantic and north-western Barents Sea are presented on a bathymetric map. Water masses and sea ice distribution are defined according to Hopkins (1991). **(B)** Close up of the study site showing the core location of JM09-KA11-GC. The core was retrieved in the Kveithola Trough surrounded by the Spitsbergen Bank at a water depth of 345 m.

The overall extent of sea ice distribution in the northern North Atlantic and the Barents Sea is closely related to the positions of the polar and Arctic fronts, which align with the average summer and winter sea ice margins, respectively (Vinje, 1977) (Fig. 1a). These fronts determine the position of the marginal ice zone and surface productivity in the summer season (e.g. Smith and Sakshaug, 1990). In the north-eastern Barents Sea, Arctic water dominates and sea ice is formed during autumn and winter (Loeng, 1991). In contrast, the southern Barents Sea is characterized by large seasonal and inter-annual sea ice distribution changes due to the strong influence of Atlantic water (Kvingedal, 2005). Nearly all the biological primary production in the Barents Sea results from a peak algal bloom during the spring as ice retreats along the ice edge (Sakshaug et al., 1992). In the western Barents Sea, Atlantic water dominates the water masses and is overlain by fresher and colder surface waters (Loeng, 1991) (Fig. 2).

3 Material and methods

Sediment core JM09-KA11-GC was retrieved in 2009 by RV *Jan Mayen* in the western Barents Sea (74.87° N, 16.48° E) at a water depth of 345 m (Rüther et al., 2012) (Fig. 1b). In this study, only the Holocene interval (past 11 900 cal yr BP) of the core was analysed. The Holocene interval is represented by the upper 1.3 m of the core and consists of sediments rich in sand and silt (Rüther et al., 2012).

3.1 Chronology

A depth–age model of JM09-KA11-GC was first developed by Rüther et al. (2012). For the current study, five additional AMS ^{14}C dates were obtained and a new depth–age model was developed using linear interpolation (Fig. 3). All 13 AMS ^{14}C dates were calibrated using Calib 7.0.0 software (Stuiver and Reimer, 1993), the Marine13 calibration curve (Reimer et al., 2013) and a local reservoir age (ΔR value) of 67 ± 34 based on existing data from near Bear Island (74.12° N, 19.07° E) (Mangerud and Gulliksen, 1975). This calibration was constrained on a 2-σ range (Table 1). Five AMS ^{14}C dates were not included in the final depth–age model (Table 1). The AMS ^{14}C date at 4.5 cm was left out as its 2-σ range was larger than the subsequent AMS ^{14}C date at 4.5 cm. Three other AMS ^{14}C dates, one at 33.0 cm and two at 82.5 cm, appeared to be too young, most likely due to the downward migration of the infaunal molluscs *Astarte elliptica* and *Nuculana minuta*. An additional AMS ^{14}C date at 111.0 cm on benthic foraminifera appeared too old when listing all AMS ^{14}C dates, including those from the lower most part of the core covering the Younger Dryas and deglaciation (Rüther et al., 2012). Although carbon dating of molluscs may be problematic (e.g. Mangerud et al., 2006), it

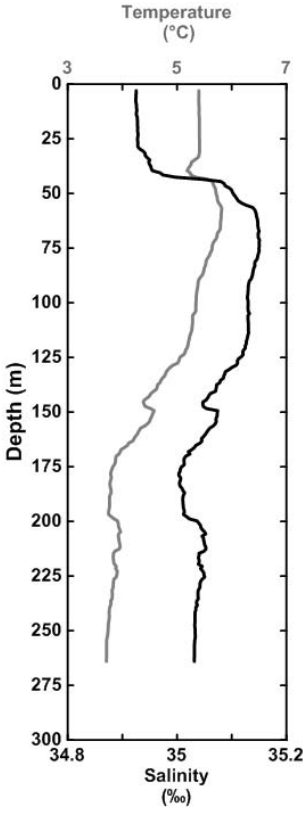

Fig. 2. Temperature (grey) and salinity (black) profile from the JM09-KA11-GC core location measured on 13 July 2009 (GlaciBar).

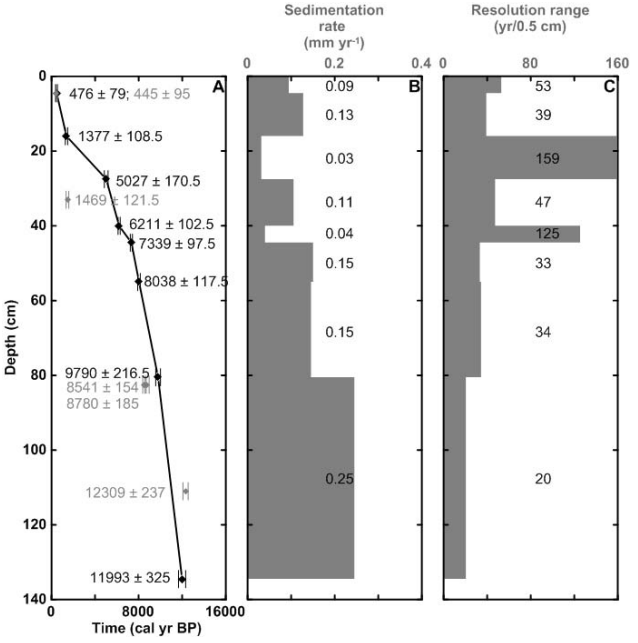

Fig. 3. (A) Depth–age model of the upper 134.5 cm of JM09-KA11-GC based on eight calibrated AMS ^{14}C dates and a linear interpolation between the calibrated radiocarbon ages. The 2-σ range of each calibrated radiocarbon age is indicated by an error bar, whereas the exact value is noted (omitted ages in grey). **(B)** Sedimentation rates versus core depth. **(C)** Resolution range versus core depth.

appears that this date is reworked when comparing it to the succession of all AMS ^{14}C dates. Hence, it was left out of the depth–age model. Other radiocarbon dates on molluscs appeared not to be reworked when evaluating all AMS ^{14}C dates together and thus they were included in the depth–age model. The resulting depth–age model showed sedimentation rates between 0.03 and 0.25 mm yr^{-1} corresponding to a sub-centennial (20–159 yr / 0.5 cm) resolution (Fig. 3).

3.2 Background to proxies

Sea surface and sub-surface temperatures are often reconstructed using faunal assemblages and stable isotopic analysis of planktic foraminifera (e.g. Eynaud, 2011) and quantitative reconstructions can be obtained through the application of transfer functions (e.g. Imbrie and Kipp, 1971; Pflaumann et al., 2003; Kucera et al., 2005). Recently, Husum and Hald (2012) developed an Arctic training set based on the >100 µm size fraction and found that the most robust reconstructions of sea surface temperatures using transfer functions were obtained when using summer temperatures from sub-surface water masses at 100 m water depth.

In recent years, seasonal Arctic sea ice conditions have been derived by analysis of the sea ice diatom biomarker IP_{25} (Belt et al., 2007; Belt and Müller, 2013). IP_{25} is a C_{25} monounsaturated highly branched isoprenoid (HBI) lipid produced specifically by Arctic sea ice diatoms and appears to be relatively stable in marine sediments (Brown et al., 2011; Belt and Müller, 2013; Stein and Fahl, 2013). Importantly, in a number of studies, variable abundances of sedimentary IP_{25} have been shown to be consistent with known sea ice trends or have provided new information regarding palaeo-sea-ice-cover conditions (Belt and Müller, 2013, and references therein). Since the absence of IP_{25} from Arctic marine sediments is believed to either represent open water or perennial ice cover, the additional determination of brassicasterol and other phytoplankton lipids has been used to distinguish between these two oceanographic extremes (e.g. Müller et al., 2009, 2011; Belt and Müller, 2013). With respect to the current study location, Vare et al. (2010) observed a good correlation between IP_{25} data and historical records of sea ice covering the last few centuries for the Barents Sea and suggested that longer term palaeo-sea-ice records beyond the historical data should therefore be achievable using the same approach. In addition, Navarro-Rodriguez et al. (2013) showed that the occurrence of IP_{25} in surface sediments from the Barents Sea was extremely sensitive to sea ice cover in recent decades.

Table 1. AMS ^{14}C dates and calibrated radiocarbon ages of JM09-KA11-GC. The calibration is based on the Marine13 calibration curve (Reimer et al., 2013) and a regional ΔR of 67 ± 34. The dates which are not used in the final depth–age model are indicated in italics.

Lab ID	Core depth	Material	^{14}C yr BP (uncorrected)	1σ	cal yr BP	2-σ range	Reference
Tra-1063	4.5 cm	Mollusc dextral part of *Bathyarca glacialis*	925	30	476	397–555	Rüther et al. (2012)
Tra-1064	*4.5 cm*	*Mollusc dextral part of Bathyarca glacialis*	*900*	*35*	*445*	*354–535*	*Rüther et al. (2012)*
Tra-1065	16.0 cm	Mollusc sinistral part of *Bathyarca glacialis*	1880	35	1377	1268–1485	Rüther et al. (2012)
Beta-324049	27.5 cm	Benthic foraminifera *Islandiella norcrossi/helenae*	4820	30	5027	4856–5197	This study
Tra-1066	*33.0 cm*	*Mollusc dextral part of Astarte elliptica*	*1990*	*35*	*1469*	*1347–1590*	*Rüther et al. (2012)*
Beta-315192	40.0 cm	Benthic foraminifera *Islandiella norcrossi/helenae*	5870	30	6211	6108–6313	This study
Beta-315193	44.5 cm	Benthic foraminifer*a Islandiella norcrossi/helenae*	6890	40	7339	7241–7436	This study
Tra-1067	55.0 cm	Mollusc sinistral part of *Astarte sulcata*	7630	45	8038	7919–8154	Rüther et al. (2012)
Beta-315194	80.5 cm	Benthic foraminifera *Islandiella norcrossi/helenae*	9140	40	9790	9573–10 006	This study
Tra-1068	*82.5 cm*	*Mollusc paired shell of Astarte elliptica*	*8140*	*50*	*8541*	*8387–8695*	*Rüther et al. (2012)*
Tra-1069	*82.5 cm*	*Mollusc sinistral part of Nuculana minuta*	*8315*	*50*	*8780*	*8595–8965*	*Rüther et al. (2012)*
Beta-315195	*111.0 cm*	*Benthic foraminifera Elphidium excavatum*	*10 900*	*50*	*12 309*	*12 072–12 546*	*This study*
Tra-1070	134.5 cm	Mollusc paired shell of *Yoldiella intermedia*	10 705	55	11 993	11 668–12 318	Rüther et al. (2012)

Table 2. Planktic foraminiferal species list.

Planktic foraminiferal species
Globigerina bulloides (d'Orbigny, 1826)
Globigerinita glutinata (Egger, 1893)
Globigerinita uvula (Ehrenberg, 1861)
Neogloboquadrina incompta (Cifelli, 1961)
Neogloboquadrina pachyderma (sinistral) (Ehrenberg, 1861)
Turborotalita quinqueloba (Natland, 1838)

3.3 Planktic foraminifera

The JM09-KA11-GC core was sampled for planktic foraminifera every 0.5 cm. The samples were freeze-dried, wet-sieved into different size fractions using 1000, 100 and 63 µm mesh size sieves and dried in an oven at 40 °C. Due to a low abundance of planktic foraminifera in the samples between 90.0 and 130.0 cm, the foraminifera in these samples were separated from the sediment using sodium polytungstate diluted with distilled water to a specific gravity of 1.8 g mL^{-1} following Knudsen (1998). One hundred and twenty-seven samples were analysed with regard to the planktic foraminifera using the 100–1000 µm size fraction according to Knudsen (1998). The identification of left- and right-coiling *Neogloboquadrina pachyderma* was done following Darling et al. (2006) (Table 2). A minimum of 300 specimens was identified for each sample, although when calculating relative and absolute abundances, 57 samples containing planktic foraminifera between 50 and 300 specimens were still included. Relative abundances (%) and fluxes (no. specimens cm^{-2} yr^{-1}) were calculated for each sample. Fluxes were calculated according to Ehrmann and Thiede (1985) using dry bulk densities, which were calculated using the water content and wet bulk density measurements of Rüther et al. (2012).

Planktic foraminifera can be exposed to carbonate dissolution associated with ocean circulation and climate (e.g. Archer and Maier-Reimer, 1994; Archer, 1996). As dissolution might have affected the planktic foraminifera assemblages in JM09-KA11-GC, it was considered important to quantify the state of foraminiferal preservation. Hence, the mean shell weight of *N. pachyderma* (sin.) was measured (Broecker and Clark, 2001; Barker and Elderfield, 2002; Beer et al., 2010). Visually well-preserved and square-shaped forms of *N. pachyderma* (sin.) were weighed using a Mettler Toledo microbalance (0.1 µg sensitivity). To minimize problems of ontogeny and variability due to size differences, the tests were picked within a narrow size fraction of 230–290 µm (Barker et al., 2004). Further, the fragmentation of foraminiferal tests was analysed in the 100–1000 µm size fraction, as this also reflects the degree of dissolution (Conan et al., 2002). The fragmentation (%) was calculated using the method of Pufhl and Shackleton (2004) (Eq. 1).

$$\text{Fragmentation (\%)} = \frac{\text{no. fragments g}^{-1}}{\text{no. fragments g}/3 + \text{no. test g}^{-1}} * 100 \quad (1)$$

In using Eq. (1), it was assumed that each shell breaks into more than one fragment, and therefore the total number of fragments per sample was divided by three. The use of a divisor reduces misinterpretations of the dissolution sensitivity in changes and progress (Le and Shackleton, 1992; Pufhl and Shackleton, 2004).

Finally, summer (July-August-September) sub-surface temperatures (sSST) were reconstructed for a water depth of 100 m using the improved modern training set of Husum and Hald (2012). The weighted average partial least square (WA-PLS) and maximum likelihood (ML) statistical models with a leave-one-out cross validation were applied (Ter Braak and Juggins, 1993; Telford and Birks, 2005). The calculations were carried out using the computer program C2 version 1.7.2 (Juggins, 2010).

3.4 Stable isotope analysis

Stable isotope analysis (δ^{13}C and δ^{18}O) was carried out on 132 samples, giving a sub-centennial resolution. Foraminiferal tests of *N. pachyderma* (sin.) from the 100–1000 µm size fraction were analysed. Measurements were performed with a Finnigan MAT 253 mass spectrometer coupled to an automated Kiel device at the Geological Mass Spectrometer (GMS) Laboratory of the University of Bergen. The data were reported on the VPDB scale (calibrated with NBS-19) and measurements were conducted with a reproducibility of ±0.04 ‰ (δ^{13}C) and ±0.06 ‰ (δ^{18}O). The resulting δ^{18}O values were corrected for the ice volume effect according to Fairbanks (1989). The isotope measurements in this study were not corrected for their species-specific vital effect as published estimates in the literature are often inconsistent, possibly due to apparent change between seasons (Jonkers et al., 2010).

3.5 Biomarker analysis

Individual sub-samples for biomarker analysis were taken at 0.5 cm intervals, freeze-dried and stored at −20 °C prior to analysis. Biomarker analysis (IP_{25} and sterols) was performed using methods described previously (Brown et al., 2011; Belt et al., 2012) but with some modifications. Briefly, three internal standards were added to each freeze-dried sediment sample to permit quantification of lipid biomarkers. Specifically, 7-hexylnonadecane (7-HND, 10 µL; 10 µg mL^{-1}) and 9-octylheptadec-8-ene (9-OHD, 10 µL; 10 µg mL^{-1}) were added for quantification of IP_{25} and 5α-androstan-3β-ol (10 µL; 10 µg mL^{-1}) was added for quantification of sterols. Sediments were then extracted using dichloromethane / methanol (3×3 mL, 2 : 1 v/v) and ultrasonication before decanting and drying (Brown et al., 2011; Belt et al., 2012). Since many total organic extracts (TOEs) were found to contain high concentrations of elemental sulfur that interfered with the subsequent gas chromatographic analyses, this was removed from the primary extracts before further purification. This was achieved through the addition of hexane (1 mL), tetrabutylammonium sulfite (TBA, 1 mL) and 2-propanol (2 mL) to the dried TOEs, which were then shaken by hand (1 min). After addition of ultra-high-purity water (3 mL), the samples were shaken again (1 min) and centrifuged. The hexane layer (containing the lipids of interest) was transferred to a clean vial and the procedure repeated twice more. Following removal of the solvent from the combined hexane extracts using nitrogen, the resulting TOEs were purified using column chromatography (silica), with IP_{25} and other hydrocarbons (hexane, 6 mL) and sterols (20 : 80 methylacetate/hexane, 6 mL) collected as two single fractions. In some cases, the identification or quantification of IP_{25} in these partially purified extracts was made difficult due to a combination of low concentrations and the occurrence of other highly abundant co-eluting organic compounds that prevented further concentration of the extracts. Therefore, hexane extracts were further fractionated into saturated and unsaturated components using glass pipettes containing silver ion solid-phase extraction (SPE) material (Supelco discovery® Ag-Ion). Saturated hydrocarbons were eluted first (hexane, 5 column volumes, then dichloromethane, 5 column volumes) and unsaturated hydrocarbons (including IP_{25}) were eluted with dichloromethane / acetone (95 / 5, 5 column volumes) before being dried (nitrogen). Analysis of individual fractions was carried out using gas chromatography–mass spectrometry (GC-MS) and operating conditions were as described previously (e.g. Belt et al., 2012; Brown and Belt, 2012). Sterols were derivatized (N,O-Bis(trimethylsilyl)trifluoroacetamide; 50 µL, 70 °C, 1 h) prior to analysis by GC-MS. Mass-spectrometric analysis was carried out either in total ion current (TIC) or single-ion monitoring (SIM) mode. Individual lipids were identified on the basis of their characteristic GC retention indices and mass spectra obtained from standards. Quantification of lipids was achieved by comparison of mass spectral responses of selected ions (SIM mode) with those of the internal standards and normalized according to relative response factors and sediment masses (Belt et al., 2012). Analytical reproducibility was monitored using a standard sediment with known abundances of biomarkers for every 16 to 18 sediment samples extracted (analytical error < 5 %, $n = 4$). All biomarker concentrations (µg g^{-1} sediment) were normalized to total organic carbon content (µg g^{-1} OC) and also converted to fluxes (µg cm^{-2} yr^{-1}) as per the method used for foraminifera.

Individual biomarker data were not combined to derive corresponding PIP_{25} data (Müller at al., 2011) for two reasons. First, Navarro-Rodriguez et al. (2013) showed that the PIP_{25}-based approach for semi-quantitative sea ice reconstruction does not work well for recent sea ice conditions for the Barents Sea. Second, the data presented here correspond to the Holocene epoch only; however, additional biomarker data from the same core covering the Younger Dryas (not shown) indicate that the so-called balance factor (c) used in the calculation of the PIP_{25} data is highly variable depending on the section of core under study. This has previously been identified as a potential limitation of this approach (Belt and Müller, 2013) and the current study exemplifies this further.

4 Results

4.1 Planktic foraminifera

The planktic foraminiferal fauna consists of six species and is dominated by two: *Neogloboquadrina pachyderma* (sin.) and *Turborotalita quinqueloba*. *Neogloboquadrina incompta*, *Globigerinita uvula* and *Globigerinita glutinata* are also observed, but as minor species. Further, *Globigerina*

bulloides is found sporadically throughout the record (Table 2; Fig. 4a–f).

The early part of the record (11 900–9900 cal yr BP) is dominated by *N. pachyderma* (sin.) with a percentage abundance of ca. 60 % and a maximum is observed at 10 800 cal yr BP (84 %) (Fig. 4a). Between 11 900 and 10 800 cal yr BP, *N. incompta* shows a decrease, followed by an increase, reaching its maximum relative abundance of 30 % at 10 400 cal yr BP. This is followed by a decrease between 10 400 and 7300 cal yr BP towards 6 % (Fig. 4c). *T. quinqueloba* becomes the most frequent species at 9900 cal yr BP and increases continuously up to 8000 cal yr BP (Fig. 4b). From 7300 to 1100 cal yr BP the relative abundances of all six recorded species remain relatively stable, with *T. quinqueloba* as the most dominant species (ca. 65 %) (Fig. 4a–f). The last 1100 cal yr BP is characterized by a decrease in *T. quinqueloba* and *N. incompta* and an increase in *G. glutinata* and *G. bulloides* (Fig. 4b–f). The most prominent feature of this period, however, is the rather sharp increase in *G. uvula* of almost 10 % (Fig. 4d).

Both the total absolute abundances of planktic foraminifera (per gram dry sediment) and the total fluxes of foraminifera show very low values in the early part of the record (11 900–9900 cal yr BP) (Fig. 4g). At ca. 10 400 cal yr BP, the total foraminiferal flux increases sharply towards 9900 cal yr BP reaching ca. 100 specimens $cm^{-2}\,yr^{-1}$. The increase in concentration starts after ca. 10 000 cal yr BP and reaches values of ca. 5000 specimens g^{-1} in ca. 1000 yr. Between 9900 and 7300 cal yr BP, the concentration continues to fluctuate around 4000 specimens g^{-1}, and the flux decreases to values around 10 to 20 specimens $cm^{-2}\,yr^{-1}$. From ca. 7300 cal yr BP, concentrations continue to gently increase, whereas fluxes remain relatively constant. In the more recent part of the record, the flux reaches a value of > 60 specimens $cm^{-2}\,yr^{-1}$ at 1100 cal yr BP, whereas the concentration shows a sharp increase, extending to values of 6000 specimens g^{-1}.

The shell weight and fragmentation are inversely correlated throughout the record (Fig. 4h). Between 11 900 and 10 300 cal yr BP, the mean shell weight decreases from approximately 5 to 3 µg, whereas the shell fragmentation increases from ca. 10 to 30 %. This period is followed by a rapid increase in shell weight from 3 to 10 µg and a simultaneous decrease in shell fragmentation from 30 to 5 %. Between 9900 and 1100 cal yr BP, the values are relatively stable, showing a mean shell weight and fragmentation of ca. 7 µg and 10 %, respectively (Fig. 4h). Finally, from 1100 cal yr BP towards the present day, the shell weight decreases to ca. 5 µg, whereas the fragmentation remains stable at around 10 %.

Different statistical models have been tested in order to reconstruct sSST records and their performance characteristics are evaluated following Birks (1995) (Table 3). A WA-PLS component 3 model is selected as the most appropriate model to obtain a precise estimation. This choice is based on a combination of the lowest root-mean-square error of prediction (RMSEP = 0.52), the highest correlation between observed and estimated values ($R^2 = 0.93$) and the lowest maximum bias (max. bias = 0.53) (Birks, 1995) (Table 3). The foram-derived sSST record shows a gradual warming from 4 to 5 °C between 11 900 and 10 400 cal yr BP (Fig. 4i). This period is interrupted by an abrupt and short cooling event of ca. 2.5 °C around 10 800 cal yr BP. From 10 400 to 8000 cal yr BP, the record shows a more gradual increase up to 6 °C, where it remains stable to present (Fig. 4i).

Table 3. Performance characteristics of transfer function models used to reconstruct palaeo-sSST of JM09-KA11-GC. Italics indicate the statistical model with the best performance values according to Birks (1995).

Transfer function	Water depth (m)	Max. bias	RMSEP	R^2
WA-PLS Component 1	100	0.60	0.56	0.91
WA-PLS Component 2	100	0.55	0.52	0.92
WA-PLS Component 3	*100*	*0.53*	*0.52*	*0.93*
WA-PLS Component 4	100	0.56	0.52	0.93
WA-PLS Component 5	100	0.55	0.52	0.93
ML	100	1.33	0.80	0.86

4.2 Stable isotope analysis

The $\delta^{18}O$ and $\delta^{13}C$ measurements of *N. pachyderma* (sin.) show similar general trends throughout the record (Fig. 5). Overall, the $\delta^{18}O$ values are in the range 1.79 to 2.90 ‰ (Fig. 5a). Between 11 900 and 11 300 cal yr BP, $\delta^{18}O$ values show a slight depletion followed by a small enrichment towards 10 800 cal yr BP. Subsequently, a sharp depletion in $\delta^{18}O$ is observed at ca. 10 400 cal yr BP (Fig. 5a), after which $\delta^{18}O$ values gradually increase up to ca. 2.50 ‰ until ca. 7300 cal yr BP. The $\delta^{18}O$ record then remains relatively stable until 1100 cal yr BP with a mean value of 2.50 ‰. For the last 1100 cal yr BP, the record shows slightly increased values (Fig. 5a).

The $\delta^{13}C$ record is within the range −0.30 to 0.86 ‰ (Fig. 5b). A slight depletion in $\delta^{13}C$ is recorded between 11 900 and 11 500 cal yr BP, followed by a small enrichment towards 10 700 cal yr BP and a sharp depletion with values of −0.26 ‰ towards ca. 10 400 cal yr BP. Between ca. 10 400 and 7300 cal yr BP, $\delta^{13}C$ values increase to 0.40 ‰. For the remaining part of the record, a relatively stable trend is observed with a mean value of ca. 0.40 ‰.

4.3 Biomarker analysis

The concentration profiles of IP_{25} and the two sterols – 24-methylcholesta-5,22E-dien-3β-ol (brassicasterol) and 24-methylcholesta-5,24(28)-dien-3β-ol (24-methylenecholesterol) – are shown in Fig. 6. At

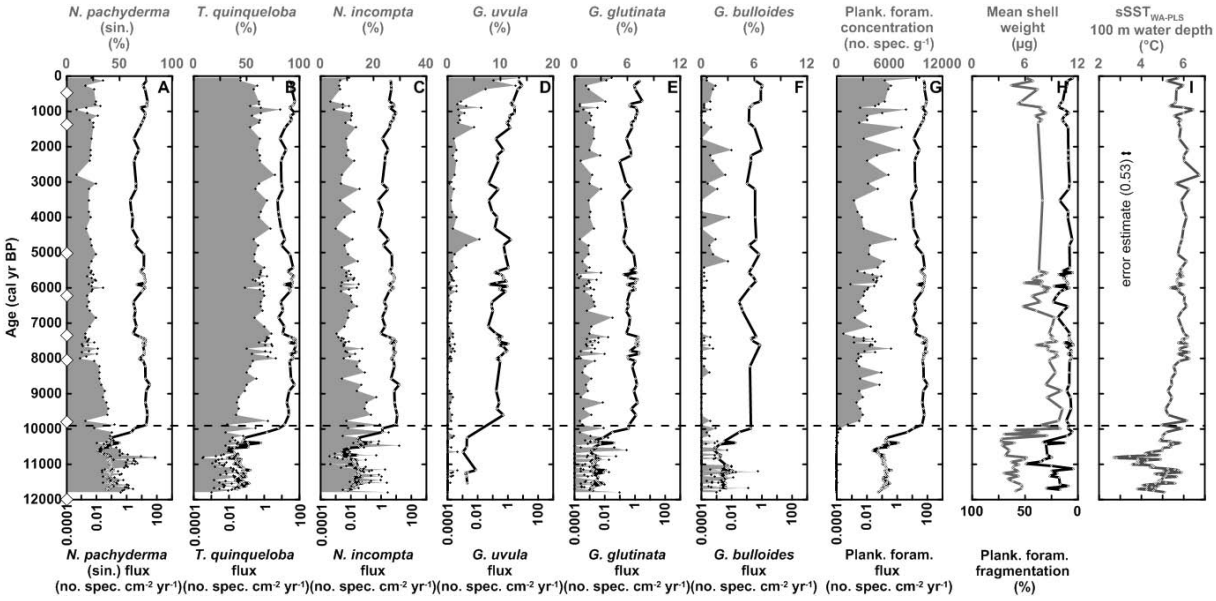

Fig. 4. Planktic foraminiferal analysis plotted versus cal yr BP. The white diamonds on the *y* axis denote the AMS ^{14}C converted to calibrated radiocarbon ages. Samples below the dotted line contain < 300 planktic foraminiferal specimens. **(A–F)** Species-specific relative distribution (grey-filled area) and flux (black line) (note the logarithmic scale for the fluxes). **(G)** Total planktic foraminiferal concentration (grey-filled area) and flux (black line) (note the logarithmic scale for the fluxes). **(H)** Mean shell weight (grey line) and planktic foraminiferal fragmentation (black line) (note the reversed axis). **(I)** Reconstructed $sSST_{WA\text{-}PLS}$.

11 900 cal yr BP the IP_{25} concentration is at its highest value (2.11 µg g^{-1} OC) in the entire record, while the brassicasterol (20.18 µg g^{-1} OC) and 24-methylenecholesterol (5.45 µg g^{-1} OC) concentrations are relatively low at this point. At the onset of the Holocene (ca. 11 700 cal yr BP), there is a sharp decrease in IP_{25} and a simultaneous increase in brassicasterol and 24-methylenecholesterol concentrations. Between ca. 11 300 and 9900 cal yr BP, IP_{25} concentrations remain relatively constant at ca. 0.25 µg g^{-1} OC, while those of brassicasterol and 24-methylenecholesterol increase after ca. 11 300 cal yr BP, reaching their highest values (51.09 and 18.97 µg g^{-1} OC, respectively) at ca. 10 400 cal yr BP followed by a decrease towards ca. 9900 cal yr BP. Between 9900 and 1100 cal yr BP, both IP_{25} and 24-methylenecholesterol are either absent or very low in concentration, but brassicasterol is still present, albeit in very low concentrations of ca. 9.00 µg g^{-1} OC. During the final part of the record (1100–0 cal yr BP), there is a clear increase in brassicasterol concentrations, reaching 60.95 µg g^{-1} OC at the top of the core. In contrast, IP_{25} continues to be present, but at a very low concentration (ca. 0.10 µg g^{-1} OC). The concentrations of all three biomarkers are substantially lower in the recent interval (< ca. 1100 cal yr BP) compared to those found in the early part of the record, with the exception of brassicasterol, which has reasonably elevated concentrations during the last ca. 500 cal yr BP. Finally, biomarker concentration profiles align closely with fluxes throughout the record (Fig. 6).

5 Discussion

The different proxy data in this study indicate palaeoceanographic changes of sub-surface temperatures and sea ice conditions in the western Barents Sea during the Holocene. These changes are discussed according to five time periods identified through analysis of all proxy data (Fig. 7). Period I represents the period 11 900 to 10 400 cal yr BP (early Holocene) with a short interval defined as sub-period Ia between 10 900 and 10 700 cal yr BP (Preboreal Oscillation). Period II constitutes the period from 10 400 to 7300 cal yr BP (early–mid-Holocene), period III represents the interval from 7300 to 1100 cal yr BP (mid–late Holocene) and period IV covers the last 1100 cal yr BP (late Holocene–present).

5.1 Period I: 11 900–10 400 cal yr BP (early Holocene)

The planktic foraminiferal fauna distribution is characterized by a clear dominance of *N. pachyderma* (sin.), which is associated with cold Arctic and polar water (Volkmann, 2000) (Fig. 7a). The high relative abundance of *N. pachyderma* (sin.) (60 %) agrees well with data from previous studies. For example, Ebbesen et al. (2007) found a high abundance of this species (up to 80 %) when investigating the > 100 µm size fraction in a sediment core from the western Svalbard margin. Further, Sarnthein et al. (2003) found a similar abundance of *N. pachyderma* (sin.) (ca. 50 %) during this time interval in a core slightly west of the current study site, although they analysed a different size fraction (> 150 µm).

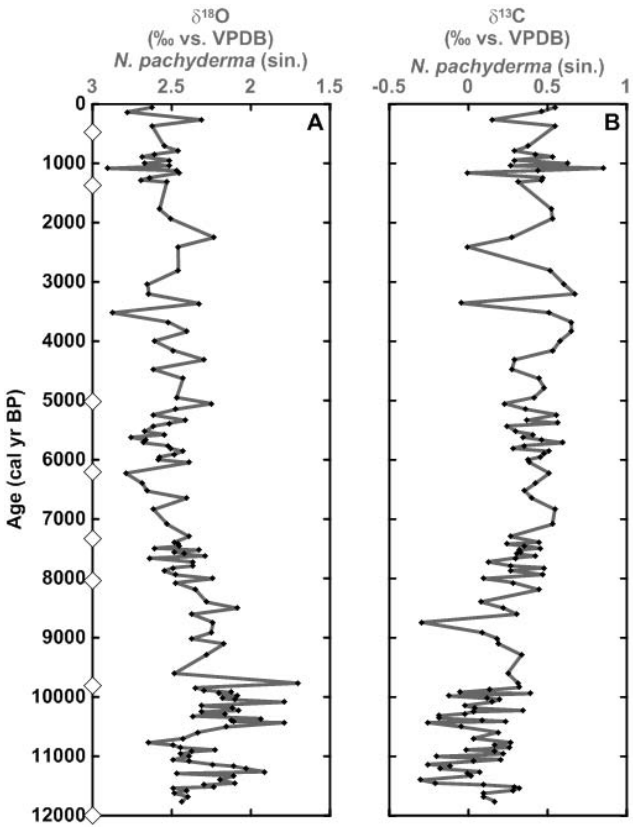

Fig. 5. Stable isotope analysis plotted versus cal yr BP. The white diamonds on the *y* axis denote the AMS ^{14}C converted to calibrated radiocarbon ages. **(A)** δ^{18}O measurements of *N. pachyderma* (sin.) corrected for ice volume effect after Fairbanks (1989). **(B)** δ^{13}C measurements of *N. pachyderma* (sin.).

The relatively low sSST values (ca. 4 °C) throughout this period (Fig. 7d) are ca. 1.5 °C lower than modern day temperatures at 100 m water depth, which argues for an enhanced influence of cold Arctic water at the core site.

Throughout period I, the mean shell weight of *N. pachyderma* (sin.) and the shell fragmentation show the least favourable preservation conditions within the record, likely reflecting increased dissolution (Fig. 7c). The core location is situated above the carbonate compensation depth (CCD); hence, the dissolution must be ascribed to other factors. Dissolution of planktic foraminifera may occur within the water column, at the sediment–water interface and in the sediments (e.g. Lohmann, 1995). Previous research has argued that the dissolution of calcareous material in the Barents Sea is caused by CO_2-rich and corrosive bottom water masses (e.g. Steinsund and Hald, 1994), which may be formed by brine rejection in the marginal ice zone (e.g. Midttun, 1985; Steinsund and Hald, 1994). Furthermore, it has been shown that the influence of seasonal sea ice might also affect the preservation conditions (Huber et al., 2000). For example, when organic material at the marginal ice zone sinks unutilized to the seafloor, the pore waters become undersaturated with respect to calcium carbonate and can thereby contribute to calcite dissolution (Scott et al., 2008). Hence, the dissolution observed in JM09-KA11-GC may provide evidence for the presence of seasonal sea ice conditions during this interval. Previously, dissolution of planktic foraminifera between 11 900 and 9000 cal yr BP was recorded in the central Fram Strait and was attributed to the increased influence of Arctic water, oceanic fronts and the marginal ice zone (Zamelczyk et al., 2012).

The low concentration of planktic foraminifera during this period may also reflect enhanced sea ice conditions (Fig. 7b), especially as areas heavily influenced by sea ice can be almost barren of planktic foraminifera (e.g. Carstens et al., 1997). Previously, a similar low concentration of planktic foraminifera was observed for this period in a core from the south-western Barents Sea, and this was attributed to high sea ice conditions (Aagaard-Sørensen et al., 2010).

Although low δ^{13}C values might be associated with poorly ventilated sub-surface water (Sarnthein et al., 1995), the low δ^{13}C values during period I could also indicate low primary production consistent with a low concentration of planktic foraminifera (Fig. 7f). On the other hand, the high sterol concentrations and TOC (Fig. 7h, Fig. 6c–e) are more consistent with enhanced primary production, probably reflecting marginal ice zone conditions. Hence, the depleted δ^{13}C data more likely suggest a strongly stratified water mass during the early Holocene (period I). This is consistent with previous research from the Barents Sea, where deglaciation processes such as a freshwater influx were suggested to have influenced the top surface water masses (Risebrobakken et al., 2010).

The stable oxygen isotope record in period I shows a general depletion from 11 900 to 10 400 cal yr BP (Fig. 7e). The sSST increases by ca. 1.5 °C during this interval, which could explain the depletion (Fig. 7d). However, it has also been shown that the surface water masses in the Barents Sea were also influenced by melt water from the retreating ice sheets during this period (Gyllencreutz et al., 2008; Risebrobakken et al., 2010). Thus, the depleted δ^{18}O values most likely reflect both a temperature increase and an influence of melt water causing a surface water freshening in the western Barents Sea.

Throughout period I, there is a progressive decrease in IP_{25} concentration (and flux), while the profiles of brassicasterol and 24-methylenecholesterol reveal a strong increasing trend (Fig. 7g–h). These biomarker data likely reflect the abrupt transition from the Younger Dryas into the early Holocene (period I) with an associated reduction in the extent of seasonal sea ice. Previously, a link between enhanced concentrations of 24-methylenecholesterol and sea ice conditions was suggested (Knies, 2005) and later supported by IP_{25} data (Cabedo-Sanz et al., 2013). However, in the current study, the abundance and flux profiles of 24-methylenecholesterol more closely resemble those of brassicasterol, indicating that

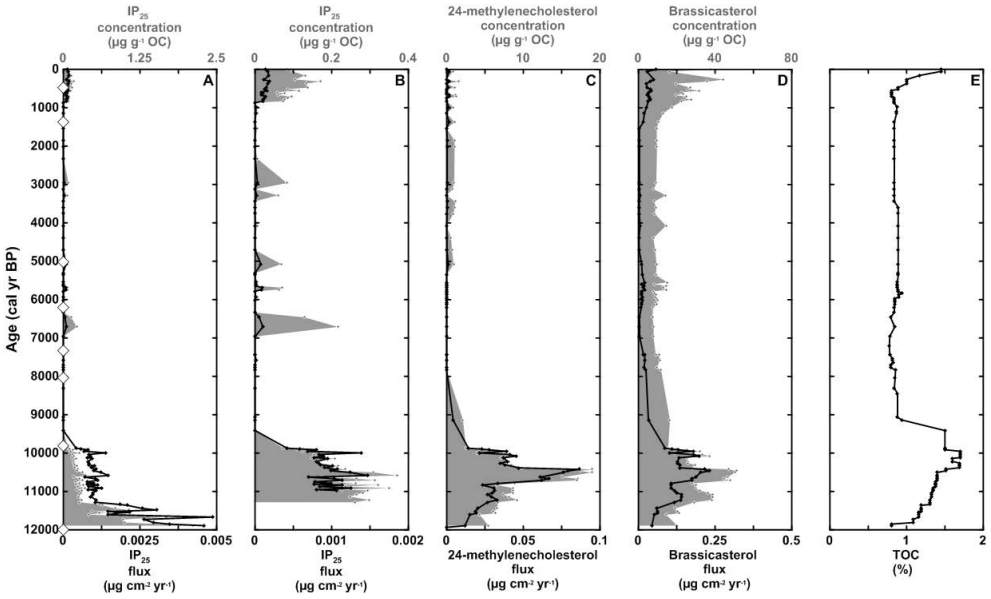

Fig. 6. Biomarker analysis plotted versus cal yr BP. The white diamonds on the *y* axis denote the AMS ^{14}C converted to calibrated radiocarbon ages. Concentration normalized against organic carbon (grey-filled area) and flux (black line) (note the logarithmic scale for the fluxes): **(A)** IP_{25} for the entire record, **(B)** IP_{25} since 11 300 cal yr BP, **(C)** 24-methylenecholesterol, **(D)** brassicasterol and **(E)** total organic carbon.

24-methylenecholesterol is not as selective a biomarker for sea ice as IP_{25}. Further, the presence of IP_{25} (albeit in low concentrations) and relatively high concentrations of both sterols, especially between ca. 10 800 and 10 300 cal yr BP, suggests that during the early Holocene, the study area was probably characterized by periods of sea ice edge conditions or close to the marginal ice zone, since this scenario results generally in enhanced primary production (Smith et al., 1985; Sakshaug, 1997). At the same time, sSST values increase rapidly, whereas δ^{18}O values are depleted, all showing a surface warming which corresponds to previous research in the region (e.g. Sarnthein et al., 2003; Rasmussen et al., 2007; Risebrobakken et al., 2010). However, a depletion in δ^{18}O during this interval for the south-western Barents Sea has also been suggested to reflect surface water freshening caused by seasonal sea ice melting (Aagaard-Sørensen et al., 2010).

Within period I, six data points between 10 900 and 10 700 cal yr BP show a rapid and large increase of *N. pachyderma* (sin.) corresponding to a cooling of ca. 2.5 °C (Figs. 7a, d). Simultaneously, a rapid δ^{18}O enrichment occurs which also reflects this cooling signal (Fig. 7e). Although this abrupt cooling signal is not recorded by the biomarker or δ^{13}C data, it seems to reflect and coincide with the so-called Preboreal Oscillation (PBO). The PBO has previously been recorded throughout the North Atlantic region in different proxy records such as ice core (e.g. Johnsen et al., 1995), terrestrial (e.g. Becker et al., 1991; Björck et al., 1996) and marine palaeo-records (e.g. Hald and Hagen, 1998; Husum and Hald, 2002), and was probably triggered by a melt water outburst hampering the thermohaline convection in the North Atlantic (Björk et al., 1996; Hald and Hagen, 1998; Husum and Hald, 2002).

5.2 Period II: 10 400–7300 cal yr BP (early–mid-Holocene)

The gradual and steady increase of *T. quinqueloba* from 10 400 to 9900 and from 9900 to 7300 cal yr BP, respectively, suggests a change in water masses from Arctic to Atlantic water (Fig. 4b). Previously, Werner et al. (2013) also attributed a high relative abundance of *T. quinqueloba* to a strong influence of Atlantic water during this period.

T. quinqueloba is associated with sub-polar conditions and Atlantic water (Bé and Tolderlund, 1971; Volkmann, 2000). Furthermore, high abundances of *T. quinqueloba* (> 80 %) have been found in close proximity to the sea ice margin in the eastern Fram Strait and northern Barents Sea (Volkmann, 2000). This species responds rapidly to changes in nutrient supply (Reynolds and Thunnel, 1985; Johannessen et al., 1994) and is associated with oceanic front conditions. In the western Barents Sea, it has also been associated with the Arctic front (Burhol, 1994).

Werner et al. (2013) also made a link between high planktic foraminiferal fluxes and ice-free conditions or a fluctuating (seasonal) sea ice margin. Further, *N. incompta* also indicates an increased influence of warmer Atlantic water during period II as it reaches its maximum abundance within the record at the beginning of this interval (Fig. 4c). *N. incompta* is a warm-water indicator, often associated with the inflow of temperate Atlantic water (Bé and Tolderlund, 1971;

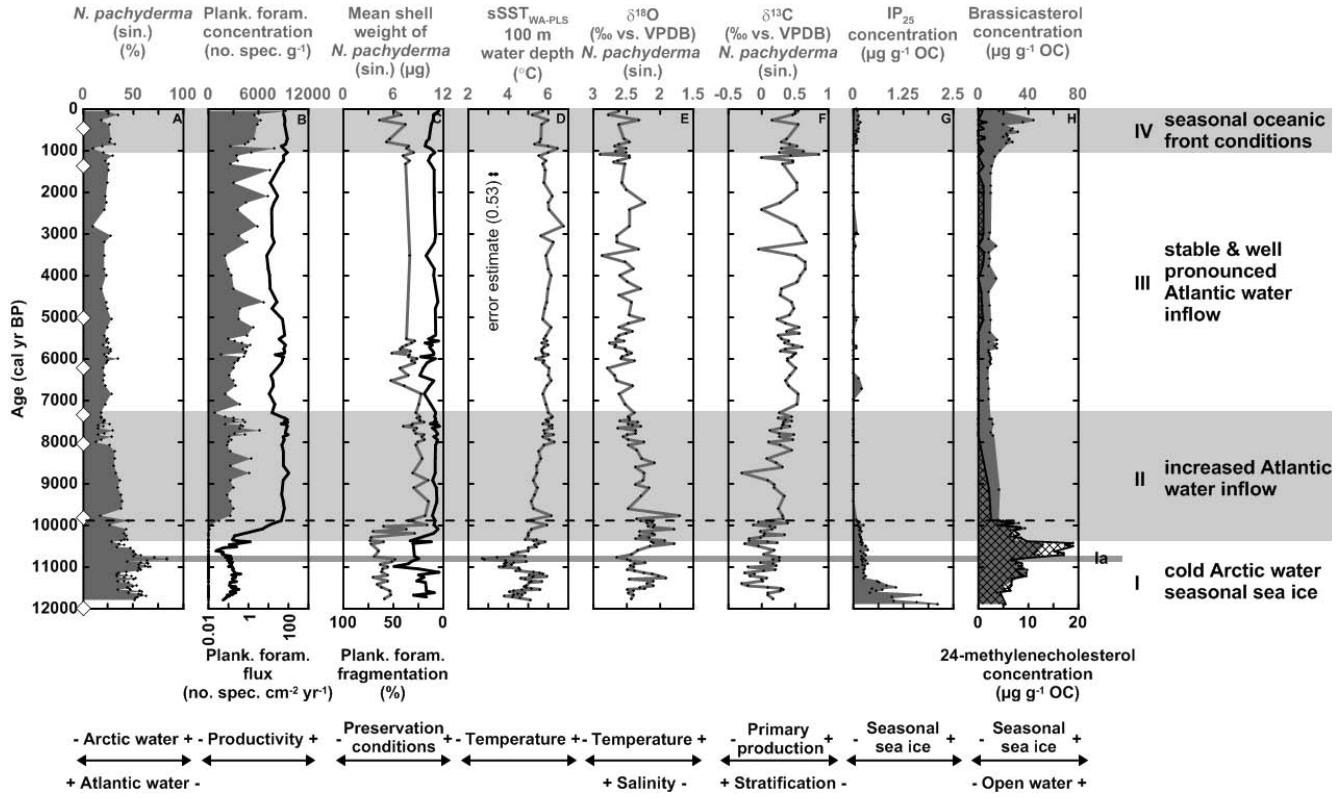

Fig. 7. Summary and palaeoceanographic development interpretation of multi-proxy data plotted versus cal yr BP. The white diamonds on the *y* axis denote the AMS ^{14}C converted to calibrated radiocarbon ages. Samples below the dotted line contain < 300 planktic foraminiferal specimens. **(A)** Relative abundance of *N. pachyderma* (sin.). **(B)** Planktic foraminiferal concentration (grey-filled area) and total planktic foraminiferal flux (black line) (note the logarithmic scale for the flux). **(C)** Mean shell weight of *N. pachyderma* (sin.) (grey line) and planktic foraminiferal fragmentation (black line) (note the reversed axis). **(D)** Reconstructed summer sea surface temperature estimates. **(E)** δ^{18}O measurements of *N. pachyderma* (sin.) corrected for ice volume effect after Fairbanks (1989). **(F)** δ^{13}C measurements of *N. pachyderma* (sin.). **(G)** Seasonal sea ice biomarker IP_{25} concentration normalized against organic carbon. **(H)** Sterol concentration normalized against organic carbon: brassicasterol (grey-filled area) and 24-methylenecholesterol (black-hatched area).

Johannessen et al., 1994; Pflaumann et al., 2003). A similar maximum of *N. incompta* (ca. 20 %) has been observed in previous studies between ca. 9000 and 10 500 cal yr BP in the western Barents Sea and western Svalbard margin (Sarnthein et al., 2003; Ebbesen et al., 2007; Hald et al., 2007). This relatively high abundance of *N. incompta* (before dropping to ca. 10 % towards the mid–late Holocene (period III)) might reflect the previously described Holocene Climate Optimum, which is linked to the increased June solar insolation at high latitudes (e.g. Koç et al., 1993; Kaufman et al., 2004; Hald et al., 2007). However, the sSST record shows a small warming trend, reaching ca. 6 °C around 8000 cal yr BP and remains relatively stable for the rest of the Holocene (Fig. 7d). This temperature trend may simply reflect stability in the temperature of the sub-surface water masses and that only the upper surface layers reflect the solar maximum, as suggested by Andersson et al. (2010). However, the reconstructed sSST also reflects the planktic foraminiferal fauna data, which differ from previous studies in the region with its very high abundance of *T. quinqueloba* (e.g. Sarnthein et al., 2003; Ebbesen et al., 2007; Hald et al., 2007; Risebrobakken et al., 2010). The current study site may be closer to the Arctic front compared to other studies, which may explain the differences in fauna between studies (e.g. Johannessen et al., 1994), although these could also be related to the state of preservation.

From 10 400 to 9900 cal yr BP, the increased shell weight and concomitant decrease in fragmentation indicate a sharp improvement in preservation conditions (Fig. 7c), a feature that was also observed between 10 800 and 8000 cal yr BP in the western Fram Strait (Zamelczyk et al., 2012). Generally good preservation conditions have been linked to Atlantic surface water where the organic matter productivity is lower, the rain of $CaCO_3$ higher and thus the pore waters supersaturated with respect to calcium (Huber et al., 2000; Henrich et al., 2002). Further, according to Edmond and Gieskes (1970), the solubility of $CaCO_3$ increases with decreasing temperatures and increasing salinities and concentrations of CO_2. However, the solubility is also influenced by pressure and thus the water depth of a core site (Archer and Maier-Reimer, 1994). The latter may explain why the dissolution indices

show generally very good preservation conditions for this core site as the water depth is only 345 m.

Dissolution, however, may be selective and is known to affect small species such as *T. quinqueloba* to a greater extent than more resistant thick-shelled species, thus changing the species composition of a foraminiferal assemblage (e.g. Berger, 1970; Thunell and Honjo, 1981; Le and Thunell, 1996). As such, the increased relative abundance of *T. quinqueloba* and the clear increase in total planktic foraminiferal concentrations and fluxes from ca. 10 400 to 9900 cal yr BP may be partially attributed to selective preservation. This selective dissolution might have potential implications for the transfer-function-derived sSST as these depend on the composition of foraminiferal assemblages.

The δ^{13}C values increase continuously throughout the early–mid-Holocene, arguing for a gradual evolution in better-ventilated surface water and/or enhanced primary production (Fig. 7f). The increasing δ^{18}O record suggests increased salinities and/or decreasing temperatures, although the planktic foraminiferal data do not indicate any changes in temperature (Fig. 7e). This increase in salinity is most likely caused by an increased Atlantic water inflow, which supports earlier observations for this time interval (e.g. Risebrobakken et al., 2010).

In terms of the biomarker data, previous studies have shown a strong positive correlation between the presence of IP_{25} and regions of known seasonal sea ice cover, while, temporally, directional changes in IP_{25} are normally consistent with corresponding changes in seasonal sea ice extent (Belt and Müller, 2013). Therefore, the declining trend in IP_{25} concentrations from period I, before disappearing from the record at ca. 9900 cal yr BP (Fig. 7g), is consistent with progressively reduced seasonal sea ice. At the same time, brassicasterol concentrations also reduce, likely reflecting the transitions from a favourable marginal ice zone scenario (c.f. period I) to reduced seasonal sea ice cover and finally open water conditions, which are less productive (Fig. 7h).

Thus, the proxy data identify changing water masses, with a steady increase of Atlantic water inflow in particular. Nonetheless, despite the gradual increase of Atlantic water inflow, Arctic front conditions and the presence of seasonal sea ice remains in the proximity of the core site, at least until ca. 9900 cal yr BP. Previous studies from the Barents Sea have recorded similar oceanic front conditions as well as an inflow of sub-surface Atlantic water during the early Holocene (e.g. Lubinski et al., 1996; Hald et al., 1999; Duplessy et al., 2005; Risebrobakken et al., 2010). The most likely north-eastwards shift of oceanic front conditions throughout the early Holocene has been linked to positive NAO index values, with an increase to the inflow of Atlantic water to the North Atlantic and Barents Sea (e.g. Aagaard-Sørensen et al., 2010).

5.3 Period III: 7300–1100 cal yr BP (mid–late Holocene)

The faunal composition in period III is marked by relatively consistent abundances of all species and a distinct dominance of *T. quinqueloba* (ca. 60 %), possibly suggesting a stable influence of Atlantic water. However, as discussed previously for period II, the high abundance of *T. quinqueloba* differs from earlier published records from this area (e.g. Sarnthein et al., 2003; Hald et al., 2004, 2007; Ebbesen et al., 2007; Werner et al., 2013), which might reflect regional oceanographic differences such as a more general proximity to the Arctic front in the Barents Sea (e.g. Volkmann, 2000; Husum and Hald, 2012). The sea ice biomarker IP_{25} is mainly absent throughout the mid–late Holocene, reflecting predominantly ice-free ocean conditions (Fig. 7g–h), meaning that the marginal ice zone was not at the core site. In contrast, increased IP_{25} concentrations (and hence inferred sea ice conditions) were observed for the West Spitsbergen Shelf during the same interval (Müller et al., 2012), likely reflecting the differences (latitude) between the two study locations.

Although the mean shell weight is slightly lower in period III compared to period II, the preservation indicators are stable throughout the mid–late Holocene (Fig. 7c), which indicates a continuation of the more favourable preservation conditions, most likely linked to the shallow water depth and presence of Atlantic water.

The stability in the relative abundances of the foraminifera is accompanied by a stable sSST record throughout the mid–late Holocene (Fig. 7d). This contrasts earlier reconstructions of SST based on diatoms (Koç et al., 1993) and alkenones (Calvo et al., 2002), which showed a cooling trend throughout the mid–late Holocene. This difference in outcomes might be due to the fact that surface cooling (or warming) that results from variability in insolation may be mainly restricted to the upper ca. 30 m of the water column (Andersson et al., 2010; Risebrobakken et al., 2011). Nonetheless, previous studies of planktic foraminifera in the region have also identified a cooling during the mid–late Holocene (e.g. Sarnthein et al., 2003; Werner et al., 2013). For example, sediment core T88-2 in the south-western Barents Sea showed a less pronounced optimum ending at 6300 cal yr BP, while sediment core MD99-2304 at the western Svalbard margin has a clear optimum ending at 8600 cal yr BP (Ebbesen et al., 2007; Hald et al., 2007; Husum and Hald, 2012). These differences are most likely due to the different study locations reflecting different water masses and settings. The SST reconstructions based on foraminiferal transfer functions do not reflect any changes of nutrition. *T. quinqueloba* depends on somewhat warmer and/or nutritious water masses (e.g. Volkmann, 2000), and hence a minor cooling signal may not be reflected if the nutrition is unchanged.

In general, the planktic foraminiferal concentrations and fluxes remain stable throughout the mid–late Holocene, suggesting that the environmental conditions remained relatively stable and favourable for planktic foraminifera throughout

this period. The consistent δ^{13}C data between 7300 and 1100 cal yr BP indicate less stratified water masses compared to the early and early–mid-Holocene, probably due to a single, well-mixed Atlantic water mass (Fig. 7f). Together with the relative warm and stable sSST values, the δ^{18}O record most likely reflects stable and high salinities throughout the mid–late Holocene and thereby indicates a stable and strong Atlantic water inflow, consistent with the outcomes from other records (e.g. Risebrobakken et al., 2010) (Fig. 7e).

5.4 Period IV: 1100–0 cal yr BP (late Holocene–present)

During the last 1100 cal yr BP, the planktic foraminiferal fauna changes slightly compared to period III, showing a minor increase of *G. glutinata* and a larger increase of *G. uvula* (Fig. 4d, e). The cosmopolitan species *G. glutinata* has also been associated with warm-water masses (Hemleben et al., 1989). *G. uvula* is a high-latitude species indicative of a high food supply and high abundances are associated with the productive zone connected with oceanic fronts (Saito et al., 1981; Boltovskoy et al., 1996; Bergami et al., 2009). Further, *G. uvula* is also connected with slightly reduced salinities and is found in high numbers in the coastal water in the south-western Barents Sea (Husum and Hald, 2012).

The sSST and δ^{18}O values might indicate a minor cooling in this period; however, the mean values are only 5.7 °C and −0.23 ‰ compared to 5.9 °C and −0.20 ‰ in the preceding period (Fig. 7d, e). The δ^{18}O values may also indicate a minor increase in salinity, but the planktic foraminiferal fauna very clearly shows slightly lower salinities in the sub-surface waters at this time. This corresponds well with previous findings that have shown a reduced salinity or freshening of the uppermost surface layer with concomitant increases in sea ice conditions during the past ca. 3000 cal yr BP in the Fram Strait (Werner et al., 2013). Additionally, a reduced salinity in the upper water masses was also observed between 2500 and 0 cal yr BP in the southern Barents Sea (Risebrobakken et al., 2010). However, Risebrobakken et al. (2010) further found that the episodes of reduced salinity were also associated with lower temperatures, which is not seen clearly in the current study. The fluctuating absence and presence of IP_{25} (at very low concentrations) and increasing brassicasterol concentrations during the last ca. 1100 cal yr BP suggests that this area experienced sea ice conditions, with alternating periods of ice-free conditions and low occurrences of seasonal sea ice close to the core site (Fig. 7g–h). A similar observation of frequently fluctuating sea ice conditions was made by Müller et al. (2012) for the West Spitsbergen Shelf, although these conditions were observed after ca. 3000 cal yr BP. Such conditions are similar to those of the present day, based on satellite imagery and biomarker reconstructions (Navarro-Rodriguez et al., 2013).

The occurrence of seasonal sea ice may also explain the decreased mean shell weight of *N. pachyderma* (sin.) as a result of some dissolution; however the fragmentation remains relatively stable (Fig. 7c). The dissolution is probably caused by the presence of sea ice as seasonal sea ice might also affect the preservation conditions (e.g. Huber et al., 2000).

The planktic foraminiferal concentration reaches its maximum value of the entire record during this period (Fig. 7b) and, together with the slightly enriched δ^{13}C values (Fig. 7f), indicates higher primary productivity associated with the oceanic front conditions. The δ^{13}C values could also reflect more stratified water masses due to a decreased influence of Atlantic water. Nonetheless, the sSST and δ^{18}O values do not show a clear cooling, which could indicate a reduced inflow of Atlantic water. Other proxies – such as coccoliths, benthic foraminifera, benthic stable isotopes (δ^{18}O) and grain size analysis – have also been investigated within the current sediment core. These show relatively stable temperatures in addition to suggesting an increased inflow of Atlantic water to the core site during this time interval (Dylmer et al., 2013; Groot et al., 2013), hence providing further evidence for stratification of the upper water column.

The sSST and planktic δ^{18}O values from the current study do not show the same cooling trend of the surface water masses during the late Holocene as found by others in the eastern Nordic Seas (e.g. Koç et al., 1993; Calvo et al., 2002; Risebrobakken et al., 2010), although it is noted that Arctic planktic foraminifera may not reflect the decreasing insolation due to their depth habitat (Andersson et al., 2010; Risebrobakken et al., 2011). The reappearance of some seasonal sea ice may be attributed to decreasing insolation, which may have caused more severe winter and sea ice conditions and hence increasing the seasonal difference. In support of this, Jernas et al. (2013) have also observed a stronger influence of seasonal (spring/summer) inflow of Atlantic water at this time at the western Svalbard margin. Werner et al. (2013) also suggest a slight re-strengthening of Atlantic water inflow based on their SST record after ca. 3000 cal yr BP, while they also observe an increase of sea ice conditions.

6 Conclusions

This paper presents a multi-proxy study of sub-surface and sea ice conditions in the western Barents Sea throughout the Holocene.

The early Holocene (11 900–10 400 cal yr BP) was characterized by cold water and a reduced Atlantic water inflow. The planktic foraminiferal fauna is dominated by the polar species *N. pachyderma* (sin.) and the sSST values were found to be around 4 °C. Stable oxygen isotope values are ca. −0.75 ‰, reflecting a surface freshening. The core site was also characterized by the transition from severe sea ice conditions at the termination of the Younger Dryas to a marginal ice zone scenario that was favourable for primary production.

Within the early Holocene, a short-term cooling event is shown by both the planktic fauna and the stable isotopes from 10 900–10 700 cal yr BP and is correlated with the so-called

Preboreal Oscillation, which is found throughout the North Atlantic region.

During the early–mid-Holocene (10 400–7300 cal yr BP), Atlantic water inflow increases as shown by planktic foraminiferal fauna dominated by *T. quinqueloba* and enriched δ^{18}O values reflecting increased salinity. Biomarkers indicate a decline in seasonal sea ice extent and the sSST record reaches values of 6 °C at ca. 8000 cal yr BP and remains relatively stable for the rest of the record.

Throughout the mid–late Holocene (7300–1100 cal yr BP), environmental conditions are stable with a pronounced inflow of Atlantic water with relatively warm sub-surface temperatures around 5.9 °C, predominantly ice-free conditions and δ^{18}O values reflecting stable high salinities.

Within the late Holocene (1100–0 cal yr BP), the planktic foraminiferal fauna changes slightly, with a higher abundance of *G. uvula* showing a reduced salinity. The sSST and δ^{18}O values may indicate a very minor cooling, but overall the values do not decrease compared to the mid–late Holocene. The presence of IP_{25}, in particular, suggests a reappearance of low-frequency seasonal sea ice. In general, all proxies from this period fluctuate rapidly, indicating more unstable oceanographic conditions.

Acknowledgements. This work was carried out within the framework of the Initial Training Network programme "Changing Arctic and Subarctic Environment" (CASE, grant agreement no. 238111) funded by the European Commission within the 7th Framework Programme FP7 2007/2013, Marie-Curie Actions and the University of Tromsø. Further, the project "Glaciations in the Barents Sea Area" (GlaciBar) funded by the Research Council of Norway, Statoil, Det Norske, British Gas and the University of Tromsø is acknowledged for providing the marine sediment core and CTD data from the core site. Jan P. Holm helped prepare the maps. Thanks are also extended to one anonymous reviewer and Juliane Müller for their helpful and informative reviews.

Edited by: J. Knies

References

Aagaard-Sørensen, S., Husum, K., Hald, M., and Knies, J.: Paleoceanographic development in the SW Barents Sea during the Late Weichselian-Early Holocene transition, Quaternary Sci. Rev., 29, 1–15, 2010.

Andersen, C., Koç, N., Jennings, A. E., and Andrews, J. T.: Nonuniform response of the major surface currents in the Nordic Seas to insolation forcing: implications for the Holocene climate variability, Paleoceanography, 19, PA2003, doi:10.1029/2002PA000873, 2004.

Andersson, C., Risebrobakken, B., Jansen, E., and Dahl, S.O.: Late Holocene surface ocean conditions of the Norwegian Sea (Vöring Plateau), Paleoceanography, 18, 1044, doi:10.1029/2001PA000654, 2003.

Andersson, C., Pausata, F. S. R., Jansen, E., Risebrobakken, B., and Telford, R. J.: Holocene trends in the foraminifer record from the Norwegian Sea and the North Atlantic Ocean, Clim. Past, 6, 179–193, doi:10.5194/cp-6-179-2010, 2010.

Archer, D.: A data-driven model of the global calcite lysocline, Global Biogeochem. Cy., 10, 511–526, 1996.

Archer, D. and Maier-Reimer, E.: Effect of deep-sea sedimentary calcite preservation on atmospheric CO_2 concentration, Nature, 367, 260–263, 1994.

Aure, J. and Strand, Ø.: Hydrographic normals and long-term variations at fixed surface layer stations along the Norwegian coast from 1936 to 2000, Fisken og Havet, 13, 1–24, 2001.

Barker, S. and Elderfield, H.: Foraminiferal calcification response to glacial interglacial changes in atmospheric CO_2, Science, 297, 883–836, 2002.

Barker, S., Kiefer, T., and Elderfield, H.: Temporal changes in North Atlantic circulation constrained by planktonic foraminiferal shell weights, Paleoceanography, 19, PA3008, doi:10.1029/2004PA001004, 2004.

Bauch, H. A. and Weinelt, M. S.: Surface water changes in the Norwegian Sea during last deglacial and Holocene times, Quaternary Sci. Rev., 16, 1115–1124, 1997.

Bé, A. W. H. and Tolderlund, D. S.: Distribution and ecology of living planktonic foraminifera in surface waters of the Atlantic and Indian Oceans, in: The micropaleontology of oceans, edited by: Funnel, B. M. and Riedel, W. R., Cambridge University Press, London, 1–100, 1971.

Becker, B., Kromer, B., and Trimborn, P.: A stable isotope tree-ring timescale of the Late Glacial/Holocene boundary, Nature, 353, 647–649, 1991.

Beer, C. J., Schiebel, R., and Wilson, P. A.: Testing planktic foraminiferal shell weight as a surface water [CO_3^{2-}] proxy using plankton net samples, Geology, 38, 103–106, 2010.

Belt, S. T. and Müller, J.: The Arctic sea ice biomarker IP_{25}: a review of current understanding, recommendations for future research and applications in palaeo sea ice reconstructions, Quaternary Sci. Rev., 79, 9–25, doi:10.1016/j.quascirev.2012.12.001, 2013.

Belt, S. T., Masseé, G., Rowland, S. J., Poulin, M., Michel, C., and LeBlanc, B.: A novel chemical fossil of palaeo sea ice: IP_{25}, Org. Geochem., 38, 16–27, 2007.

Belt, S. T., Brown, T. A., Navarro Rodriguez, A., Cabedo Sanz, P., Tonkin, A., and Ingle, R.: A reproducible method for the extraction, identification and quantification of the Arctic sea ice proxy IP_{25} from marine sediments, Anal. Method., 4, 705–713, 2012.

Bergami, C., Capotondi, L., Langone, L., Giglio, F., and Ravaioli, M.: Distribution of living planktonic foraminifera in the Ross Sea and the Pacific sector of the Southern Ocean (Antarctica), Mar. Micropaleontol., 73, 37–48, 2009.

Berger, A.: Long-term variations of daily insolation and quaternary climatic changes, J. Atmos. Sci., 35, 2363–2367, 1978.

Berger, W. H.: Planktonic foraminifera: Selective solution and the lysocline, Mar. Geol., 8, 111–138, 1970.

Birks, H. J. B.: Quantitative palaeoenvironmental reconstructions, in: Statistical modelling of quaternary science data, edited by: Maddy, D. and Brew, J. S., Quaternary Research Association, Cambridge, UK, 116–254, 1995.

Birks, C. J. A. and Koç, N.: A high-resolution diatom record of late-quaternary sea-surface temperatures and oceanographic conditions from the eastern Norwegian Sea, Boreas, 31, 323–344, 2002.

Björck, S., Kromer, B., Johnsen, S., Bennike, O., Hammarlund, D., Lemdahl, G., Possnert, G., Rasmussen, T. L., Wohlfarth, B., Hammer, C. U., and Spurk, M.: Synchronized terrestrial atmospheric deglacial records around the North Atlantic, Science, 274, 1155–1160, 1996.

Blindheim, J.: The seas of Norden, in: Norden: Man and environment, edited by: Varjo, U. and Tietze, W., Gebrüder Borntraeger, Berlin, 20–32, 1987.

Boltovskoy, E., Boltovskoy, D., Correa, N., and Brandini, F.: Planktic foraminifera from the southwestern Atlantic (30°–60°S): Species-specific patterns in the upper 50 m, Mar. Micropaleontol., 28, 53–72, 1996.

Bond, G., Showers, W., Cheseby, M., Lotti, R., Almasi, P., deMenocal, P., Priore, P., Cullen, H., Hajdas, I., and Bonani, G.: A pervasive millennial-scale cycle in North Atlantic Holocene and glacial climates, Science, 278, 1257–1266, 1997.

Broecker, W. S.: The great ocean conveyor. Oceanography, 4, 79–89, 1991.

Broecker, W. S. and Clark, E.: An evaluation of Lohmann's foraminifera weight dissolution index, Paleoceanography, 16, 531–534, 2001.

Brown, T. A. and Belt, S. T.: Identification of the sea ice diatom biomarker IP_{25} in Arctic benthic macrofauna: Direct evidence for a sea ice diatom diet in Arctic heterotrophs, Polar Biol., 35, 131–137, 2012.

Brown, T. A., Belt, S. T., Philippe, B., Mundy, C. J., Massé, G., Poulin, M., and Gosselin, M.: Temporal and vertical variations of lipid biomarkers during a bottom ice diatom bloom in the Canadian Beaufort Sea: Further evidence for the use of the IP_{25} biomarker as a proxy for spring Arctic sea ice, Polar Biol., 34, 1857–1868, 2011.

Burhol, A. L. S.: Recent distribution of planktonic foraminifera on the Svalbard-Barents margin, Master Thesis, University of Tromsø, Norway, 1994.

Cabedo-Sanz, P., Belt, S. T., Knies, J., and Husum, K: Identification of contrasting seasonal sea ice conditions during the Younger Dryas, Quaternary Sci. Rev., 79, 74–86, 2013.

Calvo, E., Grimalt, J., and Jansen, E.: High resolution U^{37}_K sea surface temperature reconstruction in the Norwegian Sea during the Holocene, Quaternary Sci. Rev., 21, 1385–1394, 2002.

Carstens, J., Hebbeln, D., and Wefer, G.: Distribution of planktic foraminifera at the ice margin in the Arctic (Fram Strait), Mar. Micropaleontol., 29, 257–269, 1997.

Cifelli, R.: Globigerina incompta, a new species of pelagic foraminifera from the North Atlantic, Contributions Cushman Foundation Foraminiferal Research, 12, 83–86, 1961.

Comiso, J. C., Parkinson, C. L., Gersten, R., and Stock, L.: Accelerated decline in the Arctic sea ice cover, Geophys. Res. Lett., 35, L01703, doi:10.1029/2007GL031972, 2008.

Conan, S. M. H., Ivanova, E. M., and Brummer, G. J. A.: Quantifying carbonate dissolution and calibration of foraminiferal dissolution indices in the Somali Basin, Mar. Geol., 182, 325–349, 2002.

Darling, K. F., Kucera, M., Kroon, D., and Wade, C. M.: A resolution for the coiling direction paradox in Neogloboquadrina pachyderma, Paleoceanography, 21, PA2011, doi:10-1029/2005PA001189, 2006.

Dieckmann, G. S. and Hellmer, H. H.: The importance of sea ice: An overview, in: Sea ice: An introduction to its physics, chemistry, biology and geology, edited by: Thomas, D. N. and Dieckmann, G. S., Blackwell Science Ltd, Oxford, UK, doi:10.1002/9780470757161.ch1, 2008.

Duplessy, J. C., Ivanova, E., Murdmaa, I., Paterne, M., and Labeyrie, L.: Holocene paleoceanography of the northern Barents Sea and variations of the northward heat transport by the Atlantic Ocean, Boreas, 30, 2–16, 2001.

Duplessy, J. C., Cortijo, E., Ivanova, E., Khusid, T., Labeyrie, L., Levitan, M., Murdmaa, I., and Paterne, M.: Paleoceanography of the Barents Sea during the Holocene, Paleoceanography, 20, A4004, doi:10.1029/2004PA001116, 2005.

Dylmer, C. V., Giraudeau, J., Eynaud, F., Husum, K., and De Vernal, A.: Northward advection of Atlantic water in the eastern Nordic Seas over the last 3000 yr: A coccolith investigation of volume transport and surface water changes, Clim. Past, 9, 1505–1518, doi:10.5194/cp-9-1505-2013, 2013.

Ebbesen, H., Hald, M., and Eplet, T. H.: Late glacial and early Holocene climatic oscillations on the western Svalbard margin, European Arctic, Quaternary Sci. Rev., 26, 1999–2011, 2007.

Edmond, J. M. and Gieskes, T. M.: On the calculation of the degree of saturation of sea water with respect to calcium carbonate under in situ conditions, Geochim. Cosmochim. Acta, 35, 1261–1291, 1970.

Ehrmann, W. U. and Thiede, J.: History of Mesozoic and Cenozoic sediment fluxes to the North Atlantic Ocean, Contributions to Sedimentology E. Schweizerbart'sche Verlagsbuchhandlung, Stuttgart, 15, 1-109, ISBN 3-510-57015-4, 1985.

Eynaud, F.: Planktonic foraminifera in the Arctic: Potentials and issues regarding modern and quaternary populations, IOP Conf. Series: Earth and Environmental Science, 14, 2011.

Fairbanks, R. G.: A 17 000-year glacia-eustatic sea level record: Influence of glacial melting rates on the Younger Dryas event and deep-ocean circulation, Nature, 342, 637–642, 1989.

Francis, J. A., Chan, W., Leathers, D. J., Miller, J. R., and Veron, D. E.: Winter Northern Hemisphere weather patterns remember summer Arctic sea-ice extent, Geophys. Res. Lett., 36, L07503, doi:10.1029/2009GL037274, 2009.

Giraudeau, J., Jennings, A. E., and Andrews, J. T.: Timing and mechanisms of surface and intermediate water circulation changes in the Nordic seas over the last 10,000 cal years: A view from the north Iceland shelf, Quaternary Sci. Rev., 23, 212-7-2139, 2004.

Goosse, H. and Holland, M.: Mechanisms of decadal and interdecadal Arctic variability in the Community Climate System Model CCSM2, J. Climate, 18, 3552–3570, 2005.

Groot, D. E., Aagaard-Sørensen, S., and Husum, K.: Reconstruction of Atlantic Water variability during the Holocene in the western Barents Sea, Clim. Past Discuss., 9, 4293–4322, doi:10.5194/cpd-9-4293-2013, 2013.

Gyllencreutz, R., Mangerud, J., Svendsen, J. I., and Lohne, Ø.: Reconstructing growth and decay of the Eurasian ice sheet during the Late Weichselian, 33rd International Geological Congress (33IGC), 6–14 August 2008, HPQ01805L, available at: http://www.cprm.gov.br/33IGC/1345819.html, 2008.

Hald, M. and Hagen, S.: Early preboreal cooling in the Nordic Sea region triggered by meltwater, Geology, 26, 615–618, 1998.

Hald, M., Kolstad, V., Polyak, L., Forman, S. L., Herlihy, F. A., Ivanov, G., and Nesheretov, A.: Late-glacial and Holocene paleoceanography and sedimentary environments in the St. Anna

trough, Eurasian Arctic Ocean margin, Paleoceanography, Paleoclimatology, Palaecology, 146, 229–249, 1999.

Hald, M., Ebbesen, H., Forwick, M., Godtliebsen, F., Khomenko, L., Korsun, S., Ringstad Olsen, L., and Vorren, T. O.: Holocene paleoceanography and glacial history of the West Spitsbergen area, Euro-Arctic margin, Quaternary Sci. Rev., 23, 2075–2088, 2004.

Hald, M., Andersson, C., Ebbesen, H., Jansen, E., Klitegaard-Kristensen, D., Risebrobakken, B., Salomonsen, G. R., Sejrup, H. P., Sarnthein, M., and Telford, R.: Variations in temperature and extent of Atlantic water in the northern North Atlantic during the Holocene, Quaternary Sci. Rev., 26, 3423–3440, 2007.

Hemleben, C., Spindler, M., and Anderson, O. R.: Modern planktonic foraminifera, Springer, New York, 363 pp., 1989.

Henrich, R., Baumann, K. H., Huber, R., and Meggers, H.: Carbonate preservation records of the past 3Myr in the Norwegian-Greenland Sea and the northern North Atlantic: Implications for the history of NADW production, Mar. Geol., 184, 17–39, 2002.

Hopkins, T. S.: The GIN Sea: A synthesis of its physical oceanography and literature review, 1972–1985, Earth Sci. Rev., 30, 175–318, 1991.

Huber, R., Meggers, H., Baumann, K. H., and Henrich, R.: Recent and Pleistocene carbonate dissolution in sediments of the Norwegian-Greenland Sea, Mar. Geol., 165, 123–136, 2000.

Husum, K. and Hald, M.: Early Holocene cooling events in Malangenfjord and the adjoining shelf, north-east Norwegian Sea, Polar Res., 21, 267–274, 2002.

Husum, K. and Hald, M.: A continuous marine record 8000–1600 cal. yr BP from the Malangenfjord, north Norway: Foraminiferal and isotopic evidence, Holocene, 14, 877–887, 2004.

Husum, K. and Hald, M.: Arctic planktic foraminiferal assemblages: Implications for subsurface temperature reconstructions, Mar. Micropaleontol., 96–97, 38–47, 2012.

Imbrie, J. and Kipp, N. G.: A new micropaleontological method for quantitative paleoclimatology: Applications to a late Pleistocene Caribbean core, in: Late Cenozoic Glacial Ages, edited by: Turkian, K. K., Yale University Press, New Haven, 71–191, 1971.

Jennings, A., Knudsen, K. L., Hald, M., Hansen, C. V., and Andrews, J. T.: A mid-Holocene shift in Arctic sea-ice variability on the East Greenland shelf, Holocene, 12, 49–58, 2002.

Jernas, P., Klitgaard Kristensen, D., Husum, K., Wilson, L., and Koç, N.: Palaeoenvironmental changes of the last two millennia on the western and northern Svalbard shelf, Boreas, 42, 236–255, 2013.

Jiang, H., Seidenkrantz, M. S., Knudsen, K. L., and Eiriksson, J.: Late-Holocene summer sea-surface temperatures based on a diatom record from the north Icelandic shelf, Holocene, 12, 137–147, 2002.

Johannessen, T., Jansen, E., Flatøy, A., and Ravelo, A. C.: The relationship between surface water masses, oceanographic fronts and plaeoclimatic proxies in surface sediments of the Greenland, Iceland, Norwegian Seas, NATO, ASI Series, 61–86, 1994.

Johnsen, S., Dahl-Jensen, D., Dansgaard, W., and Gundestrup, N.: Greenland paleotemperatures derived from GRIP bore hole temperature and ice core isotope profiles, Tellus, 5, 624–629, 1995.

Jonkers, L., Brummer, G-J. A., Peeters, F. J. C., van Aken, H. M., and De Jong, M. F.: Seasonal stratification, shell flux, and oxygen isotope dynamics of left-coiling N. pachyderma and T. quinqueloba in the western sub polar North Atlantic, Paleoceanography, 25, PA2204, doi:10.1029/2009PA001849, 2010.

Juggins, S.: C2 1.7.2, available at: http://www.staff.ncl.ac.uk/staff/stephen.juggins/ (last access: 6 March 2013), 2010.

Kaufman, D., Ager, T. A., Anderson, N. J., Anderson, P. M., Andrews, J. T., Bartlein, P. J., Brubakker, L. B., Coats, L. L., Cwynar, L. C., Duvall, M. L., Dyke, A. S., Edwards, M. E., Eisner, W. R., Gajewski, K., Geirsdottir, A., Hu, F. S., Jennings, A. E., Kaplan, M. R., Kerwin, M. W., Loshkin, A. V., MacDonald, G. M., Miller, G. H., Mock, C. J., Oswald, W. W., Otto-Bliesner, B. L., Porinchu, D. F., Rühland, K., Smol, J. P., Steig, E. J., and Wolfe, B. B.: Holocene thermal maximum in the western Arctic (0–180° N), Quaternary Sci. Rev., 23, 529–560, 2004.

Kinnard, C., Zdanowicz, C. M., Fisher, A. F., Isaksson, E., de Vernal, A., and Thompson, L. G.: Reconstructed changes in Arctic sea ice over the past 1,450 years, Nature, 479, 509–512, doi:10.1038/nature10581, 2011.

Knies, J.: Climate-induced changes in sedimentary regimes for organic matter supply on the continental shelf off northern Norway, Geochim. Cosmochim. Acta, 69, 4631–4647, 2005.

Knudsen, K. L.: Foraminiferer i Kvartær stratigrafi: Laboratorie og fremstillingsteknik samt udvalgte eksempler, Geologisk Tidsskrift, 3, 1–25, 1998.

Koç, N. and Jansen, E.: Response of the high-latitude Northern hemisphere to orbital climate forcing: evidence from the Nordic Seas, Geology, 22, 523–526, 1994.

Koç, N., Jansen, E., and Haflidason, H.: Paleoceanographic reconstructions of surface ocean conditions in the Greenland, Iceland and Norwegian seas through the last 14 ka based on diatoms, Quaternary Sci. Rev., 12, 115–140, 1993.

Kucera, M., Weinelt, M., Kiefer, T., Pflaumann, U., Hayes, A., Weinelt, M., Chen, M. T., Mix, A. C., Barrows, T. T., and Cortijo, E.: Reconstruction of sea-surface temperatures from assemblages of planktonic foraminifera: Multi-technique approach based on geographically constrained calibration data sets and its application to glacial Atlantic and Pacific Oceans, Quaternary Sci. Rev., 24, 951–998, 2005.

Kvingedal, B.: Sea-ice extent and variability in the Nordic Seas, 1967-2002, in: The Nordic seas: An integrated perspective, edited by: Drange, H., Dokken, T., Furevik, T., Gerdes, R., and Berger, W., American Geophysical Union, Geophysical Monograph, 158, 39–49, 2005.

Laskar, J., Robutel, P., Joutel, F., Gastineau, M., Correia, A. C. M., and Levrard, B.: A long-term numerical solution for the insolation quantities of the Earth, Astron. Astrophys., 428, 261–285, 2004.

Le, J. and Shackleton, N. J.: Carbonate dissolution fluctuations in the western equatorial Pacific during the late Quaternary, Paleoceanography, 7, 21–42, 1992.

Le, J. N. and Thunell, R. C.: Modelling planktic foraminiferal assemblage changes and application to sea surface temperature estimation in the western equatorial Pacific Ocean, Mar. Micropaleontol., 28, 211–229, 1996.

Loeng, H.: Features of the physical oceanographic conditions of the Barents Sea, Polar Res., 10, 5–18, 1991.

Lohmann, G. P.: A model for variation in the chemistry of planktonic foraminifera due to secondary calcification and selective dissolution, Paleoceanography, 10, 445–457, 1995.

Lubinski, D. J., Korsun, S., Polyak, L., Forman, S. L., Lehman, S. J., Herlihy, F. A., and Miller, G. H.: The last deglaciation of the Franz Victoria Trough, northern Barents Sea, Boreas, 25, 89–100, 1996.

Mangerud, J. and Gulliksen, S.: Apparent radiocarbon ages of recent marine shells from Norway, Spitsbergen, and Arctic Canada, Quaternary Res., 5, 263–273, 1975.

Mangerud, J., Bondevik, S., Gulliksen, S., Hufthammer, A. K., and Høisæter, T.: Marine 14C reservoir ages for 19th century whales and molluscs from the Nordic Atlantic, Quaternary Sci. Rev., 25, 3228–3245, 2006.

Midttun, L.: Formation of dense bottom water in the Barents Sea, Deep-Sea Res., 32, 1233–1241, 1985.

Moros, M., Emeis, K., Risebrobakken, B., Snowball, I., Kuijpers, A., McManus, J., and Jansen, E.: Sea surface temperatures and ice rafting in the Holocene North Atlantic: Climate influences on northern Europe and Greenland, Quaternary Sci. Rev., 23, 2113–2126, 2004.

Müller, J., Massé, G., Stein, R., and Belt, S. T.: Variability of sea-ice conditions in the Fram Strait over the past 30 000 years, Nature Geosci., 2, 772–776, 2009.

Müller, J., Wagner, A., Fahl, K., Stein, R., Prange, M., and Lohman, G.: Towards quantitative sea ice reconstructions in the northern North Atlantic: A combined biomarker and numerical modelling approach, Earth Planet. Sci. Lett., 306, 137–148, 2011.

Müller, J., Werner, K., Stein, R., Fahl, K., Moros, M., and Jansen E.: Holocene cooling culminates in sea ice oscillations in Fram Strait, Quaternary Sci. Rev., 47, 1–14, 2012.

Navarro-Rodriguez, A., Belt, S. T., Knies, J., Brown, T. A.: Mapping recent sea ice conditions in the Barents Sea using the proxy biomarker IP_{25}: implications for palaeo sea ice reconstructions, Quaternary Sci. Rev., 79, 26–36, 2013.

Orvik, K. A. and Skagseth, Ø.: The impact of the wind stress curl in the North Atlantic on the Atlantic inflow to the Norwegian Sea toward the Arctic, Geophys. Res. Lett., 30, 1884, doi:10.1029/2003GL017932, 2003.

Pflaumann, U., Sarnthein, M., Chapman, M., d'Abreu, L., Funnell, B., Huels, M., Kiefer, T., Maslin, M., Schulz, H., Swallow, J., van Kreveld, S., Vautravers, M., Vogelsang, E., and Weinelt, M.: Glacial North Atlantic sea-surface conditions reconstructed by GLAMAP 2000, Paleoceanography, 18, 1065, doi:10.1029/2002PA000774, 2003.

Polyak, L., Alley, R. B., Andrews, J. T., Brigham-Grette, J., Cronin, T. M., Darby, D. A., Dyke, A. S., Fitzpatrick, J. J., Funder, S., Holland, M., Jennings, A. E., Miller, G. H., O'Regan, M., Savelle, J., Serreze, M., John, K. S., White, J. W. C., and Wolff, E.: History of sea ice in the Arctic, Quaternary Sci. Rev., 29, 1757–1778, 2010.

Pufhl, H. A. and Shackleton, N. J.: Two proximal, high-resolution records of foraminiferal fragmentation and their implications for changes in dissolution, Deep-Sea Res. Pt. I, 51, 809–832, 2004.

Rasmussen, T. L., Thomsen, E., Slubowska, M. A., Jessen, S., Solheim, A., and Koç, N.: Paleoceanographic evolution of the SW Svalbard margin (76 ° N) since 20,000 ^{14}C yr BP, Quaternary Res., 67, 100–114, 2007.

Reimer, P. J., Bard, E., Bayliss, A., Beck, J. W., Blackwell, P. G., Ramsey, C. B., Buck, C. E., Cheng, H., Edwards, R. L., Friedrich, M., Grootes, P. M., Guilderson, T. P., Haflidason, H., Hajdas, I., Hatté, C., Heaton, T. J., Hoffmann, D. L., Hogg, A. G., Hughen, K. A., Kaiser, K. F., Kromer, B., Manning, S. W., Niu, M., Reimer, R. W., Richards, D. A., Scott, E. M.; Southon, J. R., Staff, R. A., Turney, C. S. M., and Van Der Plicht, J.: IntCal13 and Marine13 radiocarbon age calibration curves, 0–50 000 years cal BP, Radiocarbon, 55, 1869–1887, 2013.

Reynolds, L. and Thunnel, R. C.: Seasonal succession of planktonic foraminifera in the subpolar North Pacific, J. Foramin. Res., 15, 282–301, 1985.

Risebrobakken, B., Jansen, E., Andersson, C., Mjelde, E., and Hevrøy, K.: A high-resolution study of Holocene paleoclimatic and paleoceanographic changes in the Nordic Seas, Paleoceanography, 18, 1017, doi:10.1029/2002PA000764, 2003.

Risebrobakken, B., Morros, M., Ivanova, E. V., Chistyakova, N., and Rosenberg, R.: Climate and oceanographic variability in the SW Barents Sea during the Holocene, Holocene, 20, 609–621, 2010.

Risebrobakken, B., Dokken, T., Smedsrud, L. H., Andersson, C., Jansen, E., Moros, M., and Ivanova, E. V.: Early Holocene temperature variability in the Nordic Seas: The role of oceanic heat advection versus changes in orbital forcing, Paleoceanography, 26, PA4206, doi:10.1029/2011PA002117, 2011.

Rousse, S., Kissel, C., Laj, C., Eiriksson, J., and Knudsen, K. L.: Holocene centennial to millenial-scale climatic variability: Evidence from high resolution magnetic analyses of the last 10 cal. kyr of North Iceland (core MD99-2275), Earth Planet. Sci. Lett., 242, 390–405, 2006.

Rudels, B., Anderson, L. G., and Jones, E. P.: Formation and evolution of the surface mixed layer and the halocline of the Arctic Ocean, J. Geophys. Res., 101, 8807–8821, 1996.

Rudels, B., Björk, G., Nilsson, J., Winsor, P., Lake, I., and Nohr, C.: The interaction between waters from the Arctic Ocean and the Nordic Seas north of Fram Strait and along the East Greenland Current: Results from the Arctic Ocean-O2 Oden expedition, J. Marine Syst., 55, 1–30, 2005.

Rüther, D. C., Bjarnadóttir, L. J., Junttila, J., Husum, K., Rasmussen, T. L., Lucchi, R. G., and Andreassen, K.: Pattern and timing of the northwestern Barents Sea Ice Sheet deglaciation and indications of episodic Holocene deposition, Boreas, doi:10.1111/j.1502-3885.2011.00244.x, ISSN 0300-9483, 2012.

Sætre, R.: Short term variability and small-scale features, in: The Norwegian coastal current, edited by: Sætre, R, Tapir academic press, Trondheim, 89-99, 2007.

Saito, T., Thompson, P. R., and Breger, D.: Systematic index of recent and pleistocene planktonic foraminifera, University of Tokyo press, Tokyo, 1981.

Sakshaug, E.: Biomass and productivity distributions and their variability in the Barents Sea, ICES J. Marine Sci., 54, 341–350, 1997.

Sakshaug, E., Bjørge, A., Gulliksen, B., Loeng, H., and Mehlum, F.: Økosystem Barentshavet, Norges Allmenvitenskapelige Forskningsråd, Norges Fiskeriforskningsråd, Miljøverndepartementet, 304, 1992.

Sarnthein, M., Jansen, E., Weinelt, M., Arnold, M., Duplessy, J., Erlenkeuser, H., Flatøy, A., Johannessen, G., Johannessen, T., Jung, S., Koç, N., Labeyrie, L., Maslin, M., Pflaumann, U., and Schulz, H.: Variations in Atlantic surface ocean paleoceanography, 50–80° N: A time-slice record of the last 30,000 years, Paleoceanography, 10, 1063–1094, doi:10.1029/95PA01453, 1995.

Sarnthein, M., Van Kreveld, S., Erlenkeuser, H., Grootes, P. M., Kucera, M., Pflaumann, U., and Schulz, M.: Centennial-to-millennial-scale periodicities of Holocene climate and sediment injections off the western Barents shelf, 75° N, Boreas, 32, 447–461, 2003.

Schiermeier, Q.: Record shrinkage confounds models and portends atmospheric and ecological change, Nature, 489, 185–186, 2012.

Scott, D. B., Schell, T., Rochon, A., and Blasco, S.: Modern benthic foraminifera in the surface sediments of the Beaufort shelf, slope and Mackenzie Trough, Beaufort Sea, Canada: Taxonomy and summary of surficial distributions, J. Foramin. Res., 38, 228–250, 2008.

Semenov, V. A., Park, W., and Latif, M.: Barents Sea inflow shutdown: A new mechanism for rapid climate changes, Geophys. Res. Lett., 36, L14709, doi:10.1029/2009GL038911, 2009.

Slubowska, M. A., Koç, N., Rasmussen, T. L., and Klitgaard-Kristensen, D.: Changes in the flow of Atlantic water into the Arctic Ocean since the last deglaciation: Evidence from the northern Svalbard continental margin, 80N, Paleoceonography, 20, PA4014, doi:10.1029/2005PA001141, 2005.

Slubowska-Woldengen, M., Rasmussen, T. L., Koç, N., Klitgaard-Kristensen, D., Nilsen, F., and Solheim, A.: Advection of Atlantic Water to the western and northern Svalbard shelf since 17 500 cal yr BP, Quaternary Sci. Rev., 26, 463–478, 2007.

Smith, S. L., Smith, W. O., Codispoti, L. A., and Wilson, D. L.: Biological observations in the marginal ice zone of the East Greenland Sea, J. Marine Res., 43, 693–717, 1985.

Smith, W. O. and Sakshaug, E.: Polar phytoplankton, in: Polar oceanography, edited by: Smith, W. O., Part B: Chemistry, Biology and Geology, Academic Press, New York, 447–525, 1990.

Solignac, S., Giraudeau, J., and De Vernal, A.: Holocene sea surface conditions in the western North Atlantic: Spatial and temporal heterogeneities, Paleoceanography, 21, PA2004, doi:10.1029/2005PA001175, 2006.

Spielhagen, R. F., Werner, K., Aagaard Sørensen, S., Zamelczyk, K., Kandiano, E., Budeus, G., Husum, K., Marchitto, T. M., and Hald, M.: Enhanced modern heat transfer to the Arctic by warm Atlantic water, Science, 331, 450, doi:10.1126/science.1197397, 2011.

Stein, R. and Fahl, K.: Biomarker proxy shows potential for studying the entire Quaternary Arctic sea ice history, Org. Geochem., 55, 98–102, 2013.

Steinsund, P. I. and Hald, M.: Recent carbonate dissolution in the Barents Sea: Paleoceanographic applications, Mar. Geol., 117, 303–316, 1994.

Stroeve, J. C., Kattsov, V., Barrett, A., Serreze, M., Pavlova, T., Holland, M., and Meier, W. N.: Trends in Arctic sea ice extent from CMIP5, CMIP3 and observations, Geophys. Res. Lett., 39, L16502, doi:10.1029/2012GL052676, 2012.

Stuiver, M. and Reimer, P. J.: Extended 14C data base and revised CALIB 3.0 14C age calibration program, Radiocarbon, 35, 215–230, 1993

Swift, J. H.: The Arctic waters, in: The Nordic Seas, edited by: Hurdle, B. G., Springer New York, 129–153, 1986.

Telford, R. J. and Birks, H. J. B.: The secret assumption of transfer functions: Problems with spatial autocorrelation in evaluating model performance, Quaternary Sci. Rev., 24, 2173–2179, 2005.

Ter Braak, C. J. F. and Juggins, S.: Weighted averaging partial least squares regression (WA-PLS): An improved method for reconstructing environmental variables from species assemblages, Hydrobiologia, 269/270, 485–502, 1993.

Thunell, R. C. and Honjo, S.: Calcite dissolution and the modification of planktonic foraminiferal assemblages, Mar. Micropaleontol., 6, 169–182, 1981.

Vare, L. L., Massé, G., and Belt, S.: A biomarker-based reconstruction of sea ice conditions for the Barents Sea in recent centuries, Holocene, 20, 637–643, 2010.

Vinje, T. E.: Sea ice conditions in the European sector of the marginal seas of the Arctic, 1966–75, Aarb. Nor. Polarinst., 1975, 163–174, 1977.

Volkmann, R.: Planktic foraminifers in the outer Laptev Sea and the Fram Strait: Modern distribution and ecology, J. Foramin. Res., 30, 157–176, 2000.

Voronina, E., Polyak, L., de Vernal, A., and Peyron, O.: Holocene variations of sea-surface conditions in the southeastern Barents Sea, reconstructed from dinoflagellate cyst assemblages, J. Quaternary Sci., 16, 717–726, 2001.

Werner, K., Spielhagen, R. F., Bauch, D., Hass, H. C., and Kandiano, E.: Atlantic Water advection versus sea-ice advances in the eastern Fram Strait during the last 9 ka: Multiproxy evidence for a two-phase Holocene, Paleoceanography, 28, 283–295, doi:10.1002/palo.20028, 2013.

Zamelczyk, K., Rasmussen, T. L., Husum, K., Haflidason, H., de Vernal, A., Krogh Ravna, E., Hald, M., and Hillaire-Marcel, C.: Paleoceanographic changes and calcium carbonate dissolution in the central Fram Strait during the last 20 ka yr, Quaternary Res., 78, 405–416, 2012.

Paper II

Berben SMP, Husum K, Navarro-Rodriguez A, Belt ST and Aagaard-Sørensen S **Atlantic water inflow and sea ice distribution in the northern Barents Sea: A Holocene palaeoceanographic evolution.**
Submitted to Paleoceanography

Atlantic water inflow and sea ice distribution in the northern Barents Sea: A Holocene palaeoceanographic evolution

Berben SMP[a], Husum K[b], Navarro-Rodriguez A[c], Belt ST[c] and Aagaard-Sørensen S[a]
[a]Department of Geology, University of Tromsø, N-9037 Tromsø, Norway
[b]Norwegian Polar Institute, Fram Centre, N-9296 Tromsø, Norway
[c]Biogeochemistry Research Centre, School of Geography, Earth and Environmental Sciences, University of Plymouth, Drake Circus, Plymouth PL4 8AA, UK

Correspondence to: Berben SMP (sarah.m.berben@uit.no)

Keywords: Atlantic water inflow, sea ice distribution, northern Barents Sea, Holocene, planktic foraminifera, stable isotopes, sea ice biomarkers

Abstract

We carried out a multi-proxy analysis on a marine sediment core retrieved from the Olga Basin in the northern Barents Sea in order to investigate the interactions between, and variations in, Atlantic water inflow and sea ice distribution throughout the Holocene. This was achieved by analysing planktic foraminifera and their preservation indicators, foraminiferal stable isotopes ($\delta^{18}O$, $\delta^{13}C$) and biomarkers. The resulting sub-centennial records suggest that the early Holocene (ca. 9500 – 5800 cal yr BP) was characterised by short spring seasons and long productive summers. A strong influence of Atlantic water caused an increased heat flux which led to an active ocean feedback mechanism and hence, contributed to a reduced sea ice extent. The Holocene Thermal Optimum was recorded at different time intervals between ca. 9300 and 5800 cal yr BP indicating a proxy-specific response. Throughout the mid Holocene (ca. 5800 – 2200 cal yr BP), the sea ice edge migrated southwards and an overall cooling trend is consistent with reduced summer insolation which affected the sea surface conditions, in particular. During the late Holocene (ca. 2200 – 0 cal yr BP), the different proxies indicate a sub-surface warming, with increased Atlantic water inflow, and sea surface cooling, with extended sea ice cover, likely due to a decoupling between the ocean and the atmosphere. Longer spring seasons and shorter summers were reflected by the most extended sea ice distribution within the entire record. The generally more unstable palaeoceanographic conditions in the late Holocene are attributed to more pronounced positive NAO-like conditions.

1 Introduction

The Barents Sea is a relatively small and shallow sea, yet it plays a crucial role in the Arctic climate system, in part, because of significant heat exchange between the ocean and the atmosphere (Serreze et al., 2007). Oceanic heat is brought into the Barents Sea via the inflow of warm Atlantic water and, due to shallow depths, heat loss to the atmosphere is very efficient. Further, it has been suggested that ocean advection strongly influences sea ice extent in the Barents Sea, so the region is central to understanding ocean-sea ice-atmosphere interactions Vinje (2001).

Recently, many Arctic regions have experienced a sharp decline in sea ice cover, and this is most pronounced in the northern Barents Sea (Screen and Simmonds, 2010). Variations in sea

ice within the Barents Sea have been attributed to several different processes (e.g. atmospheric circulation variability, local wind patterns, ice import), although the role of oceanic heat advection is often emphasized as one of the most important factors. For example, Årthun et al. (2012) have argued that recent increases in Atlantic water inflow has resulted in so-called 'Atlantification' of the Barents Sea and this has contributed to a further decline in sea ice cover.

As the impacts of Arctic amplification and the associated sea ice decline reach far beyond the Arctic region (e.g. the link between recent Arctic sea ice loss and continental winter cooling (Yang and Christensen, 2012)), it is clearly necessary to better understand the interaction between Atlantic water inflow and sea ice production, together with any natural variability that occurs over longer timeframes. Instrumental records of past climate variations in the Barents Sea reach back only ca. 100 years (Smedsrud et al., 2013), so longer term records of sea ice and water mass distribution need to be derived from proxy records. Previous proxy records from the northern Barents Sea (e.g. Duplessy et al., 2001; Lubinski et al., 2001; Risebrobakken et al., 2011; Klitgaard Kristensen et al., 2013), the western Barents Sea (Berben et al., 2014) and the Svalbard margin (e.g. Slubowska et al., 2005; Rasmussen et al., 2007; Spielhagen et al., 2011; Müller et al., 2012; Werner et al., 2013) have demonstrated various fluctuations in both the influence of Atlantic water inflow and in sea ice distribution throughout the Holocene.

During the early Holocene, the so-called Holocene Thermal Maximum (HTM) has been identified in numerous previous studies and has been linked, primarily, to an increase in solar insolation and further to factors such as land-cover feedbacks and coupled atmospheric-oceanic dynamics; especially the northward penetration of relatively warm Atlantic water (e.g. Berger, 1978; Koç et al., 1993; Kaufman et al., 2004). For example, the HTM has been observed through increased sea surface temperatures (SST) and enhanced Atlantic water inflow (e.g. Duplessy et al., 2001; Sarnthein et al., 2003; Hald et al., 2007; Risebrobakken et al., 2010) along the Norwegian coast (e.g. Husum and Hald, 2004) and the Svalbard margin (e.g. Slubowska et al., 2005; Slubowska-Woldengen et al., 2007; Werner et al., 2013). The apparent timing of the HTM varies, however, possibly as a result of variable location and the depth habitat and/or response time of the different proxies to atmospheric changes (e.g. due to increased insolation), which underscores the influencing role of the interaction between the atmosphere and the ocean (Kaufman et al., 2004; Moros et al., 2004; Hald et al., 2007). In any case, the HTM was followed by the Neoglacial cooling, a period generally characterized by

the return of cooler conditions in different northern high latitude regions (e.g. Wanner et al., 2008). Marine proxy records generally show reduced SST records, a dominance of Arctic water and increased sea ice, consistent with decreasing summer insolation at high latitudes such as in the Barents Sea (e.g. Duplessy et al., 2001; Sarnthein et al., 2003; Hald et al., 2007; Risebrobakken et al., 2010; Klitgaard Kristensen et al., 2013) and the Svalbard margin (e.g. Rasmussen et al., 2007; Müller et al., 2012; Rasmussen et al., 2012; Werner et al., 2013).

During the Late Holocene, evidence for strengthened Atlantic water inflow has been presented for the Barents Sea (e.g. Duplessy et al., 2001; Lubinski et al., 2001; Berben et al., 2014) and the Svalbard margin (e.g. Slubowska-Woldengen et al., 2007; Jernas et al., 2013; Werner et al., 2013; Zamelczyk et al., 2013), while some air temperature reconstructions, based on terrestrial records from Fennoscandinavia and ice core records from Greenland and Svalbard, indicate an overall cooling (e.g. Dahl-Jensen et al., 1998; Bjune et al., 2009; Kaufman et al., 2009; Divine et al., 2011). The dominance of cold Arctic water and reduced Atlantic water inflow at the western and northern margin of Svalbard has also been identified for the late Holocene from marine records (e.g. Slubowska et al., 2005; Skirbekk et al., 2010).

Here, we combine proxy data from planktic foraminiferal fauna assemblages, stable isotopes ($\delta^{18}O$, $\delta^{13}C$) and biomarkers (including IP_{25} as a sea ice proxy; Belt et al., 2007; Belt and Müller, 2013; Brown et al., 2014) in a marine sediment core obtained from the northern Barents Sea to construct an integrated sub-surface water mass and sea ice record for the Holocene. Today, the study site is influenced by Atlantic derived water masses (Abrahamsen et al., 2006) and is covered by seasonal sea ice (Figure 1). As such, it represents a key location for investigating the palaeoceanographic evolution of Atlantic water inflow and sea ice distribution throughout the Holocene. On the basis of the combined proxy record, we propose different oceanographic scenarios that emphasize the interaction between surface water masses and sea ice distribution, and discuss these further, by comparison with outcomes from previous studies from the region.

2 Present day oceanographic setting of the Barents Sea

The Barents Sea is an epicontinental shelf located between the Norwegian-Russian coast, Novaya Zemlya and the Svalbard and Franz Josef Land archipelagos (Figure 1). The northern boundary of the Barents Sea is defined by the Nansen Basin continental slope (Jakobsson et

al., 2004). The Barents Sea is characterized by several water masses and represents a major passage for Atlantic water entering the Arctic Ocean (Carmack et al., 2006).

The Norwegian Atlantic Current (NwAC) brings relatively warm Atlantic water (>2 °C, >35 ‰) towards the high latitude North Atlantic Ocean (Hopkins, 1991) (Figure 1A). Before entering the Barents Sea, the NwAC splits into two different currents: the West Spitsbergen Current (WSC) and the North Cape Current (NCaC) (Figure 1A), both of which are responsible for the transport of warm saline Atlantic water into the Arctic Ocean, in particular the WSC (Aagaard and Greisman, 1975). The WSC continues northwards along the western Barents Sea slope and splits in the Fram Strait into three branches; the Return Atlantic Current (RAC), the Yermak Branch (YB) and the Svalbard Branch (SB) (e.g. Manley, 1995). The latter enters the Arctic Ocean north of Svalbard as a sub-surface current flowing eastward up and beyond the Franz Victoria and St. Anna Troughs. Hence, the Barents Sea becomes influenced by the sub-surface inflow of Atlantic water via the Northern Barents Sea Opening (NBSO) (Figure 1A). Subsequently, Atlantic water is advected south-westwards into the northern Barents Sea and has been observed year-round in the Olga Basin, which is the study site here (Abrahamsen et al., 2006). Further, the northern Barents Sea and, in particular, the Olga Basin, is also influenced by Atlantic water that enters as a submerged flow from the south (e.g. Novitskiy, 1961; Loeng, 1991; Pfirman et al., 1994; Aksenov et al., 2010). This Atlantic water is brought to the area by the NCaC which flows northwards via the Barents Sea Opening (BSO) into the southern Barents Sea and parallel to the coastal current system (Loeng, 1991; Loeng et al., 1993; Midttun, 1985; Rudels, 1987) (Figure 1A). Finally, after mixing and heat loss, Atlantic water leaves the Barents Sea through the Barents Sea Exit (BSX) and reaches the Arctic Ocean via the St. Anna Trough (e.g. Schauer et al., 2002) (Figure 1A). South of the NCaC, the Norwegian Coastal Current (NCC) transports Coastal water (2 - 13 °C, 32 - 35 ‰) along the Norwegian and northern Russian coasts (Hopkins, 1991) (Figure 1A). Polar water (0 - 2 °C, 33 - 33.4 ‰) is brought from the Arctic Ocean into the Barents Sea through the Franz Victoria and St. Anna Troughs, via the East Spitsbergen Current (ESC) and the Bear Island Current (BIC), respectively (Hopkins, 1991) (Figure 1A).

In contrast to the Atlantic water dominated southern Barents Sea, the northern Barents Sea is dominated by Arctic water (~0.5 °C, ~34.8 ‰) and is characterized by reduced temperature and salinity, as well as seasonal sea ice cover (Hopkins, 1991). Arctic water is formed when relatively warm Atlantic water converges and merges with cold, less saline and ice loaded Polar water. Hence, temperature and salinity values progressively decrease towards the north-

eastern Barents Sea resulting in what is classified as Atlantic derived water (>0 °C, >34.75 ‰) (Gammelsrød et al., 2009). Further, in the north-eastern Barents Sea, extensive sea ice formation, brine rejection in winter and the subsequent melting of sea ice in summer, lead to a stable and strong stratification (Wassmann et al., 2006). A small fraction of Atlantic water in the northern Barents Sea enters the area from the north as a sub-surface flow and is located below Arctic water. The majority of Atlantic water entering the region from the south is cooled due to a strong heat loss to the atmosphere, but retains high salinity. As a result, the latter, denser water mass flows below the Atlantic water mass advected from the north (Pfirman et al., 1994). Finally, dense and cold deep waters are formed through cooling and salt rejection during sea ice growth. The Barents Sea is an important contributor for the production and export of dense water into the Arctic Ocean and thereby plays a central role in the global ocean circulation and climate (Årthun et al., 2011).

The fronts dividing these different water masses are one of the main oceanographic features of the near-surface waters of the Barents Sea (Pfirman et al., 1994). Defined as a sharp climatic gradient in terms of temperature, salinity and sea ice coverage, the Polar and Arctic Fronts are the respective boundaries between Polar/Arctic and Arctic/Atlantic waters. These are closely related to the overall distribution of sea ice, in particular, and the average winter and summer sea ice margins (Vinje, 1977). Although sea ice advection from the Arctic Ocean does occur, sea ice is mainly formed locally during fall and winter (Loeng, 1991). The sea ice edge divides the Barents Sea into two different oceanographic areas, each with their own characteristics (Figure 1B). The sea ice extent is regulated by the inflow of Atlantic water into the western Barents Sea, which sets the boundary of the mainly ice-free Atlantic domain in the south-western Barents Sea (Årthun et al., 2012). In contrast, the north-eastern Barents Sea experiences large changes in seasonal sea ice distribution (Vinje, 2001; Sorteberg and Kvingedal, 2006) with maximum sea ice extent during March/April and minimum cover occurring throughout August/September (Figure 1B). Further, annual variability during recent decades might be explained by cyclone activity causing fluctuations in sea ice transport, to and from the Arctic Ocean into the north-eastern Barents Sea (Kwok et al., 2005; Sorteberg and Kvingedal, 2006; Ellingsen et al., 2009; Kwok, 2009). The interplay among the different water masses and other influences over sea ice formation determine the position of the marginal ice zone (MIZ), an area characterized by its high surface productivity during the summer season (e.g. Smith and Sakshaug, 1990). Within the Barents Sea, the major part of the biological primary production results from a peak algal bloom along the ice edge during

the spring as sea ice retreats (Sakshaug et al., 1992). Consequently, the Barents Sea is one of the most productive areas of the Arctic Seas (Wassmann et al., 2006).

3 Material and methods

A 245 cm long marine sediment core NP05-11-70GC was retrieved in 2005 by the RV *Lance* south of Kong Karls Land (Olga Basin) within the northern Barents Sea (78.40° N, 32.42° E; 293 m water depth) (Figure 1). A CTD profile taken at the same location illustrates the presence of Arctic water at the surface, with Atlantic water below ca. 150 m (Figure 2). Only the upper section of the core (0 - 124.5 cm; 1-cm intervals) was investigated in the current study.

3.1 Chronology

A depth-age model for NP05-11-70GC was developed using linear interpolation between three calibrated AMS ^{14}C dates obtained from benthic foraminifera and the assumption that the core top represents 0 cal yr BP (Figure 3). The AMS ^{14}C dates were calibrated using Calib 6.1.1 (Stuiver and Reimer, 1993) and the Marine09 calibration curve (Reimer et al., 2009). A local reservoir age (ΔR) of 105 ± 24 was indicated for the Svalbard area by Mangerud et al. (2006) and subsequently used in the calibration (Table 1). The resulting depth-age model ranges between 0 and 9417 cal yr BP (Figure 3). The sedimentation rates vary between 0.07 and 0.18 mm/yr, so the sampling resolution is 55 - 134 years (Figure 3).

3.2 Planktic foraminifera

Foraminiferal samples were freeze-dried before they were wet-sieved through three different size fractions (1000, 100 and 63 µm) and dried at 40 °C. Planktic foraminiferal assemblages were determined for 123 samples using the 100 - 1000 µm size fraction following Knudsen (1998). Following the recommendations of Forcino (2012), the relative abundances (%) of each species were calculated for samples containing more than 25 specimens (82 samples). The identification of left and right coiling *Neogloboquadrina pachyderma* was achieved following Darling et al. (2006); the left coiling form was identified as *N. pachyderma*, and the

right coiling form was identified as *Neogloboquadrina incompta*, (Cifelli, 1961). The planktic foraminiferal concentrations (#/g sediment) and fluxes (#/cm^2/yr) were also calculated; the latter being calculated following Ehrmann and Thiede (1985).

The dissolution of foraminiferal shells was investigated by calculating the mean shell weight (µg) of *N. pachyderma* (Broecker and Clark, 2001; Barker and Elderfield, 2002; Beer et al., 2010) and the fragmentation (%) of foraminiferal tests (Conan et al., 2002). 25 well preserved (visually) and square shaped *N. pachyderma* specimens were picked from a narrow size range (150 - 250 µm) in order to reduce problems of ontogeny and size difference induced variability (Barker et al., 2004). It was possible to obtain a mean weight for 110 samples of *N. pachyderma* using a Mettler Toledo microbalance (0.1 µg sensitivity). The fragmentation of planktic foraminiferal tests was calculated for the 82 samples that contained a total number of >25 specimens within the 100 - 1000 µm size fraction. The fragmentation was calculated using the equation proposed by Pfuhl and Shackleton (2004) (Equation 1).

$$Fragmentation\ (\%) = \frac{\#\ fragments/g}{\#fragments/g/3 + \#\ tests/g} * 100 \qquad \text{[Equation 1]}$$

3.3 Stable isotope analysis

Stable isotope ($\delta^{18}O$, $\delta^{13}C$) analyses were performed on the foraminiferal tests of *N. pachyderma*. All specimens were selected from a narrow size range (150 - 250 µm) in order to minimize size dependent effects on isotopic composition (Aksu and Vilks, 1988; Keigwin and Boyle, 1989; Oppo and Fairbanks, 1989; Donner and Wefer, 1994; Bauch et al., 2000). Sufficient specimens were obtained from 105 samples. Samples were analysed using a Finnigan MAT 253 mass spectrometer coupled to an automated Kiel device at the Geological Mass Spectrometer (GMS) Laboratory at the University of Bergen. These measurements were conducted with a reproducibility of ± 0.06 ‰ ($\delta^{18}O$) and ± 0.03 ‰ ($\delta^{13}C$), and data are reported on the ‰ versus VPDB scale calibrated with NBS-19. Corrections for the ice volume effect were applied on the measured $\delta^{18}O$ values according to Fairbanks (1989). No vital effect corrections were applied for the isotope measurements in this study as published estimates of species-specific vital effects are often inconsistent (e.g. Kohfeld et al., 1996; Bauch et al., 1997; Stangeew, 2001; Simstich et al., 2003), possibly due to seasonal changes of the apparent vital effect (Jonkers et al., 2010).

3.4 Biomarker analysis

Biomarker analysis was performed on 49 sub-samples (ca. 1 g) providing a centennial resolution. Prior to analysis, sub-samples were freeze-dried and stored at -20 °C. The general methodology was as described previously (Belt et al., 2012; Brown and Belt, 2012) with some modifications. Three internal standards (IS) were added to permit quantification of the biomarkers using gas chromatography-mass spectrometry (GC-MS) (Belt et al., 2012). 9-octylhetadec-8-ene (9-OHD, 10 µL; 1 µg mL^{-1}) and 7-hexylnonadecane (7-HND, 10 µL; 1 µg mL^{-1}) were added for the quantification of IP_{25}, while 5α-androstan-3β-ol (10 µL; 1 µg mL^{-1}) was used to quantify brassicasterol. Subsequently, a total organic extract was obtained according to previous descriptions (Belt et al., 2012; Brown and Belt, 2012).

Before fractionation into individual lipid classes, it was necessary to remove elemental sulfur from the TOEs that would otherwise have interfered with the GC-MS analysis. To do this, hexane (1 mL), tetrabutylammonium sulphite (TBA, 1mL) and 2-propanol (1 mL) were added to the TOEs and suspensions were shaken by hand for ca. 1 min. Thereafter, Milli-Q water (3 mL) was added, and mixtures were shaken further (1 min) and centrifuged, after which, the lipid-containing hexane layer was decanted. This procedure was repeated twice more before the hexane was removed using a nitrogen stream. Partially purified TOEs were then separated into non-polar (hexane, 6 mL) and polar fractions (20:80 methylacetate/hexane, 6 mL) using open column chromatography (SiO_2). Further separation of the hexane fraction into saturated and unsaturated components was carried out using glass pipettes containing silver ion solid phase extraction (SPE) material (Supelco discovery® Ag-Ion; 100 mg). After conditioning with acetone (3 mL) and hexane (3 mL), saturated (hexane, 1 mL) and unsaturated hydrocarbon fractions (including IP_{25}) (acetone, 2 mL) were obtained. Polar fractions containing brassicasterol were derivatized using N,O-Bis(trimethylsilyl)trifluoroacetamide (BSTFA, 50 µL, 70 °C; 1h).

All fractions were analysed using GC-MS with operating conditions as described by Belt et al. (2012). Identification of the lipids of interest was based on their characteristic GC retention times and mass spectra compared with those of reference compounds in total ion current chromatogram (TIC). Quantification of lipids was achieved by comparison of peak area integrations of selected ions with those of the internal standard in selected ion monitoring (SIM) mode (Brown et al., 2011; Belt et al., 2012). These ratios were normalized to instrumental response factors and sediment mass (and total organic carbon content) and also

converted to biomarker fluxes (µg/cm^2/yr) (Belt et al., 2012) using the same method described previously for foraminifera. Concentrations of IP_{25} and brassicasterol were also combined to derive the so-called P_BIP_{25} index that has the potential to provide semi-quantitative estimates of sea ice cover (Müller et al., 2011).

4 Results and Interpretation

Overall, the different proxies show distinct changes throughout the record time, so they are described here in terms of individual time intervals that reflect the main stages of palaeoceanographic evolution. These intervals are: early Holocene (ca. 9500 – 5800 cal yr BP), mid Holocene (ca. 5800 – 2200 cal yr BP) and late Holocene (ca. 2200 – 0 cal yr BP).

4.1 Early Holocene (ca. 9500 – 5800 cal yr BP)

The early Holocene (ca. 9500 – 5800 cal yr BP) is marked by the appearance of polar and subpolar planktic foraminifera, although the absolute abundances and fluxes remain relatively low (<2.46 #/g sediment and <0.04 #/cm^2/yr) during the first part of this period (ca. 9500 – 7300 cal yr BP) (Figure 4A; 5A). This could indicate an influence of sea ice at the core site (e.g. Carstens, 1997). Between ca. 7300 and 6500 cal yr BP, there are increases in concentration and flux of foraminifera towards 5.50 #/g sediment and 0.09 #/cm^2/yr, respectively, most likely indicating increased influence of Atlantic water (e.g. Johannessen et al., 1994). After ca. 6500 cal yr BP, foraminiferal concentrations and fluxes fall rapidly towards 2.79 #/g sediment and 0.02 #/cm^2/yr, respectively.

Within the early Holocene (ca. 9500 – 5800 cal yr BP), the extent of fragmentation falls in the range 14 - 56 % with a mean value of 32 % (Figure 4B). The mean shell weight varies between 5 and 10 µg until ca. 7300 cal yr BP, followed by more consistent values (ca. 7.5 µg) towards ca. 5800 cal yr BP (Figure 4C). Although only a few data points of fragmentation were recorded between ca. 9500 and 7300 cal yr BP, the wide range in both fragmentation and mean shell weight could indicate fluctuating preservation conditions. The relatively high and consistent mean shell weight values between ca. 7300 and 5800 cal yr BP may reflect better preservation conditions, possibly related to an increased influence of Atlantic water. Previously, better calcium carbonate preservation has been associated with increased

production of organic matter in regions of higher Atlantic water input (e.g. Hebbeln et al., 1998; Henrich et al., 2002).

The foraminiferal assemblages in the early Holocene are dominated by *N. pachyderma* (ca. 95 %) (Figure 5B), indicating Arctic conditions at the study site (Volkmann, 2000). Between ca. 7300 and 5800 cal yr BP, the relative abundances of *Turborotalita quinqueloba, N. incompta* and *Globigerinita glutinata* show increased values, up to ca. 24, 27 and 4 %, respectively (Figure 5C-E). These species are associated with subpolar conditions and relatively warm Atlantic (sub-surface) water (Bé and Tolderlund, 1971; Johannessen et al., 1994; Carstens et al., 1997). These foraminiferal fauna changes between ca. 7300 and 5800 cal yr BP are most likely reflecting the HTM at the core site. In addition, *T. quinqueloba* has also been found to be characteristic of Arctic Front conditions in the western Barents Sea (Burhol, 1994), where it responds to a plentiful nutrient supply (Reynolds and Thunnel, 1985; Johannessen et al., 1994).

Studies of recent foraminiferal calcite and the isotopic composition of water masses by Lubinski et al. (2001) demonstrate that, in the Barents Sea, the planktic foraminiferal oxygen isotope signals are controlled mainly by temperature changes, since modern surface water temperatures vary much more than salinity. However, the water masses in the region were also influenced by meltwater and reduced salinities during the very early Holocene, but this influence ended around ca. 11 000 cal yr BP and thus, well before the onset of the current oxygen isotope record (Klitgaard Kristensen et al., 2013). Therefore, it is assumed that the stable oxygen isotope record of the current study is mainly controlled by temperature. During the early Holocene (ca. 9500 – 5800 cal yr BP), the $\delta^{18}O$ record has a value of 3.87 ‰ (Figure 6A). $\delta^{18}O$ values then reduce to ca. 3.78 ‰ towards ca. 8800 cal yr BP, followed by a period (ca. 8800 – 7300 cal yr BP) characterized by more depleted values (ca. 3.58 ‰). This depletion (ca. 0.2 ‰) might indicate a small temperature rise, possibly indicating a gradual shift towards warmer conditions due to increased inflow of Atlantic water. The sharp enrichment in $\delta^{18}O$ between ca. 7600 and 7300 cal yr BP is followed by values that fluctuate around ca. 3.70 ‰ until ca. 5800 cal yr BP. This possibly indicates cooler conditions after ca. 7300 cal yr BP, and that the core site became more influenced by oceanic front conditions. Here, the relatively light $\delta^{18}O$ values between ca. 8800 and 7300 cal yr BP coincide with high insolation values, thus indicating the HTM at the core site (Figure 6). Throughout the early Holocene (ca. 9500 – 5800 cal yr BP), $\delta^{13}C$ values show depletion from 0.37 to 0.01 ‰ between ca. 9500 and 8500 cal yr BP (Figure 6B) consistent with reduced primary production

and/or increased stratification. This trend is reversed at ca. 5800 cal yr BP, with enriched $\delta^{13}C$ values (ca. 0.80 ‰) indicating increased primary production and/or enhanced ventilation (e.g. Spielhagen and Erlenkeuser, 1994) (Figure 6B).

The concentration and flux of the sea ice biomarker IP_{25} (Belt et al., 2007; Belt and Müller, 2013; Brown et al., 2014) shows a rapid decrease (<200 cal yr) at the start of the early Holocene (ca. 9500 – 5800 cal yr BP), whereas those of brassicasterol increase (Figure 7A-B). Consistent with these observations, a reduction in the P_BIP_{25} index from 0.37 to 0.16 also indicates a reduction in sea ice cover with the presence of more open water conditions (Müller et al., 2011) (Figure 7D). From ca. 9300 to 6500 cal yr BP, IP_{25} values increase, but still remain relatively low (ca. 0.05 to 0.10 µg/g OC) (Figure 7A). On the other hand, brassicasterol shows an opposite trend, albeit with some fluctuations around ca. 23 µg/g OC (Figure 7B). Consistent with the foraminiferal assemblages and $\delta^{18}O$ record, these biomarker data also indicate the occurrence of the HTM at the core site throughout the early Holocene. The biomarker data reflects the HTM between ca. 9300 and 6500 cal yr BP, after which, IP_{25} abundances increase, suggesting termination of the HTM. The early Holocene is also characterized by a decreasing trend in TOC, although values remain relatively high (ca. 1.65 to 2.00 %) (Figure 7C). The P_BIP_{25} index shows the lowest values of the record (0.16 - 0.40) suggesting a period characterized by low or variable seasonal sea ice cover and influenced substantially by open water conditions (Müller et al., 2011) (Figure 7D).

4.2 Mid Holocene (ca. 5800 – 2200 cal yr BP)

Throughout the mid Holocene (ca. 5800 – 2200 cal yr BP), both planktic foraminiferal concentrations and fluxes show a general increase towards ca. 8.00 #/g sediment and ca. 0.15 #/cm^2/yr, respectively (Figure 4A; 5A). The mean shell weight remains relatively stable (ca. 7 µg) with a small decrease towards the end of the interval, whereas the fragmentation record exhibits an overall decrease from ca. 42 to 16 %, indicating improved preservation (Figure 4C-B). The relative abundances of *T. quinqueloba* and *N. incompta* reduce after ca. 5800 cal yr BP and remain relatively stable (ca. 3 - 4 %) towards ca. 2200 cal yr BP (Figure 5C-D). Throughout this period, *N. pachyderma* clearly dominates (ca. 90 %) the planktic foraminiferal fauna (Figure 5B), suggesting a relatively stable period characterized by a dominance of colder Arctic water (Volkmann, 2000).

The $\delta^{18}O$ record remains relatively stable throughout the mid Holocene (ca. 5800 – 2200 cal yr BP) (Figure 6A) with relatively high values (ca. 3.70 ‰) most likely also indicating a decreased influence of Atlantic water. The $\delta^{13}C$ record continues to increase from 0.76 towards 0.90 ‰, indicative of increased ventilation (Spielhagen and Erlenkeuser, 1994) (Figure 6B), although increased $\delta^{13}C$ values might also be attributed to an increase in primary production resulting from a stronger influence of oceanic front conditions.

IP_{25} increases to ca. 0.25 µg/g OC during the mid Holocene (ca. 5800 – 2200 cal yr BP), while brassicasterol shows a decreasing trend to 10 µg/g OC (Figure 7A-B). Combined, the P_BIP_{25} values continue their increasing trend from the early Holocene (0.4 - 0.7) (Figure 7D), reaching values indicative of MIZ conditions according to Müller et al. (2011). As such, the biomarker data indicate a gradual increase in seasonal (spring) sea ice cover, most likely related to the reduced July insolation causing a cooling at the sea surface.

4.3 Late Holocene (ca. 2200 – 0 cal yr BP)

During the late Holocene (ca. 2200 – 0 cal yr BP), three episodes of increased values for both planktic foraminiferal concentrations and fluxes are observed between ca. 2200 and 2000 cal yr BP, ca. 1600 and 700 cal yr BP, and ca. 400 and 0 cal yr BP (Figure 4A; 5A). These three episodes show the highest fluxes and concentrations of the entire record (up to 0.16 #/cm^2/yr and 10 #/g sediment, respectively). The degree of fragmentation also generally increases (to ca. 50 %), whereas the mean shell weight shows a general decrease towards ca. 4.5 µg (Figure 4B-C). In addition to these general trends, the mean shell weight and, in particular, the planktic foraminiferal fragmentation, show highly fluctuating values (ca. 9 - 83 %) (Figure 4C-B). Despite these fluctuations, however, this interval shows an overall change towards enhanced dissolution. This may be caused by an increased influence of the MIZ and its associated high surface productivity causing a reduced preservation of calcium carbonate (Huber et al., 2000; Scott et al., 2008). Additionally, brine rejection may form corrosive bottom water masses causing dissolution at the sea floor (e.g. Midttun, 1985; Steinsund and Hald, 1994). This has been observed for recent benthic foraminiferal faunas in the Barents Sea (Steinsund and Hald, 1994).

The relative abundance of *N. pachyderma* shows a general decrease towards ca. 65 % suggesting a reduced dominance of Arctic water at the core site (Figure 5B). The

corresponding increasing trend in relative abundances of other species is also seen in their individual fluxes (Figure 5C-G). Thus, in the periods between ca. 2200 – 2000, 1600 – 700 and 400 – 0 cal yr BP, *T. quinqueloba* and *N. incompta* both reach very high abundance and flux values. These changes argue for episodes of enhanced influence of Atlantic water and/or front conditions. After ca. 2000 cal yr BP, increasing values of *G. bulloides* (ca. 8 %) and in particular *G. glutinata* (ca. 5 %) mark the faunal assemblages (Figure 5F-E). The period from ca. 400 – 0 cal yr BP is characterized by a clear increase of *G. bulloides* to ca. 6 %, in addition to a remarkable increase of *G. glutinata* and *G. uvula* (both to ca. 7 %) (Figure 5F; 5E; 5G). *G. uvula* has previously been associated with reduced salinities (e.g. Husum and Hald, 2012) and high food supply related to a productive oceanic front (Saito et al., 1981; Boltovskoy et al., 1996; Bergami et al., 2009).

Both $\delta^{18}O$ and $\delta^{13}C$ show a general depletion within the late Holocene with values in the ranges 3.49 - 3.98 ‰ and 0.34 - 0.84 ‰ for $\delta^{18}O$ and $\delta^{13}C$, respectively (Figure 6). Depleted values of $\delta^{18}O$ most likely reflect warmer temperatures due to an increased influence of Atlantic derived water. The $\delta^{13}C$ record shows a clear depletion towards values below 0.7 ‰, thus indicating enhanced stratification between the surface and sub-surface waters, likely related to a returned influence of Atlantic water.

The late Holocene (ca. 2200 – 0 cal yr BP) is characterized by the highest abundances of IP_{25} (0.35 µg/g OC) and relatively low (but stable) brassicasterol (12.5 µg/g OC) (Figure 7A-B). Although the TOC values fluctuate somewhat throughout the late Holocene, the absolute values (ca. 1.62 %) are the lowest within the entire TOC record (Figure 7C). Consistent with the opposing trends in the IP_{25} and brassicasterol records, the P_BIP_{25} values reach their highest value (0.87) of the record at ca. 0 cal yr BP (Figure 7D). An increase in P_BIP_{25} suggests a further extension in sea ice cover, reflecting Arctic Front conditions (Müller et al., 2011), most similar to modern conditions.

5 Holocene palaeoceanographic evolution

Our palaeoceanographic record from the Olga Basin shows generally gradual but distinct changes in seasonal sea ice distribution and Atlantic water inflow to the northern Barents Sea throughout the Holocene. These variations are discussed here, and placed in further context by comparison with previously published records from the region (Figure 1). In terms of sea

ice cover, we interpret our combined proxy data by proposing different seasonal sea ice scenarios. In order to obtain realistic representations for such variations in sea ice cover, we have considered known scenarios derived from modern and historical observations (NSIDC) (Figure 1B). For example, the modern sea ice context has been derived from maximum (March) and seasonal variability (April/August) in sea ice extent using satellite data obtained between 1981 and 2010 (NSIDC) (Figure 8D). In terms of temporal changes, historical data for the Barents Sea show variations in the mean sea ice edge position in April for four sub periods between 1870 and 2002 (i.e. 1870 – 1920; 1921 – 1961; 1962 – 1988; 1989 – 2002) (Divine and Dick, 2006). This north-easterly retreat of the sea ice edge since the second half of the 19th century took place after a significant cooling in the second half of the 18th century and occurred in a north-easterly direction (Divine and Dick, 2006). This key dataset illustrates that, even on a decadal time scale, the migration pattern of the sea ice extent associated with climatic conditions can reflect those observed during seasonal or annual sea ice edge change. Such observations and changes therefore provide precedent for our proposed sea ice scenarios (and changes to these) during the Holocene.

5.2 Subpolar conditions and long productive summers ca. 9500 – 5800 cal yr BP

The high relative abundances of *N. pachyderma* in the early part of the record indicate the dominance of Arctic water masses. Nonetheless, the increased abundances of subpolar species and of total planktic foraminifera between ca. 7300 and 5800 cal yr BP indicate a pronounced influence of Atlantic water inflow at the core site, most likely indicative of the HTM. Elevated planktic foraminiferal concentrations were also recorded in the north-eastern Barents Sea around ca. 9800 cal yr BP by Duplessy et al. (2001), who suggested an early intrusion of Atlantic water and high surface water productivity (Figure 1). Similarly, Klitgaard Kristensen et al. (2013) related their observed high planktic foraminiferal concentrations in the northern Barents Sea between ca. 7600 and 6500 cal yr BP to a renewed and stronger influence of Atlantic water (Figure 1). Berben et al. (2014) reached the same conclusion having found a strong increase in the planktic foraminiferal concentrations and relative abundances of subpolar species such as *N. incompta* and *T. quinqueloba* in the western Barents Sea at ca. 10 000 cal yr BP (Figure 1). However, for the West Svalbard margin, Werner et al. (2013) associated high planktic foraminiferal fluxes ca. 8000 cal yr BP to ice-free or seasonally fluctuating sea ice margin conditions (Figure 1).

The depleted stable isotope ($\delta^{18}O$, $\delta^{13}C$) values between ca. 8800 and 7300 cal yr BP most likely reflect the HTM, with the strong enrichment in $\delta^{18}O$ between ca. 7600 and 7300 cal yr BP probably corresponding to the termination phase of the HTM. The latter is consistent with the observations of Duplessy et al. (2001) (Figure 1) who observed decreasing $\delta^{18}O$ values between ca. 10 000 and 7850 cal yr BP and attributed these to a deglacial warming with an increased influence of Atlantic water inflow. Light $\delta^{18}O$ values between ca. 7850 and 6900 cal yr BP were associated with the abrupt termination of the HTM. In addition, Lubinski et al. (2001) linked decreasing $\delta^{18}O$ values between ca. 10 000 and 6800 cal yr BP with a possible surface temperature increase of ca. 1 - 2 °C due to a return inflow of warm water (Figure 1). Klitgaard Kristensen et al. (2013) found low $\delta^{18}O$ values between ca. 7600 and 6500 cal yr BP related to a possible return of stronger inflow of Atlantic water (Figure 1). Similar reports of low $\delta^{18}O$ have be made for a nearby location in the western Barents Sea (ca. 10 000 cal yr BP; Berben et al., 2014) and for the southern Barents Sea (ca. 11 000 – 9500 cal yr BP; Risebrobakken et al., 2010) (Figure 1).

Depleted $\delta^{18}O$ values attributed to a stronger inflow of Atlantic water delivered by the SB have also been recorded at the western and northern Svalbard margin ca. 8000 cal yr BP (Slubowska et al., 2005; Werner et al., 2013) and in the Franz Victoria Trough ca. 7500 cal yr BP (Duplessy et al., 2001) (Figure 1). However, the depleted $\delta^{18}O$ values reported in the current study do not correspond with this observed time-transgressive pattern of the SB and it is assumed, therefore, that throughout the HTM, the core site was influenced by Atlantic water entering the Barents Sea via the NCaC through the BSO. This conclusion is consistent with observations in the southern Barents Sea ca. 11 000 – 9800 cal yr (Risebrobakken et al., 2010) and the north-western Barents Sea ca. 7000 cal yr BP (Klitgaard Kristensen et al., 2013) (Figure 1).

In our record, the increasing $\delta^{13}C$ after ca. 8500 cal yr BP indicates that the early Holocene is further characterized by an increasing trend in primary production and/or less stratified water masses; however, maximum TOC values throughout this period suggest the former, and is consistent with previous findings from the northern Barents Sea (Duplessy et al., 2001; Lubinski et al., 2001), the western Barents Sea (Berben et al., 2014) and the West Svalbard margin (Werner et al., 2013) (Figure 1).

Relatively low IP_{25} concentrations with increased brassicasterol abundances indicate reduced seasonal (spring) sea ice cover and longer (warmer) summers with open water conditions

suitable for phytoplankton production. The occurrence of reduced sea ice cover and longer summers is consistent with increased planktic foraminiferal concentrations (reported here and Carstens et al., 1997) and with longer ice-free seasons and a retreated ice margin in the northern Barents Sea (Duplessy et al., 2001) as well as increased phytoplankton production in the northern Fram Strait (Müller et al., 2009) (Figure 1). Reduced spring sea ice cover also indicates the HTM recorded at the sea surface between ca. 9300 and 6500 cal yr BP, which probably results from maximum summer insolation at 78° N. Similar conclusions regarding the timing and termination of the HTM based on IP_{25} records have been made for the Fram Strait (ending at ca. 8400 cal yr BP; Müller et al., 2009) and at the West Svalbard margin, where the last phase of the HTM was recorded ca. 8500 – 7000 cal yr BP (Müller et al., 2012) (Figure 1).

Previously, Risebrobakken et al. (2011) emphasized that, throughout the HTM, high latitude radiative forcing was not responsible for the overall conditions of the water column and ocean dynamics. They suggested instead, that an intensified heat advection which peaked at ca. 10 000 cal yr BP was the result of a major reorganization of the ocean circulation following the deglaciation. Additionally, atmospheric forcing further enhanced the transport of warm and salty water (Risebrobakken et al., 2011). As the surface layer was directly influenced by the high summer insolation, relatively high air temperatures might also have increased sea surface temperatures which could, additionally, have contributed to reduced seasonal sea ice cover. Further, Smedsrud et al. (2013) showed how increased inflow of Atlantic water via the BSO led to relatively warm and reduced sea ice conditions in the Barents Sea which caused an increased heat flux between the ocean and atmosphere, thus enhancing the formation of dense water. This led to a strong outflow through the BSX, causing a stronger inflow of Atlantic water and thereby maintaining an ocean feedback mechanism. Thus, a strengthening of warm and saline Atlantic water input into the Barents Sea might have contributed to the observed sea ice extent retreat, a possible physical mechanism corresponding to the previously proposed (and recent) 'Atlantification' (Årthun et al., 2012). Consistent with these suggestions, relatively low sea ice biomarker (IP_{25}) concentrations are accompanied by maximum brassicasterol abundances which, combined, indicate reduced sea ice cover during relatively short spring seasons, with longer summers leading to enhanced phytoplankton production within the proximity of the sea ice edge. Hence, throughout the early Holocene the sea ice edge was in the proximity of the core site at ca. 78° N (Figure 8A). The elevated brassicasterol concentrations might have resulted from lower seasonality shifts of the sea ice

edge or from longer and warmer summers, so the minimum (summer) sea ice position is less predictable compared to the maximum (Figure 8A). In any case, our proposed sea ice scenario suggests that water masses south of the study area were ice free, which agrees with open water conditions observed in the western Barents Sea (Berben et al., 2014) and the West Svalbard margin (Müller et al., 2012) (Figure 8A) during the early Holocene.

5.1.1 Holocene Thermal Maximum: onset and termination

Within the current study, the proxies indicate the timing of the HTM to be between ca. 9300 and 5800 cal yr BP, although with some differences. The biomarker data record the HTM between ca. 9300 and 6500 cal yr BP, the stable oxygen isotope record indicate maximum temperatures between ca. 8800 and 7300 cal yr BP, whereas the planktic faunal assemblages argue for maximum temperatures from ca. 7300 to 5800 cal yr BP. Since all analyses were carried out on sediment material from the same horizons and the variations in timing (HTM) are larger than the radiocarbon dating errors in the depth-age model (Figure 3), these differences in occurrence and duration of the HTM between proxies demonstrate the variability in proxy-specific response time.

Sea ice biomarkers record the HTM at the sea surface, which is influenced mainly by maximum insolation values. In contrast, the $\delta^{18}O$ record and the faunal assemblages record the HTM within the sub-surface water masses which is the habitat of the polar planktic foraminifera (Volkmann, 2000). These sub-surface water masses are not influenced directly by solar insolation as this is mainly restricted to the sea surface (ca. upper 30 m) (Andersson et al., 2010; Risebrobakken et al., 2011). Hence, the HTM recorded by the oxygen isotopes and planktic foraminiferal fauna reflect warmer water temperatures linked to an increased influence of Atlantic water. A time-transgressive inflow of Atlantic water from south to north along the Norwegian and Svalbard margins as documented by Hald et al. (2007) most likely caused the lag in response time between biomarker and planktic foraminiferal data.

A second lag in response time is observed between the stable isotope and planktic foraminiferal fauna data. The planktic foraminiferal fauna reflect an annual signal whereas, in the Arctic Ocean, the calcification of *N. pachyderma* is linked to phytoplankton blooms and occurs mainly in August (Kohfeld et al., 1996; Volkmann, 2000). However, sea-ice conditions may have caused a shift in the growing season (e.g. Farmer et al., 2008) and it has

also been found that planktic foraminifera may change their depth habitat for the calcification and thus reflect different temperatures compared to the general fauna (Simstich et al., 2003). In particular, *N. pachyderma* is found throughout the upper water column (50 - 100 m), but calcification occurs at depths between 100 - 200 m (e.g. Bauch et al., 1997; Stangeew, 2001; Simstich et al., 2003). Furthermore, the foraminiferal fauna response might also depend on factors other than temperature and salinity. For example, the subpolar species *T. quinqueloba* also depends on the available food supply (e.g. Volkmann, 2000) and increased nutrition might have followed later. Indeed, such a delay in food supply is suggested by increasing $\delta^{13}C$ values which likely reflect enhanced primary production, possibly associated with increased seasonal sea ice cover. After ca. 6500 cal yr BP, the increased concentrations of sea ice biomarkers certainly argue for the appearance of a MIZ which is associated with a high food supply on which *T. quinqueloba* seems to thrive (e.g. Volkmann, 2000). Hence, the timing of increased relative abundances of subpolar species is probably related to a combination of enhanced Atlantic water influence and increased nutrition availability due to a strengthening of the seasonal sea ice cover. Such a conclusion agrees with the observation of the HTM associated with Atlantic water, high primary productivity and food availability in the northern Barents Sea (Duplessy et al., 2001).

5.2 Well-ventilated water masses and moderated seasonality ca. 5800 – 2200 cal yr BP

Throughout the mid Holocene, the relative abundances of the subpolar foraminifera decrease indicating a reduced influence of Atlantic water inflow. In addition, the clear and stable dominance of *N. pachyderma* demonstrate the prevailing presence of Arctic water at the core site. Correspondingly, the enriched $\delta^{18}O$ values argue for lower temperatures consistent with previous records. Most notably, a similar cooler mid Holocene with a strongly reduced Atlantic water inflow and/or colder Atlantic water has been observed in the northern Barents Sea (Duplessy et al., 2001; Klitgaard Kristensen et al., 2013) (Figure 1) and it has also been suggested that Arctic water from the north-eastern Barents Sea might have influenced the western Barents Sea due to less heat advection from the south (Hald et al., 2007). In the eastern Fram Strait, Werner et al. (2013) observed cold conditions after ca. 5200 cal yr BP, with a profound decrease of *T. quinqueloba* and low planktic foraminiferal fluxes (Figure 1).

Compared with the early Holocene, lower TOC values indicate that the enriched $\delta^{13}C$ values reflect better ventilation of the water masses throughout the mid Holocene, consistent with previous research (Spielhagen and Erlenkeuser, 1994). For the northern Barents Sea, Lubinski et al. (2001) suggested that enriched $\delta^{13}C$ values might even reflect the ventilation conditions over a broad area (Figure 1) and similar $\delta^{13}C$ trends have indeed been reported for the northern Barents Sea (Duplessy et al., 2001), the western Barents Sea (Berben et al., 2014) and the West Svalbard margin (Werner et al., 2013) (Figure 1).

For the biomarkers, higher concentrations of IP_{25} with concomitant decreases in brassicasterol indicate an increased and consistent seasonal sea ice cover and similar IP_{25}-based observations of sea ice have been linked to the mid Holocene Neoglacial cooling for the northern Fram Strait (Müller et al., 2009) and West Svalbard margin (Müller et al., 2012) (Figure 1).

Overall, the climatic changes show a period marked by a continuous cooling trend with a dominance of cold Arctic water and an accompanying increase in seasonal sea ice cover. As the summer insolation decreased, it probably caused the surface layer to cool with increased production of seasonal sea ice. Consequently, the strongly reduced Atlantic water inflow could not have affected the sea ice distribution in the same way as was proposed for the early Holocene (i.e. via the ocean feedback mechanism). These changes are translated into a scenario consisting of an overall advance of the sea ice extent (Figure 8B). The minimum sea ice edge was probably further south compared to the early Holocene, consistent with previous observations in the northern Barents Sea after ca. 6000 cal yr BP. For example, Duplessy et al. (2001) recorded a southwards shift of the summer sea ice margin and Klitgaard Kristensen et al. (2013) argued for generally increased sea ice cover, with the MIZ advancing towards the south (Figure 8B). In the northern Fram Strait, Müller et al. (2009) found very low (almost absent) amounts of brassicasterol and increased concentrations of IP_{25}, which also indicates a more general southwards advance of the minimum sea ice edge at this time (Figure 8B). During winter, we suggest that the maximum sea ice edge ranged between 76 - 77° N or, at least, further south compared to the early Holocene (Figure 8A-B) and corresponds well to the sea ice conditions inferred from IP_{25} measurements at the continental slope of western Svalbard (Müller et al., 2012) (Figure 8B). In the western Barents Sea, however, IP_{25} was mainly absent, reflecting predominantly ice free conditions during this interval (Berben et al., 2014) (Figure 8B).

5.3 Stratified water masses and long icy winters ca. 2200 – 0 cal yr BP

The general decrease of *N. pachyderma* and increased relative abundances of subpolar foraminifera, indicate a returned influence of Atlantic water during the late Holocene. In addition to the overall observed trend, the planktic foraminiferal concentrations and fauna show additional fluctuations that argue for intervals of varying Atlantic water influence, an observation supported by an overall depleting trend and periods of even more depleted $\delta^{18}O$ values. These observations agree well with previous reports of more unstable oceanographic conditions throughout the late Holocene with episodic increases in Atlantic water into the northern Barents Sea (Duplessy et al., 2001; Lubinski et al., 2001), the western Barents Sea (Wilson et al., 2011; Berben et al., 2014) and the Svalbard margin (Jernas et al., 2013; Werner et al., 2013) (Figure 1).

An overall depletion in $\delta^{13}C$ values indicates enhanced stratification between the surface and sub-surface layers. A similar trend was found within the northern Barents Sea after ca. 3000 cal yr BP and was attributed to decreased ventilation and/or decreased primary production (Duplessy et al., 2001; Lubinski et al., 2001; Risebrobakken et al., 2011) (Figure 1). In addition, Werner et al. (2013) suggested that gradually decreasing $\delta^{13}C$ values at the West Svalbard margin could also be related to the density-driven downward migration of *N. pachyderma* as a response to the less-ventilated sub-surface waters (Kozdon et al., 2009) (Figure 1). The latter is suggested to be a result of the thickening of the surface layer due to the influence of sea ice and a freshening of the uppermost surface water layer. Werner et al. (2013) also found a similar increased in *G. uvula* throughout the late Holocene and noted similar findings at the south-west Svalbard margin (Rasmussen et al., 2007) (Figure 1) which were attributed to an increased contribution of cool productive coastal waters according to Husum and Hald (2012). A similar increased relative abundance of *G. uvula* was found in the western Barents Sea throughout the last ca. 1100 cal yr BP (Berben et al., 2014), and this was associated with slightly reduced salinities (Figure 1). However, since *G. uvula* is a rather small species, the increased relative abundance could also be created by the advection of tests by Atlantic water transport.

An increase in sea ice during the late Holocene is also indicated from the biomarker (IP_{25}) data. Previously, Berben et al. (2014) reported increased IP_{25} concentrations throughout the last ca. 1100 cal yr BP in the western Barents Sea, arguing for a south-westwards transgression of the sea ice edge (Figure 1). Further, and consistent with the episodes of

elevated planktic foraminiferal concentrations, the biomarker and TOC data also reveal episodes where the general trend is amplified (i.e. simultaneous increase in sea ice and phytoplankton biomarkers), most likely indicating intervals of intensified primary production. An intensified sea ice cover with intervals of sea ice fluctuations was also observed in the eastern Fram Strait throughout the last 3000 cal yr BP (Müller et al., 2012) (Figure 1).

Compared to the early Holocene, the observed sub-surface warming versus a sea surface cooling might seem contradictory, but indicates that the late Holocene was most likely characterized by a strong vertical stratification and a decoupling between the atmosphere and the oceanic sub-surface. Summer insolation was lower during the late Holocene resulting in cooler atmospheric temperatures and potentially enhanced sea ice production and/or reduced sea ice melt. In addition to the stronger vertical stratification of the water column, the increased sea ice cover probably also limited the heat flux between the atmosphere and the sub-surface water masses. In terms of seasonality, we suggest that relatively long spring seasons with extensive sea ice cover and maximum IP_{25} would have been followed by shorter (and probably cooler compared to previous periods) summers with lower phytoplankton production (brassicasterol) (Figure 8C). Overall, the site was characterized by an extensive sea ice cover with the maximum (and possibly minimum) sea ice edge further south of the core site (Figure 8C). Our observations and interpretations are also consistent with intensified sea ice occurrence in the northern Barents Sea (Duplessy et al., 2001; Klitgaard Kristensen et al., 2013), increasing sea ice cover in the Fram Strait (Müller et al., 2009; 2012) and the western Barents Sea (Berben et al., 2014) (Figure 8C). Finally, we note that concentrations of IP_{25} and brassicasterol in surface sediment material from a nearby location (78.39° N, 32.07° E; Navarro-Rodriguez, 2014) are, respectively, slightly lower and higher than those in the upper sections of the NP05-11-70GC core. We interpret these data as representing a slight reversal in the extent of spring sea ice cover during recent decades (Figure 8D) and a return to more open water conditions during summer (c.f. Mid Holocene). Of course, precedent for such a reversal in sea ice extent is evident during the last ca. 100 yr from observational records (Divine and Dick, 2006), but the biomarker data provide further evidence that sea ice cover likely exceeded the modern extent during the (pre-industrial) late Holocene (Figure 8C).

5.2.1 Sub-surface warming versus increased sea ice extent

The observed increase in sea ice extent corresponds well with the overall cooling throughout the late Holocene as recorded previously by various Arctic terrestrial (e.g. Bjune et al., 2009; Kaufman et al., 2009), ice core (e.g. Kaufman et al., 2009; Divine et al., 2011) and marine records (e.g. Slubowska et al., 2005; Skirbekk et al., 2010). The overall increased sea ice extent is most likely a direct result of the low insolation directly affecting the sea surface, possibly strengthened by a negative solar irradiance anomaly between ca. 2850 and 2600 cal yr BP which would have triggered the increased sea ice extent and decreased ventilation of the sub-surface waters. The probability of such a mechanism was illustrated further by a modelling experiment performed by Renssen et al. (2006).

The increased influence of Atlantic water inflow also correlates well to previous studies arguing for warmer sub-surface water masses throughout the late Holocene in the Barents Sea (Lubinski et al., 2001; Duplessy et al., 2005; Risebrobakken et al., 2010; Wilson et al., 2011) and at the Svalbard margin (Jernas et al., 2013; Werner et al., 2013). The increased Atlantic water influence is attributed to prevailing positive North Atlantic Oscillation (NAO) conditions, amplified by stronger stratification among the upper layers (Lubinski et al., 2001; Duplessy et al., 2005).

As it is suggested here that a positive NAO situation could have forced the general increased influence of Atlantic water, it might be that even more pronounced positive NAO conditions caused the observed intervals showing amplified conditions of Atlantic water inflow. Thus, Duplessy et al. (2005) correlated their minor fluctuations in temperatures to centennial to millennial-scale variations in the intensity of westerlies in the North Atlantic. These intervals also show further elevated levels of sea ice and phytoplankton biomarker concentrations. Müller et al. (2012) observed similar in-phase fluctuations of IP_{25} and phytoplankton biomarkers in the eastern Fram Strait and assumed that they might have been triggered by a temporarily strengthened inflow of Atlantic water and/or changed atmospheric circulation pattern and also argue that positive NAO-like conditions could have prevailed during intervals of elevated biomarker contents.

6 Conclusions

Holocene palaeoceanographic evolution in the northern Barents Sea has been reconstructed using multi-proxy data obtained from a marine sediment core taken from the Olga Basin. The observed changes of Atlantic water inflow and seasonal sea ice cover have illustrated natural oceanic variability and some possible physical driving forces and aspects of ocean-sea ice-atmosphere dynamics are discussed. Three major palaeoceanographic settings can be summarised as follows:

The early Holocene (ca. 9500 – 5800 cal yr BP)

Overall warm subpolar conditions, i.e. a pronounced inflow of Atlantic water, a reduced seasonal sea ice cover and an increased primary production, were determined, primarily, by the high summer insolation. The core site was influenced by Atlantic water entering the Barents Sea via the NCaC through the BSO which caused an increased heat flux between the ocean and the atmosphere. This led to an active ocean feedback mechanism that contributed to a reduced sea ice extent. Seasonally, the interval was characterised by short spring seasons, long productive summers and potentially less variability in sea ice. Some differences in the timing of the HTM between ca. 9300 and 5800 cal yr BP are attributed to proxy-specific responses. We suggest that sea ice responded most directly to solar insolation at the sea surface, whereas sub-surface water masses were more influenced by the inflow of Atlantic water. Stable isotopes (foraminifera) responded to changes in temperature and salinity changes, whereas the planktic foraminiferal distributions also depended on food availability. Furthermore, the latter two proxies reflect different seasons throughout the year and/or different depth habitats.

The mid Holocene (ca. 5800 – 2200 cal yr BP)

In this interval, an overall cooling trend was characterized by cold Arctic water, well-ventilated water masses and an advanced seasonal sea ice cover. These are associated with the Neoglacial cooling, consistent with reduced summer insolation at high latitudes. Due to the lowered summer insolation, reduced atmospheric temperatures likely affected sea surface conditions and increased sea ice production. This interval was also characterized by a general increase southwards in sea ice edge position during winter and summer.

The late Holocene (ca. 2200 – 0 cal yr BP)

This period was marked by an increased Atlantic water inflow, enhanced stratification and extensive seasonal sea ice cover. The overall increased sea ice cover was probably induced by lowered insolation. The observed sub-surface warming and sea surface cooling co-existed due to a decoupling between the atmosphere and the ocean, with the sea ice acting as a barrier between the two. Long spring seasons with extensive sea ice cover were followed by relatively short and less productive summers. Sea ice distribution was at its greatest extent within the entire record. Some reversal of sea ice expansion is proposed in recent decades. Elevated levels of Atlantic water inflow, primary production and seasonal sea ice cover suggest more unstable oceanographic conditions. These intervals are attributed to more pronounced positive NAO-like conditions that amplified the general trends.

Acknowledgements

This work was carried out within the framework of the Initial Training Network program "Changing Arctic and Subarctic Environments" (CASE, Grant Agreement No. 238111) funded by the European Commission within the 7th Framework Program People, the Research Council of Norway in addition to the University of Tromsø and Norwegian Polar Institute. Thanks are also extended to Trine Dahl and Julia Sen for assisting with laboratory work in addition to Patricia Cabedo-Sanz for valuable discussions.

References

Aagaard K and Greisman P (1975) Towards new mass and heat budgets in the Arctic Ocean. *J. Geophys. Res.* 80: 3821-3827.

Abrahamsen E, Østerhus S and Gammelsrød T (2006) Ice draft and current measurements from the north-western Barents Sea, 1993-96. *Polar Res.* 25: 25-37.

Aksenov Y, Bacon S, Coward AC and Nurser AJG (2010) The North Atlantic inflow to the Arctic Ocean: high-resolution model study. *J. Mar. Syst.* 79: 1-22.

Aksu AE and Vilks G (1988) Stable isotopes in planktonic and benthic foraminifera from Arctic Ocean surface sediments. *Can. J. Earth Sci.* 25: 701-709.

Andersson C, Pausata FSR, Jansen E, Risebrobakken B and Telford RJ (2010) Holocene trends in the foraminifer record from the Norwegian Sea and the North Atlantic Ocean. *Clim. Past* 6: 179-193, doi:10.5194/cp-6-179-2010.

Årthun M, Ingvaldsen RB, Smedsrud LH and Schrum C (2011) Dense water formation and circulation in the Barents Sea. *Deep-Sea Res. I* 58: 801-817.

Årthun M, Eldevik T, Smedsrud LH, Skagseth Ø and Ingvaldsen R (2012) Quantifying the influence of Atlantic heat on Barents Sea ice variability and retreat. *J. Clim.* 25: 4736-4743.

Barker S and Elderfield H (2002) Foraminiferal calcification response to glacial interglacial changes in atmospheric CO_2. *Science* 297: 883-836.

Barker S, Kiefer T and Elderfield H (2004) Temporal changes in North Atlantic circulation constrained by planktonic foraminiferal shell weights. *Paleoceanography* 19: PA3008.

Bauch D, Carstens J and Wefer G (1997) Oxygen isotope composition of living Neogloboquadrina pachyderma (sin.) in the Arctic Ocean. *Earth Planet. Sc. Lett.* 146: 47-58.

Bauch D, Carstens J, Wefer G and Thiede J (2000) The imprint of anthropogenic CO_2 in the Arctic Ocean: evidence from planktic $d^{13}C$ data from water column and sediment surfaces. *Deep-Sea Res. Pt. II* 9-11: 1791-1808.

Bé AWH and Tolderlund DS (1971) Distribution and ecology of living planktonic foraminifera in surface waters of the Atlantic and Indian Oceans. In Funnell BM and Riedel WR (eds) *The micropaleontology of oceans.* Cambridge University Press, London, 105-149.

Beer CJ, Schiebel R and Wilson PA (2010) Testing planktic foraminiferal shell weight as a surface water [CO_3^{2-}] proxy using plankton net samples. *Geology* 38: 103-106.

Belt ST, and Müller J (2013) The Arctic sea ice biomarker IP_{25}: a review of current understanding, recommendations for future research and applications in palaeo sea ice reconstructions. *Quaternary Sci. Rev. Doi: 10.1016/j.quascirev.2012.12.001.*

Belt ST, Massé G, Rowland SJ, Poulin M, Michel C and LeBlanc B (2007) A novel chemical fossil of palaeo sea ice: IP_{25}. *Org. Geochem.* 38: 16-27.

Belt ST, Brown TA, Navarro Rodriguez A, Cabedo Sanz P, Tonkin A and Ingle R (2012) A reproducible method for the extraction, identification and quantification of the Arctic sea ice proxy IP_{25} from marine sediments. *Anal. Method.* 4: 705-713.

Berben SMP, Husum K, Cabedo-Sanz P and Belt ST (2014) Holocene sub-centennial evolution of Atlantic water inflow and sea ice distribution in the western Barents Sea. *Clim. Past* 10: 181-198, doi:10.5194/cp-10-181-2014.

Bergami C, Capotondi L, Langone L, Giglio F and Ravaioli M (2009) Distribution of living planktonic foraminifera in the Ross Sea and the Pacific sector of the Southern Ocean (Antarctica). *Mar. Micropaleontol*. 73: 37-48.

Berger A (1978) Long-term variations of daily insolation and quaternary climatic changes. *J. Atmos. Sci.* 35: 2363-2367.

Bjune AE, Seppä H and Birks HJB (2009) Quantitative summer temperature reconstructions for the last 2000 years based on pollen-stratigraphical data from northern Fennoscandia. *J. Paleolimnol.* 41: 43-56.

Boltovskoy E, Boltovskoy D, Correa N and Brandini F (1996) Planktic foraminifera from the southwestern Atlantic (30° – 60°S): Species-specific patterns in the upper 50 m. *Mar. Micropaleontol.* 28: 53–72.

Broecker WS and Clark E (2001) An evaluation of Lohmann's foraminifera weight dissolution index. *Paleoceanography* 16: 531-534.

Brown TA and Belt ST (2012) Identification of the sea ice diatom biomarker IP_{25} in Arctic benthic macrofauna: Direct evidence for a sea ice diatom diet in Arctic heterotrophs. *Polar Biol.* 35: 131-137.

Brown TA, Belt ST, Philippe B, Mundy CJ, Massé G, Poulin M and Gosselin M (2011) Temporal and vertical variations of lipid biomarkers during a bottom ice diatom bloom in the Canadian Beaufort Sea: Further evidence for the use of the IP_{25} biomarker as a proxy for spring Arctic sea ice. *Polar Biol.* 34: 1857-1868.

Brown TA, Belt ST, Tatarek A and Mundy CJ (2014) Source identification of the Arctic sea ice proxy IP_{25}. *Nat. Commun.* 5:4197 doi: 10.1038/ncomms5197.

Burhol ALS (1994) Recent distribution of planktonic foraminifera on the Svalbard-Barents margin. Master Thesis, University of Tromsø, Tromsø, Norway.

Carmack E, Barber D, Christensen J, Macdonald R, Rudels B and Sakshaug E (2006) Climate variability and physical forcing of the food webs and the carbon budget on panarctic shelves. *Prog. Oceanogr.* 71: 145-181.

Carstens J, Hebbeln D and Wefer G (1997) Distribution of planktic foraminifera at the ice margin in the Arctic (Fram Strait). *Mar. Micropaleontol.* 29: 257-269.

Cifelli R (1961) Globigerina incompta, a new species of pelagic foraminifera from the North Atlantic. *Contributions Cushman Foundation Foraminiferal Research* 12: 83-86.

Conan SMH, Ivanova EM and Brummer G-JA (2002) Quantifying carbonate dissolution and calibration of foraminiferal dissolution indices in the Somali Basin. *Mar. Geol.* 182: 325-349.

Dahl-Jensen D, Moesgaard K, Gundestrup N, Clow GD, Johnsen SJ, Hansen AW and Balling N (1998) Past temperatures directly from the Greenland Ice Sheet. *Science* 282: 268-271.

Darling KF, Kucera M, Kroon D and Wade CM (2006) A resolution for the coiling direction paradox in Neogloboquadrina pachyderma. *Paleoceanography* 21: PA2011, doi:10-1029/2005PA001189.

Divine DV and Dick C (2006) Historical variability of sea ice edge position in the Nordic Seas. *J. Geophys. Res.* 111: C01001, doi:10.1029/2004JC002851.

Divine D, Isaksson E, Martma T, Meijer HAJ, Moore J, Pohjola V, van de Wal RSW and Godtliebsen F (2011) Thousand years of winter surface air temperature variations in Svalbard and northern Norway reconstructed from ice-core data. *Polar Research* 30: 7379, doi: 10.3402/polar.v30i0.7379.

Donner B and Wefer G (1994) Flux and stable isotope composition of Neogloboquadrina pachyderma and other planktonic foraminifers in the Southern Ocean (Atlantic sector). *Deep-Sea Res. Pt. I* 41: 1733-1743.

Duplessy JC, Ivanova E, Murdmaa I, Paterne M and Labeyrie L (2001) Holocene paleoceanography of the northern Barents Sea and variations of the northward heat transport by the Atlantic Ocean. *Boreas* 30: 2-16.

Duplessy JC, Cortijo E, Ivanova E, Khusid T, Labeyrie L, Levitan M, Murdmaa I and Paterne M (2005) Paleoceanography of the Barents Sea during the Holocene. *Paleoceanography* 20: A4004.

Ehrmann WU and Thiede J (1985) History of Mesozoic and Cenozoic sediment fluxes to the North Atlantic Ocean. Contributions to Sedimentology E. Schweizerbart'sche Verlagsbuchhandlung, Stuttgart, 15: 1-109, ISBN 3-510-57015-4.

Ellingsen I, Slagstad D and Sundfjord A (2009) Modification of water masses in the Barents Sea and its coupling to ice dynamics: A model study. *Ocean. Dyn.* 59: 1095-1108.

Fairbanks RG (1989) A 17 000-year glacia-eustatic sea level record: Influence of glacial melting rates on the Younger Dryas event and deep-ocean circulation. *Nature* 342: 637-642.

Farmer EJ, Chapman MR and Andrews JE (2008) Centennial-scale Holocene North Atlantic surface temperatures from Mg/Ca ratios in *Globigerina bulloides*, *Geochemistry, Geophysics, Geosystems*. Epub ahead of print 31December, DOI: 10.1029/2008GC002199.

Forcino FL (2012) Multivariate assessment of the required sample size for community paleoecological research. *Palaeogeogr. Palaeocl.* 315-316: 134-141.

Gammelsrød T, Leikvin Ø, Lien V, Budgell WP, Loeng H and Maslowski W (2009) Mass and heat transports in the NE Barents Sea: Observations and models. *J. Marine Syst.* 75: 56-69.

Hald M, Andersson C, Ebbesen H, Jansen E, Klitegaard-Kristensen D, Risebrobakken B, Salomonsen GR, Sejrup HP, Sarnthein M and Telford R (2007) Variations in temperature and extent of Atlantic water in the northern North Atlantic during the Holocene. *Quaternary Sci. Rev.* 26: 3423-3440.

Hebbeln D, Henrich R and Baumann K-H (1998) Paleoceanography of the last glacial/interglacial cycle in the Polar North Atlantic. *Quat. Sci. Rev.* 17: 125-153.

Henrich R, Baumann KH, Huber R and Meggers H (2002) Carbonate preservation records of the past 3Myr in the Norwegian-Greenland Sea and the northern North Atlantic: Implications for the history of NADW production. *Mar. Geol.* 184: 17-39.

Hopkins TS (1991) The GIN Sea: A synthesis of its physical oceanography and literature review, 1972–1985. *Earth Sci. Rev.* 30: 175-318.

Huber R, Meggers H, Baumann KH and Henrich R (2000) Recent and Pleistocene carbonate dissolution in sediments of the Norwegian-Greenland Sea. *Mar. Geol.* 165: 123-136.

Husum K and Hald M (2004) A continuous marine record 8000–1600 cal. yr BP from the Malangenfjord, north Norway: Foraminiferal and isotopic evidence. *Holocene* 14: 877-887.

Husum K and Hald M (2012) Arctic planktic foraminiferal assemblages: Implications for subsurface temperature reconstructions. *Mar. Micropaleontol.* 96-97: 38-47.

Jakobsson M, Grantz A, Kristoffersen Y and Macnab R (2004) Physiography and bathymetry of the Arctic Ocean. In: Stein R and Macdonald RW (eds) *The Organic Carbon Cycle in the Arctic Ocean*. Springer, New York, 1-5.

Jernas P, Klitgaard Kristensen D, Husum K, Wilson L and Koç N (2013) Palaeoenvironmental changes of the last two millennia on the western and northern Svalbard shelf. *Boreas* 42: 236-255.

Johannessen T, Jansen E, Flatøy A and Ravelo AC (1994) The relationship between surface water masses, oceanographic fronts and plaeoclimatic proxies in surface sediments of the Greenland, Iceland, Norwegian Seas. In: Zahn R, Pedersen TF, Kaminski MA and Labeyrie L (eds) *Carbon Cycling in the Glacial Ocean: Constraints of the Ocean's Role in Global Change*. Springer, Berlin, 61-86.

Jonkers L, Brummer G-JA, Peeters FJC, van Aken HM and De Jong MF (2010) Seasonal stratification, shell flux, and oxygen isotope dynamics of left-coiling N. pachyderma and T. quinqueloba in the western sub polar North Atlantic. *Paleoceanography* 25: PA2204.

Kaufman D, Ager TA, Anderson NJ, Anderson PM, Andrews JT, Bartlein PJ, Brubakker LB, Coats LL, Cwynar LC, Duvall ML, Dyke AS, Edwards ME, Eisner WR, Gajewski K, Geirsdottir A, Hu FS, Jennings AE, Kaplan MR, Kerwin MW, Loshkin AV, MacDonald GM, Miller GH, Mock CJ, Oswald WW, Otto-Bliesner BL, Porinchu DF, Rühland K, Smol JP, Steig EJ and Wolfe BB (2004) Holocene thermal maximum in the western Arctic (0 - 180 °N). *Quaternary Sci. Rev.* 23: 529-560.

Kaufman DS, Schneider DP, McKay NP, Ammann CM, Bradley RS, Briffa KR, Miller GH, Otto-Bliesner BL, Overpeck JT and Vinther BM (2009) Recent warming reverses long-term arctic cooling. *Science* 325(5945): 1236-1239.

Keigwin LD and Boyle EA (1989) Late Quaternary paleochemistry of high-latitude surface waters. *Palaeogeogr. Palaeocl.* 73: 85-106.

Klitgaard Kristensen D, Rasmussen TL and Koç N (2013) Paleoceanographic changes in the northern Barents Sea during the last 16 000 years – new constraints on the last deglaciation of the Svalbard-Barents Ice Sheet. *Boreas* 42: 798-813.

Knudsen KL (1998) Foraminiferer i Kvartær stratigrafi: Laboratorie og fremstillingsteknik samt udvalgte eksempler. *Geologisk Tidsskrift* 3: 1-25.

Koç N, Jansen E and Haflidason H (1993) Paleoceanographic reconstructions of surface ocean conditions in the Greenland, Iceland and Norwegian seas through the last 14 ka based on diatoms. *Quaternary Sci. Rev.* 12: 115-140.

Kohfeld KE, Fairbanks RG and Smith SL (1996) *Neogloboquadrina pachyderma* (sinistral coiling) as paleoceanographic tracers in polar oceans: Evidence from northeast water polynya plankton tows, sediments traps, and surface sediments. *Paleoceanography* 11: 679-699.

Kozdon R, Eisenhauer A, Weinelt M, Meland MY and Nuernberg D (2009) Reassessing Mg/Ca temperature calibrations of Neogloboquadrina pachyderma (sinistral) using paired d44/40Ca and Mg/Ca measurements. *Geochem. Geophys. Geosyst.* 10: Q03005, doi:10.1029/2008GC002169.

Kwok R (2009) Outflow of Arctic Ocean sea ice into the Greenland and Barents Seas: 1979-2007. *J. Clim.* 22(9): 2438-2457.

Kwok R, Maslowski W and Laxon S (2005) On large outflows of Arctic sea-ice into the Barents Sea. *Geophys. Res. Lett.* 32: L22503. Doi:10.1029/2005GL024485.

Laskar J, Robutel P, Joutel F, Gastineau M, Correia ACM and Levrard B (2004) A long-term numerical solution for the insolation quantities of the Earth. *Astron. Astrophys.* 428: 261-285.

Loeng H (1991) Features of the physical oceanographic conditions of the Barents Sea. *Polar Res.* 10: 5-18.

Loeng H, Ozhigin V, Ådlandsvik B and Sagen H (1993) Current Measurements in the northeastern Barents Sea. International Council for the Exploration of the Sea, Council Meeting 1993/C:41, Hydrographic Committee, 22.

Lubinski DJ, Polyak L and Forman SL (2001) Freshwater and Atlantic water inflows to the deep northern Barents and Kara seas since ca 13 ^{14}Cka: foraminifera and stable isotopes. *Quaternary Sci. Rev.* 20: 1851-1879.

Mangerud J, Bondevik S, Gulliksen S, Hufthammer AK and Høisæter T (2006) Marine ^{14}C reservoir ages for 19th century whales and molluscs from the North Atlantic. *Quaternary Sci. Rev.* 25: 3228-3245.

Manley TO (1995) Branching of Atlantic water within the Greenland—Spitsbergen passage: an estimate of recirculation. *J. Geophys. Res.* 100: 20627-20634.

Midttun L (1985) Formation of dense bottom water in the Barents Sea *Deep-Sea Res.* 32: 1233-1241.

Moros M, Emeis K, Risebrobakken B, Snowball I, Kuijpers A, McManus J and Jansen E (2004) Sea surface temperatures and ice rafting in the Holocene North Atlantic: Climate influences on northern Europe and Greenland. *Quaternary Sci. Rev.* 23: 2113-2126.

Müller J, Massé G, Stein R and Belt ST (2009) Variability of sea-ice conditions in the Fram Strait over the past 30000 years. *Nat. Geosci.* 2 (11): 772-776.

Müller J, Wagner A, Fahl K, Stein R, Prange M and Lohman G (2011) Towards quantitative sea ice reconstructions in the northern North Atlantic: A combined biomarker and numerical modelling approach. *Earth Planet. Sci. Lett.* 306: 137-148.

Müller J, Werner K, Stein R, Fahl K, Moros M and Jansen E (2012) Holocene cooling culminates in sea ice oscillations in Fram Strait. *Quaternary Sci. Rev.* 47: 1-14.

National Snow and Ice Data Center (NSIDC), Boulder Colorado, www.nsidc.com

Navarro-Rodriguez A (2014) Reconstruction of recent and palaeo sea ice conditions in the Barents Sea. PhD Thesis, Plymouth University, Plymouth, UK.

Novitskiy VP (1961) Permanent currents of the northern Barents Sea. *Tr. Gos. Okeanogr. Inst.* 64: 1-32. (English Translation)

Oppo DW and Fairbanks RG (1989) Carbon isotope composition of tropical surface water during the past 22,000 years. *Paleoceanography* 4: 333-351.

Pfirman SL, Bauch D and Gammelsrød T (1994) The Northern Barents Sea: water mass distribution and modification. In: Johannessen OM, Muench RD and Overland JE (eds) *The Polar Oceans and Their Role in Shaping the Global Environment*. *AGU Geoph. Monog. Series.* 85: 77-94.

Pfuhl HA and Shackleton NJ (2004) Two proximal, high-resolution records of foraminiferal fragmentation and their implications for changes in dissolution. *Deep-Sea Res. Pt. I* 51: 809-832.

Rasmussen TL, Thomsen E, Slubowska MA, Jessen S, Solheim A and Koç N (2007) Paleoceanographic evolution of the SW Svalbard margin (76 °N) since 20 000 ^{14}C yr BP. *Quaternary Res.* 67: 100-114.

Rasmussen TL, Forwick M and Mackensen A (2012) Reconstruction of inflow of Atlantic Water to Isfjorden, Svalbard during the Holocene: Correlation to climate and seasonality. *Mar. Micropaleontol.* 94-95: 80-90.

Reimer PJ, Baillie MGL, Bard E, Bayliss A, Beck JW, Blackwell PG, Ramsey CB, Buck CE, Burr GS, Edwards RL, Friedrich HM, Grootes PM, Guilderson TP, Hajdas I, Heaton TJ, Hogg AG, Hughen KA, Kaiser KF, Kromer B, Mccormac FG, Manning SW, Reimer RW, Richards DA, Southon JR, Talamo S, Turney CSM, Van Der Plicht J and Weyhenmeyer CE (2009) IntCal09 and Marine09 radiocarbon age calibration curves, 0-50 000 years cal BP. *Radiocarbon* 51: 1111-1150.

Renssen H, Goosse H and Muscheler R (2006) Coupled climate model simulation of Holocene cooling events: oceanic feedback amplifies solar forcing. *Clim. Past* 2: 79-90, doi:10.5194/cp-2-79-2006.

Reynolds L and Thunnel RC (1985) Seasonal succession of planktonic foraminifera in the subpolar North Pacific. *J. Foramin. Res.* 15: 282-301.

Risebrobakken B, Morros M, Ivanova EV, Chistyakova N and Rosenberg R (2010) Climate and oceanographic variability in the SW Barents Sea during the Holocene. *Holocene* 20: 609-621.

Risebrobakken B, Dokken T, Smedsrud LH, Andersson C, Jansen E, Moros M and Ivanova EV (2011) Early Holocene temperature variability in the Nordic Seas: The role of oceanic heat advection versus changes in orbital forcing. *Paleoceanography* 26: PA4206.

Rudels B (1987) On the mass balance of the Polar Ocean, with special emphasis on the Fram Strait. *Norsk Polarinst. Skri.* 188: 53.

Saito T, Thompson PR and Breger D (1981) Systematic index of recent and pleistocene planktonic foraminifera. University of Tokyo press, Tokyo, Japan.

Sakshaug E, Bjørge A, Gulliksen B, Loeng H and Mehlum F (1992) Økosystem Barentshavet. Norges Allmenvitenskapelige Forskningsråd, Norges Fiskeriforskningsråd, Miljøverndepartementet, 304.

Sarnthein M, Van Kreveld S, Erlenkeuser H, Grootes PM, Kucera M, Pflaumann U and Schulz M (2003) Centennial- to millennial-scale periodicities of Holocene climate and sediment injections off the western Barents shelf, 75 N. *Boreas* 32: 447-461.

Schauer U, Loeng H, Rudels B, Ozhigin VK and Dieck W (2002) Atlantic Water flow through the Barents and Kara Seas. *Deep-Sea Res. I* 49: 2281-2298.

Scott DB, Schell T, Rochon A and Blasco S (2008) Modern benthic foraminifera in the surface sediments of the Beaufort shelf, slope and Mackenzie Through, Beaufort Sea, Canada: Taxonomy and summary of surficial distributions. *J. Foramin. Res.* 38: 228-250.

Screen JA and Simmonds I (2010) The central role of diminishing sea ice in recent Arctic temperature amplification. *Nature* 464: 1334-1337.

Serreze M, Barrett A, Slater A, Steele M, Zhang J and Trenberth K (2007) The large-scale energy budget of the Arctic. *J. Geophys. Res.* 112: D11122, doi.:10.1029/2006JD008230.

Simstich J, Sarnthein M and Erlenkeuser H (2003) Paired $\delta^{18}O$ signals of N. pachyderma (s) and T. quinqueloba show thermal stratification structure in the Nordic Seas *Mar. Micropaleontol.* 48: 107-125.

Skirbekk K, Klitgaard Kristensen D, Rasmussen TL, Koç N and Forwick M (2010) Holocene climate variations at the entrance to a warm Arctic fjord: evidence from Kongsfjorden trough, Svalbard. *Geological society, London, Special Publications 2010* 344: 289-304, doi:10.1144/SP344.20.

Slubowska MA, Koç N, Rasmussen TL and Klitgaard-Kristensen D (2005) Changes in the flow of Atlantic water into the Arctic Ocean since the last deglaciation: Evidence from the northern Svalbard continental margin, 80N. *Paleoceonography* 20: PA4014, doi:10.1029/2005PA001141.

Slubowska-Woldengen M, Rasmussen TL, Koç N, Klitgaard-Kristensen D, Nilsen F and Solheim A (2007) Advection of Atlantic Water to the western and northern Svalbard shelf since 17 500 cal yr BP. *Quaternary Sci. Rev.* 26: 463-478.

Smedsrud LH, Esau I, Ingvaldsen RB, Eldevik T, Haugan PM, Li C, Lien VS, Olsen A, Omar AM, Otterå OH, Risebrobakken B, Sandø AB, Semenov VA and Sorokina SA (2013) The role of the Barents Sea in the Arctic climate system. *Rev. Geophys.* 51: 415-449, doi:10.1002/rog.20017.

Smith WO and Sakshaug E (1990) Polar phytoplankton. In: Smith WO (ed) *Polar oceanography, Part B: Chemistry, Biology and Geology*. Academic Press, New York, 447-525.

Sorteberg A and Kvingedal B (2006) Atmospheric forcing on the Barents Sea winter ice extent. *J. Clim.* 19: 4772-4784.

Spielhagen RF and Erlenkeuser H (1994) Stable oxygen and carbon isotopes in planktic foraminifera from the Arctic Ocean surface sediments: Reflection of the low salinity surface water layer. *Mar. Geol.* 119: 227-250.

Spielhagen RF, Werner K, Aagaard-Sørensen S, Zamelczyk K, Kandiano E, Budeus G, Husum K, Marchitto T and Hald M (2011) Enhanced modern heat transfer to the Arctic by warm Atlantic water. *Science* 331: 450-453.

Stangeew E (2001) Distribution and isotopic composition of living planktonic foraminifera N. pachyderma (sinistral) and T. quinqueloba in the high latitude North Atlantic. Ph.D. thesis, Math.-Naturwiss. Fak., Christian-Albrechts-Univ., Kiel, Germany. (Available at http://e-diss.uni-kiel.de/diss_464/pp).

Steinsund PI and Hald M (1994) Recent carbonate dissolution in the Barents Sea: Paleoceanographic applications. *Mar. Geol.* 117: 202-316.

Stuiver M and Reimer PJ (1993) Extended ^{14}C data base and revised CALIB 3.0 ^{14}C age calibration program. *Radiocarbon* 35: 215-230.

Vinje TE (1977) Sea ice conditions in the European sector of the marginal seas of the Arctic, 1966-75. *Aarb. Nor. Polarinst.* 1975: 163-174.

Vinje T (2001) Anomalies and trends of sea-ice extent and atmospheric circulation in the Nordic Seas during the period 1864-1998. *J. Clim.* 14(3): 255-267.

Volkmann R (2000) Planktic foraminifers in the outer Laptev Sea and the Fram Strait: Modern distribution and ecology. *J. Foramin. Res.* 30: 157-176.

Wanner H, Beer J, Bütikofer J, Crowley TJ, Cubasch U, Flückiger J, Goosse H, Grosjean M, Joos F, Kaplan JO, Küttel M, Müller SA, Prentice C, Solomina O, Stocker TF, Tarasov P, Wagner M and Widmann M (2008) Mid- to Late Holocene climate change: An overview. *Quat. Sci. Rev.* 27(19–20): 791-1828.

Wassmann P, Reigstad M, Haug T, Rudels B, Carroll ML, Hop H, Gabrielsen GW, Falk-Petersen S, Denisenko G, Arashkevich E, Slagstad D and Pavlova O (2006) Food webs and carbon flux in the Barents Sea. *Prog. Oceanogr.* 71: 232-287.

Werner K, Spielhagen RF, Bauch D, Hass HC and Kandiano E (2013) Atlantic Water advection versus sea-ice advances in the eastern Fram Strait during the last 9 ka: Multi proxy evidence for a two-phase Holocene. *Paleoceanography* 28: 283-295.

Wilson LJ, Hald M and Godtliebsen F (2011) Foraminiferal faunal evidence of twentieth-century Barents Sea warming. *Holocene*, 21(4): 527-537.

Yang S and Christensen JH (2012) Arctic sea ice reduction and European cold winters in CMIP5 climate change experiments. *Geophys. Res. Lett.* 39: L20707, doi:10.1029/2012GL053338.

Zamelczyk K, Rasmussen TL, Husum K and Hald M (2013) Marine calcium carbonate preservation vs. climate change over the last two millennia in the Fram Strait: Implications for planktic foraminiferal paleostudies. *Mar. Micropaleontol.* 98: 14-27.

Figure captions

Table 1: Depth-age model of NP05-11-70GC calibrated using Calib 6.1.1 (Stuiver and Reimer, 1993), the Marine09 calibration curve (Reimer et al., 2009) and a local reservoir age (ΔR) of 105 ± 24 after Mangerud et al. (2006).

Figure 1: The modern oceanography is presented on a bathymetric map of the Barents Sea area. The core location of NP05-11-70GC is indicated by a green circle, whereas previously published records are indicated by number: 1) Risebrobakken et al. (2010) 2) Wilson et al. (2011) 3) Berben et al. (2014) 4) Sarnthein et al. (2003) 5) Rasmussen et al. (2007) 6) Müller et al. (2012); Werner et al. (2013) 7) Skirbekk et al. (2010); Jernas et al. (2013) 8) Müller et al. (2009) 9) Slubowska et al. (2005); Jernas et al. (2013) 10) Klitgaard Kristensen et al. (2013) 11) Lubinski et al. (2001) 12) Duplessy et al. (2001); (2005) 13) Risebrobakken et al. (2011) 14) Duplessy et al. (2005). Northern Barents Sea Opening (NBSO), Barents Sea Opening (BSO), Barents Sea Exit (BSX). A) The main surface currents (Hopkins, 1991). Atlantic water (red): Norwegian Atlantic Current (NwAC), North Cape Current (NCaC), West Spitsbergen Current (WSC), Return Atlantic Current (RAC), Yermak Branch (YB) and Svalbard Branch (SB). Polar water (blue): Bear Island Current (BIC) and East Spitsbergen Current (ESC). Coastal water (black): Norwegian Coastal Current (NCC). B) Seasonal sea ice extent (April (blue) and August (orange)) for the period 1981 – 2010 (National Snow and Ice Data Centre (NSIDC) Boulder Colorado, www.nsidc.com). The observed sea ice extent for April (dotted) and August (dashed) from historical data for four sub periods between 1870 and 2002: 1870 – 1920 (red), 1921 – 1961 (yellow), 1962 – 1988 (pink) and 1989 – 2002 (black) (Divine and Dick, 2006).

Figure 2: Temperature (black) and Salinity (grey) profile at the NP05-11-70GC core site (78.40° N, 32.42° E). Water masses are defined according Gammelsrød et al., 2009.

Figure 3: Depth-age model of NP05-11-70GC. A) Calibrated radiocarbon ages plotted versus depth with a linear interpolation between the dated levels. Error bars indicate the sampled depth intervals and a 2-σ error on the calibrated ages. B) Sedimentation rate versus depth. C) Resolution range versus depth.

Figure 4: Planktic foraminiferal concentration, flux and preservation indicator analysis versus calendar years BP. The black diamonds on the Y-axis denote the AMS ^{14}C converted to calibrated radiocarbon ages. The in grey highlighted periods are characterized by an increased influence of Atlantic water. A) Total planktic foraminiferal concentration (line) and flux (fill) versus age. B) Planktic foraminiferal fragmentation versus age. C) Mean shell weight of *N. pachyderma* versus age.

Figure 5: Planktic foraminiferal fauna analysis versus calendar years BP. The black diamonds on the Y-axis denote the AMS ^{14}C converted to calibrated radiocarbon ages. The in grey highlighted periods are characterized by an increased influence of Atlantic water. A) Total planktic foraminiferal concentration (line) and flux (fill) versus age. B-G) Species-specific relative abundance (line) and flux (fill) versus age. H) July insolation at 78° N (Laskar et al., 2004) (note the reversed axis) versus age.

Figure 6: Stable isotopes analysis performed on *N. pachyderma* versus calendar year BP. The black diamonds on the Y-axis denote the AMS ^{14}C converted to calibrated radiocarbon ages. The in grey highlighted periods are characterized by an increased influence of Atlantic water. A) δ^{18}O measurements corrected for ice volume effect after Fairbanks (1989) versus age. B) δ^{13}C measurements versus age. C) July insolation at 78° N (Laskar et al., 2004) (note the reversed axis) versus age.

Figure 7: Biomarker analysis versus calendar years BP: biomarker-specific fluxes (fill) and concentrations normalized to sediment (black line) and to total organic carbon (grey line). The black diamonds on the Y-axis denote the AMS ^{14}C converted to calibrated radiocarbon ages. The in grey highlighted periods are characterized by an increased influence of Atlantic water. A) Sea ice biomarker IP_{25} versus age. B) Phytoplankton biomarker brassicasterol versus age. C) Total organic carbon versus age. D) P_BIP_{25} (fill) and July insolation at 78° N (line) (Laskar et al., 2004) (note the reversed axis) versus age.

Figure 8: Scenarios of the proposed biomarker production (scheme) and seasonal sea ice distribution (map) scenarios at the NP05-11-70GC core location (green circle). A-C) Proposed biomarker production and seasonal sea ice distribution scenarios for, respectively, the early Holocene, the mid Holocene and the late Holocene. The shaded areas represent the proposed variability of the sea ice edge whereas the numbers indicate the core locations of previous studies: 1) Berben et al. (2014), 2) Müller et al. (2012), 3) Müller et al. (2009), 4) Klitgaard Kristensen et al. (2013), and 5) Duplessy et a. (2001). D) Present day situation based on mean sea ice extent

(1981 - 2010) for March (black), April (blue) and August (orange) (National Snow and Ice Data Centre (NSIDC) Boulder Colorado, www.nsidc.com).

Table 1

Lab ID	Core depth (cm)	Material	Uncorrected AMS ^{14}C age	1σ	Calibrated age 2-σ range	Calibrated age used in depth-age model (cal yr BP)
Beta-331327	47 - 53	Benthic foraminifera	2780	30	2281 - 2496	2389
Beta-346803	77 - 82	Benthic foraminifera	6110	40	6298 - 6536	6417
Beta-331328	132 - 137	Benthic foraminifera	8870	50	9307 - 9527	9417
Beta-331329	223 - 240	Benthic foraminifera	> 43500			

Figure 1

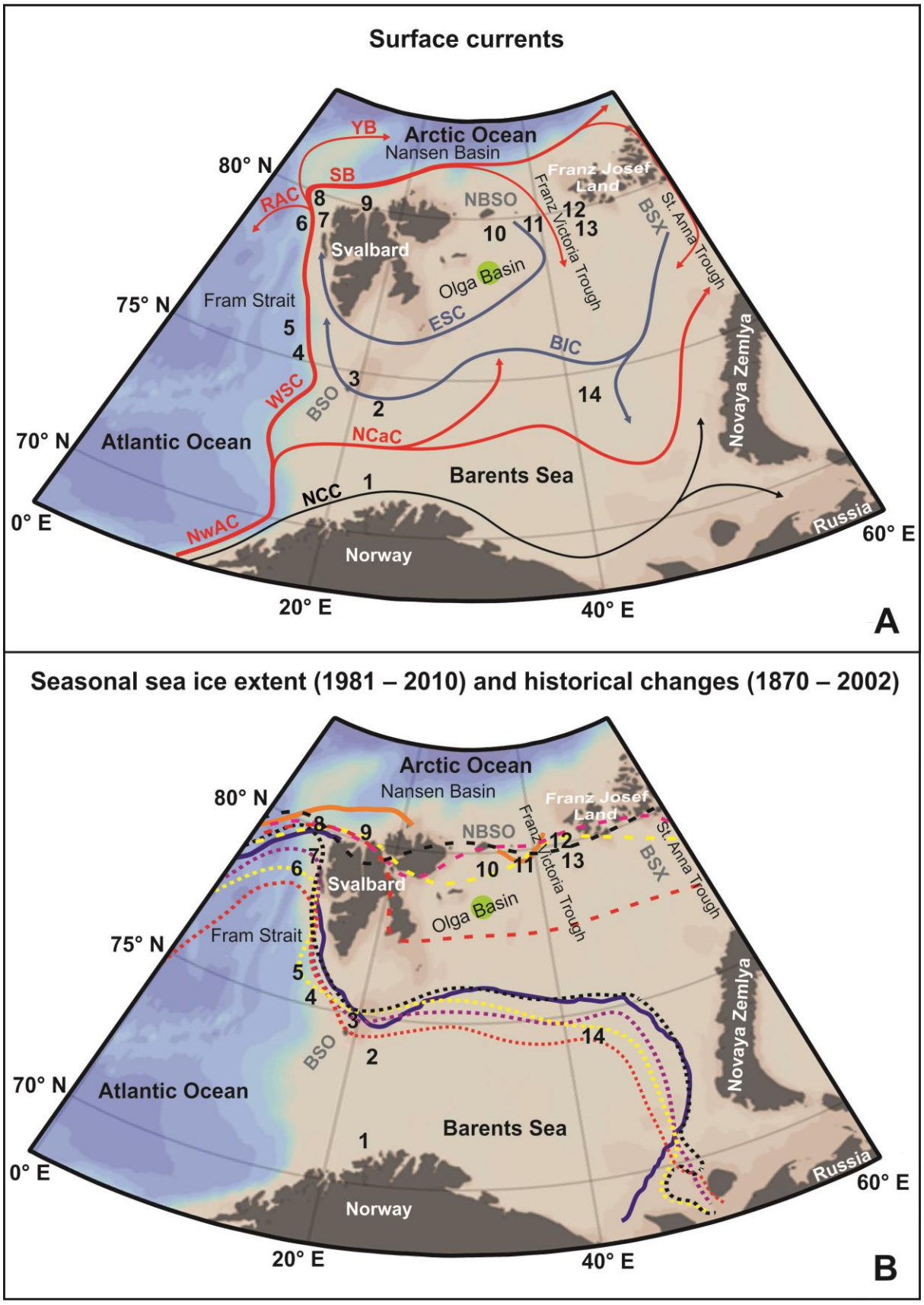
Surface currents
Arctic Ocean
Nansen Basin
YB
SB
RAC
80° N
75° N
70° N
0° E
20° E
40° E
60° E
Fram Strait
Svalbard
NBSO
Franz Victoria Trough
Franz Josef Land
BSX
St. Anna Trough
Olga Basin
ESC
BIC
WSC
BSO
NCaC
NCC
NwAC
Atlantic Ocean
Barents Sea
Norway
Russia
Novaya Zemlya
1
2
3
4
5
6
7
8
9
10
11
12
13
14
A
Seasonal sea ice extent (1981 – 2010) and historical changes (1870 – 2002)
Arctic Ocean
Nansen Basin
80° N
75° N
70° N
0° E
20° E
40° E
60° E
Fram Strait
Svalbard
NBSO
Franz Victoria Trough
Franz Josef Land
BSX
St. Anna Trough
Olga Basin
BSO
Atlantic Ocean
Barents Sea
Norway
Russia
Novaya Zemlya
1
2
3
4
5
6
7
8
9
10
11
12
13
14
B

Figure 2

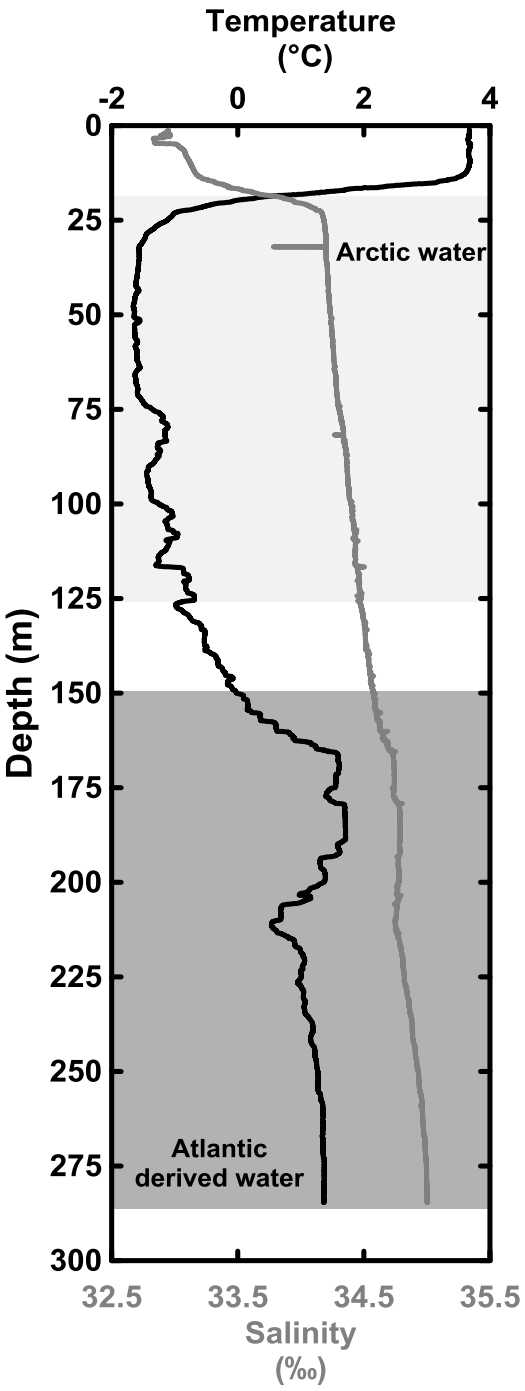
Temperature
(°C)
-2
0
2
4
0
25
50
75
100
125
150
175
200
225
250
275
300
Depth (m)
Arctic water
Atlantic
derived water
32.5
33.5
34.5
35.5
Salinity
(‰)

Figure 3

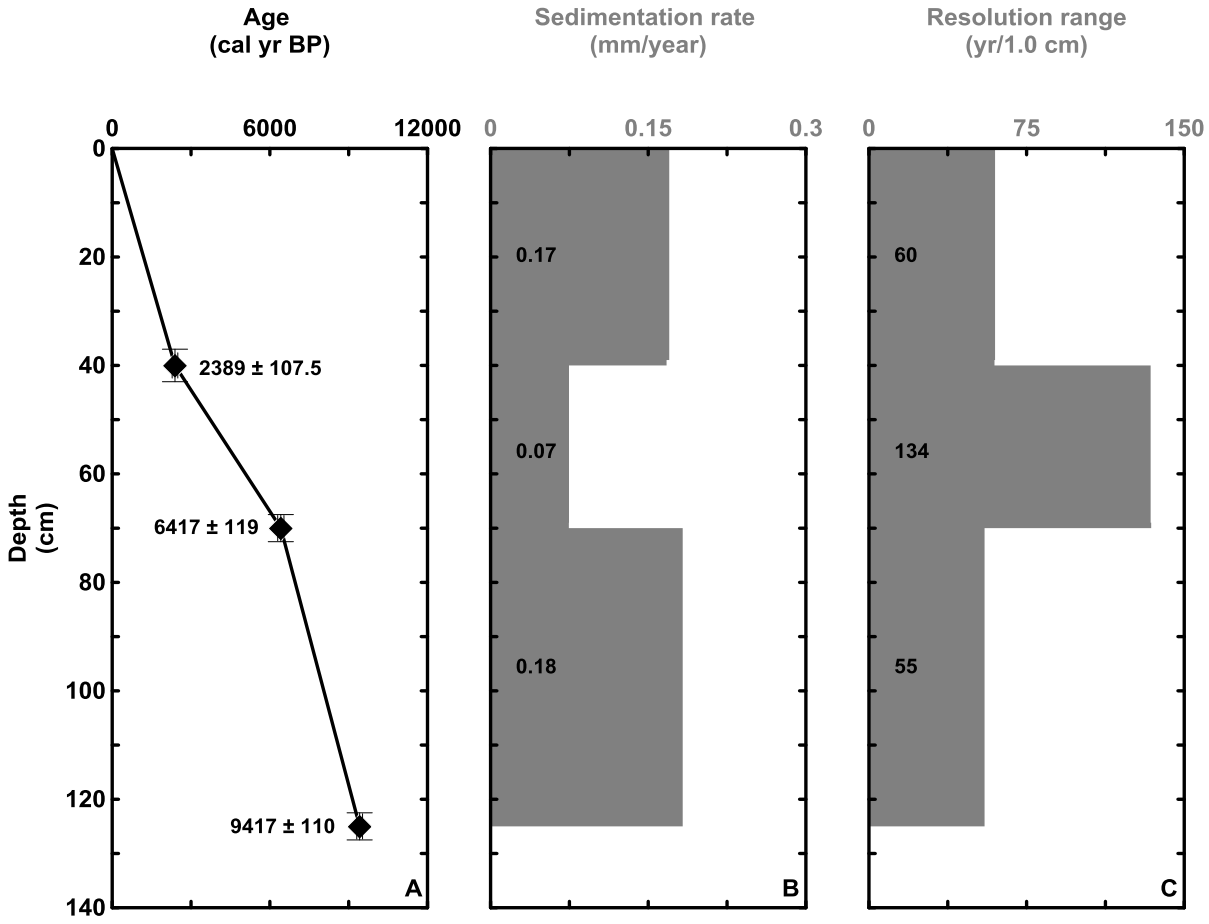
Age
(cal yr BP)
Sedimentation rate
(mm/year)
Resolution range
(yr/1.0 cm)
0
6000
12000
0
0.15
0.3
0
75
150
Depth
(cm)
0
20
40
60
80
100
120
140
2389 ± 107.5
6417 ± 119
9417 ± 110
A
0.17
0.07
0.18
B
60
134
55
C

Figure 4

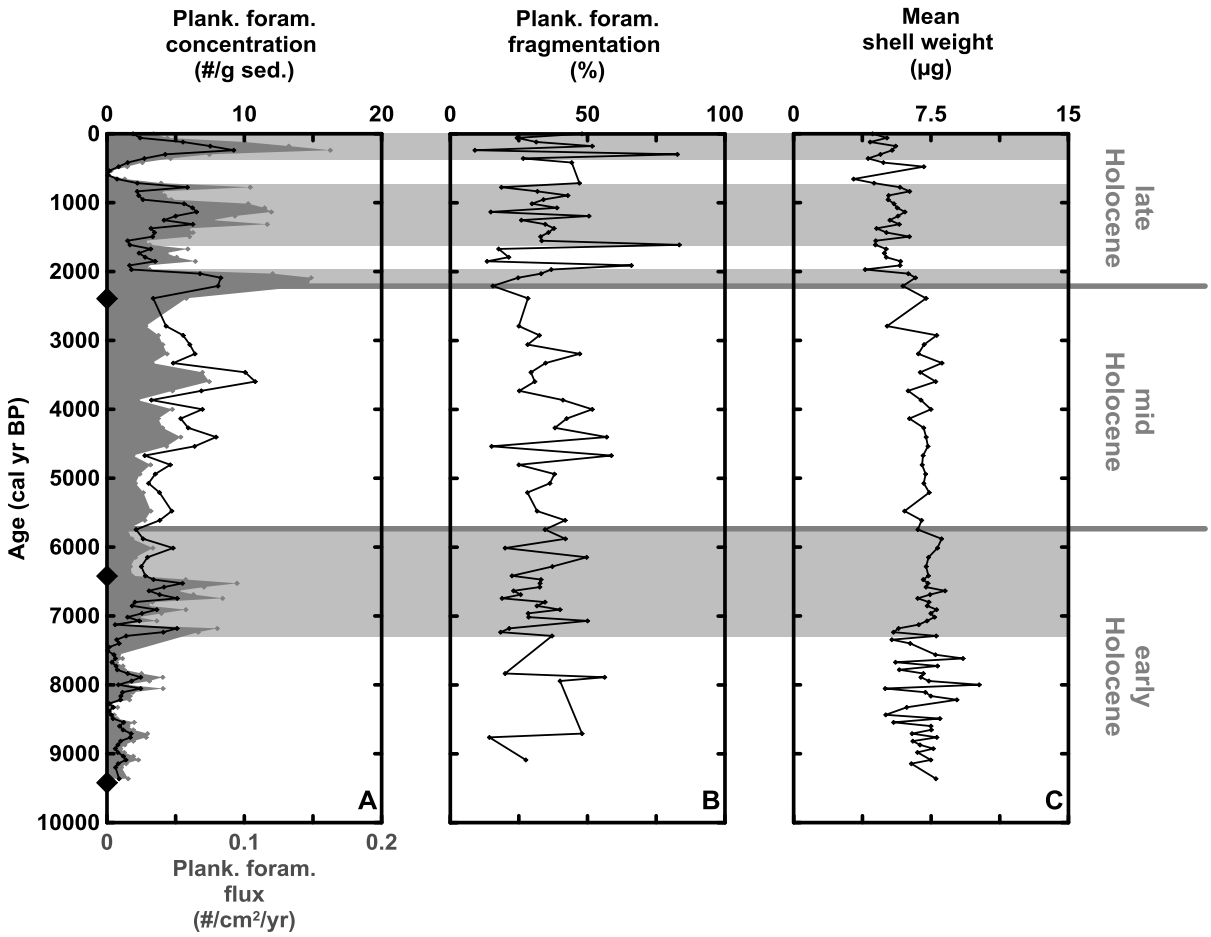
Plank. foram. concentration (#/g sed.)
Plank. foram. fragmentation (%)
Mean shell weight (µg)
0
10
20
50
100
7.5
15
Age (cal yr BP)
0
1000
2000
3000
4000
5000
6000
7000
8000
9000
10000
late Holocene
mid Holocene
early Holocene
A
B
C
0
0.1
0.2
Plank. foram. flux (#/cm²/yr)

Figure 5

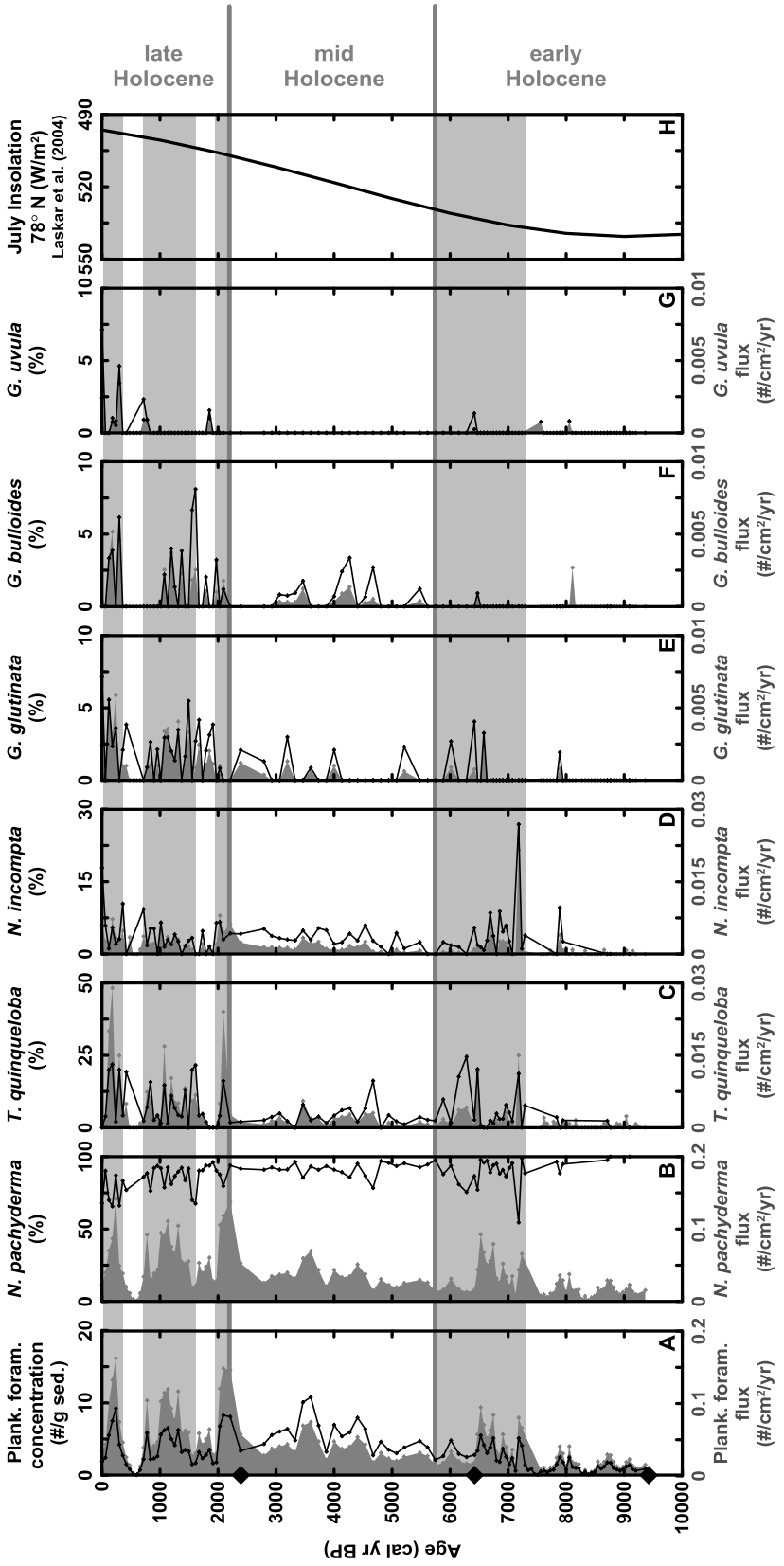
late Holocene
mid Holocene
early Holocene
July Insolation 78° N (W/m²) Laskar et al. (2004)
Plank. foram. concentration (#/g sed.)
N. pachyderma (%)
T. quinqueloba (%)
N. incompta (%)
G. glutinata (%)
G. bulloides (%)
G. uvula (%)
Plank. foram. flux (#/cm²/yr)
N. pachyderma flux (#/cm²/yr)
T. quinqueloba flux (#/cm²/yr)
N. incompta flux (#/cm²/yr)
G. glutinata flux (#/cm²/yr)
G. bulloides flux (#/cm²/yr)
G. uvula flux (#/cm²/yr)
A
B
C
D
E
F
G
H
Age (cal yr BP)

Figure 6

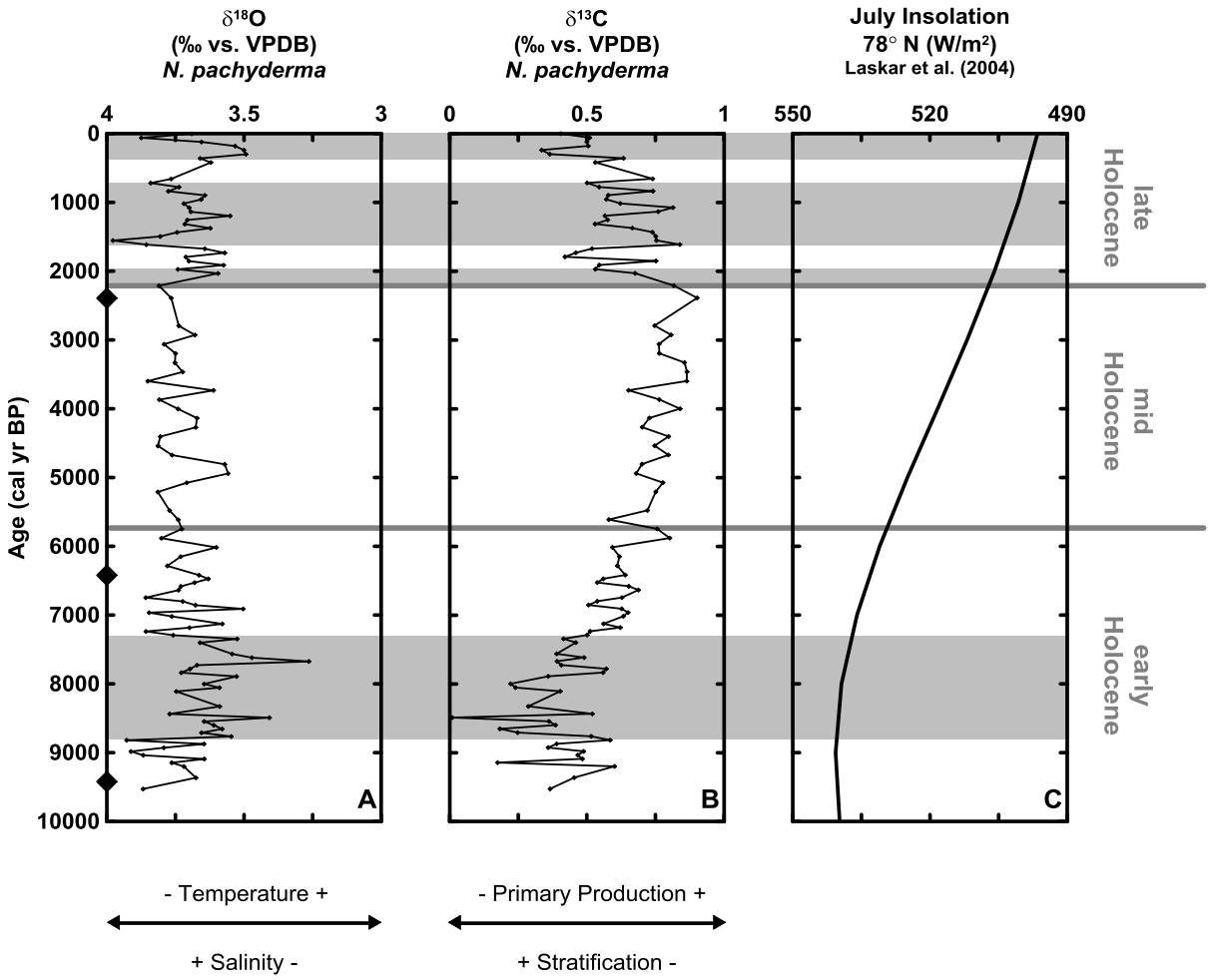
δ18O
(‰ vs. VPDB)
N. pachyderma
δ13C
(‰ vs. VPDB)
N. pachyderma
July Insolation
78° N (W/m2)
Laskar et al. (2004)
4
3.5
3
0
0.5
1
550
520
490
Age (cal yr BP)
0
1000
2000
3000
4000
5000
6000
7000
8000
9000
10000
late Holocene
mid Holocene
early Holocene
A
B
C
- Temperature +
+ Salinity -
- Primary Production +
+ Stratification -

Figure 7

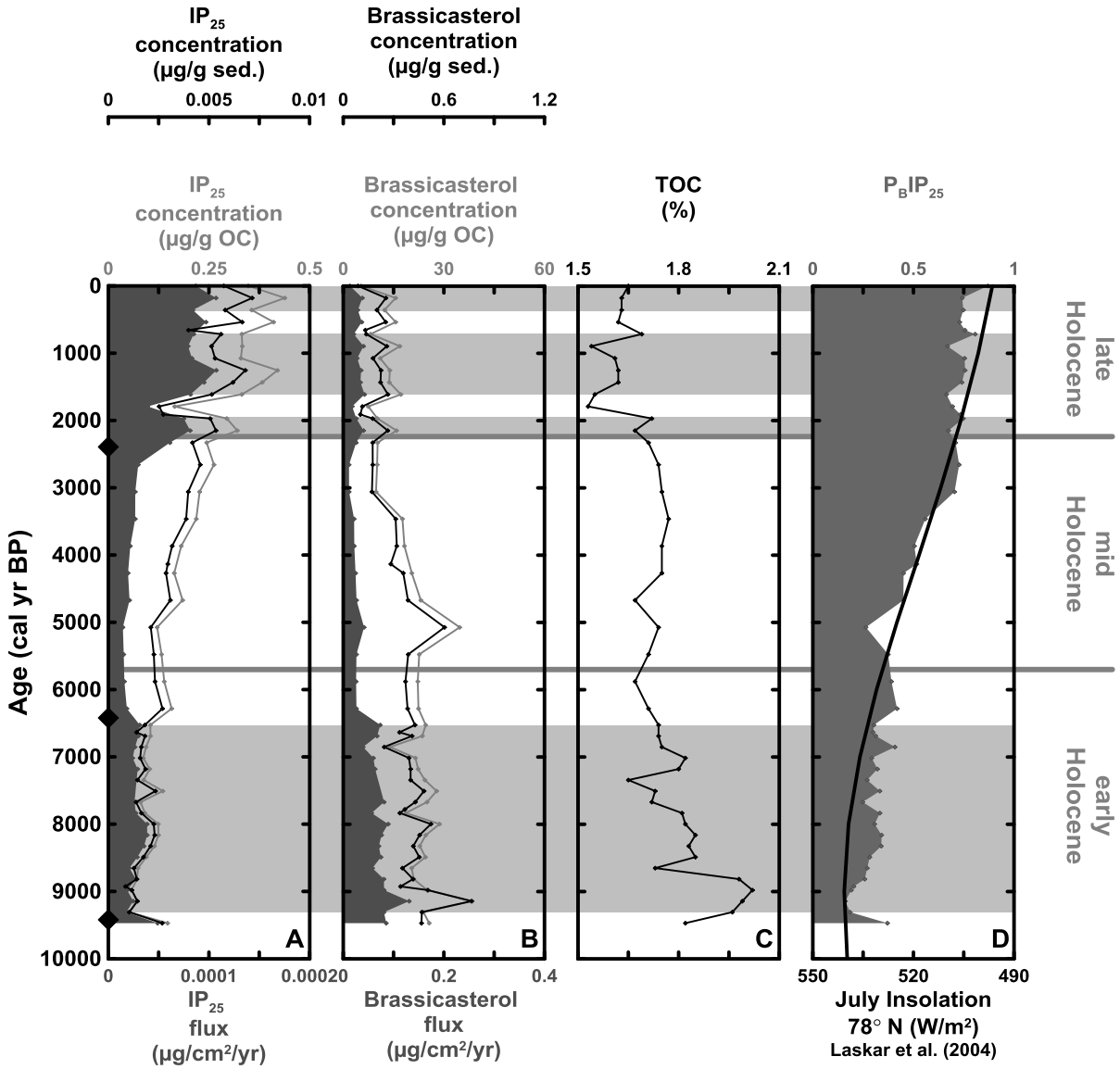
IP25 concentration (µg/g sed.)
0 0.005 0.01
Brassicasterol concentration (µg/g sed.)
0 0.6 1.2
IP25 concentration (µg/g OC)
0 0.25 0.5
Brassicasterol concentration (µg/g OC)
0 30 60
TOC (%)
1.5 1.8 2.1
PBIP25
0 0.5 1
Age (cal yr BP)
0 1000 2000 3000 4000 5000 6000 7000 8000 9000 10000
late Holocene
mid Holocene
early Holocene
A
B
C
D
0 0.0001 0.00020
IP25 flux (µg/cm²/yr)
0 0.2 0.4
Brassicasterol flux (µg/cm²/yr)
550 520 490
July Insolation 78° N (W/m²)
Laskar et al. (2004)

Figure 8

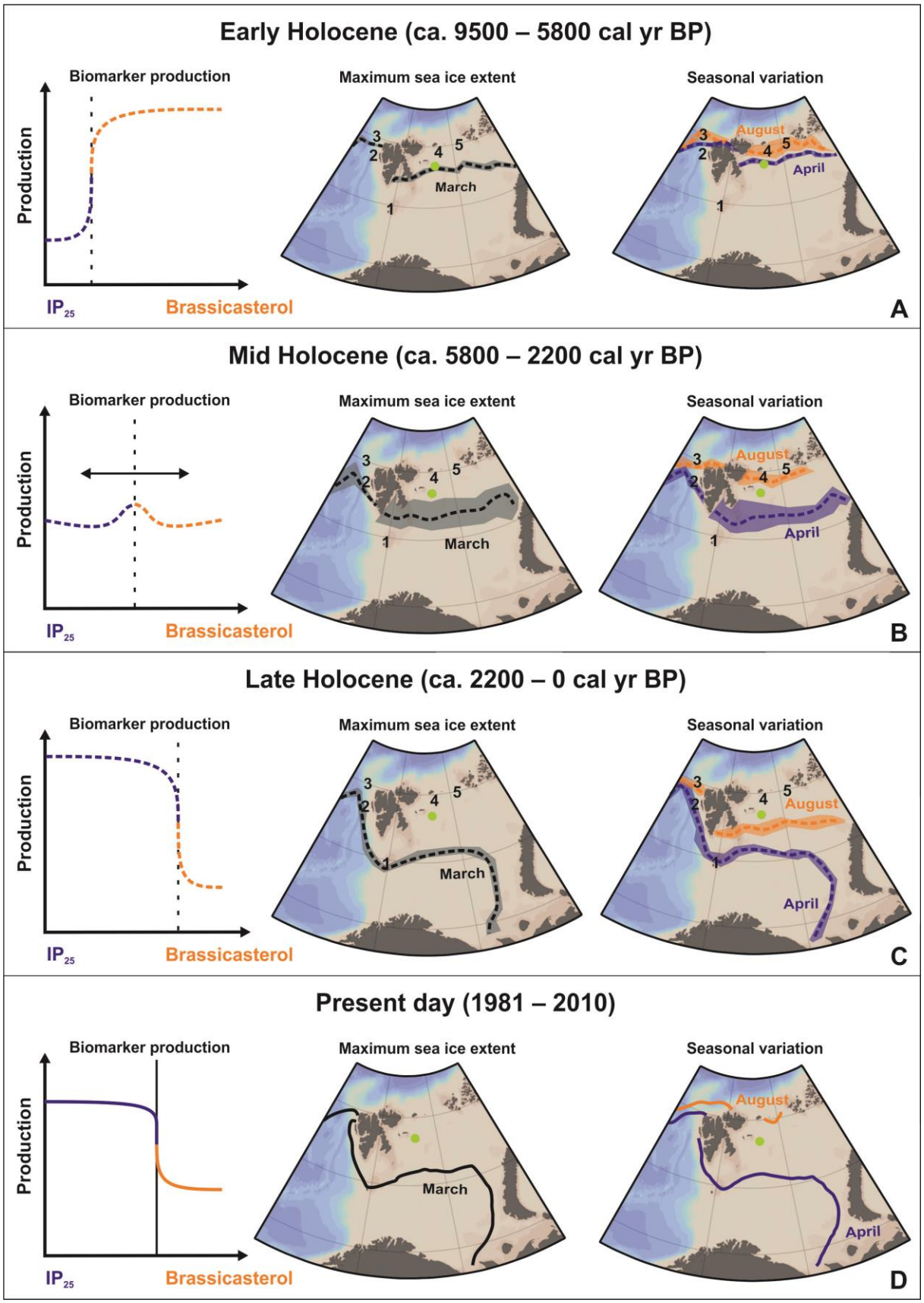
Early Holocene (ca. 9500 – 5800 cal yr BP)
Biomarker production
Production
IP25
Brassicasterol
Maximum sea ice extent
Seasonal variation
August
April
March
1
2
3
4
5
A
Mid Holocene (ca. 5800 – 2200 cal yr BP)
Biomarker production
Production
IP25
Brassicasterol
Maximum sea ice extent
Seasonal variation
August
April
March
1
2
3
4
5
B
Late Holocene (ca. 2200 – 0 cal yr BP)
Biomarker production
Production
IP25
Brassicasterol
Maximum sea ice extent
Seasonal variation
August
April
March
1
2
3
4
5
C
Present day (1981 – 2010)
Biomarker production
Production
IP25
Brassicasterol
Maximum sea ice extent
Seasonal variation
August
April
March
D

Paper III

Berben SMP, Husum K and Aagaard-Sørensen S **A late Holocene multi-proxy record from the northern Norwegian margin: temperature and salinity variability.**
In prep. Intended for The Holocene

A late Holocene multi-proxy record from the northern Norwegian margin: temperature and salinity variability

Berben SMP[a], Husum K[b] and Aagaard-Sørensen S[a]
[a]Department of Geology, University of Tromsø, N-9037 Tromsø, Norway
[b]Norwegian Polar Institute, Fram Centre, N-9296 Tromsø, Norway

Correspondence to: Berben SMP (sarah.m.berben@uit.no)

Keywords: Atlantic water inflow, Coastal water, NAO, northern Norwegian margin, late Holocene, planktic foraminifera, stable isotopes, Mg/Ca

Abstract

This study presents a late Holocene multi-proxy analysis performed on a marine sediment core from the northern Norwegian margin. Palaeo sub-surface temperature and salinity estimates were reconstructed in order to elucidate the natural variability of Atlantic and Coastal water influences. Planktic foraminiferal fauna and their preservation indicators, stable isotopes ($\delta^{18}O$, $\delta^{13}C$) and trace elements were analysed. Paired Mg/Ca and $\delta^{18}O$ measurements of *N. pachyderma* resulted in temperature ($SST_{Mg/Ca}$) and salinity reconstructions in addition to transfer function derived temperature ($SST_{Transfer}$) estimates. The overall poor preservation conditions at the core site might have influenced the Mg/Ca ratios and are therefore likely the primary cause of the recorded underestimated $SST_{Mg/Ca}$ and SSS values. The high resolution record shows a general cooling trend with fluctuating palaeoceanographic conditions which are attributed to shifting NAO conditions. Period I (ca. 3500 – 2900 cal yr BP) is characterized by a stronger influence of Coastal water and stratified water masses most likely associated with negative NAO-like conditions. During period II (ca. 2900 – 1600 cal yr BP) warm Atlantic water linked with a positive NAO mode dominates the core site. A returned influence of Coastal water is observed throughout period III (ca. 1600 – 950 cal yr BP). The stable and colder sub-surface temperatures during this period correlate with the Dark Ages. Within period IV (ca. 950 – 550 cal yr BP) the core site experienced a stronger influence of Atlantic water likely due to positive NAO conditions correlating to the Medieval Warm Period.

1 Introduction

Throughout the late Holocene, a general cooling trend has been observed in the North Atlantic associated with a reduced influence of warm Atlantic water (e.g. Slubowska et al., 2005; Hald et al., 2007; Skirbekk et al., 2010). A similar cooling trend, recorded by lake and tree records from north-western Europe, has been ascribed to reduced insolation at high latitudes (e.g. Bjune et al., 2009; Kaufman et al., 2009). Contradictory, fluctuations of a strengthened Atlantic water inflow towards the Arctic Ocean have been observed at the Vøring plateau (e.g. Andersson et al., 2003; Risebrobakken et al., 2003; Andersson et al., 2010), the Barents Sea (e.g. Duplessy et al., 2001; Lubinski et al., 2001; Berben et al., 2014)

and the Svalbard margin (e.g. Slubowska-Woldengen et al., 2007; Jernas et al., 2013; Werner et al., 2013; Zamelczyk et al., 2013). Additionally, throughout the late Holocene, several observations of fluctuating climatic conditions have been found in the Nordic Seas (e.g. Giraudeau et al., 2004; Nyland et al., 2006; Solignac et al., 2006; Slubowska-Woldengen et al., 2007) as well as in north-western Europe (e.g. Lauritzen and Lundberg, 1999; Bjune and Birks, 2008). These include the 'Roman Warm Period' (RWP, ca. BCE 50 – CE 400), the 'Dark Ages' (DA, ca. CE 400 - 800), the 'Medieval Warm Period' (MWP, CE 900 – 1500) and the 'Little Ice Age' (LIA, ca. CE 1500 - 1900) (e.g. Lamb, 1977).

These fluctuating conditions have been ascribed to different causes such as solar forcing, volcanic eruptions (e.g. Bryson and Goodman, 1980; Lean, 2002; Jiang et al., 2005; Wanner et al., 2008) or changes in atmospheric forcing linked to the North Atlantic Oscillation (NAO) controlling the inflow of Atlantic water to the Arctic Ocean (e.g. Trouet et al., 2009; Olsen et al., 2012). Warm and salty Atlantic water is brought into the Nordic Seas by the North Atlantic Current (NAC) and flows parallel with colder and less saline Coastal water along the Norwegian margin. These two water masses possess opposite characteristics with respect to temperature and salinity. Further, they respond opposite to the strengthened or reduced westerlies attributed to positive and negative NAO modes, respectively (e.g. Sætre, 2007). A positive versus negative NAO mode affects the climatic conditions in north-western Europe by generating warmer and wetter versus colder and dryer conditions (e.g. Wanner et al., 2001). Along the Norwegian coast the impact of the variable NAO is seen in precipitation, temperature and wind intensity changes (Ottersen et al., 2001). And thus, the northern Norwegian margin is a key location to investigate the natural variability of Atlantic water inflow throughout the late Holocene linked to fluctuating NAO modes. With respect to the recent global warming, it is of great importance to understand the natural variability of the Atlantic water inflow towards the Arctic Ocean as it strongly influences north-western Europe climatic conditions.

For the Nordic Seas, several studies have reconstructed water mass properties based on planktic foraminiferal fauna. Transfer functions reflect sub-surface temperatures whereas stable oxygen isotopes reflect both the temperature and $\delta^{18}O$ of ambient sea water (e.g. Sarnthein et al., 2003; Rasmussen and Thomsen, 2010; Risebrobakken et al., 2010; Berben et al., 2014). However, in order to reconstruct palaeo sub-surface salinities, additional proxies are required. The Mg-uptake in foraminiferal calcite is primarily temperature depended (e.g.

Nürnberg, 1995). The positive correlation between the Mg-uptake in foraminiferal calcite and temperature of the ambient sea water during growth allows palaeo reconstructions of sub-surface temperatures based on Mg/Ca ratio measurements (e.g. Mashiotta et al., 1999; Elderfield and Ganssen, 2000; Kozdon et al., 2009). Therefore, paired calcite $\delta^{18}O$ and Mg/Ca measurements enable the reconstruction of palaeo seawater $\delta^{18}O$ (e.g. Thornalley et al., 2009; Elderfield et al., 2010) and subsequently, via modern $\delta^{18}O_{seawater}$:salinity relationships, enable the reconstruction of palaeo salinity.

In order to investigate the fluctuating interplay of Atlantic and Coastal water related to variable NAO modes throughout the late Holocene, the variability of sub-surface temperature and salinity has been reconstructed. Paired Mg/Ca and $\delta^{18}O$ measurements of *Neogloboquadrina pachyderma* were analysed in addition to the distribution of planktic foraminiferal fauna and preservation conditions. Subsequently, a new record of both palaeo sub-surface temperature and salinity estimates from the northern Norwegian margin is presented.

2 Present day oceanography

The Norwegian Sea is dominated by relatively warm and saline Atlantic water (>2 °C, >35 ‰; Hopkins, 1991). Atlantic water is brought to the area by the two-branched Norwegian Atlantic Current (NwAC) (Orvik and Niiler, 2002) (Figure 1A). Both branches follow a topographically steered northwards pathway through the Nordic Seas and eventually reach the Arctic Ocean via the Fram Strait. The western branch crosses the Iceland-Faroe Ridge entering the Norwegian Sea as the Iceland-Faroe frontal jet (Perkins et al., 1998) (Figure 1A). The eastern branch passes through the Faroe-Shetland channel and follows a pathway along the Norwegian shelf edge towards the Arctic Ocean with a branch flowing into the Barents Sea (Orvik and Niiler, 2002) (Figure 1A).

The Norwegian Coastal Current (NCC) transports Coastal water (2-13 °C, 32-35 ‰; Hopkins, 1991) northwards originating from the North Sea, the Baltic and the Norwegian coast (Figure 1A). Coastal water is characterized by its low salinities due to the influence of freshwater run off from the Norwegian mainland. The NCC is density driven which is mainly influenced by its salinity distribution. Mixing with Atlantic water takes place and increases northwards, and

thus salinity increases whereas stratification reduces. In general, cold Coastal water can be found above warmer Atlantic water in the upper 50 to 100 m of the water column as a thinning wedge westwards (Ikeda et al., 1989) (Figure 1B). A boundary is formed as a well-defined front between the cold, low salinity Coastal water and the warmer, more saline Atlantic water (Ikeda et al., 1989). The overall properties and movements of the NCC are influenced by several factors such as freshwater, tides, wind conditions, bottom topography and Atlantic water (Sætre, 2007). In the study area, the topography causes the NCC to extend much further westwards and hence, closer to the influence of the NwAC (Figure 1C). Therefore, this is a key area to investigate the interplay between Atlantic and Coastal water fluctuations as a result of climatic variability.

3 Material and methods

For this study, a marine sediment core from the northern Norwegian margin (Vøring plateau in front of Trænadjupet south of the Lofoten) was investigated. The core (W00-SC3) (67.24° N, 08.31° E) was retrieved in 2000 by the SV *Geobay* at a water depth of 1184 m (Laberg et al., 2002) (Figure 1). Its recovery was 385 cm from which the top 19 cm was disturbed and therefore not used. The core consists of very soft clay sediments and was sampled for each 1.0 cm between 19 and 263 cm. CTD data nearby the core site (67.10° N, 08.26° E) indicate the presence of Atlantic water till a water depth of ca. 375 m for present day conditions (Blaume, 2002) (Figure 2).

3.1 Chronology

A depth-age model of W00-SC3 based on four AMS ^{14}C dates measured on *N. pachyderma* was developed. All four AMS ^{14}C dates were calibrated using Calib 7.0.0 software (Stuiver and Reimer, 1993), the Marine13 calibration curve (Reimer et al., 2013) and a local reservoir age (ΔR value) of 71 ± 21 following recommendations by Mangerud et al. (2006) (Table 1). The calibration was constrained on a 2-σ range for both calendar years Before Present (cal yr BP) and calendar years Before Common Era (BCE)/Common Era (CE) (cal yr BCE/CE). For this study the cal yr BP depth-age model will be used, however, the cal yr BCE/CE scale was

added for all the plotted data in order to compare with different studies. The AMS ^{14}C date at 23.5 cm was omitted from the final depth-age model as it appeared too old. The new depth-age model was constrained using linear interpolation between dated levels. Further, based on the homogeneous lithology throughout the core, the sedimentation rate from 120-40 cm was extrapolated towards the top, more specifically between 40 and 19 cm (Figure 3). The resulting depth-age model is constrained between 3485 and 550 cal yr BP (1536 BCE – 1395 CE) and showed sedimentation rates between 0.79 and 0.87 mm/yr and thus, enabled the sampling on a multi-decadal temporal resolution (Figure 3).

3.2 Planktic foraminifera and preservation indicators

All samples were freeze-dried, wet-sieved through three different size fractions (1000, 100 and 63 µm) and subsequently dried in an oven at 40 °C. Every 4 cm from the 100 - 1000 µm size fraction was analysed for its planktic foraminiferal content (>300 specimens) following Knudsen (1998). The identification of left and right coiling *N. pachyderma* was done following Darling et al. (2006), meaning that the right coiling form is identified as *Neogloboquadrina incompta* (Cifelli, 1961). Subsequently, relative abundances (%) of each species were calculated for 62 samples. The planktic foraminiferal concentration (#/g sediment) and fluxes (#/cm^2/yr) were calculated. For the latter, a theoretical value for the dry bulk density of 0.76 g/cm^3 was assumed based on marine sediment core T-88-2 (Aspeli, 1994) and subsequently calculated according Ehrmann and Thiede (1985).

As carbonate dissolution might affect the planktic foraminiferal assemblages, it is important to investigate the preservation conditions in order to assess the potential dissolution induced pre- and post-depositional alterations (e.g. Zamelczyk et al., 2013). Preservation indicators such as the mean shell weight (µg) of *N. pachyderma* (Broecker and Clark, 2001; Barker and Elderfield, 2002; Beer et al., 2010) and fragmentation (%) of planktic foraminiferal tests (Conan et al., 2002) were inspected. The mean shell weight of *N. pachyderma* was determined for 118 samples using a Mettler Toledo microbalance (0.1 µg sensitivity). In order to minimize problems of variations due to size difference and ontogeny, 50 square shaped and well preserved (visually) specimens were selected from a narrow size range (150 - 250 µm) (Barker et al., 2004). For 62 samples within the 100 - 1000 µm size fraction, the fragmentation was calculated using the equation of Pufhl and Shackleton (2004) (Equation 1).

$$Fragmentation\ (\%) = \frac{\#\ fragments/g}{\#fragments/g/2 + \#\ tests/g} * 100 \qquad \text{[Equation 1]}$$

Within this equation, a divisor (2) is included as it is most likely that each test breaks into more than one fragment. The latter is in order to reduce possible misinterpretations of the dissolution sensitivity in changes and progress (Le and Shackleton, 1992; Pufhl and Shackleton, 2004).

3.3 Geochemical analysis

Weight percentages (wt. %) of total carbon (TC) and total organic carbon (TOC) were analysed at one cm resolution using a LECO SC-444 (ES-2) at the Laboratory of the Geological Survey of Norway (NGU). Prior to TOC analysis, the inorganic carbon (carbonate) was removed by treating the samples with 10 % hydrochloric acid (HCl). The calcium carbonate ($CaCO_3$) content was calculated according Espitalié et al. (1977) (Equation 2).

$$CaCO_3 = (TC - TOC) * 8{,}33 \qquad \text{[Equation 2]}$$

3.4 Stable isotope analysis

Stable isotope analysis ($\delta^{18}O$, $\delta^{13}C$) was performed on 117 samples containing 50 specimens of *N. pachyderma*. In order to minimize size dependent effects on isotopic composition, all specimens were picked in a 150 - 250 µm size fraction (Keigwin and Boyle, 1989; Oppo and Fairbanks, 1989; Donner and Wefer, 1994; Aksu and Vilks, 1998; Bauch et al., 2000). The stable isotope measurements were performed with a Finnigan MAT 253 Mass Spectrometer coupled to an automated Kiel device at the Geological Mass Spectrometer (GMS) Laboratory of the University of Bergen. The analytical errors for $\delta^{18}O$ and $\delta^{13}C$ were ± 0.06 ‰ and ± 0.03 ‰ respectively. The data were reported in ‰ versus VPDB and calibrated with NBS-19. For $\delta^{18}O$, a vital effect of 0.6 ‰ has been applied. This value has previously been suggested for the Nordic Seas (Simstich et al., 2003) as well as for the Norwegian Sea (Nyland et al., 2006).

3.5 Trace element analysis

Trace element analysis was performed on 101 samples containing an average of 75 visually well preserved specimens of the planktic foraminifer *N. pachyderma.* In order to minimize the possible size-dependent bias on the Mg/Ca measurements, the tests were picked from a narrow (as narrow as possible) size fraction (150 - 250 µm) (Elderfield et al., 2002). The tests were cracked open between glass plates in order to optimize the chemical cleaning procedure which consisted of a reduction step to remove metal oxides and an oxidation step to remove any organic matter (e.g. Boyle and Keigwin, 1985). Subsequently, the samples were analysed by ICP-MS method for foraminiferal analysis including simultaneous measurements of Mg, Mn, Al, and Fe, all of which are reported as ratios to Ca. The measurements were performed on a Finnigan Element2 at the Marine Science Institute, UC Santa Barbara with an analytical precision of 1.2 % for Mg/Ca. Fe, Al and Mn are tracers of contaminating phases and thus investigated in order to identify remnant post cleaning sample contamination which might bias the measured Mg/Ca ratios in foraminiferal calcite (Barker et al., 2003).

3.6 Temperature and salinity reconstructions

To reconstruct summer sub-surface temperatures ($SST_{Transfer}$) (July-August-September) for a water depth of 100 m, a transfer function and the modern training set of Husum and Hald (2012) were used. Although the core site lays at the geographical southern boundary of this modern training set, it was assumed to be the most appropriated as it uses material analysed at the >100 µm size fraction and thus include smaller specimens as *Turborotalita quinqueloba* and *Globigerinita uvula*. The transfer function derived $SST_{Transfer}$ reconstructions were performed using C2 version 1.7.2. (Juggins, 2010) and a three component Weighted Average-Partial Least Square (WA-PLS) statistical model with a leave-one-out cross validation (Ter Braak and Juggins, 1993; Telford and Birks, 2005).

Mg/Ca derived sub-surface temperature estimates ($SST_{Mg/Ca}$) were reconstructed using the refined species-specific temperature:Mg/Ca equation of Kozdon et al. (2009) (Equation 3).

$$Mg/Ca\,(mmol/mol) = 0.13\ (\pm 0.037) * T\ (°C) + 0.35\ (\pm 0.17) \qquad \text{[Equation 3]}$$

This equation is based on cross-calibrated $\delta^{44/40}$Ca and Mg/Ca temperature estimates from Holocene core top samples of *N. pachyderma* from the Norwegian Sea and Arctic domain. Although the Mg-uptake into foraminiferal calcite is controlled by exponential thermodynamics (Mashiotta et al., 1999), in Equation 3, it is assumed that within the narrow temperature range occupied by *N. pachyderma*, a linear temperature function is appropriate and works well for reconstructed temperatures above ca. 2.5 °C (Kozdon et al., 2009). However, for temperatures below 2.5 °C, associated with salinities less than 34.5 ‰, the method loses its precision (Kozdon et al., 2009).

In order to reconstruct sub-surface salinities, the oxygen isotope ratios of the ambient seawater ($\delta^{18}O_w$) were first calculated using the temperature:δ^{18}O equation of Shackleton (1974) modified after O'Neil et al. (1969) (Equation 4).

$$T\ (°C) = 16.90 - 4.38 * (\delta^{18}O_c - \delta^{18}O_w) + 0.10 * (\delta^{18}O_c - \delta^{18}O_w)^2 \quad \text{[Equation 4]}$$

Within this equation, T refers to the previously calculated $SST_{Mg/Ca}$, $\delta^{18}O_c$ to the measured oxygen isotope value of foraminiferal calcite (*N. pachyderma*) and $\delta^{18}O_w$ to the oxygen isotope composition of ambient seawater. Both $\delta^{18}O_c$ and $\delta^{18}O_w$ are expressed as ‰ VPDB. In order to convert $\delta^{18}O_w$ VPDB values to the $\delta^{18}O_w$ VSMOW scale, the following equation was applied (Hut, 1987) (Equation 5).

$$\delta^{18}O_{w\,VPDB} = \delta^{18}O_{w\,VSMOW} - 0.27\ ‰ \quad \text{[Equation 5]}$$

Subsequently, Equation 4 and 5 are rearranged in order to calculate $\delta^{18}O_w$ VSMOW which results in Equation 6 (Nyland et al., 2006).

$$\delta^{18}O_w = \delta^{18}O_c + 0.27 - \left[\frac{4.38 - \sqrt{4.38^2 - 0.4 * (16.9 - T_{Mg/Ca})}}{0.2}\right] \quad \text{[Equation 6]}$$

Subsequently, sub-surface salinities (SSS) were reconstructed using the salinity (S) to $\delta^{18}O_w$ relation for the central and eastern Nordic Seas by Simstich et al. (2003) (Equation 7).

$$\delta^{18}O_w = -12.17 + 0.36 * S \quad \text{[Equation 7]}$$

4 Results

4.1 Planktic foraminifera and preservation indicators

The planktic foraminiferal fauna consist of six species: *N. pachyderma*, *T. quinqueloba*, *N. incompta*, *Globigerinita glutinata*, *Globigerina bulloides* and *Globigerinita uvula* (Table 2) (Figure 4). Overall, the record is dominated by *N. incompta* and *T. quinqueloba* with a mean value of ca. 34 and 29 % respectively.

Between ca. 3500 and 2900 cal yr BP, the planktic foraminiferal concentration and flux show relative low values of ca. 750 #/g sediment and ca. 50 #/cm^2/yr (Figure 4A; 5E). *N. pachyderma* and *N. incompta* show a small decrease from ca. 18 to 14 % and from ca. 40 to 22 % (Figure 4B; 4D). Simultaneously, *T. quinqueloba* and *G. uvula* show a gradual increase from ca. 28 to 35 % and from ca. 5 to 20 % (Figure 4C; 4G). *G. glutinata* and *G. bulloides* show relative abundances of ca. 6 and 3 % (Figure 4E; 4F).

The planktic foraminiferal concentration and flux show slightly higher values of ca. 1000 #/g sediment and ca. 65 #/cm^2/yr between ca. 2900 and 2300 cal yr BP which are followed by a sharp increase reaching the highest recorded values (3765 #/g sediment, 226 #/cm^2/yr) towards ca. 1600 cal yr BP (Figure 4A; 5E). Between ca. 2900 and 1600 cal yr BP, stable abundances of *N. pachyderma* (ca. 11 %) and relative high and stable values of *N. incompta* (ca. 33 %) are recorded (Figure 4B; 4D). *T. quinqueloba* shows high values (ca. 32 %) with a gentle decrease towards ca. 1600 cal yr BP (Figure 4C). *G. glutinata* and *G. bulloides* show, in particular between ca. 2900 and 2300 cal yr BP, the highest recorded values (ca. 7 and 5 %) followed by a small reduction between 2300 and 1600 cal yr BP (Figure 4E; 4F).

At ca. 1600 cal yr BP, the concentration and flux records show a rapid drop from 3765 to 865 # g/sediment and from 226 to 52 #/cm^2/yr followed by stable values (ca. 1330 #/g sediment, ca. 80 #/cm^2/yr) between ca. 1600 and 950 cal yr BP (Figure 4A; 5E). Gently increasing values of *G. uvula* (ca. 15 to 26 %) and *G. glutinata* (ca. 2 to 5 %) are recorded; whereas *T. quinqueloba* shows a slight decrease from ca. 25 to 16 % (Figure 4G; 4E; 4C). *N. pachyderma*, *N. incompta* and *G. bulloides* remain relatively constant throughout this period (Figure 4B; 4D; 4F).

Between ca. 950 and 550 cal yr BP, the concentration and flux record show slightly decreasing values towards 450 #/g sediment and 27 #/cm^2/yr (Figure 4A; 5E). *N. pachyderma* and *N. incompta* both show an increase with values up to ca. 23 and 42 % (Figure 4B; 4D). Simultaneously, decreasing values are recorded for *G. glutinata* from ca. 5 to 2 % and for *G. uvula* from ca. 26 to 8 % (Figure 4E; 4G). *T. quinqueloba* and *G. bulloides* remain constant around values of ca. 21 and 2 % respectively (Figure 4C; 4F).

The preservation indicators show overall values between 47 and 94 % of planktic foraminiferal fragmentation and between 1.6 and 4.8 µg for the mean shell weight of *N. pachyderma* (Figure 5A-B). Between ca. 3500 and 2900 cal yr BP, the fragmentation shows generally high values around ca. 75 %, whereas the mean shell weight decreases slightly from 3.7 to 2.6 µg. Between ca. 2900 and 1600 cal yr BP, the fragmentation remains relatively stable around slightly reduced values of ca. 69 %. The mean shell weight of *N. pachyderma* shows decreasing values towards 1.7 µg at ca. 2300 cal yr BP followed by an increase reaching ca. 3 µg at ca. 1600 cal yr BP. Between ca. 1600 and 950 cal yr BP, the fragmentation increases from 49 to 79 % and the mean shell weight remains stable around ca. 2.7 µg. Between ca. 950 and 550 cal yr BP, both preservation indicators show a pronounced increase from ca. 47 to 90 % for the planktic foraminiferal fragmentation and from 2.0 to 3.2 µg for the mean shell weight of *N. pachyderma*.

4.2 Geochemical analysis

The TOC and $CaCO_3$ results show an overall increasing trend with values between 0.7 and 1.3 wt. % and 17.0 and 30.6 wt. %, respectively (Figure 5C-D). Between ca. 3500 and 2900 cal yr BP, both records show an increase of ca. 0.7 to 0.9 wt. % for TOC and ca. 17 to 22 wt. % for $CaCO_3$. Towards ca. 2300 cal yr BP, TOC values increase reaching 1.1 wt. % followed by a quick drop to 0.8 wt. % around ca. 2200 cal yr BP and remain further stable around this value towards ca. 1600 cal yr BP. Between ca. 2900 and 1600 cal yr BP, the $CaCO_3$ continues its increasing trend from ca. 22 to 30 wt. %. Between ca. 1600 and 950 cal yr BP, the TOC values increase gradually from 1.0 to 1.1 wt. %, whereas the $CaCO_3$ data decreases from ca. 30 to 24 wt. %. Between ca. 950 and 550 cal yr BP, TOC values remain relatively stable around ca. 1.0 wt. %, whereas the $CaCO_3$ record increases slightly towards ca. 26 wt. %.

4.3 Stable isotope analysis

The stable isotope analysis results in values between 2.3 and 3.1 ‰ for $\delta^{18}O$ and within the range -0.4 to 0.6 ‰ for $\delta^{13}C$ (Figure 6). Between ca. 3500 and 2900 cal yr BP, $\delta^{18}O$ values decrease gently from ca. 2.9 to 2.7 ‰ whereas the $\delta^{13}C$ record shows simultaneously increasing values from ca. 0.2 to 0.4 ‰. Between ca. 2900 and 1600 cal yr BP, the $\delta^{18}O$ record continues its decreasing trend towards values of 2.5 ‰ at ca. 1600 cal yr BP. The $\delta^{13}C$ values decrease from ca. 0.4 ‰ at ca. 2900 cal yr BP towards ca. 0.1 ‰ at ca. 2300 cal yr BP followed by relative stable values around ca. 0.3 ‰ towards ca. 1600 cal yr BP. Between ca. 1600 and 950 cal yr BP, $\delta^{18}O$ values initially continue their decreasing trend towards 2.4 ‰ at ca. 1300 cal yr BP before increasing to values of ca. 2.7 ‰ between ca. 1200 and 950 cal yr BP. The $\delta^{13}C$ record shows increasing values from ca. 0.1 to 0.4 ‰ during this time interval. Between ca. 950 and 550 cal yr BP both records increase simultaneously towards ca. 2.8 ‰ for $\delta^{18}O$ and ca. 0.5 ‰ for $\delta^{13}C$.

4.4 Trace element analysis

Tracers of contamination are plotted against Mg/Ca ratios (Figure 7). Fe and Al are tracers of detrital material contamination such as silicate minerals, whereas Mn is a tracer of secondary diagenetic Mn-rich carbonate (Boyle, 1983). The results show high correlations between Mg/Ca and Fe and Al tracers, with $R^2 = 0.57$ for Fe/Ca and $R^2 = 0.47$ for Al/Ca (Figure 7A-B). The correlation between Mg/Ca and Mn/Ca is low ($R^2 = 0.06$) and thus further not relevant (Figure 7C). When deleting samples with ratios higher than 100 µmol/mol of the contamination tracers following the contamination threshold used by Barker et al. (2003), the correlations are strongly reduced to non-existing with $R^2 = 0.05$ for Fe/Ca and $R^2 = 0.09$ for Al/Ca (Figure 7D-E). This change suggests that contamination by detrital material (i.e. high values of Fe/Ca and/or Al/Ca) impact the results by elevating the Mg/Ca values. Therefore, all samples (n=32) with ratios >100 µmol/mol of Fe and Al are omitted from the further study.

The resulting Mg/Ca record consists of 69 data points with ratios in the range 0.70 to 0.96 mmol/mol (Figure 8A). Between ca. 3500 and 2900 cal yr BP, the Mg/Ca record shows relative stable values around ca. 0.76 mmol/mol. Between ca. 2900 and 2500 cal yr BP, the ratios increase towards 0.89 mmol/mol. Due to the omitted data as a result of possible

contamination, there is no reliable data between ca. 2500 and 2100 cal yr BP. Between ca. 2100 and 1600 cal yr BP, the record remains relatively stable around ca. 0.81 mmol/mol. Around ca. 1600 cal yr BP the Mg/Ca ratios drop quickly towards 0.70 mmol/mol, thereafter they remain stable around ca. 0.78 mmol/mol towards the top of the record (i.e. due to the omitted values after ca. 800 cal yr BP).

4.5 Temperature and salinity reconstructions

The transfer function derived temperature ($SST_{Transfer}$) reconstructions (n=62) range between 6.3 and 7.7 °C (Figure 8C; 4H). Between ca. 3500 and 2900 cal yr BP, the $SST_{Transfer}$ record decreases from 7.2 to 6.7 °C. Thereafter, the $SST_{Transfer}$ values increase towards ca. 7.7 °C at ca. 2500 cal yr BP. Hereafter the $SST_{Transfer}$ record decreases towards ca. 1600 cal yr BP reaching ca. 6.6 °C. Between ca. 1600 and 950 cal yr BP, the $SST_{Transfer}$ estimates remain relatively stable around ca. 6.6 °C. Eventually, between ca. 950 and 550 cal yr BP, the $SST_{Transfer}$ record shows a decrease of ca. 0.5 °C (from ca. 6.8 to 6.3 °C).

The Mg/Ca derived sub-surface temperature reconstructions ($SST_{Mg/Ca}$) (n=69) range between 2.7 and 4.7 °C (Figure 8B). Between ca. 3500 and 3300 cal yr BP, the $SST_{Mg/Ca}$ values show a small decrease from 3.1 to 2.7 °C followed by relatively stable values of ca. 3.2 °C towards ca. 2900 cal yr BP. Between ca. 2900 and 2500 cal yr BP, the $SST_{Mg/Ca}$ values show a gradual increase from ca. 3.2 to 4.2 °C and between ca. 2100 and 1600 cal yr BP, $SST_{Mg/Ca}$ values are relatively stable around 3.5 °C. Between ca. 1600 and 950 cal yr BP, the $SST_{Mg/Ca}$ estimates are slightly lower around ca. 3.2 °C with one exception around ca. 1300 cal yr BP where $SST_{Mg/Ca}$ estimates peak to 4.7 °C.

Reconstructed sub-surface salinities (SSS) (n=65) range between 31.6 and 34.0 ‰ (Figure 8D). Between ca. 3500 and 2900 cal yr BP, the reconstructed SSS estimates show a gradual decrease from ca. 33 to 32 ‰. After ca. 2900 cal yr BP, the SSS data increases to 33.6 ‰ at ca. 2800 cal yr BP followed by a decrease to ca. 2500 cal yr BP. Between ca. 2100 and 1600 cal yr BP, palaeo SSS estimates are stable around ca. 33 ‰, showing the highest values of the record (i.e. 34.0 ‰). Between ca. 1600 and 950 cal yr BP, the SSS values show stable values of ca. 32 ‰.

5 Discussions

5.1 Palaeo SST and SSS assessment

Modern sea temperature measured nearby the core site is ca. 7 °C within the upper 300 m of the water column (Blaume, 2002) (Figure 2), and thus corresponds to the reconstructed palaeo $SST_{Transfer}$ estimates (Figure 4H; 8C). However, the $SST_{Mg/Ca}$ estimates, which range 3.0 to 3.6 °C lower than the $SST_{Transfer}$, do not correspond with the modern sea temperature data (Figure 8B). Further, the SSS estimates (ca. 33 ‰) show (consequently) lower values than the modern salinity values (>35 ‰) (Blaume, 2002) (Figure 2). Furthermore, the $SST_{Mg/Ca}$ estimates also seem to be rather low compared to palaeo reconstructions of the last 1200 years from the Vøring plateau (Nyland et al., 2006). This dissimilarity is in the first place attributed to the use of a different temperature:Mg/Ca equation by Nyland et al. (2006), more specifically the equation from Elderfield and Ganssen (2000). The temperature:Mg/Ca equations from Elderfield and Ganssen (2000) and Kozdon et al. (2009) are calibrated differently resulting in two different potential temperature ranges of the equations, 0 to 7 °C and 3 to 6 °C respectively. In this study, applying the temperature:Mg/Ca equation of Elderfield and Ganssen (2000) would have resulted in 0.7 to 1.8 °C warmer $SST_{Mg/Ca}$ and 0.71 to 0.88 ‰ higher SSS estimates. Nonetheless, a different equation would still have resulted in lower $SST_{Mg/Ca}$ estimates in comparison with the $SST_{Transfer}$ and/or present day instrumental data. This discrepancy might be caused by variability of the species-specific habitat depth preference and/or main calcification period (i.e. season) of *N. pachyderma*, in addition to initial low Mg/Ca values (Meland et al., 2006; Kozdon et al., 2009).

Whereas the $SST_{Transfer}$ record is reconstructed for a water depth of 100 m, the $SST_{Mg/Ca}$ record reflects the average calcification depth of *N. pachyderma*. Studies have shown a poor correlation between modern Mg/Ca inferred temperatures and their corresponding hydrographic data and thus, contest the previously made assumption that the $SST_{Mg/Ca}$ reflects a constant average calcification depth (Meland et al., 2006; Nyland et al., 2006). The water depth of chamber formation and encrustation of *N. pachyderma* is linked to the stratification of the water column and can therefore be highly variable (e.g. Kohfeld et al., 1996; Stangeew, 2001; Simstich et al., 2003). Furthermore, Kozdon et al. (2009) argued that the main factor controlling the habitat depth of *N. pachyderma* in the Nordic Seas is the density-driven water mass stratification. Therefore, it seems that the by Mg/Ca recorded temperature signal is

bound to the isopycnal layer and hence, only reflects a narrow temperature range. Hemleben et al. (1989) indicated that *N. pachyderma* is probably a passive dweller implying that the water mass stratification is preconditioning the habitat and thus, causing a lower temperature response of the Mg/Ca signal. This effect might even be amplified in high latitudes due to the stronger water mass stratification. It is thus most likely that *N. pachyderma* does not possess a constant calcification depth and that the species therefore records a dampened amplitude of the total sub-surface water temperature range. Due to the distinctive seasonality and strong stratification in high latitude regions, the assignment of a true calcification depth and hence temperature remains one of the major issues (Barker et al., 2003). The apparent calcification depth of *N. pachyderma* can be found around ca. 250 m water depth off Norway (Simstich et al., 2003). Palaeo water mass properties at ca. 250 m might have differed from those at ca. 100 m and thereby possibly partly contributed to the observed discrepancy between $SST_{Mg/Ca}$ and $SST_{Transfer}$ estimates.

On an annual time scale, the biological production of *N. pachyderma* peaks in spring and a second time during maximum stratification in late summer (Jonkers et al., 2010). Therefore, the Mg-uptake by *N. pachyderma* reflects a combined spring and summer temperature signal resulting in lower $SST_{Mg/Ca}$ estimates compared to the $SST_{Transfer}$ values which are reconstructed for summer. However, Jonkers et al. (2013) measured Mg/Ca values of *N. pachyderma* from sediment traps in the central Irminger Sea which only show a weak seasonal trend. Jonkers et al. (2013) speculate that the Mg-uptake is controlled by other factors than temperature such as sensitivity of *N. pachyderma* to $[CO_3^{2-}]$ changes which could partly mask the summertime increases due to a parallel increase in $[CO_3^{2-}]$.

In addition to temperature, several secondary factors might influence the absolute Mg/Ca ratios including variability in salinity (Nürnberg et al., 1996; Lea et al., 1999), calcite dissolution (Dekens et al., 2002), test size (e.g. Elderfield et al., 2002) and the applied cleaning protocol (e.g. Barker et al., 2003), which may provide an explanation to the initially low Mg/Ca values. The presented Mg/Ca ratios are relatively low and are ca. 0.16 mmol/mol lower than previous observations from the Vøring plateau performed within a comparable size fraction using a similar cleaning method (Nyland et al., 2006). In particular, the "Cd cleaning method" (Boyle and Keigwin, 1985) comprising a reductive cleaning step could result in absolute lowering of Mg/Ca ratios of up to ~15 % (Barker et al., 2003; Meland et al., 2006). Artificially correcting the present Mg/Ca data for this potential reduction would translate into

0.8 to 1.1 °C higher $SST_{Mg/Ca}$ and 0.6 to 0.8 ‰ higher SSS estimates, which are still lower than modern day values and the $SST_{Transfer}$ record. Hence, this cleaning step does not seem to explain the differences observed between the two temperature proxies. This was also concluded by Aagaard-Sørensen et al. (2013) after comparisons between transfer function and Mg/Ca derived temperature estimates from a core retrieved in the Polar North Atlantic.

The observed preservation indicators show generally high planktic foraminiferal fragmentation and low mean shell weights of *N. pachyderma* and thereby, argue for overall poor preservation conditions (Figure 5A-B). In addition, the generally low $CaCO_3$ record (<30 wt. %) corresponds to earlier findings of low carbonate contents of surface sediments on the Norwegian continental margin associated with poor preservation conditions (Huber et al., 2000) (Figure 5D). At the continental margins, dilution by terrigenous material might lead to low percentages of sedimentary carbonate (Hebbeln et al., 1998), whereas high fertility results in a high input of organic matter and thereby, to enhanced carbonate dissolution (Berger, 1971; Emerson and Bender, 1981; Archer, 1991). Previous studies highlighted that Mg-rich parts might have been removed from the foraminiferal test due to dissolution and thereby, bias the Mg/Ca ratios resulting in underestimated $SST_{Mg/Ca}$ values (Brown and Elderfield, 1996; Rosenthal et al., 2000; Johnstone et al., 2011). Although the risk of measuring biased material was minimized by picking the visually most preserved tests, it remains impossible to quantify the degree of preservation influence on the measured Mg/Ca ratios and hence, the reconstructed $SST_{Mg/Ca}$ and SSS estimates. Due to the observed overall poor preservation conditions, it is likely that the Mg/Ca measurements were influenced by carbonate dissolution.

5.2 Palaeoceanographic evolution of the late Holocene

Throughout the late Holocene, the current proxy records show an overall cooling, with $SST_{Transfer}$ values decreasing from 7.7 to 6.3 °C (Figure 4H; 8C), associated with an overall decreased inflow of Atlantic water. This corresponds well to previous observations of decreased Atlantic water inflow in the Nordic Seas (e.g. Slubowska et al., 2005; Hald et al., 2007; Skirbekk et al., 2010) as well as to lake and tree records from north-western Europe arguing for a late Holocene trend towards colder and dryer conditions (e.g. Bjune et al., 2009; Kaufman et al., 2009). Contrary, at the Vøring plateau south of the study site, planktic

foraminiferal data show an overall increased inflow of Atlantic water throughout this time period (Andersson et al., 2003; Risebrobakken et al., 2003; Andersson et al., 2010). In addition to the overall cooling, the current study also shows smaller scale fluctuations of the sub-surface water masses which will be discussed further for four separate time periods. The interpretation of the fluctuating influence of sub-surface water masses and their possible link with NAO conditions is presented as schematic profiles across the northern Norwegian margin (Figure 9).

5.2.1 Period I: ca. 3500 – 2900 cal yr BP

Between ca. 3500 and 2900 cal yr BP, the relative faunal abundances show increased values of *G. uvula* (ca. 5 to 20 %) and high values (ca. 30 %) of *T. quinqueloba* (Figure 4G; 4C). The latter has been associated with sub-polar conditions and Atlantic water (Bé and Tolderlund, 1971; Volkmann, 2000) and additionally considered to respond rapidly to changes in nutrient supply (Reynolds and Thunnel, 1985; Johannessen et al., 1994). *G. uvula* has been associated with Coastal water and reduced salinities (Husum and Hald, 2012) as well as with high food supplies and cold productive surface waters (e.g. Saito et al., 1981; Boltovskoy et al., 1996; Bergami et al., 2009). Hence, the high relative abundances of both *T. quinqueloba* and *G. uvula* argue for enhanced productivity most likely due to an increased influence of colder, less saline and more productive Coastal water. Additionally, the enriching $\delta^{13}C$ values might also argue for increased primary production corresponding to an increased influence of more productive Coastal water (Figure 6B).

However, the relatively low planktic foraminiferal concentrations and fluxes seem to argue for a rather low primary production (Figure 4A; 5E). These relatively low values might result from relatively poor preservation conditions as indicated by generally high planktic foraminiferal fragmentation, a decreasing mean shell weight of *N. pachyderma* and low $CaCO_3$ values (<22 wt. %) (Figure 5A; 5B; 5D). The latter might reflect the dilution by terrigenous material enhancing carbonate dissolution at the continental margin off Norway (Huber et al., 2000). In addition, the solubility of $CaCO_3$ increases with decreasing temperatures (Edmond and Gieskes, 1970), and thus, the enhanced dissolution conditions are most likely due to a combination of the core location at the continental margin and an increased influence of colder Coastal water.

The depleting $\delta^{18}O$ trend might indicate an increased temperature and/or decreased salinity signal (Figure 6A). The planktic foraminiferal fauna data and decreasing $SST_{Transfer}$ estimates (7.2 to 6.7 °C) with an average value of ca. 6.9 °C argue strongly that the $\delta^{18}O$ record reflects less saline water masses associated with an increased influence of Coastal water (Figure 4H; 8C). Correspondingly, the reconstructed SSS estimates confirm the overall trend towards less saline conditions (Figure 8D). Nonetheless, contrary to decreasing $SST_{Transfer}$ estimations, the overall lower $SST_{Mg/Ca}$ values remain relatively stable throughout this period which might illustrate the different water depths and/or season that the two proxies represent (see section 5.1.3) possibly arguing for more stratified water masses (Figure 8B-C).

Overall, the multi-proxy data argue for an increased influence of Coastal water and possibly more stratified water masses at the core site. This is likely the result of a more westwards located thinning wedge of Coastal water above Atlantic water that might have been the result of a dominating negative NAO-like mode throughout this time interval (Figure 9A). Previously, a 5200 year NAO-index has been reconstructed using a multi-proxy geochemical record from a lake in south-west Greenland (Olsen et al., 2012). Although this NAO-index shows mainly positive values, Olsen et al. (2012) observed a stronger influence of negative NAO conditions between ca. 4500 and 2500 cal yr BP which might correspond to the negative NAO-like conditions suggested here (Figure 8E). Negative NAO conditions are generally associated with a reduced inflow of Atlantic water and a stronger influence of Coastal water (e.g. Sætre, 2007; Hurrell et al., 2013). Correspondingly, between ca. 3500 and 2500 cal yr BP, reconstructed SST estimates from the Vøring plateau (66.58° N, 07.38° E) show decreasing values arguing for a reduced influence of Atlantic water (Andersson et al., 2003; Risebrobakken et al., 2003; Andersson et al., 2010). Additionally, negative NAO conditions result in a colder and dryer climate in north-western Europe (e.g. Wanner et al., 2001). A decreasing temperature and precipitation trend throughout this time interval was observed by pollen and plant macrofossil analyses from a lake record in northern Norway (Svanåvatnet; 66.25° N, 14.03° E) (Bjune and Birks, 2008). Furthermore, based on the mean ablation-season temperature and winter snow accumulation, a decreased winter precipitation was also observed in western Norway (Nesje et al., 2001) and between 3500 and 3200 cal yr BP, a speleothem record from northern Norway indicates decreased surface ground temperatures (Lauritzen and Lundberg, 1999).

5.2.2 Period II: ca. 2900 –1600 cal yr BP

Between ca. 2900 and 1600 cal yr BP, the planktic foraminiferal fauna is characterized by high relative abundances of *T. quinqueloba*, *N. incompta*, *G. glutinata* and *G. bulloides* (Figure 4C-F). These species have all been associated with subpolar conditions and warm Atlantic surface water masses (e.g. Bé and Tolderlund, 1971; Johannessen et al., 1994; Carstens et al., 1997; Simstich et al., 2003) and thus, argue for a pronounced influence of Atlantic water brought to the study area by the NwAC.

The total planktic foraminiferal concentration and flux values show higher and increasing values, especially between ca. 2300 and 1600 cal yr BP, possibly indicating for increased primary production (Figure 4A; 5E). However, the $\delta^{13}C$ record shows an initial depletion towards ca. 2300 cal yr BP followed by relative stable values (ca. 0.3 ‰) arguing for less primary production (Figure 6B). The seemingly increased primary production, reflected by higher flux and concentration, likely results from the generally improved preservation conditions. The observed overall reduced fragmentation and increasing trend of $CaCO_3$ (up to ca. 30 wt. %) argue for a gradual trend towards reduced dissolution conditions throughout this period (Figure 5A; 5D). More favourable preservation conditions have previously been associated with increased influence of Atlantic surface water where pore waters are supersaturated with respect to calcium due to the lower organic matter productivity and a higher rain of $CaCO_3$ (e.g. Huber et al., 2000; Henrich et al., 2002).

The $\delta^{18}O$ record continues its depleting trend from Period I possibly reflecting an increased temperature and/or reduced salinity signal (Figure 6A). The planktic foraminiferal fauna data and the therefrom derived high $SST_{Transfer}$ estimates (ca. 7.3 °C) argue for increasing temperatures which are most likely related to an increased inflow of Atlantic water (Figure 4H; 8C). Correspondingly, the palaeo SSS record shows overall higher values up to ca. 34 ‰ and thus, correlates to an increased influence of more saline Atlantic water (Figure 8D). Additionally, the $SST_{Mg/Ca}$ estimates show, compared to Period I, ca. 0.5 - 1.0 °C higher temperatures associated with an increased influence of Atlantic water (Figure 8B).

The increased influence of Atlantic water inflow suggested here might result from positive NAO conditions. The latter are associated with stronger westerlies across the North Atlantic (e.g. Hurrell et al., 2013). This resulted in an enhanced inflow of Atlantic water which possibly reduced the influence of Coastal water leading to a more eastwards located thinning

wedge of Coastal water above Atlantic water (Figure 9B). Throughout this time period, Olsen et al. (2012) observed a general increasing trend in their NAO-index which might correspond to the influence of a positive NAO mode suggested here **(Figure 8E)**. Similarly high sub-surface temperatures associated with a strengthened inflow of Atlantic water have been observed at the Vøring plateau between ca. 2500 and 1600 cal yr BP (Andersson et al., 2003; Risebrobakken et al., 2003; Andersson et al., 2010). Throughout the time interval of period II, increased temperatures in northern Norway have been observed from a lake record (Bjune and Birks, 2008) and a speleothem record (Lauritzen and Lundberg, 1999). In addition, between ca. 2700 and 1900 cal yr BP increased winter precipitation has been observed in western Norway (Nesje et al., 2001). This correlates well to the warmer and wetter climate scenarios attributed to positive NAO conditions in north-western Europe (e.g. Wanner et al., 2001). Further, the last part of this period might be corresponding to the earlier observed Roman Warm Period between ca. 2000 and 1550 cal yr BP (ca. BCE 50 – CE 400) (Lamb, 1977) and additionally correlate to the findings of warmer temperatures in northern Norway also linked to the Roman Warm Period by Lauritzen and Lundberg (1999).

5.2.3 Period III: ca. 1600 – 950 cal yr BP

Between ca. 1600 and 950 cal yr BP, the planktic foraminiferal fauna shows stable values for all species with particularly high values of *G. uvula* (ca. 25 %) (Figure 4G). This likely reflects a stable period characterized by a strongly increased influence of Coastal water (e.g. Husum and Hald, 2012). At ca. 1600 cal yr BP, both the planktic foraminiferal concentration and flux drop rapidly where after the record remains stable until ca. 950 cal yr BP (Figure 4A; 5E). The planktic foraminiferal fragmentation increases, whereas the $CaCO_3$ record shows an overall decreasing trend (Figure 5A; 5D). This might indicate slightly reduced preservation conditions, possibly related to an enhanced influence of Coastal water and dilution of terrigenous material (e.g. Huber et al., 2000). Correspondingly, the enriched $\delta^{13}C$ record indicates enhanced primary production conditions arguing for a returned influence of Coastal water (Figure 6B).

Although $\delta^{18}O$ values initially continue their decreasing trend towards ca. 1300 cal yr BP, they eventually increase and thereby argue for a possible reduction in temperature (Figure 6A). Compared to Period II, the $SST_{Transfer}$ (ca. 6.6 °C) and $SST_{Mg/Ca}$ records both reflect

stable conditions with ca. 0.5 - 1.0 °C lower estimates indicative of a reduced influence of relatively warm Atlantic water (Figure 8B-C). Additionally, the SSS estimates show a rapid decrease followed by stable, and compared to period II, ca. 0.5 - 1.0 ‰ lower values and thus, also arguing for a reduced influence of Atlantic water or enhanced influence of Coastal water (Figure 8D).

The multi-proxy data argues for a strong influence of Coastal water which is interpreted as a westwards migrated thinning wedge of Coastal water (Figure 9C) which would suggest a shift towards negative NAO conditions (e.g. Sætre, 2007). However, the negative NAO conditions suggested here do not correlate with the overall positive NAO mode reconstructed by Olsen et al. (2012) during this time interval (Figure 8E). The current multi-proxy record corresponds well with other marine and terrestrial observations from nearby the study area within this time interval. Palaeo SST estimates from the Vøring plateau showed a sharp decrease at ca. 1600 cal yr BP where after they remained stable around lower temperatures (compared to values before ca. 1600 cal yr BP) (Andersson et al., 2003; Risebrobakken et al., 2003; Andersson et al., 2010). This also suggests a reduced influence of Atlantic water towards the core site. Further, a colder and dryer climate associated with the Dark Ages was suggested by low surface ground temperatures between ca. 1500 and 900 cal yr BP in northern Norway (e.g. Lauritzen and Lundberg, 1999). Additionally, Bjune and Birks (2008) also observed decreasing air temperatures between ca. 1800 and 800 cal yr BP in northern Norway.

5.2.4 Period IV: ca. 950 – 550 cal yr BP

The increased relative abundance of *N. incompta* indicates a stronger influence of subpolar conditions and thus, a stronger influence of Atlantic water (e.g. Bé and Tolderlund, 1971) (Figure 4D). The concomitant decreasing values of *G. glutinata* and *G. uvula* correspondingly argue for a possible decreased influence of Coastal water (Figure 4E; 4G). The increased abundance of *N. pachyderma* argues for increased polar conditions (e.g. Bé and Tolderlund, 1971; Volkmann, 2000) (Figure 4B). A similar increased abundance of *N. pachyderma* was also found throughout the last ca. 1000 cal yr BP at the Vøring plateau (Risebrobakken et al., 2003). The planktic foraminiferal concentrations and fluxes slightly decrease which might indicate a reduction in primary production (Figure 4A; 5E). Fragmentation and mean shell weight records show a pronounced increase arguing for deteriorated preservation conditions

in the sediment, i.e. increased fragmentation as well as to reduced dissolution of calcite, i.e. increased shell weight (Figure 5A-B). In addition, the $CaCO_3$ record shows a slight increase indicating somewhat reduced dissolution conditions associated with an increased influence of Atlantic water (Huber et al., 2000) (Figure 5D). The increasing $\delta^{13}C$ record might indicate a reduced stratification at the core site resulting from an increased influence of Atlantic water (Figure 6B).

Based on the planktic foraminiferal fauna and the therefrom derived decreasing $SST_{Transfer}$ record, the enriching $\delta^{18}O$ values might reflect a reduced temperature signal (Figure 6A). The $SST_{Transfer}$ record reaches its lowest estimate (ca. 6.3 °C) by the end of the record around ca. 550 cal yr BP (Figure 4H; 8C). The latter contradicts with the previously suggested returned influence of Atlantic water, however, the generally colder temperature estimates are most likely due to the overall cooling trend observed throughout the record and linked to decreasing solar insolation values throughout the late Holocene (e.g. Hald et al., 2007; Kaufman et al., 2009). Nonetheless, contemporaneous reconstructed SST estimates from the Vøring plateau have shown increasing values (Andersson et al., 2003; Risebrobakken et al., 2003; Andersson et al., 2010).

Despite the overall cooling trend, the increased influence of Atlantic water seems to be the result of generally positive NAO conditions (Figure 9D). The reconstructed NAO-index from south-west Greenland also indicate positive NAO conditions during this time interval which are associated with the Medieval Warm Period (Olsen et al., 2012) (Figure 8E). Furthermore, this also corresponds to the results of a NAO reconstruction based on tree rings and speleothems that indicate a dominating positive NAO mode associated with an intensified AMOC (Trouet et al., 2009). These conditions are expressed by a reduced influence of Coastal water and a stronger moisture and heat transport to Norway by the NwAC resulting in warmer and wetter climate conditions (e.g. Wanner et al., 2001; Hurrell et al., 2013). This correlates well to terrestrial records from northern Norway which show slightly increasing air temperatures for this time interval (Bjune and Birks, 2008) and high surface ground temperature estimates between ca. 800 and 500 cal yr BP (Lauritzen and Lundberg, 1999). This time interval most likely reflects the warmer conditions associated with the Medieval Warm Period correlating with observation at the Vøring plateau between ca. 1150 and 650 cal yr BP (ca. 800 – 1300 AD) (Nyland et al., 2006) and in northern Norway between ca. 800 and 500 cal yr BP (ca. 1150 – 1450 AD) (Lauritzen and Lundberg, 1999).

6 Conclusions

A marine core from the northern Norwegian margin was investigated to elucidate the natural variability of water mass properties throughout the late Holocene. In this study, paired Mg/Ca and $\delta^{18}O$ measurements of *N. pachyderma* were presented in order to reconstruct palaeo sub-surface temperature and salinity estimates. Additionally, preservation conditions were analysed and the reconstructed palaeo $SST_{Mg/Ca}$ and SSS estimates were assessed. The palaeoceanographic evolution of the late Holocene was discussed in terms of changing influences of Atlantic and Coastal water and linked to fluctuating modes of the NAO.

The recorded discrepancy between the reconstructed $SST_{Mg/Ca}$ and $SST_{Transfer}$ estimations is likely caused by a combination of several factors such as the restriction of Mg/Ca recordings to a narrow temperature signal, inaccurate estimations of the preferred depth habitat and calcification season of *N. pachyderma* and the initially low Mg/Ca measurements. The overall low measured Mg/Ca ratios might have been influenced by the cleaning method including a reductive step. However, they are likely a direct result of the overall poor preservation conditions associated with the continental margin, resulting in potential underestimations of true $SST_{Mg/Ca}$ and SSS values.

Overall, the proxy results indicate a general cooling trend (7.7 to 6.3 °C, $SST_{Transfer}$) throughout the late Holocene. In addition, fluctuating conditions of Atlantic and Coastal water intensity are observed. Period I (ca. 3500 – 2900 cal yr BP) is influenced by relatively cold (ca. 6.9 °C, $SST_{Transfer}$), less saline and more productive Coastal waters and a stronger vertical stratification of the water column. These conditions are attributed to dominating negative NAO-like conditions. Throughout Period II (ca. 2900 – 1600 cal yr BP), the core site experiences a stronger influence of warm Atlantic water (ca. 7.3 °C, $SST_{Transfer}$) with more favourable preservation conditions associated with positive NAO conditions. The last part of this period likely corresponds to the Roman Warm Period. Within period III (ca. 1600 – 950 cal yr BP), stable conditions and cold sub-surface temperatures (ca. 6.6 °C, $SST_{Transfer}$) are observed indicating a returned and stronger influence of Coastal water. This period correspond very well with the colder and dryer Dark Ages. Period IV (ca. 950 – 550 cal yr BP) experienced a returned stronger influence of Atlantic water attributed to dominating positive NAO conditions and correlates well with the Medieval Warm Period. Nonetheless,

Atlantic water reaching the core site was less warm (ca. 6.3 °C, $SST_{Transfer}$) compared to period II due to the overall late Holocene cooling.

Acknowledgements

This work was carried out within the framework of the Initial Training Network program "Changing Arctic and Subarctic Environments" (CASE, Grant Agreement No. 238111) funded by the European Commission within the 7th Framework Program People, the Research Council of Norway in addition to the University of Tromsø and Norwegian Polar Institute. Jan Sverre Laberg is acknowledged for providing the marine sediment core. Georges Paradis and Dorothy K. Pak are gratefully thanked for cleaning and analysing the Mg/Ca samples at the University of California, Santa Barbara, USA. Additionally, thanks are also extended to Jan P. for his help preparing the maps and Trine Dahl, Julia Sen and Karina Monsen for assisting with laboratory work at the University of Tromsø.

References

Aagaard-Sørensen S, Husum K, Hald M, Marchitto T and Godtliebsen F (2013) Sub sea surface temperatures in the Polar North Atlantic during the Holocene: Planktic foraminiferal Mg/Ca temperature reconstructions. *The Holocene* 24(1): 93-103.

Aksu AE and Vilks G (1988) Stable isotopes in planktonic and benthic foraminifera from Arctic Ocean surface sediments. *Can. J. Earth Sci.* 25: 701-709.

Andersson C, Risebrobakken B, Jansen E and Dahl SO (2003) Late Holocene surface ocean conditions of the Norwegian Sea (Voring Plateau). *Paleoceanography* 18: PA1044, doi: 10.1029/2001PA000654.

Andersson C, Pausata FSR, Jansen E, Risebrobakken B and Telford RJ (2010) Holocene trends in the foraminifer record from the Norwegian Sea and the North Atlantic Ocean. *Clim. Past* 6: 179-193.

Archer D (1991) Modeling the calcite lysocline. *J. Geophys. Res.* 96(C9): 17037-17050.

Aspeli R (1994) Late Quaternary benthic foraminiferal stratigraphy on the western Barents slope Sea. Unpublished thesis, University of Tromsø (in Norwegian).

Barker S and Elderfield H (2002) Foraminiferal calcification response to glacial interglacial changes in atmospheric CO_2. *Science* 297: 883-836.

Barker S, Greaves M and Elderfield H (2003) A study of cleaning procedures used for foraminiferal Mg/Ca paleothermometry. *Geochem. Geophys. Geosyst.* 4(9): 8407, doi:10.1029/2003GC000559.

Barker S, Kiefer T and Elderfield H (2004) Temporal changes in North Atlantic circulation constrained by planktonic foraminiferal shell weights. *Paleoceanography* 19: PA3008.

Bauch D, Carstens J, Wefer G and Thiede J (2000) The imprint of anthropogenic CO_2 in the Arctic Ocean: evidence from planktic $d^{13}C$ data from water column and sediment surfaces. *Deep-Sea Res. Pt. II* 9(11): 1791–1808.

Bé AWH and Tolderlund DS (1971) Distribution and ecology of living planktonic foraminifera in surface waters of the Atlantic and Indian Oceans. In: Funnell BM and Riedel WR (eds) *The Micropaleontology of the Oceans*. Cambridge University Press, London, 105-149.

Beer CJ, Schiebel R and Wilson PA (2010) Testing planktic foraminiferal shell weight as a surface water [CO_3^{2-}] proxy using plankton net samples. *Geology* 38: 103-106.

Berben SMP, Husum K, Cabedo-Sanz P and Belt ST (2014) Holocene sub-centennial evolution of Atlantic water inflow and sea ice distribution in the western Barents Sea. *Clim. Past* 10: 181-198, doi:10.5194/cp-10-181-2014.

Bergami C, Capotondi L, Langone L, Giglio F and Ravaioli M (2009) Distribution of living planktonic foraminifera in the Ross Sea and the Pacific sector of the Southern Ocean (Antarctica). *Mar. Micropaleontol.* 73: 37-48.

Berger WB (1971) Sedimentation of planctonic foraminifera. *Mar. Geol.* 11: 325-358.

Bjune AE and Birks HJB (2008) Holocene vegetation dynamics and inferred climate changes at Svanåvatnet, Mo i Rana, northern Norway. *Boreas* 37: 146-156.

Bjune AE, Seppä H and Birks HJB (2009) Quantitative summer temperature reconstructions for the last 2000 years based on pollen-stratigraphical data from northern Fennoscandia. *J. Paleolimnol.* 41: 43-56.

Blaume F (2002) Physical oceanography from CTD PO181_311. doi:10.1594/PANGAEA.77314.

Boltovskoy E, Boltovskoy D, Correa N and Brandini F (1996) Planktic foraminifera from the southwestern Atlantic (30° – 60°S): Species-specific patterns in the upper 50 m. *Mar. Micropaleontol.* 28: 53–72.

Boyle EA (1983) Manganese carbonate overgrowths on foraminifera tests. *Geochim. Cosmochim. Acta* 47: 1815-1819.

215,000 years: Changes in deep ocean circulation and chemical inventories. *Earth Planet. Sci. Lett.* 76: 135-150.

Broecker WS and Clark E (2001) An evaluation of Lohmann's foraminifera weight dissolution index. *Paleoceanography* 16: 531-534.

Brown SJ and Elderfield H (1996) Variations in Mg/Ca and Sr/Ca ratios of planktonic foraminifera caused by postdepositional dissolution: Evidence of shallow Mg-dependent dissolution. *Paleoceanography* 11(5): 543-551.

Bryson RA and Goodman BM (1980) Volcanic activity and climate change. *Science* 207: 1041-1044.

Carstens J, Hebbeln D and Wefer G (1997) Distribution of planktic foraminifera at the ice margin in the Arctic (Fram Strait). *Mar. Micropaleontol.* 29: 257-269.

Cifelli R (1961) Globigerina incompta, a new species of pelagic foraminifera from the North Atlantic. Contributions Cushman Foundation Foraminiferal Research 12: 83-86.

Conan SMH, Ivanova EM and Brummer GJA (2002) Quantifying carbonate dissolution and calibration of foraminiferal dissolution indices in the Somali Basin. *Mar. Geol.* 182: 325-349.

Darling KF, Kucera M, Kroon D and Wade CM (2006) A resolution for the coiling direction paradox in Neogloboquadrina pachyderma. *Paleoceanography* 21: PA2011, doi:10-1029/2005PA001189.

Dekens PS, Lea DW, Pak DK and Spero HJ (2002) Core top calibration of Mg/Ca in tropical foraminifera: Refining paleotemperatures estimation. *Geochem. Geophys. Geosyst.* 3(4): 1022, doi:10.1029/2001GC000200.

Donner B and Wefer G (1994) Flux and stable isotope composition of Neogloboquadrina pachyderma and other planktonic foraminifers in the Southern Ocean (Atlantic sector). *Deep-Sea Res. Pt. I* 41: 1733-1743.

Duplessy JC, Ivanova E, Murdmaa I, Paterne M and Labeyrie L (2001) Holocene paleoceanography of the northern Barents Sea and variations of the northward heat transport by the Atlantic Ocean. *Boreas* 30: 2-16.

Edmond JM and Gieskes TM (1970) On the calculation of the degree of saturation of sea water with respect to calcium carbonate under in situ conditions. *Geochim. Cosmochim. Acta* 35: 1261-1291.

Ehrmann WU and Thiede J (1985) History of Mesozoic and Cenozoic sediment fluxes to the North Atlantic Ocean. Contributions to Sedimentology E. Schweizerbart'sche Verlagsbuchhandlung, Stuttgart, 15: 1-109, ISBN 3-510-57015-4.

Elderfield H and Ganssen G (2000) Past temperature and d18O of surface ocean waters inferred from foraminiferal Mg/Ca ratios. *Nature* 405: 442-445, doi:10.1038/35013033.

Elderfield H, Vautravers M and Cooper M (2002) The relationship between shell size and Mg/Ca, Sr/Ca, δ18O, and δ13C of species of planktonic foraminifera. *Geochem. Geophys. Geosyst.* 3(8): 1-13.

Elderfield H, Greaves M, Barker S, Hall IR, Tripati A, Ferretti P, Crowhurst S, Booth L and Daunt C (2010) A record of bottom water temperature and seawater [delta]18O for the Southern Ocean over the past 440 kyr based on Mg/Ca of benthic foraminiferal Uvigerina spp. *Quaternary Sci. Rev.* 29: 160-169.

Emerson S and Bender M (1981) Carbon fluxes at the sediment-water interface of the deep-sea: calcium carbonate preservation. *J. Mar. Res.* 39: 139-162.

Espitalié J, Laporte JL, Madec M, Marquis F, Leplat P, Paulet J and Boutefeu A (1977) Méthode rapide de characterisation des roches-mere, de leur potential petrolier et de leur degre d'évolution. *Revue de l'Institute Francais du Petrole* 32: 23-42.

Giraudeau J, Jennings AE and Andrews JT (2004) Timing and mechanisms of surface and intermediate water circulation changes in the Nordic seas over the last 10,000 cal years: A view from the north Iceland shelf. *Quaternary Sci. Rev.* 23: 2127-2139.

Hald M, Andersson C, Ebbesen H, Jansen E, Klitegaard-Kristensen D, Risebrobakken B, Salomonsen GR, Sejrup HP, Sarnthein M and Telford R (2007) Variations in temperature and extent of Atlantic water in the northern North Atlantic during the Holocene. *Quaternary Sci. Rev.* 26: 3423-3440.

Hebbeln C, Henrich R and Baumann KH (1998) Paleoceanography of the last glacial/interglacial cycle in the Polar North Atlantic. *Quat. Sci. Rev.* 17: 125-153.

Hemleben C, Spindler M and Anderson OR (1989) Modern planktonic foraminifera. Springer, New York, 363.

Henrich R, Baumann KH, Huber R and Meggers H (2002) Carbonate preservation records of the past 3Myr in the Norwegian-Greenland Sea and the northern North Atlantic: Implications for the history of NADW production. *Mar. Geol.* 184: 17-39.

Hopkins TS (1991) The GIN Sea: A synthesis of its physical oceanography and literature review, 1972–1985. *Earth Sci. Rev.* 30: 175-318.

Huber R, Meggers H, Baumann KH and Henrich R (2000) Recent and Pleistocene carbonate dissolution in sediments of the Norwegian-Greenland Sea. *Mar. Geol.* 165: 123-136.

Hurrell JW, Kushnir Y, Ottersen G and Visbeck M (2013) An overview of the North Atlantic Oscillation. The North Atlantic Oscillation: Climatic significance and environmental impact. American Geophysical Union, 1-35.

Husum K and Hald M (2012) Arctic planktic foraminiferal assemblages: Implications for subsurface temperature reconstructions. *Mar. Micropaleontol.* 96(97): 38-47.

Hut G (1987) Stable isotope reference samples for geochemical and hydrological investigations. paper presented at Consultants Group Meeting, Int. At. Energy Agency, Vienna.

Ikeda M, Johannessen JA, Lygre K and Sandven S (1989) A process study of mesoscale meanders and eddies in the Norwegian Coastal Current. *J. Phys. Oceanogr.* 19: 20-35.

Jernas P, Klitgaard Kristensen D, Husum K, Wilson L and Koç N (2013) Palaeoenvironmental changes of the last two millennia on the western and northern Svalbard shelf. *Boreas* 42: 236-255.

Jiang H, Eiriksson J, Schulz M, Knudsen KL, Seidenkrantz MS (2005) Evidence for solar forcing of sea-surface temperature on the North Icelandic Shelf during the Late Holocene. *Geology* 33(1): 73-76.

Johannessen T, Jansen E, Flatøy A and Ravelo AC (1994) The relationship between surface water masses, oceanographic fronts and plaeoclimatic proxies in surface sediments of the Greenland, Iceland, Norwegian Seas. In: Zahn R, Pedersen TF, Kaminski MA and Labeyrie L (eds) *Carbon Cycling in the Glacial Ocean: Constraints of the Ocean's Role in Global Change*. Berlin, Springer, 61-86.

Johnstone HJH, Yu J, Elderfield H and Schulz M (2011) Improving temperature estimates derived from Mg/Ca of planktonic foraminifera using X-ray computed tomography-based dissolution index, XDX. *Paleoceanography* 26(1): PA1215, DOI: 10.1029/2009pa001902.

Jonkers L, Brummer GJA, Peeters FJC, van Aken HM and De Jong MF (2010) Seasonal stratification, shell flux, and oxygen isotope dynamics of left-coiling N. pachyderma and T. quinqueloba in the western sub polar North Atlantic. *Paleoceanography* 25: PA2204.

Jonkers L, Jiménez-Amat P, Graham Mortyn P and Brummer GJA (2013) Seasonal Mg/Ca variability of N. pachyderma (s) and G. bulloides: Implications for seawater temperature reconstruction. *Earth Planet. Sci. Lett.* 376: 137-144.

Juggins S (2010) C2 1.7.2 available at http://www.staff.ncl.ac.uk/staff/stephen.juggins/.

Kaufman DS, Schneider DP, McKay NP, Ammann CM, Bradley RS, Briffa KR, Miller GH, Otto-Bliesner BL, Overpeck JT, Vinther BM and Arctic Lakes 2k Project Members (2009) Recent warming reverses long-term Arctic cooling. *Science* 325: 1236-1239.

Keigwin LD and Boyle EA (1989) Late Quaternary paleochemistry of high-latitude surface waters. *Palaeogeogr. Palaeocl.* 73: 85-106.

Knudsen KL (1998) Foraminiferer i Kvartær stratigrafi: Laboratorie og fremstillingsteknik samt udvalgte eksempler. *Geologisk Tidsskrift* 3: 1-25.

Kohfeld KE, Fairbanks RG and Smith SL (1996) *Neogloboquadrina pachyderma* (sinistral coiling) as paleoceanographic tracers in polar oceans: Evidence from northeast water polynya plankton tows, sediments traps, and surface sediments. *Paleoceanography* 11: 679-699.

Kozdon R, Eisenhauer A, Weinelt M, Meland MY and Nuernberg D (2009) Reassessing Mg/Ca temperature calibrations of Neogloboquadrina pachyderma (sinistral) using paired d44/40Ca and Mg/Ca measurements. *Geochem. Geophys. Geosyst.* 10: Q03005, doi:10.1029/2008GC002169.

Laberg JS, Vorren TO, Mienert J, Bryn P and Lien R (2002) The Trænadjupet slide: a large slope failure affecting the continental margin of Norway 4,000 years ago. *Geo. Mar. Lett.* 22: 19-24.

Lamb HH (1977) Climate, Present, Past and Future. Volume 2. Climatic History and the Future. Methuen & Co Ltd, London, 835.

Lauritzen SE and Lundberg J (1999) Calibration of the speleothem delta function: an absolute temperature record for the Holocene in northern Norway. *The Holocene* 9(6): 650-669.

Le J and Shackleton NJ (1992) Carbonate dissolution fluctuations in the western equatorial Pacific during the late Quaternary. *Paleoceanography* 7: 21-42.

Lea DW, Mashiotta TA and Spero HJ (1999) Controls on magnesium and strontium uptake in planktonic foraminifera determined by live culturing. *Geochim. Cosmochim. Acta* 63: 2369-2379.

Lean J (2002) Solar forcing of climate change in recent millennia. In: Wefer G, Berger WH, Behre KE and Jansen E (eds) *Climate development and history of the North Atlantic realm*. Berlin, Springer-Verlag, 75-88.

Lubinski DJ, Polyak L and Forman SL (2001) Freshwater and Atlantic water inflows to the deep northern Barents and Kara seas since ca 13 ^{14}Cka: foraminifera and stable isotopes. *Quaternary Sci. Rev.* 20: 1851-1879.

Mangerud J, Bondevik S, Gulliksen S, Hufthammer AK and Høisæter T (2006) Marine ^{14}C reservoir ages for 19th century whales and molluscs from the North Atlantic. *Quaternary Sci. Rev.* 25: 3228-3245.

Mashiotta TA, Lea DW and Spero HJ (1999) Glacial interglacial changes in Subantarctic sea surface temperature and d18O-water using foraminiferal Mg. *Earth Planet. Sci. Lett.* 170: 417-432, doi:10.1016/S0012-821X(99)00116-8.

Meland MY, Jansen E, Elderfield H, Dokken TM, Olsen A and Bellerby RGJ (2006) Mg/Ca ratios in the planktonic foraminifer Neogloboquadrina pachyderma (sinistral) in the northern North Atlantic/Nordic seas. *Geochem. Geophys. Geosyst.* 7: Q06P14, doi:10.1029/2005GC001078.

Nesje A, Matthews JA, Dahl SO, Berrisford MS and Andersson C (2001) Holocene glacier fluctuation of Flatebreen and winter-precipitation changes in the Jostedalsbreen region, western Norway, based on glaciolacustrine sediment records. *The Holocene* 11: 267–280.

Nürnberg D (1995) Magnesium in tests of Neogloboquadrina pachyderma sinistral from high northern and southern latitudes. *J. Foraminiferal Res.* 25(4): 350-368.

Nürnberg D, Bijma J and Hemleben C (1996) Assessing the reliability of magnesium in foraminiferal calcite as a proxy for water mass temperatures. *Geochim. Cosmochim. Acta* 60: 803-814, doi:10.1016/0016-7037(95)00446-7.

Nyland B, Jansen E, Elderfield H and Andersson C (2006) Neogloboquadrina pachyderma (dex. and sin.) Mg/Ca and d18O records from the Norwegian Sea. *Geochem. Geophys. Geosyst.* 7: Q10P17, doi:10.1029/2005GC001055.

O'Neil JR, Clayton RN and Mayeda TK (1969) Oxygen isotope fractionation in divalent metal carbonates. *J. Chem. Phys.* 51(12): 5547-5558, doi:10.1063/1.1671982.

Olsen J, Anderson NJ and Knudsen MF (2012) Variability of the North Atlantic Oscillation over the past 5200 years. *Nature Geoscience* 5: 808-812. 28 July 2014, ftp://ftp.ncdc.noaa.gov/pub/data/paleo/paleolimnology/greenland/lake-ss1220-2012.xls.

Oppo DW and Fairbanks RG (1989) Carbon isotope composition of tropical surface water during the past 22,000 years. *Paleoceanography* 4: 333-351.

Orvik KA and Niiler P (2002) Major pathways of Atlantic water in the northern North Atlantic and Nordic Seas toward Arctic. *Geophys. Res. Lett.* 29(19): 1896, doi:10.1029/2002GL015002.

Ottersen G, Planque B, Belgrano A, Post E, Reid P and Stenseth N (2001) Ecological effects of the North Atlantic Oscillation. *Oecologia* 128: 1-14.

Perkins H, Hopkins TS, Malmberg SA, Poulain PM and Warn-Varnas A (1998) Oceanographic conditions east of Iceland. *J. Geophys. Res.* 103: 21531-21542.

Pufhl HA and Shackleton NJ (2004) Two proximal, high-resolution records of foraminiferal fragmentation and their implications for changes in dissolution. *Deep-Sea Res. Pt. I* 51: 809-832.

Rasmussen TL and Thomsen E (2010) Holocene temperature and salinity variability of the Atlantic Water inflow to the Nordic Seas. *The Holocene* 20(8): 1223-1234.

Reimer PJ, Bard E, Bayliss A, Beck JW, Blackwell PG, Ramsey CB, Buck CE, Cheng H, Edwards RL, Friedrich M, Grootes PM, Guilderson TP, Haflidason H, Hajdas I, Hatté C, Heaton TJ, Hoffmann DL, Hogg AG, Hughen KA, Kaiser KF, Kromer B, Manning SW, Niu M, Reimer RW, Richards DA, Scott EM, Southon JR, Staff RA, Turney CSM and van der Plicht J (2013) Intcal13 and Marine13 radiocarbon age calibration curves. *Radiocarbon* 55(4): 1869-1887.

Reynolds L and Thunnel RC (1985) Seasonal succession of planktonic foraminifera in the subpolar North Pacific. *J. Foramin. Res.* 15: 282-301.

Risebrobakken B, Jansen E, Mjele E and Hevrøy K (2003) A high resolution study of Holocene paleoclimatic and paleoceanographic changes in the Nordic Seas. *Paleoceanography* 18: 1017, doi:10.1029/2002PA000764.

Risebrobakken B, Morros M, Ivanova EV, Chistyakova N and Rosenberg R (2010) Climate and oceanographic variability in the SW Barents Sea during the Holocene. *Holocene* 20: 609-621.

Rørvik KL, Laberg JS, Hald M, Ravna EK and Vorren TO (2010) Behavior of the northwestern part of the Fennoscandian ice sheet during the Last Glacial Maximum – a response to external forcing. *Quaternary Sci. Rev.* 29: 2224-2237.

Rosenthal Y, Lohmann GP, Lohmann KC and Sherrell RM (2000) Incorporation and preservation of Mg in *Globigerinoides sacculifer*: Implications for reconstructing the temperature and 18O/16O of seawater. *Paleoceanography* 15(1): 135-145.

Sætre R (2007) The Norwegian coastal current. Tapir academic press, Trondheim, 89-99.

Saito T, Thompson PR and Breger D (1981) Systematic index of recent and pleistocene planktonic foraminifera. University of Tokyo press, Tokyo, 1-190.

Sarnthein M, Van Kreveld S, Erlenkeuser H, Grootes PM, Kucera M, Pflaumann U and Schulz M (2003) Centennial-to-millennial-scale periodicities of Holocene climate and sediment injections off the western Barents shelf, 75 °N. *Boreas* 32: 447-461.

Shackleton NJ (1974) Attainment of isotopic equilibrium between ocean water and the benthonic foraminifera genus uvigerina: Isotopic changes in the ocean during the last glacial. *Colloq. Int. CNRS* 219: 203-209.

Simstich J, Sarnthein M and Erlenkeuser H (2003) Paired δ18O signals of N. pachyderma (s) and T. quinqueloba show thermal stratification structure in the Nordic seas. *Mar. Micropaleontol.* 48: 107–125.

Skirbekk K, Klitgaard Kristensen D, Rasmussen TL, Koç N and Forwick M (2010) Holocene climate variations at the entrance to a warm Arctic fjord: evidence from Kongsfjorden trough, Svalbard. *Geological society, London, Special Publications*, 344: 289-304, doi:10.1144/SP344.20.

Slubowska MA, Koç N, Rasmussen TL and Klitgaard-Kristensen D (2005) Changes in the flow of Atlantic water into the Arctic Ocean since the last deglaciation: Evidence from the northern Svalbard continental margin, 80N. *Paleoceonography* 20: PA4014, doi:10.1029/2005PA001141.

Slubowska-Woldengen M, Rasmussen TL, Koç N, Klitgaard-Kristensen D, Nilsen F and Solheim A (2007) Advection of Atlantic Water to the western and northern Svalbard shelf since 17 500 cal yr BP. *Quaternary Sci. Rev.* 26: 463-478.

Solignac S, Giraudeau J and De Vernal A (2006) Holocene sea surface conditions in the western North Atlantic: Spatial and temporal heterogeneities. *Paleoceanography* 21: PA2004, doi:10.1029/2005PA001175.

Stangeew E (2001) Distribution and isotopic composition of living planktonic foraminifera N. pachyderma (sinistral) and T. quinqueloba in the high latitude North Atlantic. Ph.D. thesis, Math.-Naturwiss. Fak., Christian-Albrechts-Univ., Kiel, Germany. (Available at http://e-diss.uni-kiel.de/diss_464/pp).

Stuiver M and Reimer PJ (1993) Extended 14C data base and revised CALIB 3.0 14C age calibration program. *Radiocarbon* 35: 215-230.

Telford RJ and Birks HJB (2005) The secret assumption of transfer functions: Problems with spatial autocorrelation in evaluating model performance. *Quaternary Sci. Rev.* 24: 2173-2179.

Ter Braak CJF and Juggins S (1993) Weighted averaging partial least squares regression (WA-PLS): An improved method for reconstructing environmental variables from species assemblages. *Hydrobiologia* 269(270): 485-502.

Thornalley DJR, Elderfield H and McCave IN (2009) Holocene oscillations in temperature and salinity of the surface subpolar North Atlantic. *Nature* 457: 711-714.

Trouet V, Esper J, Graham NE, Baker A, Scourse JD and Frank DC (2009) Persistent positive North Atlantic Oscillation mode dominated the Medieval Climate Anomaly. *Science* 324: 78-80.

Volkmann R (2000) Planktic foraminifers in the outer Laptev Sea and the Fram Strait: Modern distribution and ecology. *J. Foramin. Res.* 30: 157-176.

Wanner H, Brönnimann S, Casty C, Gyalistras D, Luterbacher J, Schmutz C, Stephenson D and Xoplaki E (2001) North Atlantic Oscillation – Concepts and studies. *Surveys in Geophysics* 22: 321-381.

Wanner H, Beer J, Bütikofer J, Crowley TJ, Cubasch U, Flückiger J, Goosse H, Grosjean M, Joos F, Kaplan JO, Küttel M, Müller SA, Prentice IC, Solomina O, Stocker TF, Tarasov P, Wagner M and Widmann M (2008) Mid- to Late Holocene climate change: an overview. *Quaternary Sci. Rev.* 27(19-20): 1-38, doi:10.1016/j.quascirev.2008.06.013.

Werner K, Spielhagen RF, Bauch D, Hass HC and Kandiano E (2013) Atlantic Water advection versus sea-ice advances in the eastern Fram Strait during the last 9 ka: Multiproxy evidence for a two-phase Holocene. *Paleoceanography* 28: 283-295.

Zamelczyk K, Rasmussen TL, Husum K and Hald M (2013) Marine calcium carbonate preservation vs. climate change over the last two millennia in the Fram Strait: Implications for planktic foraminiferal paleostudies. *Mar. Micropaleontol.* 98: 14-27.

Figure captions

Table 1: AMS ^{14}C dates and calibrated radiocarbon ages of W00-SC3. The calibration is performed using Calib 7.0.0 software (Stuiver and Reimer, 1993), the Marine13 calibration curve (Reimer et al., 2013) and a local reservoir age (ΔR value) of 71 ± 21 following Mangerud et al. (2006). The AMS ^{14}C date highlighted in grey is omitted from the final depth-age model.

Table 2: Planktic foraminiferal species list.

Figure 1: Study area of W00-SC3 (67.24° N, 08.31° E) (green) with the main surface currents: Norwegian Atlantic Current (NwAC) (red) and Norwegian Coastal Current (NCC) (black). A) Surface currents presented on a bathymetric map. B) Generalized schematic profile across the northern Norwegian margin modified after Rørvik et al. (2010). Coastal water (CW), Atlantic water (AW), Atlantic intermediate water (AIW) and Deep water (DW). C) Detail map of the surface currents nearby the core site modified after Sætre (1983). Red and black arrows indicate Atlantic and Coastal water respectively.

Figure 2: CTD data from PO181_311 (67.10° N, 08.26° E) (Blaume, 2002). Temperature (black) and salinity (grey) versus water depth. Atlantic water mass is highlighted in grey.

Figure 3: Depth-age model of W00-SC3 based on three calibrated AMS ^{14}C dates. The 2-σ range of the calibrated radiocarbon ages is indicated by an error bar. The exact values are noted in black for the used dates and grey for one omitted AMS ^{14}C date. A) Calibrated calendar years BP versus core depth. B) Sedimentation rates versus core depth.

Figure 4: Planktic foraminiferal fauna versus cal yr BP (left y-axis) and cal yr BCE/CE (right y-axis). The black diamonds on the Y-axis indicate the AMS ^{14}C converted to calibrated radiocarbon ages. The horizontal lines (grey) in the background indicate the boundaries between the different periods. A) Planktic foraminiferal concentration (black) and flux (grey) versus age. B-G) Species-specific relative abundances (black) and fluxes (grey) of planktic foraminifera versus age. H) Transfer function derived $SST_{Transfer}$ estimates using a modern foraminiferal dataset by Husum and Hald (2012) versus age.

Figure 5: Preservation and geochemical analysis versus cal yr BP (left y-axis) and cal yr BCE/CE (right y-axis). The black diamonds on the Y-axis indicate the AMS ^{14}C converted to calibrated radiocarbon ages. The horizontal lines (grey) in the background indicate the boundaries between the different periods. A) Planktic foraminiferal fragmentation versus age. B) Mean shell weight of *N. pachyderma* versus age. C) Total organic carbon versus age. D) Calcium carbonate versus age. E) Planktic foraminiferal concentration (black) and flux (grey) versus age.

Figure 6: Stable isotopes analysis performed on *N. pachyderma* versus cal yr BP (left y-axis) and cal yr BCE/CE (right y-axis). The black diamonds on the Y-axis indicate the AMS ^{14}C converted to calibrated radiocarbon ages. The horizontal lines (grey) in the background indicate the boundaries between the different periods. A) $\delta^{18}O$ measurements corrected for a vital effect of 0.6 ‰ according Simstich et al. (2003) and Nyland et al. (2006) versus age. B) $\delta^{13}C$ measurements versus age.

Figure 7: Trace element analysis plotted as correlations of contamination tracers versus Mg/Ca ratios. A-C) Correlations are plotted for all measurements. D-F) Samples with ratios higher than 100 µmol/mol are omitted following the contamination threshold of Barker et al. (2003). A; D) Fe/Ca versus Mg/Ca. B; E) Al/Ca versus Mg/Ca. C;F) Mn/Ca versus Mg/Ca.

Figure 8: Water mass properties versus cal yr BP (left y-axis) and cal yr BCE/CE (right y-axis). The black diamonds on the Y-axis indicate the AMS ^{14}C converted to calibrated radiocarbon ages. The horizontal lines (grey) in the background indicate the boundaries between the different periods. A) Mg/Ca ratios of *N. pachyderma* versus age. B) $SST_{Mg/Ca}$ estimates obtained by the temperature:Mg/Ca equation of Kozdon et al. (2009) versus age. C) $SST_{Transfer}$ estimates using the modern foraminiferal dataset by Husum and Hald (2012) versus age. D) SSS estimates derived by a combined $\delta^{18}O_c$ and $SST_{Mg/Ca}$ approach using the salinity to $\delta^{18}O_w$ relation for the central and eastern Nordic Seas by Simstich et al. (2003) versus age. E) Reconstructed NAO-index from a lake record in south-west Greenland (Olsen et al., 2012) versus age.

Figure 9: The interpretation of fluctuating influence of sub-surface water masses based on multi-proxy data from the study area is presented as a schematic profile across the northern Norwegian margin for four separate time periods. Coastal water (CW), Atlantic water (AW), Atlantic intermediate water (AIW) and Deep water (DW).

Table 1

Lab ID	Core depth (cm)	Material	Uncorrected ^{14}C age	cal yr BP	2-σ range BP	cal yr BCE/CE	2-σ range BCE/CE	Reference
Beta-334422	23.5	*N. pachyderma*	1590 ± 30	1069	968 - 1170	881 CE	780 - 982 CE	This study
TUa-2931	40.0	*N. pachyderma*	1360 ± 65	821.5	684 - 959	1128.5 CE	991 - 1266 CE	Laberg et al., 2002
TUa-2930	120.0	*N. pachyderma*	2305 ± 55	1836	1688 - 1984	114.5 CE	35 BC - 262 CE	Laberg et al., 2002
TUa-2929	263.0	*N. pachyderma*	3660 ± 95	3484.5	3237 - 3732	1535.5 BCE	1783 - 1288 BCE	Laberg et al., 2002

Table 2

Planktic foraminiferal species
Globigerina bulloides (d'Orbigny), 1826
Globigerinita glutinata (Egger), 1893
Globigerinita uvula (Ehrenberg), 1861
Neogloboquadrina incompta (Cifelli), 1961
Neogloboquadrina pachyderma (sinistral) (Ehrenberg), 1861
Turborotalita quinqueloba (Natland), 1838

Figure 1

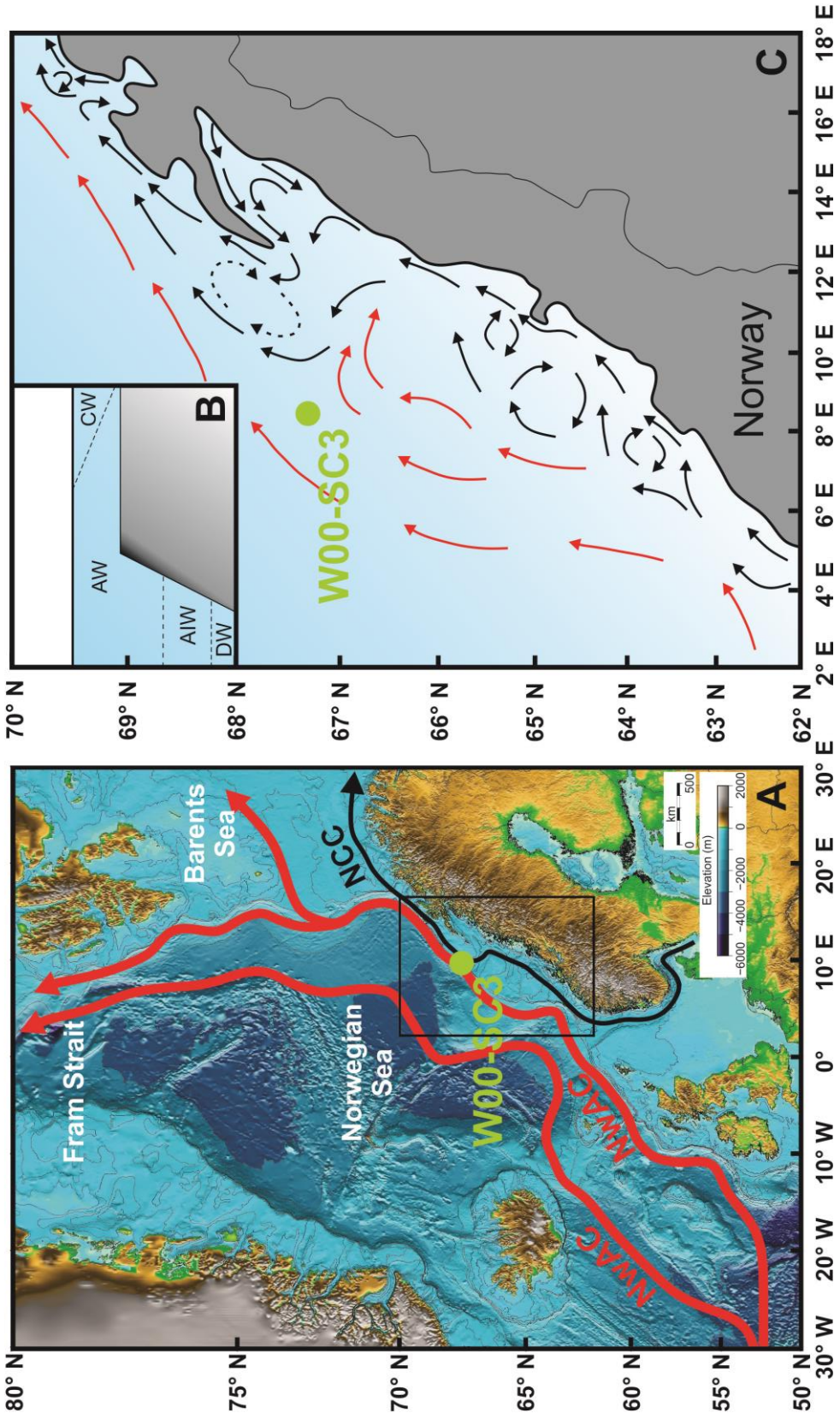
A
B
C
Fram Strait
Barents Sea
Norwegian Sea
NCC
W00-SC3
NwAC
NwAC
W00-SC3
Elevation (m)
km
AW
AIW
DW
CW
Norway
80° N
75° N
70° N
65° N
60° N
55° N
50° N
30° W
20° W
10° W
0°
10° E
20° E
30° E
70° N
69° N
68° N
67° N
66° N
65° N
64° N
63° N
62° N
2° E
4° E
6° E
8° E
10° E
12° E
14° E
16° E
18° E

Figure 2

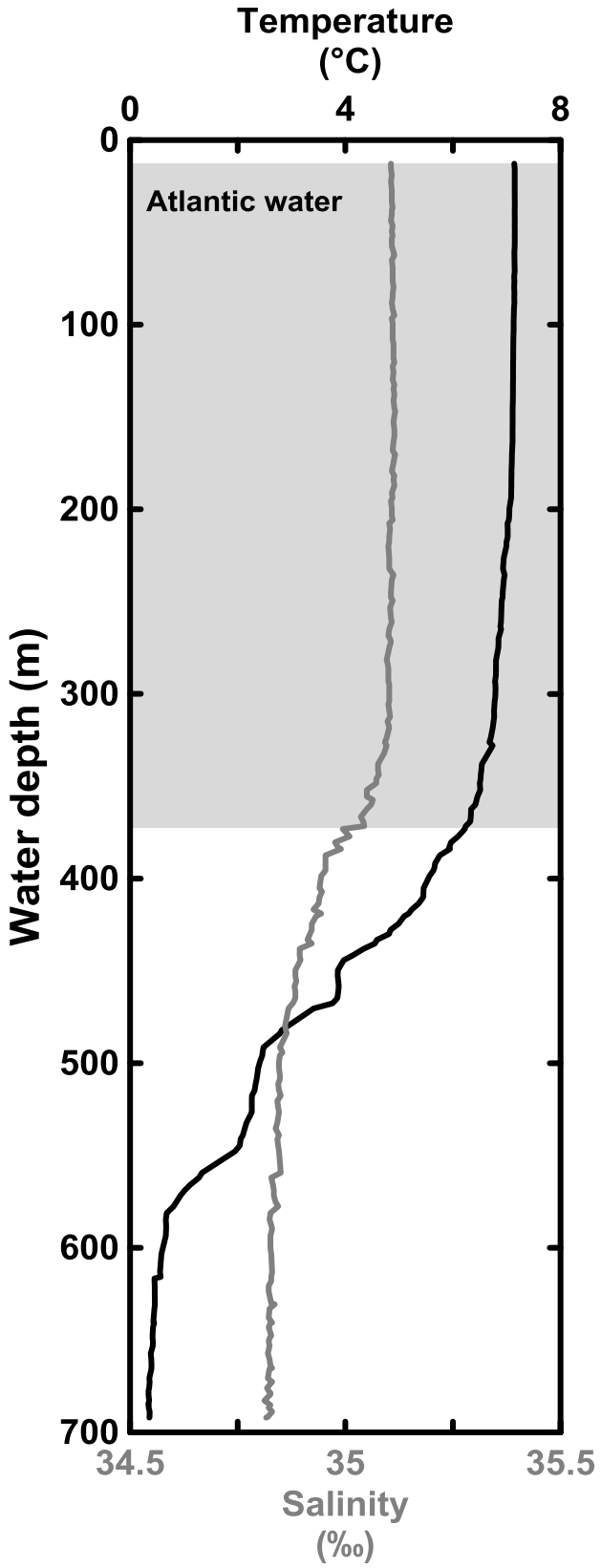
Temperature
(°C)
0
4
8
0
Atlantic water
100
200
300
400
500
600
700
Water depth (m)
34.5
35
35.5
Salinity
(‰)

Figure 3

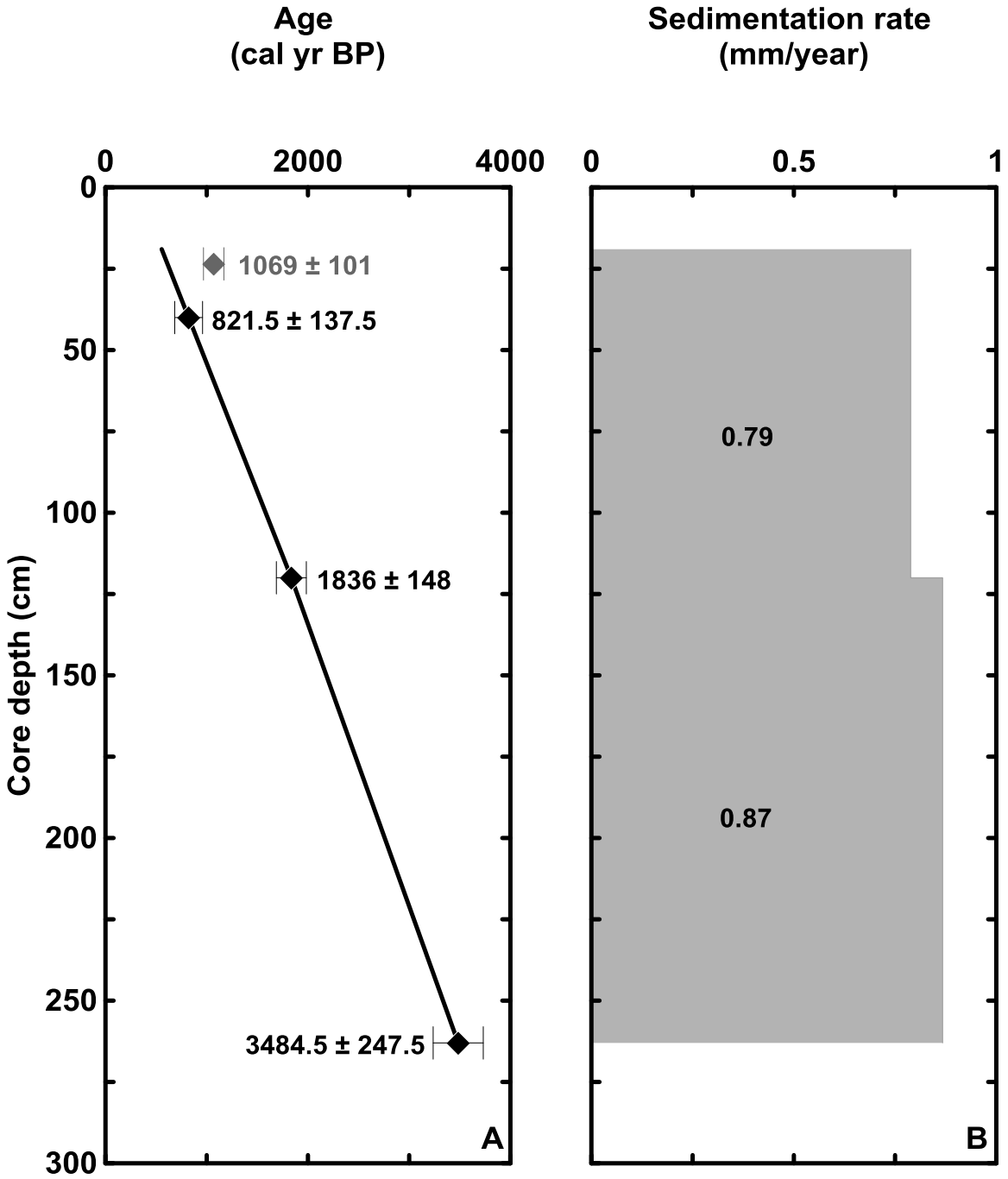
Age
(cal yr BP)
Sedimentation rate
(mm/year)
0
2000
4000
0
0.5
1
Core depth (cm)
0
50
100
150
200
250
300
1069 ± 101
821.5 ± 137.5
1836 ± 148
3484.5 ± 247.5
0.79
0.87
A
B

Figure 4

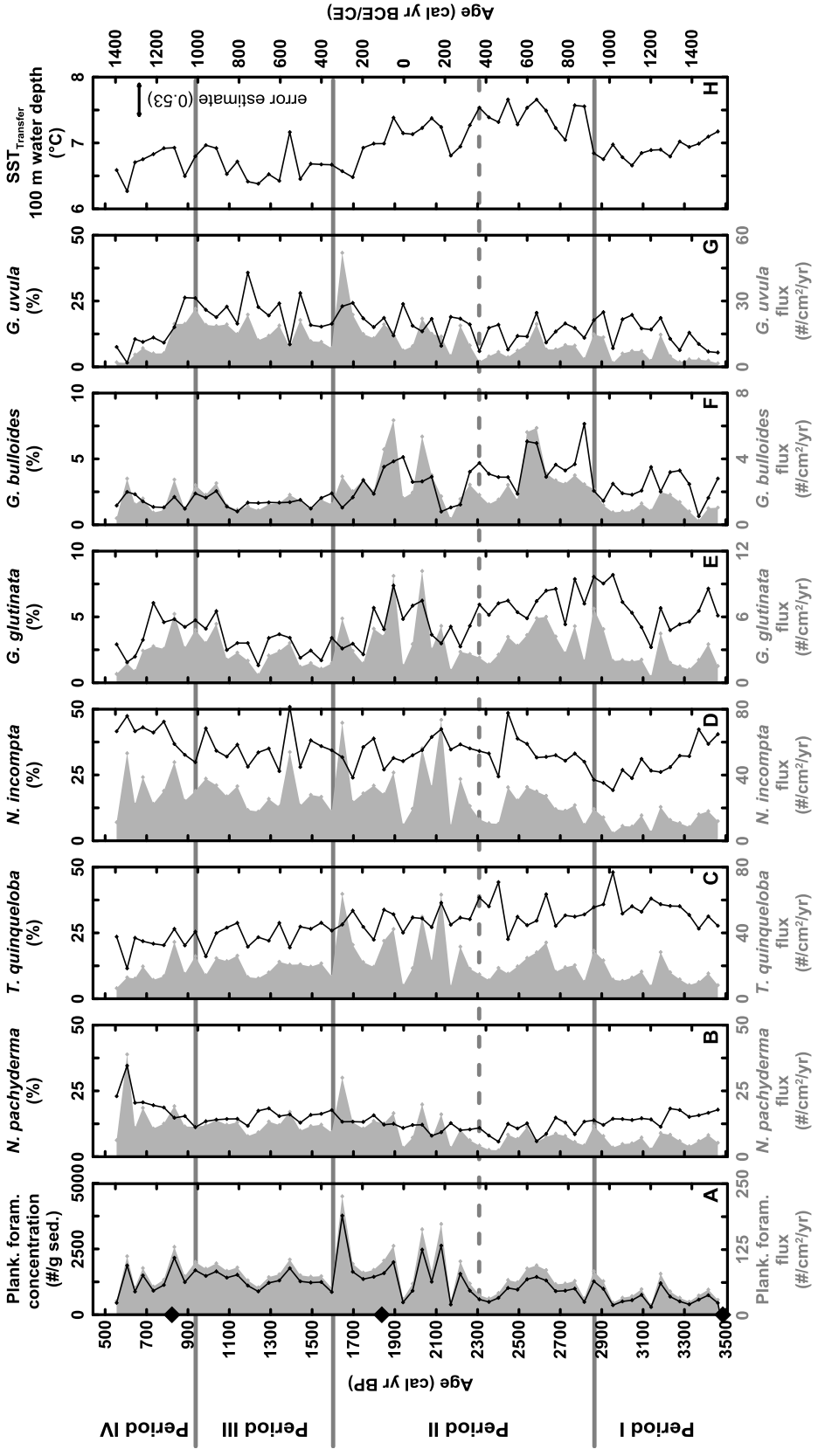
Age (cal yr BCE/CE)
1400 1200 1000 800 600 400 200 0 200 400 600 800 1000 1200 1400
SST Transfer 100 m water depth (°C)
error estimate (0.53)
H
G. uvula (%)
G. uvula flux (#/cm²/yr)
G
G. bulloides (%)
G. bulloides flux (#/cm²/yr)
F
G. glutinata (%)
G. glutinata flux (#/cm²/yr)
E
N. incompta (%)
N. incompta flux (#/cm²/yr)
D
T. quinqueloba (%)
T. quinqueloba flux (#/cm²/yr)
C
N. pachyderma (%)
N. pachyderma flux (#/cm²/yr)
B
Plank. foram. concentration (#/g sed.)
Plank. foram. flux (#/cm²/yr)
A
500 700 900 1100 1300 1500 1700 1900 2100 2300 2500 2700 2900 3100 3300 3500
Age (cal yr BP)
Period IV
Period III
Period II
Period I

Figure 5

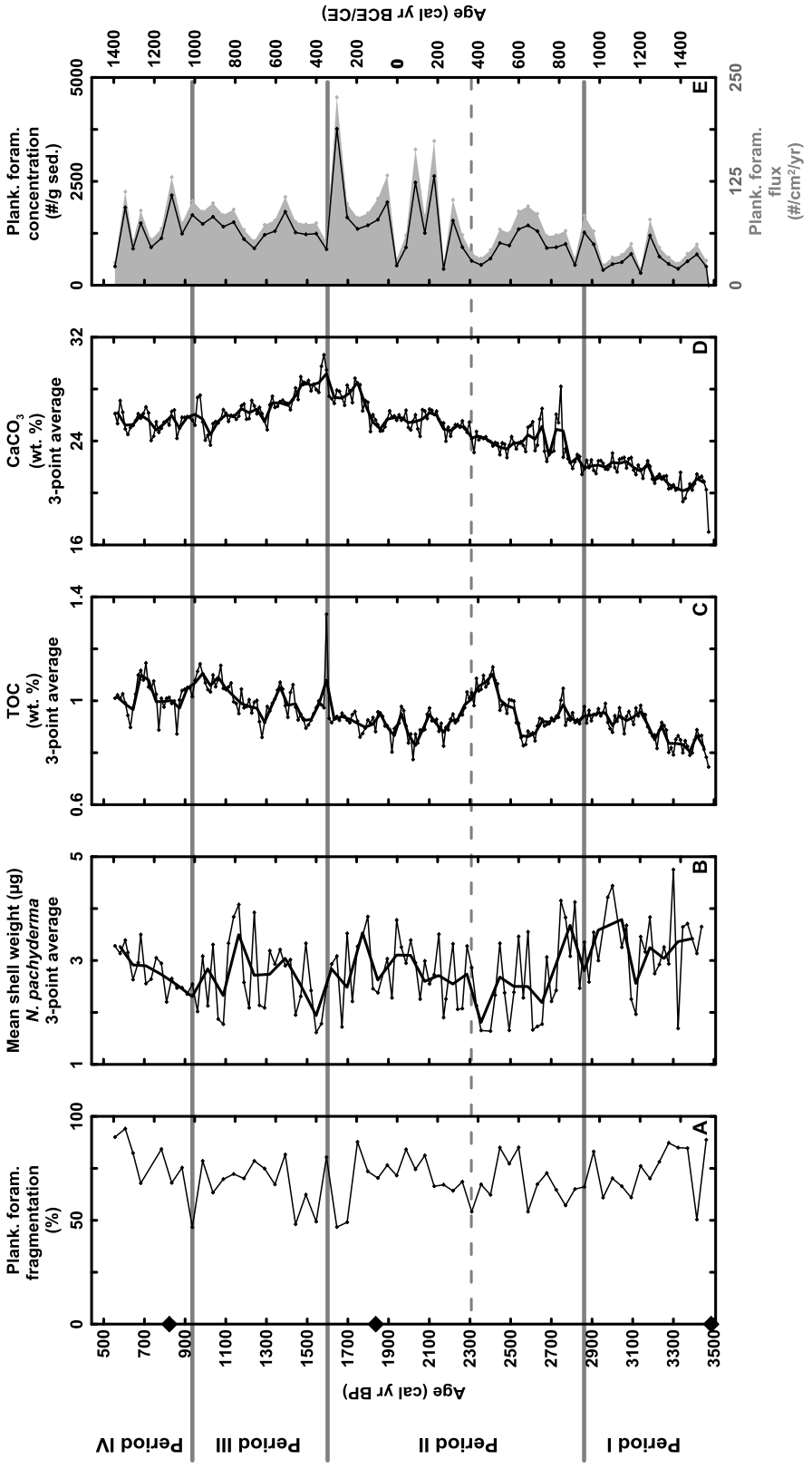
Age (cal yr BCE/CE)
1400 1200 1000 800 600 400 200 0 200 400 600 800 1000 1200 1400
Plank. foram. concentration (#/g sed.)
0 2500 5000
Plank. foram. flux (#/cm²/yr)
0 125 250
E
CaCO3 (wt. %) 3-point average
16 24 32
D
TOC (wt. %) 3-point average
0.6 1 1.4
C
Mean shell weight (µg) N. pachyderma 3-point average
1 3 5
B
Plank. foram. fragmentation (%)
0 50 100
A
Age (cal yr BP)
500 700 900 1100 1300 1500 1700 1900 2100 2300 2500 2700 2900 3100 3300 3500
Period IV
Period III
Period II
Period I

Figure 6

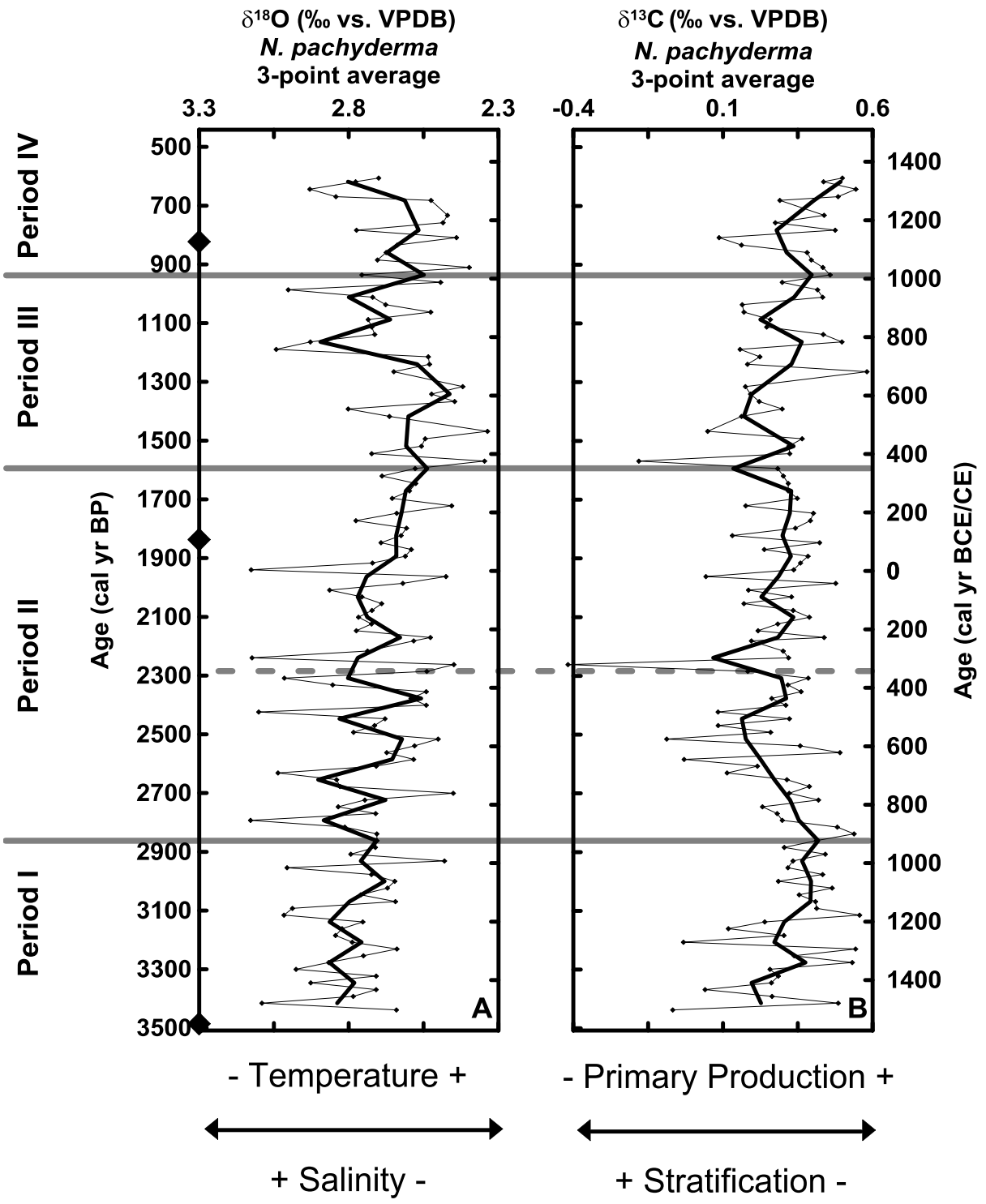
δ18O (‰ vs. VPDB)
N. pachyderma
3-point average
3.3
2.8
2.3
δ13C (‰ vs. VPDB)
N. pachyderma
3-point average
-0.4
0.1
0.6
Period IV
Period III
Period II
Period I
Age (cal yr BP)
500
700
900
1100
1300
1500
1700
1900
2100
2300
2500
2700
2900
3100
3300
3500
1400
1200
1000
800
600
400
200
0
200
400
600
800
1000
1200
1400
Age (cal yr BCE/CE)
A
B
- Temperature +
+ Salinity -
- Primary Production +
+ Stratification -

Figure 7

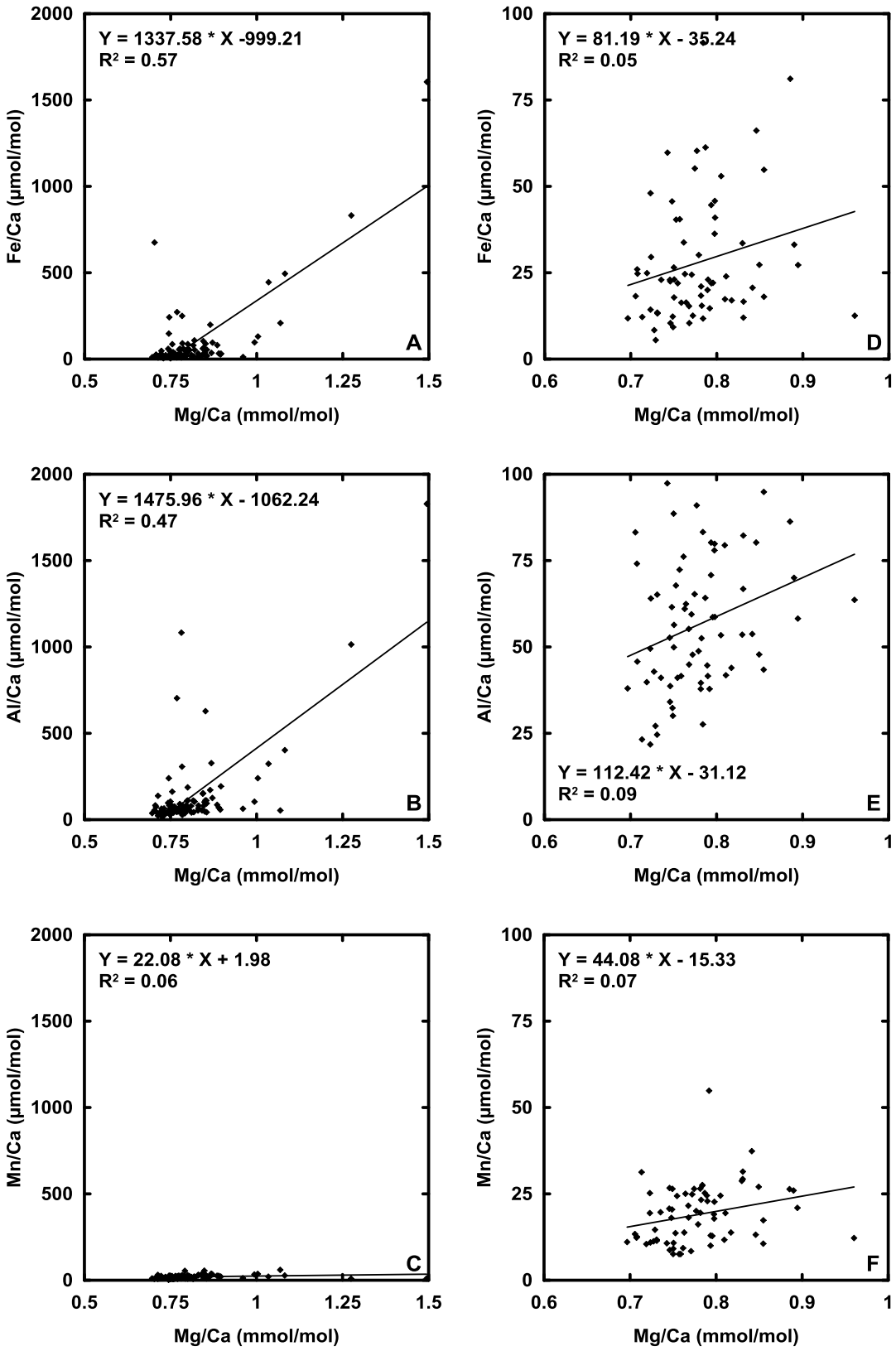
Y = 1337.58 * X -999.21
R² = 0.57
Fe/Ca (µmol/mol)
Mg/Ca (mmol/mol)
A
Y = 81.19 * X - 35.24
R² = 0.05
Fe/Ca (µmol/mol)
Mg/Ca (mmol/mol)
D
Y = 1475.96 * X - 1062.24
R² = 0.47
Al/Ca (µmol/mol)
Mg/Ca (mmol/mol)
B
Y = 112.42 * X - 31.12
R² = 0.09
Al/Ca (µmol/mol)
Mg/Ca (mmol/mol)
E
Y = 22.08 * X + 1.98
R² = 0.06
Mn/Ca (µmol/mol)
Mg/Ca (mmol/mol)
C
Y = 44.08 * X - 15.33
R² = 0.07
Mn/Ca (µmol/mol)
Mg/Ca (mmol/mol)
F

Figure 8

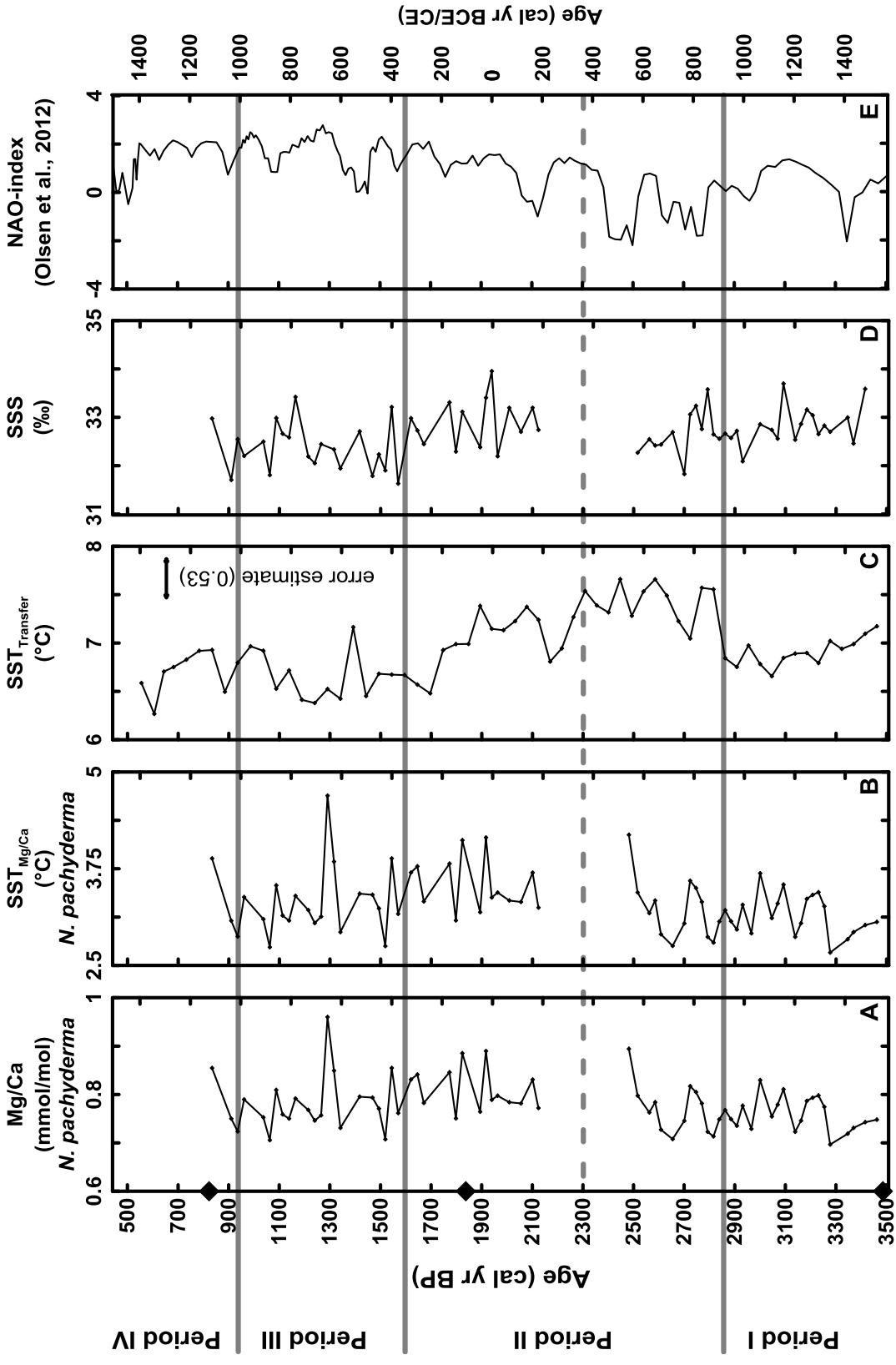
Age (cal yr BCE/CE)
1400
1200
1000
800
600
400
200
0
200
400
600
800
1000
1200
1400
NAO-index
(Olsen et al., 2012)
4
0
-4
E
SSS
(‰)
35
33
31
D
SST Transfer
(°C)
8
7
6
error estimate (0.53)
C
SST Mg/Ca
(°C)
N. pachyderma
5
3.75
2.5
B
Mg/Ca
(mmol/mol)
N. pachyderma
1
0.8
0.6
A
500
700
900
1100
1300
1500
1700
1900
2100
2300
2500
2700
2900
3100
3300
3500
Age (cal yr BP)
Period IV
Period III
Period II
Period I

Figure 9

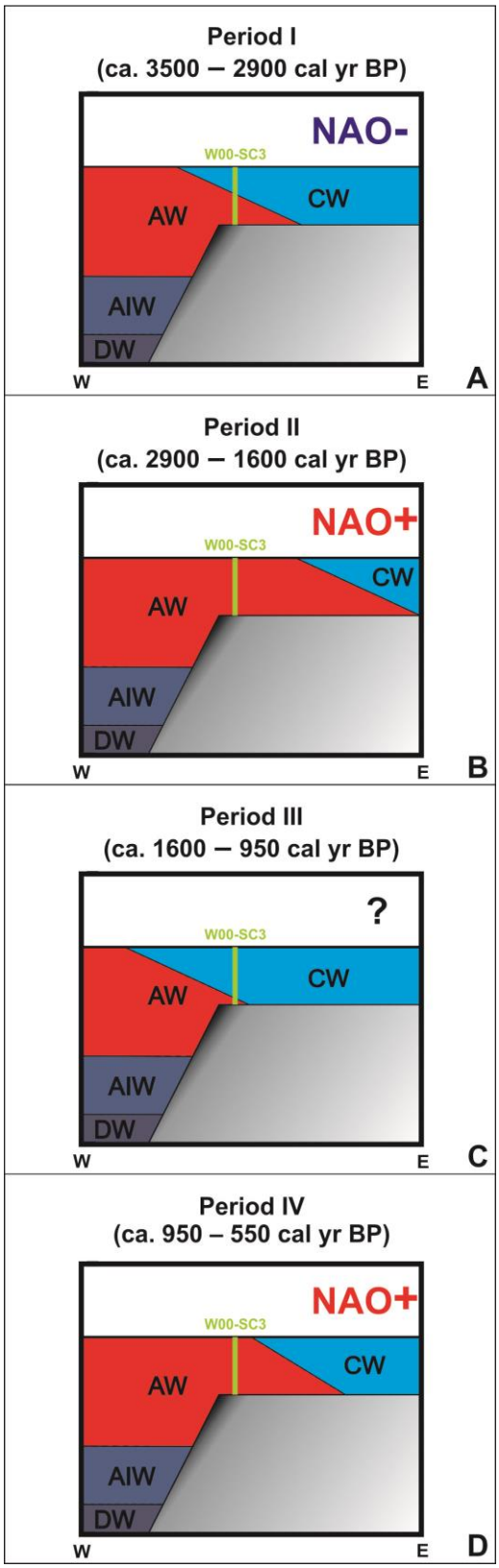
Period I
(ca. 3500 – 2900 cal yr BP)
NAO-
W00-SC3
AW
CW
AIW
DW
W
E
A
Period II
(ca. 2900 – 1600 cal yr BP)
NAO+
W00-SC3
AW
CW
AIW
DW
W
E
B
Period III
(ca. 1600 – 950 cal yr BP)
?
W00-SC3
AW
CW
AIW
DW
W
E
C
Period IV
(ca. 950 – 550 cal yr BP)
NAO+
W00-SC3
AW
CW
AIW
DW
W
E
D